NASA CR-132633

DESIGN AND ANALYSIS

OF A

SUPERSONIC PENETRATION/MANEUVERING FIGHTER

Prepared by

R. D. Child

April 1975

Prepared Under Contract NAS1-13496
By Los Angeles Aircraft Division
ROCKWELL INTERNATIONAL CORPORATION
Los Angeles, California
For
LANGLEY RESEARCH CENTER
NATIONAL AERONAUTICS AND SPACE ADMINISTRATION

ABSTRACT

The ability to cruise at supersonic speeds provides a tactical fighter with advantages in: (1) terminal combat effectiveness, (2) survival during penetration of enemy territory, and (3) attack of time-critical targets.

In air-to-air combat, a supersonic speed capability provides a number of benefits. The speed advantage can be used either to initiate combat at a high energy state or, if desired, to avoid combat. A long endurance speed advantage can be used to run down or run away from today's supersonic aircraft because existing supersonic aircraft can maintain supersonic speeds for only a few minutes.

The object of this study was to design three candidate air combat fighters which would cruise effectively at freestream Mach numbers of 1.6, 2.0, and 2.5 while maintaining good transonic maneuvering capability. These fighters were designed to deliver aerodynamically controlled dogfight missiles at the design Mach numbers. Studies performed by Rockwell International in May 1974 and guidance from NASA determined the shape and size of these missiles.

The principal objective of this study was the aerodynamic design of the vehicles; however, configurations were sized to have realistic structure, mass properties, and propulsion systems. The results of this study showed that air combat fighters in the 15,000 to 23,000 pound class would cruise supersonically on dry power and still maintain good transonic maneuvering performance.

TABLE OF CONTENTS

LIST OF ILLUSTRATIONS

LIST OF ILLUSTRATIONS (CONTINUED)

LIST OF ILLUSTRATIONS (CONTINUED)

LIST OF ILLUSTRATIONS (CONTINUED)

LIST OF TABLES

INTRODUCTION

The ability to cruise at supersonic speeds provides a tactical fighter with advantages in: (1) terminal combat effectiveness, (2) survival during penetration of enemy territory, and (3) attack of time-critical targets.

In air-to-air combat, a supersonic speed capability provides a number of benefits. The speed advantage can be used either to initiate combat at a high energy state or, if desired, to avoid combat. A long endurance speed advantage can be used to run down or run away from today's supersonic aircraft because existing supersonic aircraft can maintain supersonic speeds for only a few minutes.

In combat with any but the most advanced enemy aircraft, supersonic "hit and run" missile attacks can be made without giving the opponent an opportunity to launch his missiles. If the enemy has exhausted his supply of missiles, supersonic speed can be used to make hit and run attacks without being exposed to return gunfire.

The object of this study was to design three air combat fighters which would cruise effectively at freestream Mach numbers of 1.6, 2.0, and 2.5 while maintaining good transonic maneuvering capability. These fighters were designed to deliver aerodynamically controlled dogfight missiles at the design Mach numbers. Studies performed by Rockwell International in May of 1974 and guidance from NASA determined the shape and size of these missiles.

The principal objective of this study was the aerodynamic design of the vehicles, however, configurations were sized to have realistic structure, mass properties, and propulsion systems. The results of this study showed that air combat fighters in the 15,000 to 23,000 pound class would cruise supersonically on dry power and still maintain good transonic maneuvering performance.

NOMENCLATURE

A	1. Area, sq cm (sq in.) 2. Aspect ratio
A_c	Engine inlet capture area, sq cm (sq in.)
A_i	Engine inlet area, sq cm (sq in.)
A_o	Freestream tube area, sq cm (sq in.)
A_t	Engine throat area, sq cm (sq in.)
A_x	Engine auxiliary inlet area, sq cm (sq in.)
AR	Aspect ratio = b^2/S_{REF}
Axi	Axisymmetric
BLC	Boundary layer control
BPR	Engine bypass ratio
b	Span of planar surface
C_D	Drag coefficient
$C_{D_{add}}$	Additive drag coefficient
C_{D_i}	1. Inlet drag coefficient 2. Coefficient of drag due to lift (induced drag)
C_{D_K}	Drag factor
C_{D_M}	Wave drag coefficient
C_L	Lift coefficient
C_{L_K}	Lift factor
C_{L_o}	Lift at α = 0.0 degrees
C_{L_α}	Lift curve slope, per degree
C_ℓ	1. Section lift coefficient 2. Rolling moment coefficient
C_m	Pitching moment coefficient
C_n	Yawing moment coefficient

C_p	Static-pressure coefficient
C_R, C_r	Planar surface root chord, cm (in.)
C_{REF}	Reference chord, cm (in.)
C_T, C_t	Planar surface tip chord, cm (in.)
C_y	Sideforce coefficient
c	Chord length, cm (in.)
$\bar{c}$	Mean aerodynamic chord, MAC
C.G.	Center of gravity
D_h	Inlet hydraulic diameter, cm (in.)
daN	DecaNewton
E_L	Young's modulus parallel to filament direction, $\frac{Kg}{sq\ cm}(\frac{LB}{sq\ in.})$
E_T	Transverse Young's modulus of a filament, $\frac{Kg}{sq\ cm}(\frac{LB}{sq\ in.})$
ECI	External compression inlet
ECS	Environmental control system
EI	Bending stress, Kg-sq cm (LB-sq in.)
F_{cu}	Ultimate compression stiffness, $\frac{Kg}{sq\ cm}(\frac{LB}{sq\ in.})$
F_N	Net thrust, daN (LB)
F_{NE}	Net propulsive effort, daN (LB)
F_{su}	Ultimate shear stress, $\frac{Kg}{sq\ cm}(\frac{LB}{sq\ in.})$
F_{tu}	Ultimate tension stress, $\frac{Kg}{sq\ cm}(\frac{LB}{sq\ in.})$
FDWT	Flight design gross weight, Kg (LB)

FRP	Fuselage reference plane
F.S.	Fuselage longitudinal station
G_{LT}	Shear modulus of a filament, $\frac{Kg}{sq\ cm}$ ($\frac{LB}{sq\ in.}$)
g	Acceleration due to gravity
GJ	Torsional stiffness, Kg-sq cm (LB-sq in.)
K	Induced drag factor
L	Reference length, m(ft)
LDWT	Landing design gross weight
M, M_o	Freestream Mach number
M_d	Design Mach number
M_ℓ	Local Mach number
M_H	Maximum continuous level flight Mach number
M_L	Limit Mach number
M_t'	Mach number at throat (with isentropic internal contraction)
M_x	Wing ultimate bending moment, cm-Kg (in.-LB)
M_y	1. Wing ultimate torque, cm-Kg (in.-LB) 2. Fuselage ultimate bending moment cm-Kg (in.-LB)
M.A.C.	Mean aerodynamic chord = $\bar{c}$, cm (in.)
MCI	Mixed compression inlet
MTOWT	Maximum takeoff gross weight
OPR	Overall pressure ratio
P	Static pressure
$\Delta P/P_2$	Duct exit hammershock pressure ratio
P_u^*	Unstarted sonic throat static pressure

NOMENCLATURE (CONTINUED)

q	Dynamic pressure $=\frac{1}{2} \rho V^2$, $\frac{Kg}{sq\ cm}$ $(\frac{LB}{sq\ in.})$
R	Mission radius, nm (miles)
$(\Delta REC)_{SRS}$	Pressure recovery penalty for self-restarting operation
r	Inside lip radius of engine inlet, cm(in.)
S, S_{REF}	Reference area, sq m (sq ft)
S_W	Gross wing area, sq m (sq ft)
S_{WET}	Wetted area, sq m (sq ft)
S_Z	Wing vertical shear, Kg (LB)
SEP	Specific excess power = V(T-D)/W
S.F.C.	Specific fuel consumption, Kg/hr/daN(LB/HR/LB)
S.L.	Sea level
SP/MF	Supersonic Penetration/Maneuvering Fighter
T	Thrust, daN (LB)
TOGW	Takeoff gross weight, Kg (LB)
t/2c	Wing nondimensional half thickness
V	Velocity, M/sec (ft/sec)
V_1	Engine failure speed, Km/Hr (knots)
W	1. Weight, Kg (LB) 2. Airflow rate, Kg/sec(LB/sec)
W_{c_2}	Engine corrected airflow
X	Airplane longitudinal dimension, cm (in.) (except for pages 7, 76, 77, 78)
Y	Airplane lateral dimension, cm (in.)
Z	Airplane vertical dimension, cm (in.)
2-D	Two-dimensional

α	Angle of attack, degrees
α_o	Angle of attack at $C_{L=0.0}$
β	Sideslip angle, degrees
Γ	Dihedral angle, degrees
Δ	Increment
δ	Pressure ratio
ϵ	Twist angle, degrees
η	Wing spanwise station
θ	1. Temperature ratio 2. Deflection of engine inlet ramp with respect to freestream 3. Angle of skin ply with respect to wing reference system
Λ	Sweep of wing, degrees
λ	Taper ratio = $\frac{C_t}{C_r}$
ξ	Trailing edge cutout ratio
ρ	Density
ϕ	Roll angle, degrees
ψ	Outwash angle, degrees

SUBSCRIPTS

AVG	Average value
a	Aileron
a.c.	Aerodynamic center
B	Body
c	1. camber 2. capture
c.p.	Center of pressure

SUBSCRIPTS (Continued)

e	Elevator
F	Fuselage
i	Inlet of engine
L.E.	Leading edge of planar surface
ℓ	Local value
MAX.	Maximum value
MIN.	Minimum value
NAC.	Nacelle
o	Freestream
P	Aircraft roll axis
R	Rudder
REF.	Reference
t	1. Throat of engine 2. Total value
t_2	Engine downstream station total value
us	Engine unstart value
W	Wing

Section I

PRELIMINARY SIZING

The preliminary or initial sizing for the three air vehicles designed for 1.6, 2.0 and 2.5 Mach number cruise respectively was based on an in-house developed supercruiser airplane. Propulsion data used in the sizing exercises and subsequent air vehicle design was that developed using the Pratt & Whitney Parametric Engine computer program. The engines were the PW 74-09 for the 1.6 Mach design, the PW 74-17 for the 2.0 Mach design and the PW 74-18 for the 2.5 Mach design. Basic weight and aerodynamic scaling were made to the modified supercruiser design. The airplanes were sized using the appropriate engine data, aerodynamics, geometry and weight characteristics along with the mission requirements shown in figure 1. Si 'ng was accomplished using the Vehicle Sizing and Performance Evaluation Program (VSPEP). This computer program produced vehicles for various wing loadings and thrust-to-weight values that meet the desired 300.0 n.mi. design mission radius. Additional performance evaluation was made to establish take off distance over a 50 ft obstacle and Specific Excess Power (SEP) at 0.9M/ 30,000 ft/5g maneuver condition.

Selected airplanes were chosen by cross plotting the above generated data for each of the three airplanes and picking the minimum gross weight airplane having a takeoff distance no greater than 3000 feet and a SEP no less than -300 ft/sec as well as a mission radius of 300 nm. Characteristics of the selected airplanes are shown on Table I.

The M=1.6 airplane generated by this sizing was drawn and shown on figure 2 (D575-1). Aerodynamic and weight analysis of this airplane were made and the results are shown in table III and figures 3 through 5. This airplane was then set up on the VSPEP program and a second iteration sizing exercise was performed for each of the three airplanes using the D575-1 as a baseline vehicle. The 1.6 Mach cruise airplane in this case used propulsion data for the PW 74-16 engine. The sizing procedure used was identical to that described above for the first pass preliminary sizing.

Characteristics of the three refined airplanes are shown on Table II. The reduction in size over the results of the first iteration were found to be due mainly to weight in the center section and lower skin friction drag.

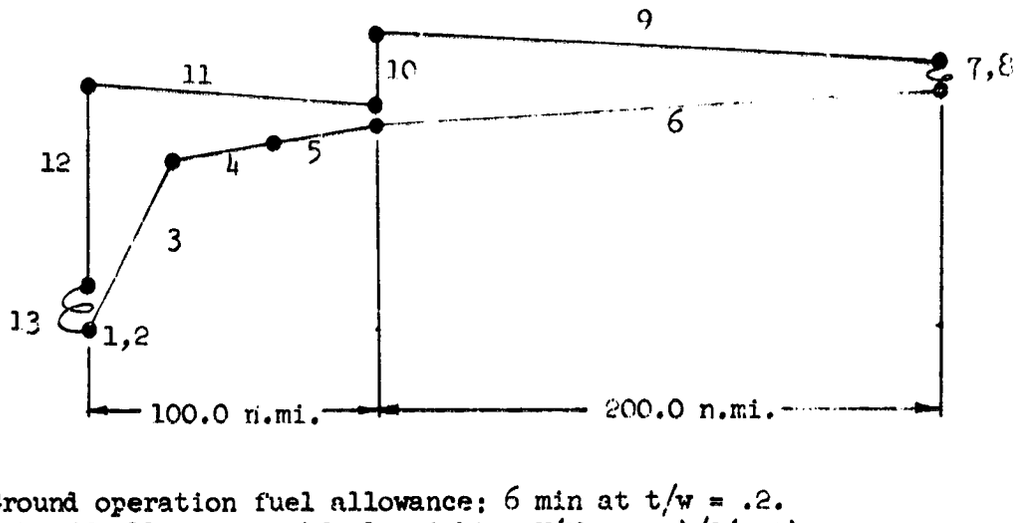

1. Ground operation fuel allowance: 6 min at t/w = .2.
2. Takeoff allowance: Δfuel weight $= mV(W_o - W_i)/2(T-D)$
   where $m = W/g$ where W is the weight at start of climb
   W_o = sea level static maximum power fuel flow
   W_i = sea level maximum power fuel flow at initial climb speed
   T = maximum thrust at start of climb
   D = trimmed drag at start of climb
3. Intermediate power climb to best subsonic cruise altitude.
4. Subsonic cruise at best cruise speed and altitude.
5. Accelerate and climb to design Mach number at maximum power.
6. Cruise at design Mach number, best altitude on dry power.
7. Maneuver at design Mach number with 50 percent initial fuel.
   Fuel = (energy required) (fuel flow)/SEP
   SEP = specific excess power $V(T-D)/W$
   V = velocity feet/second
   T = maximum power thrust at design Mach
   D = trimmed drag at design Mach

Design Mach Number	Altitude (Ft)	Energy Required (Ft)
1.6	30,000	74,000
2.0	40,000	105,000
2.5	50,000	144,000

8. Deliver payload = 1000 lbs.
9. Cruise at design Mach number, best altitude on dry power.
10. Descend and decelerate with no time, fuel or distance.
11. Subsonic cruise at best cruise speed and altitude.
12. Descend to sea level with no time, fuel or distance.
13. Sea level loiter for 20.0 minutes at best loiter speed.

Figure 1. Design Mission Details

TABLE I

Characteristics of the Selected Airplanes

DESIGN CRUISE MACH NO.		1.6	2.0	2.5
Gross Wt.	(lb)	21650	27350	30950
W_o/S	(psf)	65	75	75
T/W_o		.65	.686	.72
Radius	(nm)	300	300	300
Takeoff Distance	(ft)	2650	2630	2660
SEP at .9M/30K/5g	(fps)	-300	-300	-300

TABLE II

Characteristics of the Refined Airplanes

DESIGN CRUISE MACH NO.		1.6	2.0	2.5
Gross Wt	(lb)	15700	18304	23469
Fuel Wt	(lb)	3894	5424	8467
Wing Area	(ft^2)	185	215	276
Engines	(#-%)	2-45.3	2-52.4	2-62.6
Radius	(nm)	300	300	300
Takeoff Distance	(ft)	3000	3000	3000
SEP at .9M/30K/5g	(fps)	-175	-167	-170

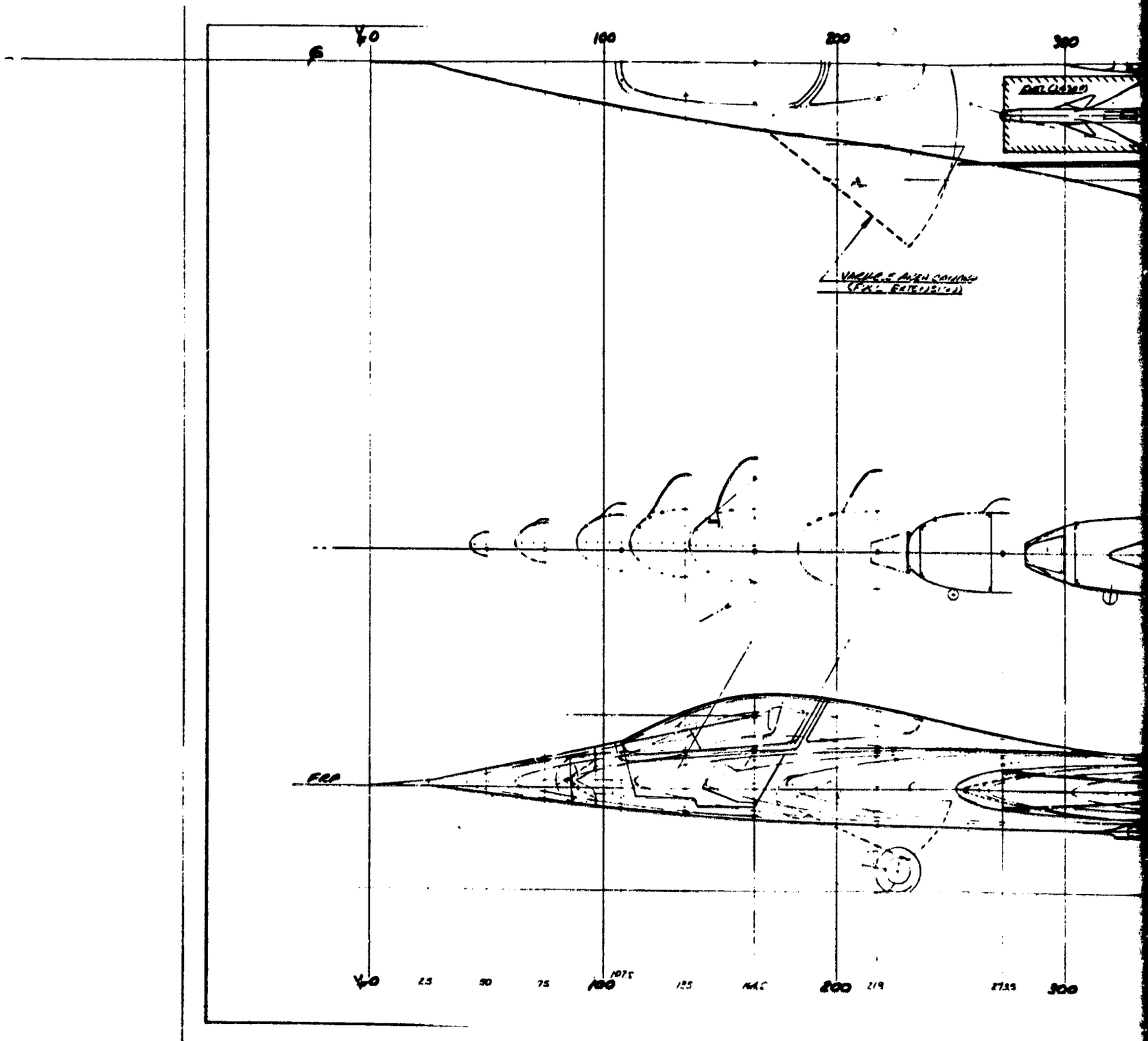

PRECEDING PAGE BLANK NOT FILMED

FOLDOU

FOLDOUT FRAME

1

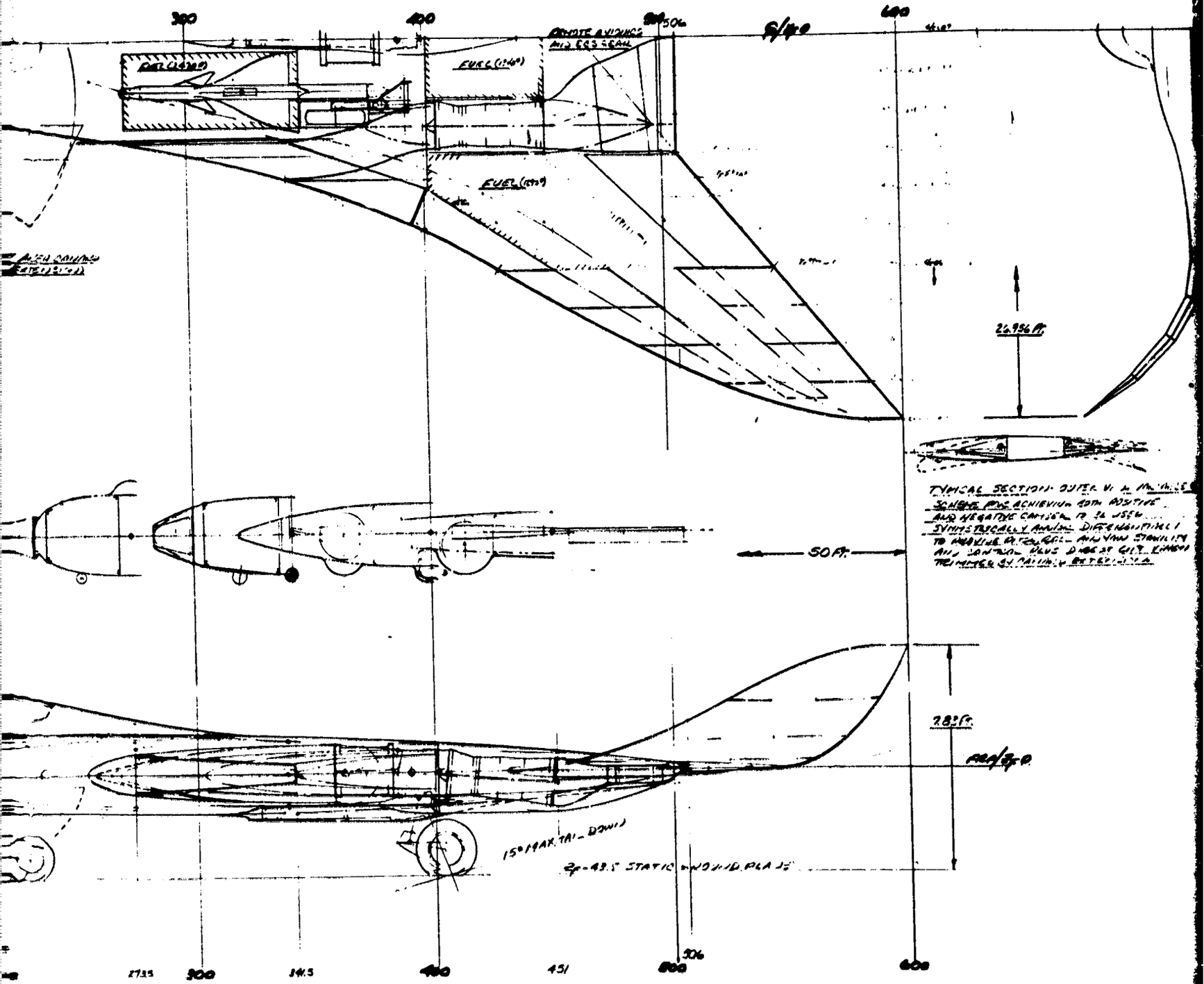

FOLDOUT FRAME

2

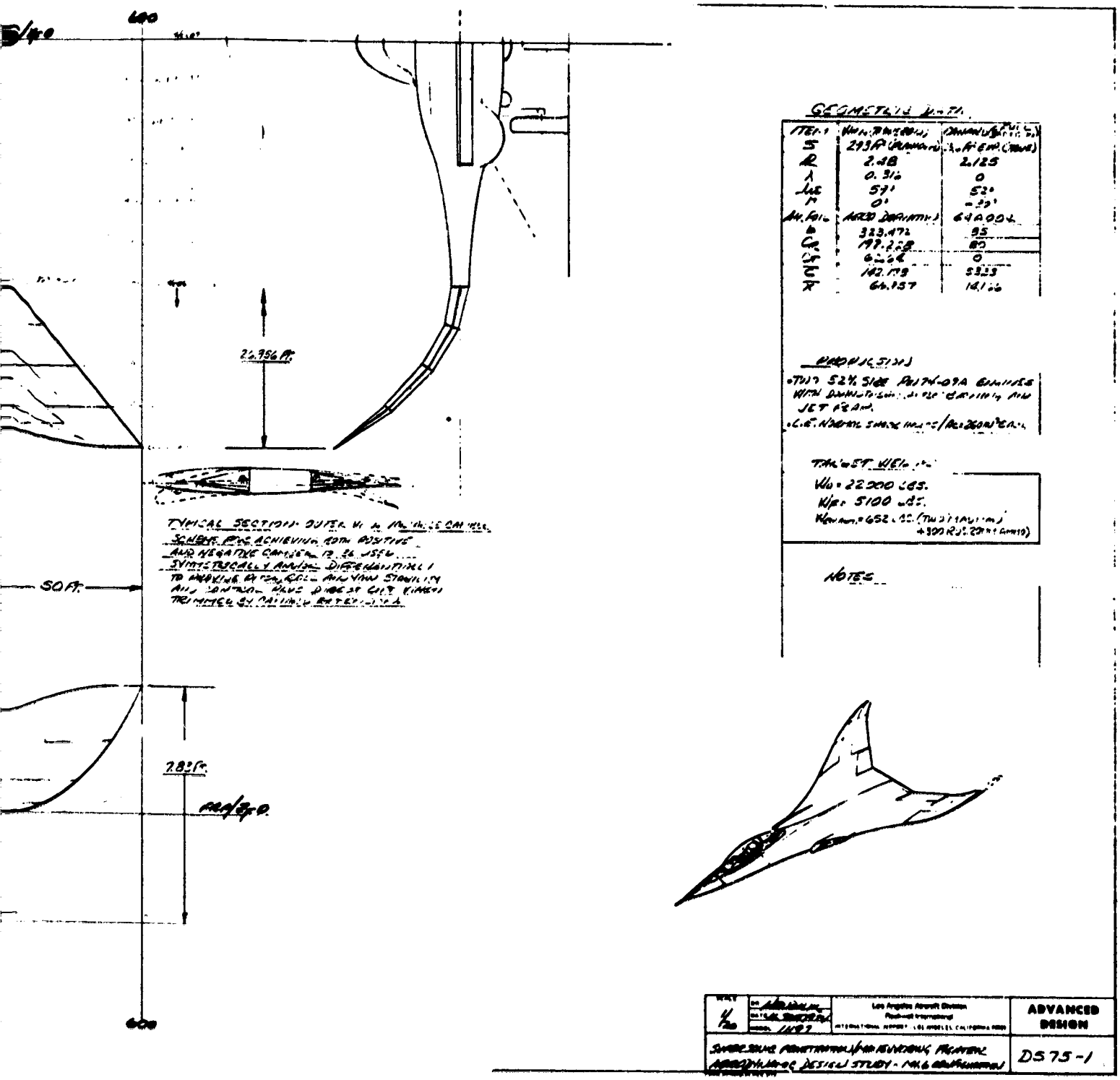

Figure 2. Configuration Layout-Supersonic Penetration/ Maneuvering Fighter (SP/MF), D575-1

FOLDOUT FRAME

TABLE III. WEIGHT SUMMARY – SP/MF, D575-1

	WEIGHT	C. G.	% MAC	MOMENT	WTS. FOL ACCD. FIRING
TOTAL STRUCTURE	(5875)	(377.5)		(2211570)	
WING GROUP (COMPOSITE)	1800	482			2000
TAIL GROUP HORIZONTAL (COMPOSITE)	120	220			
VERTICAL					
BODY GROUP (COMPOSITE)	2250	313			2050
ALIGHTING GEAR GROUP - MAIN	680	379			
- AUXILIARY	160				
SURFACE CONTROLS	750	31-			
ENGINE SECTION OR NACELLE GROUP	115	440			
PROPULSION GROUP	(2950)	(446.1)		(1315960)	
ENGINE (INSTALLED)	1100	426			
ACCESSORY GEAR BOXES & DRIVES	100	397			
AIR INDUCTION SYSTEM (COMPOSITE)	300	344			
EXHAUST SYSTEM	820	485			
COOLING & DRAIN PROVISIONS	10	426			
LUBRICATING SYSTEM	20	426			
FUEL SYSTEM	530	380			
ENGINE CONTROLS	40	235			
STARTING SYSTEM	30	426			
PROPELLER INSTALLATION					
FIXED EQUIPMENT	(2725)	(303.5)		(827120)	
INSTRUMENTS	190	201			
HYDRAULIC & PNEUMATIC GROUP	340	376			
ELECTRICAL GROUP	445	352			
ELECTRONICS GROUP	580	247			
ARMAMENT PROVISIONS	670	340			
FURNISHINGS	270	187			
AIR CONDITIONING EQUIPMENT	220	360			
PHOTOGRAPHIC					
AUXILIARY GEAR	10	370			
TOTAL WEIGHT EMPTY	(11550)	377.5	- 0.7 %	(4360650)	
CREW	215	157			
FUEL					
INTERNAL	5100	375			
TRAPPED	75	375			
OIL					
ENGINE	30	426			
TRAPPED					
ARMAMENT GUN (M-101)	255	378			
AMMO (300 RDS)	170	373			
2- MADMAN MISSILES	480	324			
EQUIPMENT GUN CAMERA	5	140			
N_2	10	380			
O_2	25	200			
TOTAL USEFUL LOAD	6365	363.2		(2311980)	
DESIGN GROSS WEIGHT	17915	372.5	- 4.2 %	6672630	
FUEL FOR EXPANDED GROSS WEIGHT					
EXPANDED GROSS WEIGHT					

FIGURE 3. WAVE DRAG VERSUS MACH NUMBER

0575 -1

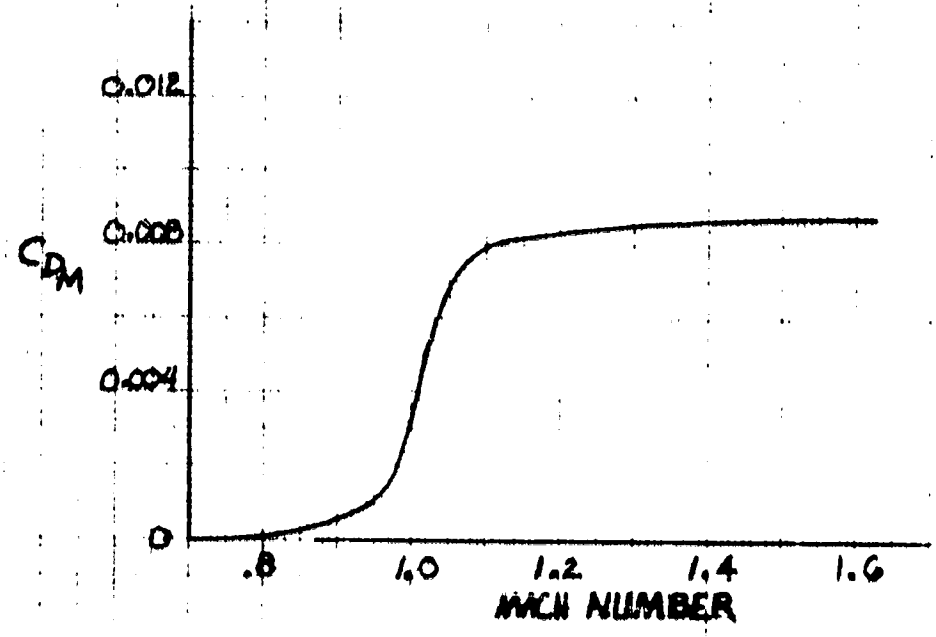

FIGURE 4. VARIATION OF INDUCED DRAG FACTOR WITH MACH NUMBER

D575-1

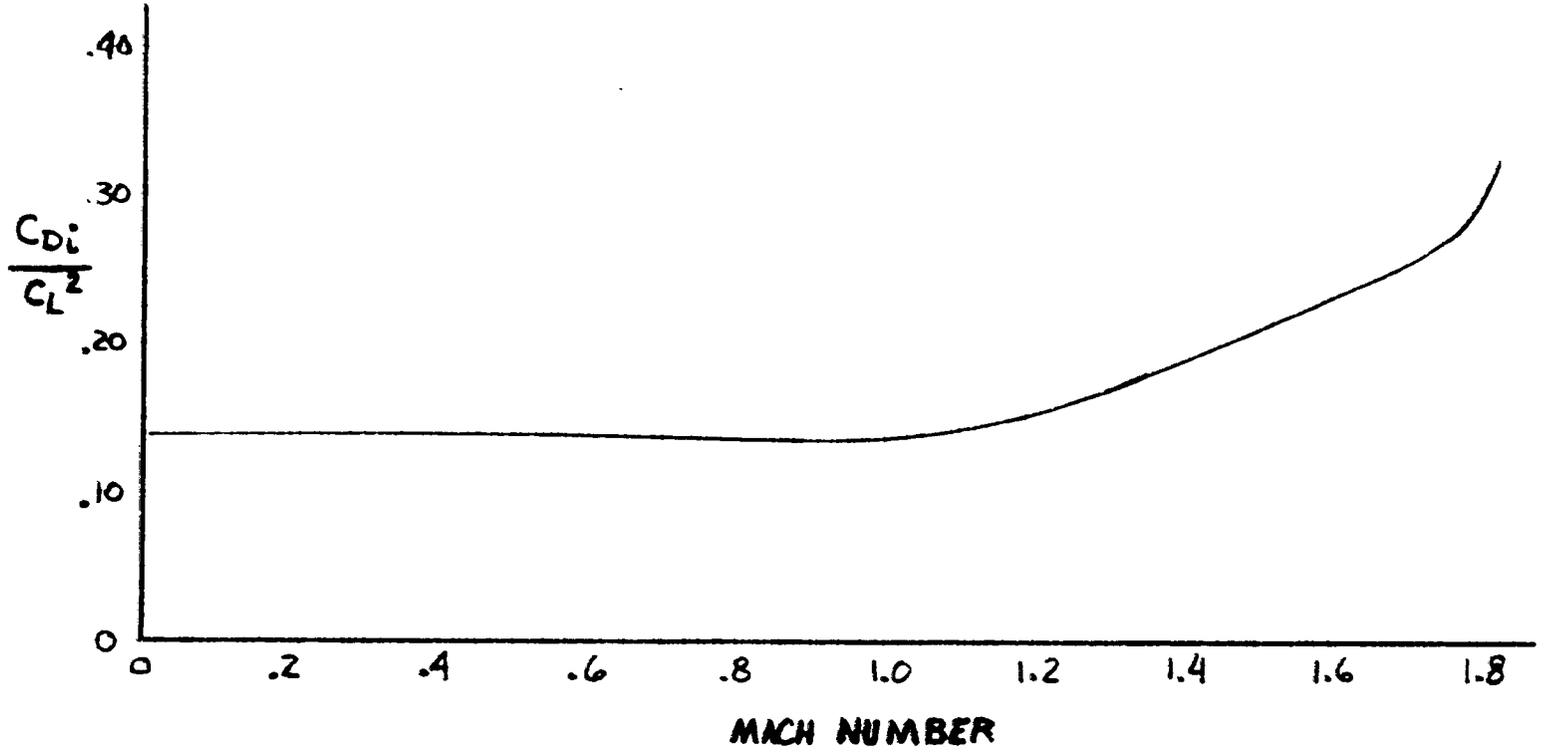

** SKIN FRICTION DRAG * INPUT DATA **

D575-1 SKIN FRICTION DRAG AT M=.6 AND 25000 FT

MACH= 0.600	PRESS= 786.000	TEMP= 429.000	SREF= 293.000	KS= 0.000100	TAU= 0.0	
5	1.000000	0.000100	0.0	1.000000	0.0	
10	3.000000	0.0	0.0	0.0	0.0	
20	3.000000	2.000000	2.000000	1.000000	1.000000	
25	1.000000	1.000000	1.000000	1.000000	1.000000	
30	1.000000	1.000000	1.000000	1.000000	1.000000	
35	1.000000	1.000000	1.000000	1.000000	1.000000	
40	40.080002	11.850000	4.440000	0.0	0.0	
60	656.000000	265.000000	47.000000	1.000000	1.000000	
65	1.000000	1.000000	1.000000	1.000000	1.000000	
70	1.000000	1.000000	1.000000	1.000000	1.000000	
75	1.000000	1.000000	1.000000	1.000000	1.000000	
80	0.130500	0.050000	0.040000	0.0	0.0	
120	0.0	1.200000	1.200000	0.0	0.0	

COMP NO.	COMP TYPE	WET SURF AREA	COMP LENGTH	X TRANS.	X/L TRANS.	REYNOLDS NO.	CF SMOOTH	CF ROUGH	CF USED	
1	3.0	656.000	40.080	0.946	0.02360	0.81105E+08	0.00489	0.00543	0.00543	WING-BODY .00785
2	2.0	265.000	11.850	0.946	0.07983	0.23979E+08	0.00222	0.00252	0.00252	
3	2.0	47.000	4.440	0.946	0.21306	0.89847E+07	0.00041	0.00047	0.00047	

** TOTAL SKIN FRICTION DRAG = 0.00842
INCLUDING BASE AND MISCELLANEOUS DRAG = 0.0

FIGURE 5. AERODYNAMIC SKIN FRICTION DRAG ANALYSIS, D575-1

Section II

INLET DESIGN AND PROPULSION PERFORMANCE

This report documents the air induction system conceptual design studies for the Supersonic Penetration/Maneuvering Fighter (SP/MF). Five inlets were configured for design Mach numbers of 1.6, 2.0, and 2.5. The Mach 1.6 design inlet is a refinement of the Supercruiser wing root inlet of reference 1. The Mach 2.0 and 2.5 design inlets are multi-shock systems configured in advance of precise air vehicle definition. The performance estimates for the Mach 2.0 and 2.5 inlets include the assumptions of a freestream flow field and design angle of attack.

ENGINE AIR DEMAND TRENDS

The PW74 cycle deck, reference 2, is used as representative of 1980 engine technology, and permits a wide variation in Overall Pressure Ratio (OPR), Bypass Ratio (BPR) and Turbine Inlet Temperature. The 100 percent size engine has a design corrected airflow of 130 pounds per second, and a fan inlet diameter of 28.3 inches. A 2.3 percent airflow bleed from the inlet duct for the cooling air for the Environmental Control System (ECS) was included for inlet sizing.

The left side of figure 6 shows the effects of OPR and BPR on engine corrected airflow vs ram temperature, T_{t2}. Increasing the OPR from 15 to 29 significantly depresses the engine air demand at T_{t2} above 700 degrees Rankine. Increasing the BPR from 0.2 to 0.6 increases the air demand at high T_{t2} levels and low OPR designs. These curves indicate the degree of inlet variable geometry required for exact inlet/engine matching. An inlet throat Mach number of about 0.7 is desired for good pressure recovery and low spillage drag. If the inlet throat area cannot be reduced to match the engine air demand schedule the excess inlet air supply must be spilled externally or bypassed.

The right side of the figure compares the trends of freestream tube area, A_o, vs Mach number in the isothermal atmosphere. These curves show the virtually impossible task of designing an efficient inlet for an OPR = 29 engine in a Mach 2.5 air vehicle. Achieving a 50 percent throat area regulation between Mach 1.0 and 2.5 with a capture area only 20 - 30 percent greater than the maximum throat area cannot be done without an extremely complicated variable geometry inlet. In addition, the low corrected airflow connotates a low engine thrust/weight ratio at supersonic cruise. Therefore, the OPR = 15 engines should be used for the Mach 2.5 cruise air vehicle studies.

INLET SPILLAGE DRAG

The inlet drags contained in this report include all drags due to operation at inlet capture area ratios, A_o/A_c, below unity. All form and friction drags on surfaces external to the inlet projected area, A_c, are included in the air vehicle drags. In this report, the spillage drag is the summation of boundary layer control air momentum drag, compression surface pressure drag at maximum mass flow ratio, and additive drag due to subcritical air spillage or the drag associated with bypassing the excess inlet air capacity.

A comparison of additive drag for the B-1 inlet, reference 3 and a NACA 1 series (B747, DC-10, L1011 type) inlet, reference 4. is given on figure 7. This figure shows that the $\Delta C_D/(A_o/A_c)$ slopes are quite similar for these inlets; therefore, the B-1 additive drag trends were used for all inlets employing external compression surfaces in this study.

PRESSURE RECOVERY AT LOW SPEED

Sharp inlet lips are needed for efficient supersonic operation, but these sharp lips create flow separation losses at inlet mass flow ratios greater than unity. The take-off pressure recovery can be improved with auxiliary inlets. Figure 8 shows experimental pressure recovery data for sharp lip inlets, the .-100D inlet with an r/D_h (inside lip radius/inlet hydraulic diameter) of 0.02, and auxiliary inlets. An auxiliary inlet/capture area ratio of 0.25 is used for most of the inlets in this study.

The Mach 1.6 design wing root inlet is too short for a conventional auxiliary inlet. Figure 9 illustrates a technique of over-rotation of the variable camber feature of this wing root design to open an auxiliary inlet slot in the top of the wing. The estimated take-off pressure recovery gains with this slot are shown on figure 10.

INLET CONFIGURATIONS

In the initial Supercruiser configuration development, it was assumed that the inlet would be located behind the detached shock generated by the subsonic wing leading edge. However, the inlet evolved into a wing root location in a near-freestream flow field.

Figure 11 presents D572-2 Supercruiser flow field data and a station cut comparison of the D572-2 and D575 air vehicle at F.S. 350. The flow field data for α_o of 0 and 4 degrees were developed with the slender body flow theory program, reference 5. These flow field data show that the wing root inlet location involves the smallest flow field transients. The top of the fuselage is a completely unsatisfactory location for an inlet. A bottom outboard inlet ($Y \geq 40$ inches) would be the preferred alternate to the D575-1 inlet location.

The highly swept inlet sidewalls and the short subsonic diffuser preclude the use of a conventional external compression ramp. The figure 9 inlet

has converging sidewalls designed to provide the shock compression equivalent to a six degree ramp at Mach 1.6. The subsonic diffuser losses were estimated with the aid of the offset diffuser parametric data in reference 6. The subsonic diffuser loss coefficients for the figure 9 inlet configuration are tabulated below:

Mi	Pt/q
0.7	0.12
0.8	0.14
0.9	0.16

Two inlet configurations were developed for the Mach 2.0 cruise vehicles. Both inlets are designed for "shock-on cowl" at Mach 2.2 to provide a maneuvering capability at cruise conditions and an overshoot or escape speed tolerance. The figure 12 rectangular (2-D) configuration is based upon the Rockwell F-15 proposal design with the shock system geometry scaled down from the 2.5M "shock-on-cowl" F-15 design. The second Mach 2.0 design, figure 13, is similar to the F-111 or Tailor-Mate concepts, reference 7. This inlet was configured as a semi-cone design with an expanding second cone located on the fuselage side or, preferably, under the wing or fuselage.

The rectangular inlet utilizes two fixed ramps, 5 and 10 degrees from the inlet reference plane and a third compression ramp variable from 5 to 26 degrees. The maximum throat to capture area ratio is 77 percent and the internal diffuser loss coefficient is 10 percent q_i for throat Mach numbers below 0.7. The two compartment ramp boundary layer control bleed system is designed for three percent bleed at $M_o = 2.0$.

The semi-cone design was based upon data in references 7 and 8. The initial 12.5 degrees translating semi-cone is followed by a cone segment variable between 8 and 26 degrees. This inlet will also have a design BLC bleed flow of three percent and a 10 percent diffuser loss coefficient.

Internal compression inlets are needed for Mach 2.5 cruise vehicles to achieve high pressure recovery and low cowl pressure drag. However, a maneuvering vehicle cannot afford violent unstarts a la SR-71. This can be avoided by conservatism in selecting the internal contraction ratio and throat Mach number. Figure 14 presents B-1 MCl data on several unstarts at $M_o = 2.2$, lip station Mach number = 1.72. These data show that the magnitude and rate of unstart duct exit pressure decay become more severe with decreasing design throat Mach number. Since the probability of an engine over-temperature and stall is proportional to the rate of airflow loss, the chances and severity of the unstart can be reduced by selecting throat Mach numbers above 1.3.

The left side of figure 15 illustrates the aerodynamic principles of the Self-Restarting Inlet. The supersonic bleed zone is compartmented to create a controlled bleed flow reversal under the second ramp during the unstart to create a separated boundary layer aerodynamic ramp which produces more external air spillage, increased external compression, and a reduced internal aerodynamic area contraction. The result is an automatic restart if the unstart initiating back pressure pulse is removed. The right side of the

figure presents the experimental pressure recovery penalty for self-restarting operation due to the increased normal shock loss as a result of the throat Mach number schedule shown below. Theoretically, the self-restarting concept requires an unstarted sonic throat static pressure P_u^* higher than the static pressure P_i, on the external ramp forward of the cowl lips to create the necessary ramp boundary bleed flow reversal. The theoretical curve assumed an isentropic internal contraction process to the terminal shock for the started inlet and ignored the effects of boundary layer bleed. The experimental restarts, at off design Mach numbers, involved three-dimensional external air spillage and boundary layer bleed flows that moderated the flow processes and permitted restarts at below the isentropic theory throat Mach number schedules. The data points above the theoretical curve illustrate the effects of non-isentropic internal contraction and incomplete boundary layer removal at higher M_i levels. The square and circle symbols denote the design throat Mach numbers for the M 2.5 SP/MF inlets.

Figure 16 shows the Mach 2.5 2-D inlet (shock on cowl at 2.6M) with a design point shock system pressure recovery of 93 percent and a duct exit recovery of 87 percent. The design point boundary layer bleed is six percent. The inlet geometry is controlled by the double angle compression ramp.

The Mach 2.5 semi-cone inlet has only two external oblique shocks, a shock system recovery of 90.2 percent and a duct exit recovery of 84 percent. The decreased compression surface area permits a design point bleed flow of 5 percent. Configuration details are given on figure 17.

INLET PERFORMANCE ESTIMATES FOR PROPULSION SYSTEM ANALYSES

The inlet performance estimates for propulsion system analyses are given on figures 18 through 22. The format permits solving for pressure recovery by input of corrected airflow (engine plus ECS) to the appropriate $W\sqrt{\theta}/\delta_{t2}\ A_c$ curves. The capture area ratio, A_o/A_c, and inlet drag coefficient, C_{D_i}, can be computed from $W\sqrt{\theta}/\delta_{t2}\ A_c$, P_{t2}/P_{to}, and A/A^* for the particular flight Mach number. These drag curves include all corrections to A_o/A_c as explained in a previous section.

The design capture areas for a SLS engine corrected airflow of 130 pounds per second and 2.3 percent ECS bleed flow from the inlet are tabulated below:

INLET	A_c~sq in.	Sizing Criteria
M1.6, Wing Root	460	T/O, M= 0.9, 36K
M2.0, 2-D	522.5	T/O, M= 0.9, 36K
M2.0, Semi-cone	522.5	T/O, M= 0.9, 36K
M2.5, 2-D	575.0	T/O, M= 0.9, 36K**
M.25, Semi-cone	565.0	T/O, M= 0.9, 36K**

** These inlets are oversized at 2.5M for OPR greater than 15, BPR = 0.2. Circle symbols on figures 21 and 22 denote inlet control points for mixed compression operation.

The pressure recovery decay at subcritical $W\sqrt{\theta}/\delta_{t2}\ A_c$ levels at $M_o > 1.6$ show the effect of bypassing duct airflow through a B-1 type bypass door on the cowl side of the inlet. This bypass process removes part of the above average total pressure air and necessitates a pressure decreasing mixing of the remaining airflow. These data can be refined when air vehicle configuration development efforts permit an exact definition of the bypass design.

Installed propulsion performance data for SP/MF studies are given in reference 23. The selected propulsion systems are as follows:

Design M_o	1.6	2.0	2.5
Engine	PW74-16	-17	-18
Bypass Ratio	0.2	0.2	0.2
Overall Pressure Ratio	29	29	15
Inlet Type	Wing Root	2-D	2-D
(Reference Figure)	9	12	16

HAMMERSHOCK PRESSURES

Duct exit pressures for operation on 1500 and 2000 psf 'q' limits are presented on figure 23. The hammershock pressures were estimated by the methods outlined in references 10 and 11. The duct exit hammershock pressure ratios, $\Delta P/P_2$, are shown for a bypass ratio of 0.2 and Overall Pressure Ratios of 15, 22, and 29. Hard engine stalls will create duct exit hammershock pressure pulses of 15 - 20 psi for 1500 q designs and over 20 psi for 2000 q air vehicles. The Overall Pressure Ratio has a significant effect on the hammershock pressure pulse at low altitudes and Mach numbers. Increasing the Bypass Ratio to 0.6 will reduce the hammershock pressure pulse by 5 - 6 psi at low Mach numbers.

Hammershock pressures are a very important design factor for long inlet diffusers. The gains in engine thrust/weight by decreasing bypass ratio can be cancelled by increased diffuser weight due to higher hammershock pressures. The hammershock pressure pulse, $\Delta P/P_2$, may be attenuated in the forward duct by 10 - 20 percent at high speeds due to duct area variation and boundary layer bleed, but experimental data show little attenuation at low speeds.

MACH 2.5 MISSION INLET EVALUATION

Three candidate inlets for the M2.5 SP/MF (D575-4) are compared on figure 24. The 1/10 scale sketches and P_t/P_{to} vs A_o/A_c plots compare:

2-D Mixed Compression Inlet (MCI), 4 oblique shocks, design point $P_{t_2}/P_{t_o} = 0.87$, reference figure 16.

Axisymmetric MCI, 3 oblique shocks, design point $P_{t_2}/P_{t_o} = 0.84$, figure 17.

Axisymmetric External Compression Inlet (ECI), 2 oblique shocks, design point P_{t_2}/P_{t_o} = 0.79. This is the Tailor-Mate, reference 7 B-3 inlet with the pressure recovery reduced a calculated three percent from the experimental level to correct for the large offset in the D575-4 diffuser.

The propulsion performance data in reference 23, PW74-18 engine, were based on the 2-D MCI configuration.

Figure 25 compares the propulsion system performances for the several inlets. These curves represent the changes in net propulsive effort, F_{NE}, and specific fuel consumption, S.F.C., due to differences in pressure recovery and spillage drag. The F_{NE} differences were insignificant for maximum power operation at Mach numbers below 1.6.

The basic assumptions for approximate mission analyses were: (1) No change in air vehicle weight between inlets, (2) No differences in air vehicle drag for inlet mass flow ratio = 1, and (3) No change in total fuel load. For simplicity in calculation, a common climb-acceleration to M 1.6 and a common 100 mile subsonic cruise and loiter at the end of the mission were assumed. The basepoint mission for the 2-D MCI inlet installation was evaluated with the Rockwell Mission Analysis Program, the mission segments for the other inlet installations were approximated by desk calculation adjustments for the differences in net propulsive effort and specific fuel consumption shown on figure 25.

The dominant segment of the M2.5 SP/MF mission is the maneuver at 50,000 ft maximum power, to achieve a total energy maneuverability, $\int V/W(F_N-D)dt$ of 144,000 feet. The M2.5 cruise legs were adjusted to accommodate the changes in fuel consumption for the combat maneuver. The effects of the performance differences are graphically illustrated on figure 26 and tabulated below:

Effect	Inlet	
	A_{xi} MCI	A_{xi} ECI
Change in Net Propulsive Effort, ΔF_{NE}	-4.6%	-13.9%
Change in Maneuverability ΔSEP	-12.5%	-37.8%
Increase in Maneuvering Fuel	+12.2%	+42.4%
Change in Combat Radius	-23 nm	-89 nm

If the mission requirements were changed to a constant 2071 pounds of fuel for the combat maneuver the loss in radius will be 10 nm for the A_{xi} MCI inlet and 30 nm for the A_{xi} ECI inlet installation.

The preliminary analyses show significant effects of inlet performance on mission capability for the D575-4 air vehicle. It does not appear that a detailed configuration and mission analysis study will markedly change the results. All three inlets have two variable compression surfaces and fair into the same diffuser; therefore, the weight differences should be a fraction of one percent of the air vehicle structural weight. A shock-expansion theory analysis of inlet cowl pressure drags showed no significant differences in isolated inlet pressure drag.

Mixed compression inlets will be required for the M2.5 SP/MF. However, the relatively small size (A_c of $1/4 \rightarrow 1/3$ of existing variable geometry inlets) and the relatively brief supersonic flight time dictate a careful review of variable geometry features. For example, adding another variable ramp or cone plus actuation and control to achieve another 1 to 2 percent pressure recovery would not be cost effective.

FIGURE 6. ENGINE AIRFLOW TRENDS
PW 74 PARAMETRIC DECK

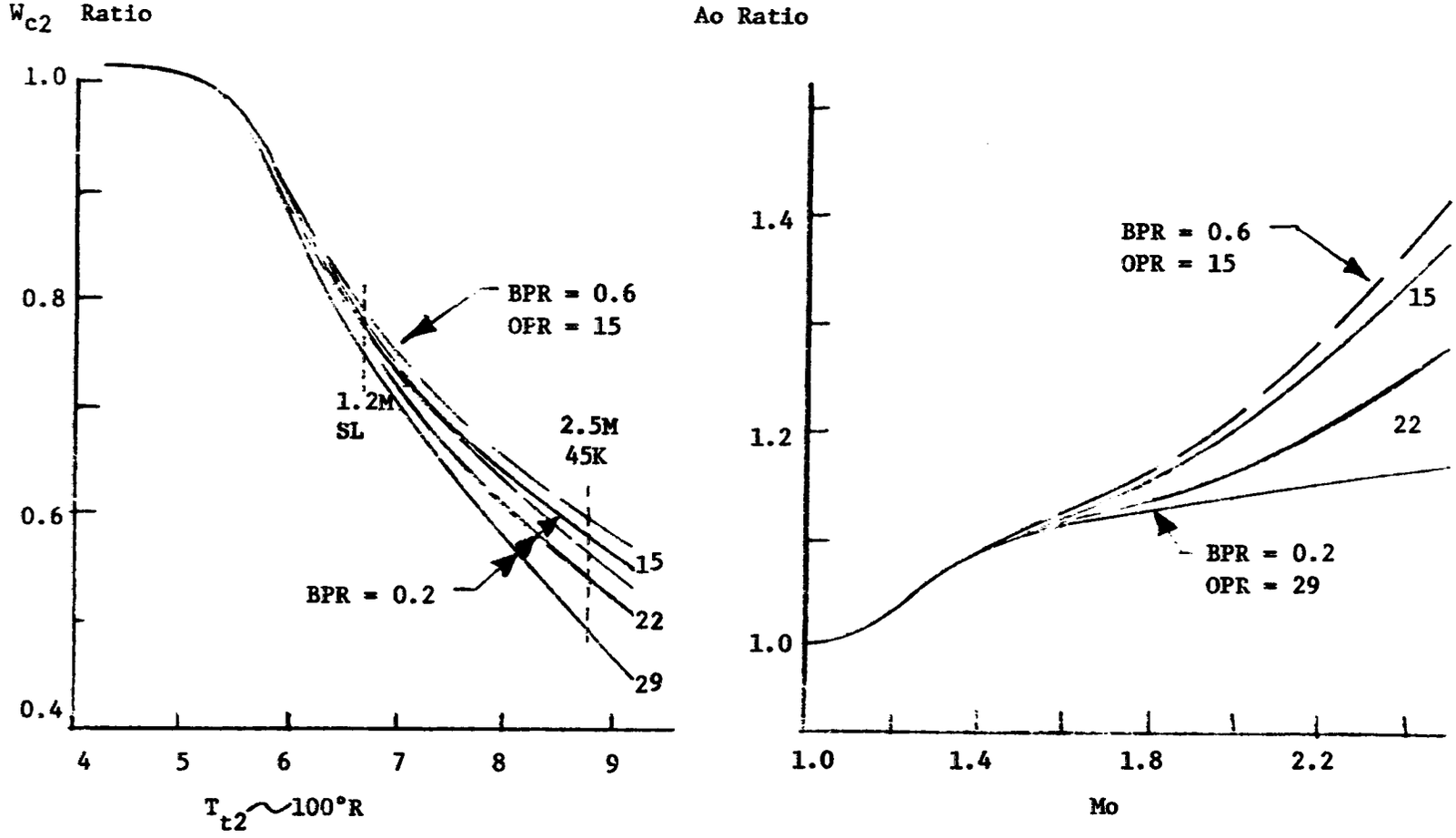

FIGURE 7. ADDITIVE DRAG TRENDS

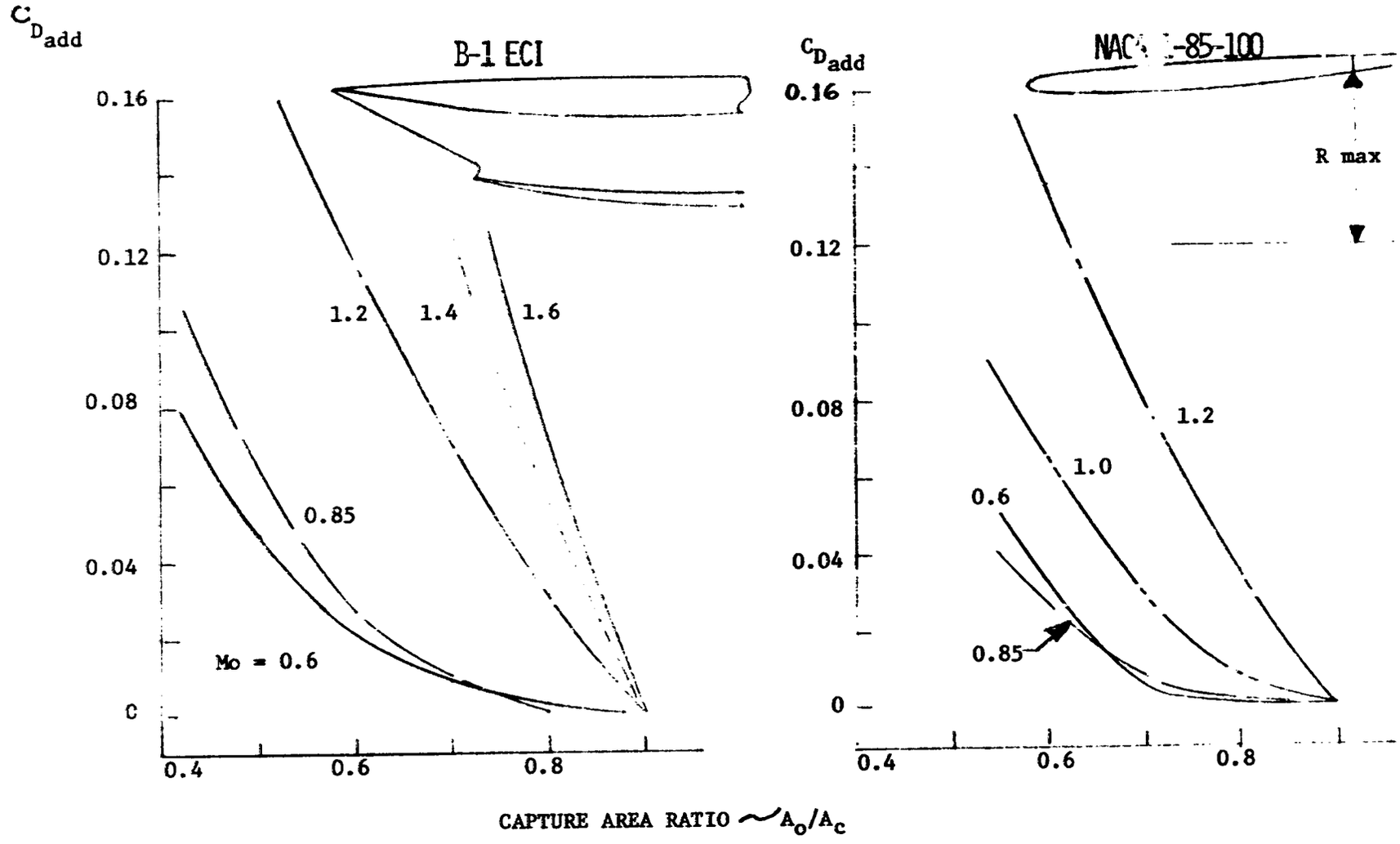

FIGURE 8. EXPERIMENTAL PRESSURE RECOVERY DATA TRENDS

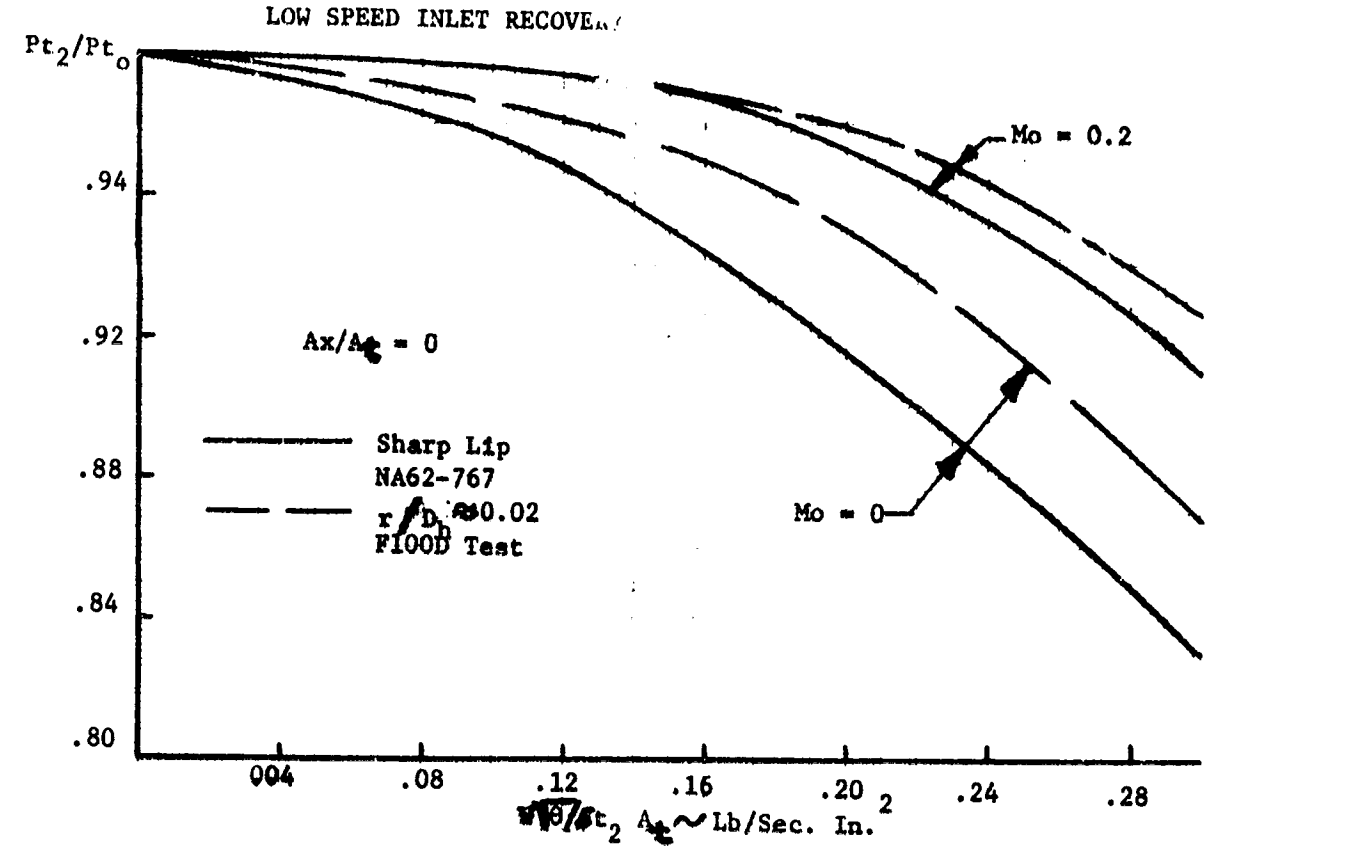

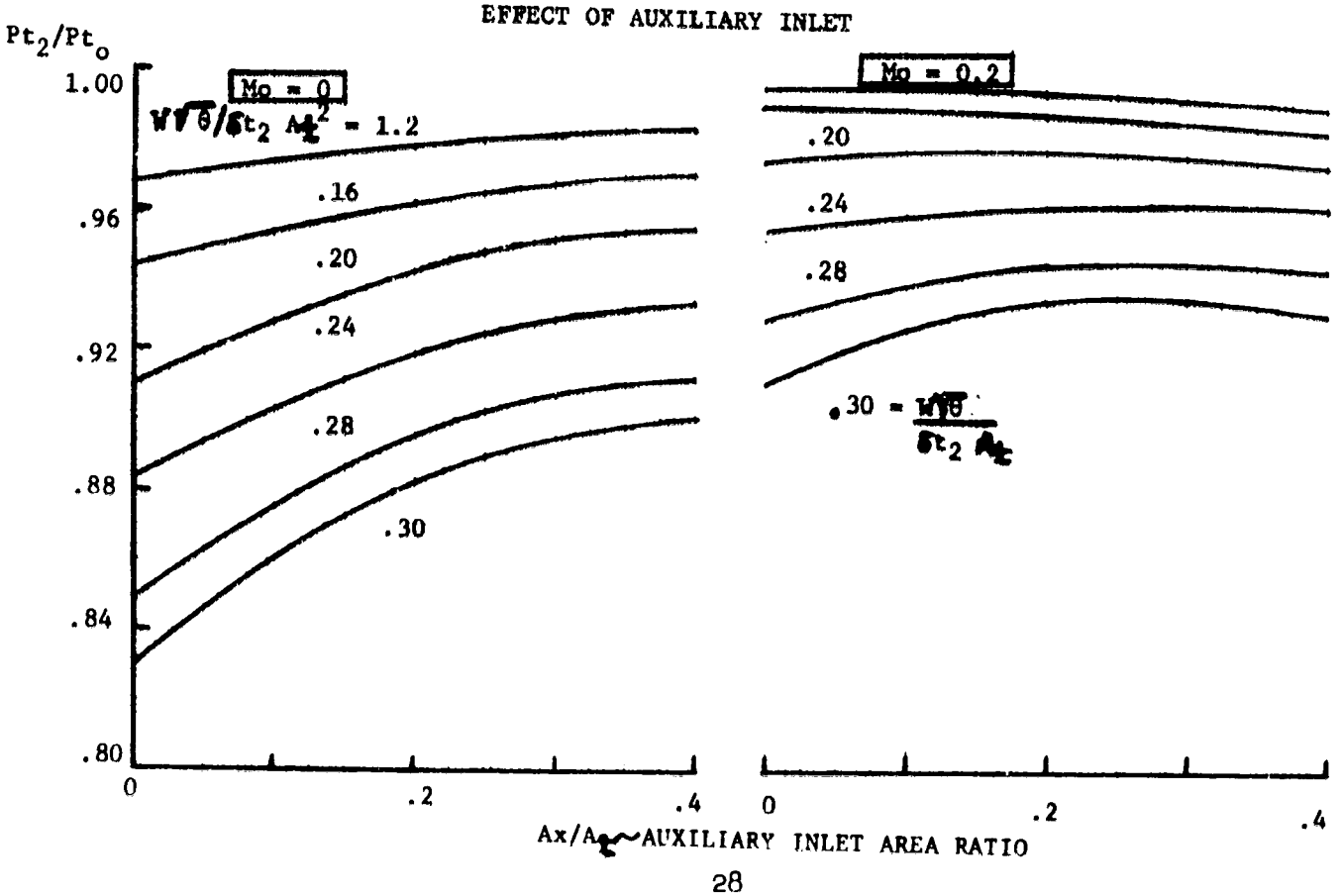

FIGURE 9. SUPERCRUISER AUXILIARY INLET GEOMETRY

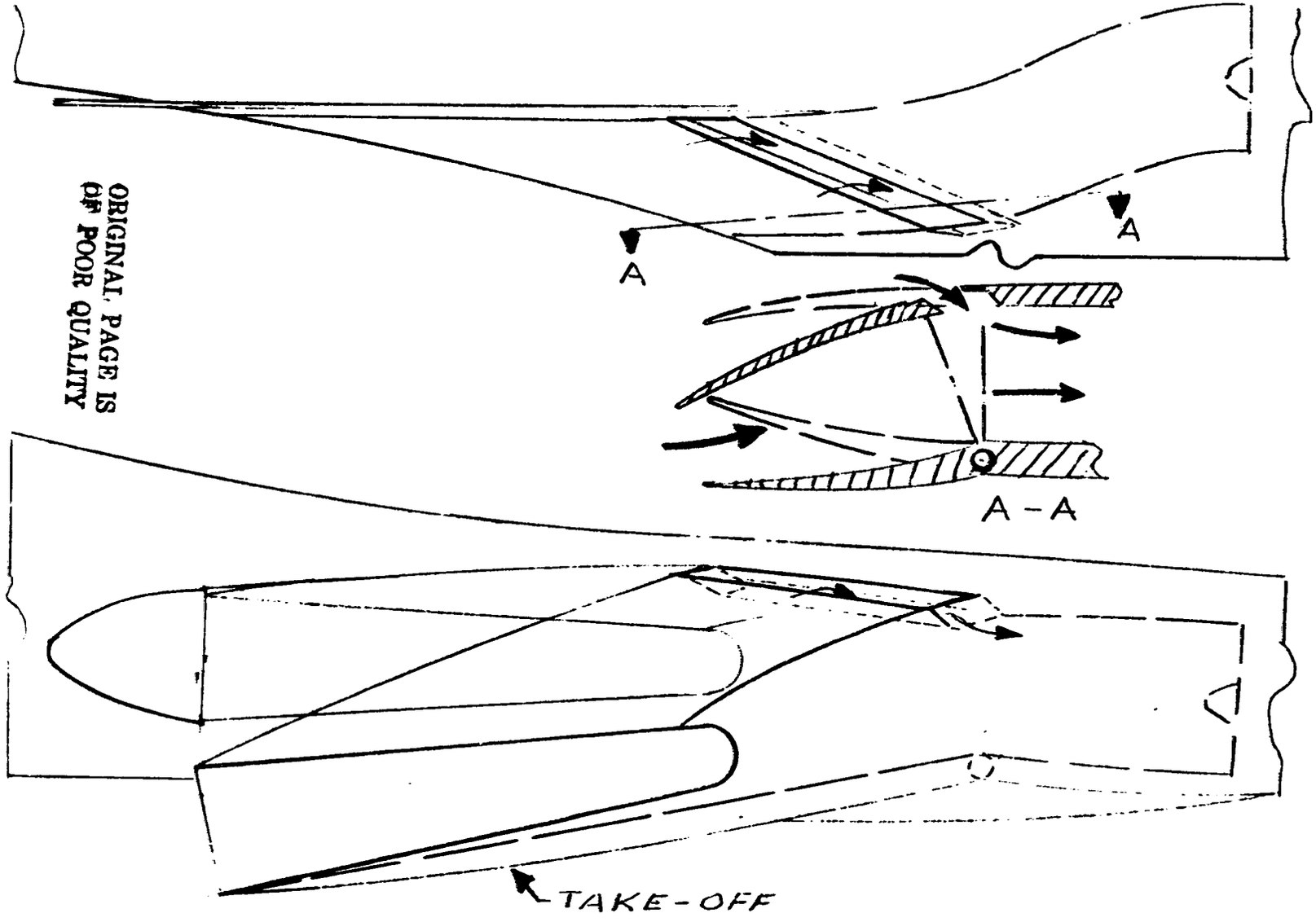

FIGURE 10. D525 AUXILIARY INLET DATA, $M_d = 1.6$

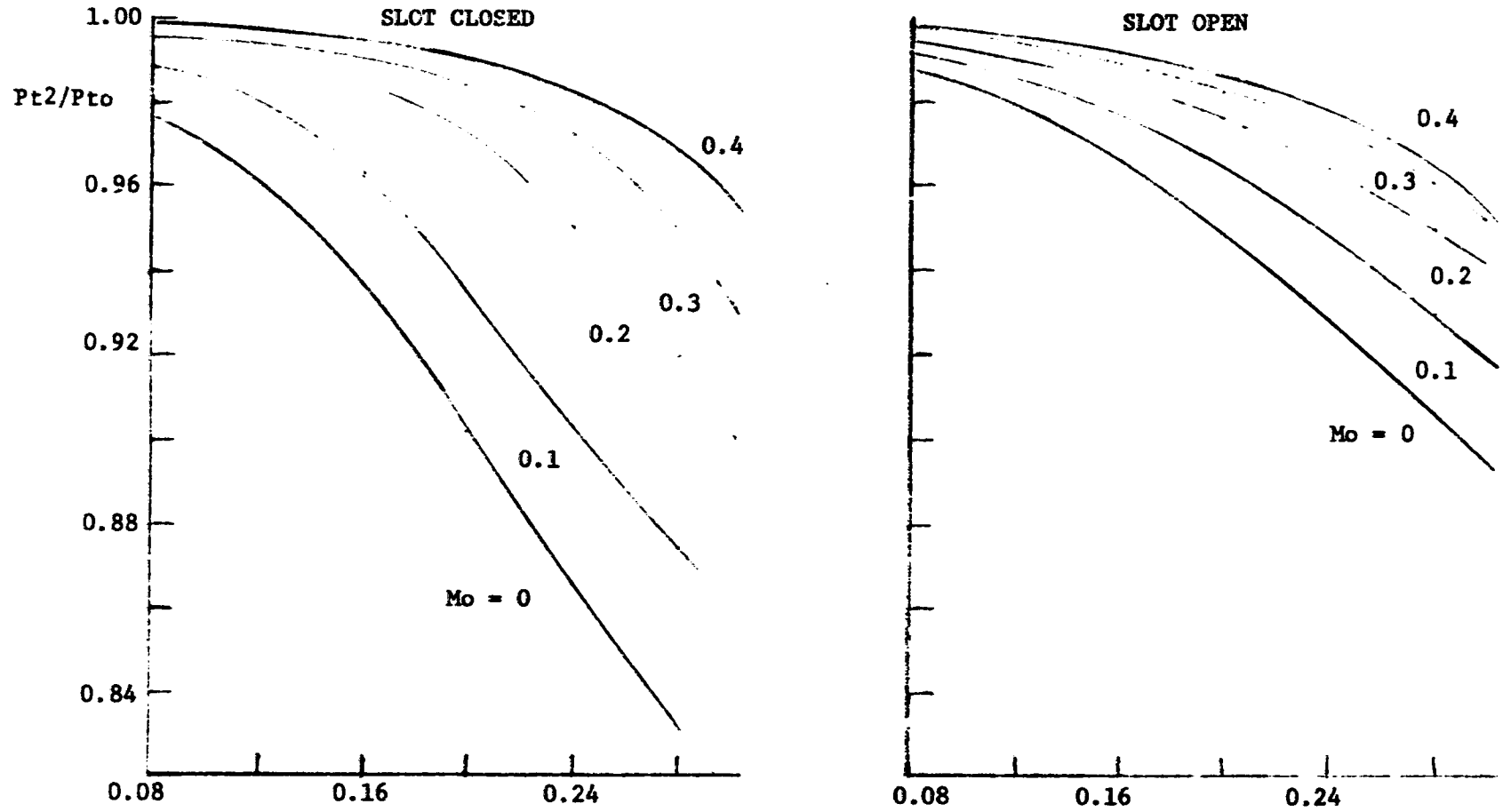

FIGURE 11. SP/MF INLET FLOW FIELD

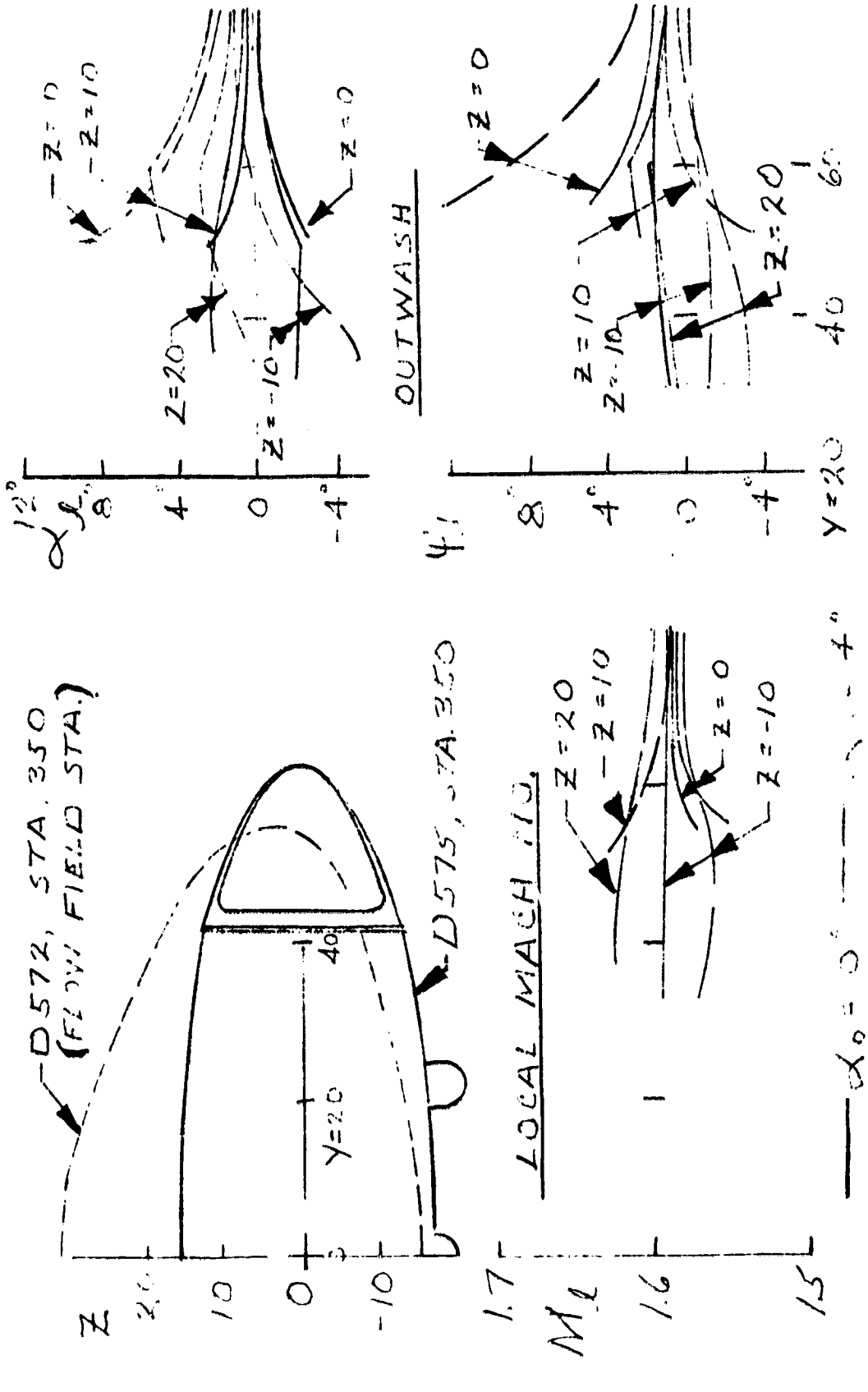

ORIGINAL PAGE IS
OF POOR QUALITY

FIGURE 12. 2-D INLET GEOMETRY, DESIGN MACH = 2.0

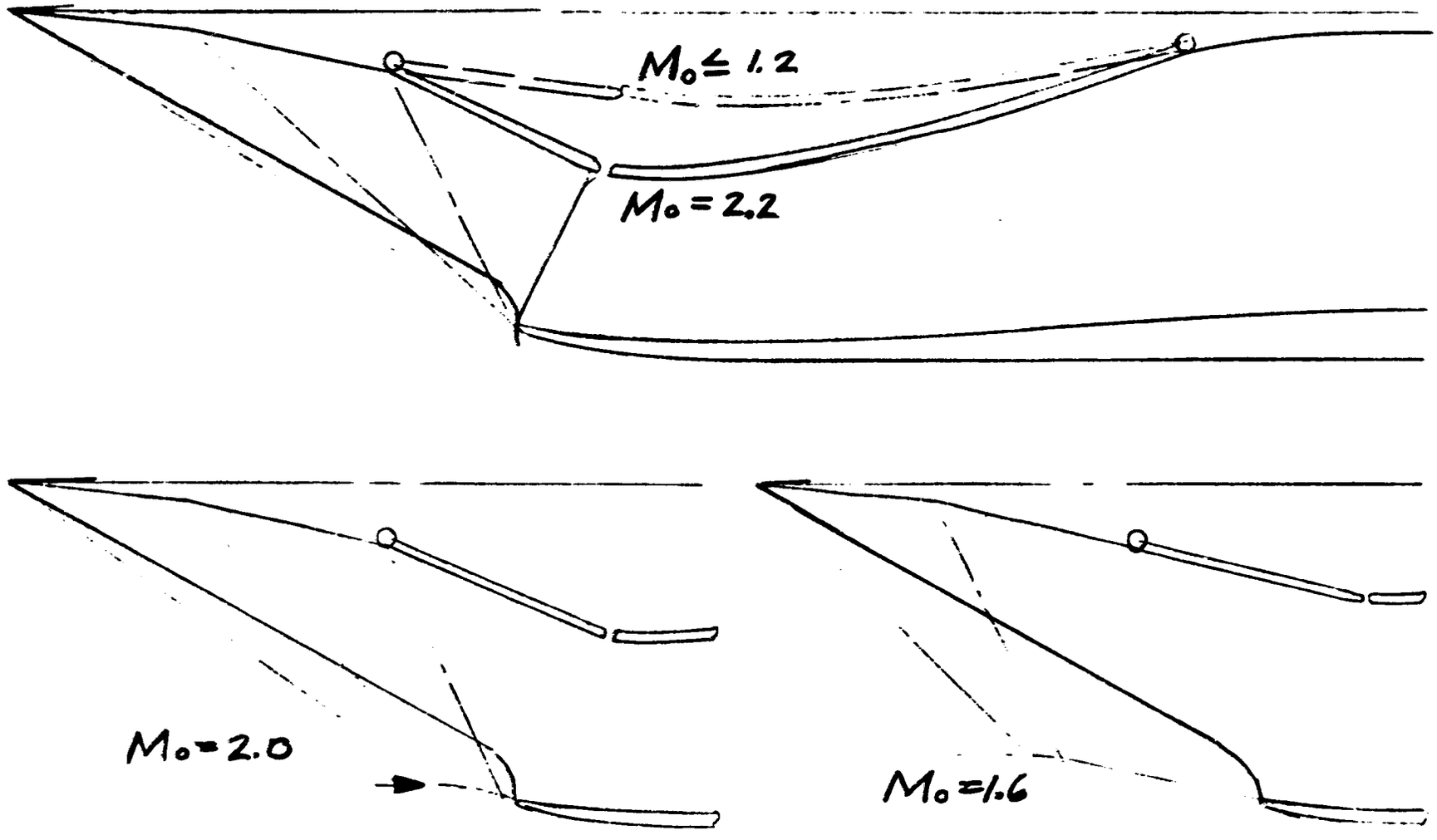

FIGURE 13. SEMI-CONE INLET GEOMETRY
DESIGN MACH = 2.0

FIGURE 14. INLET UNSTART PRESSURES

Mo = 2.2 Mi = 1.72

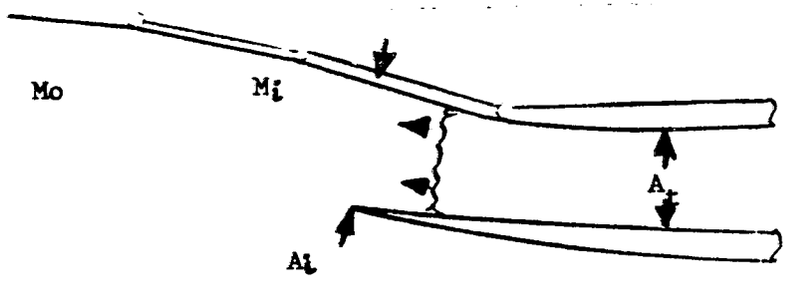

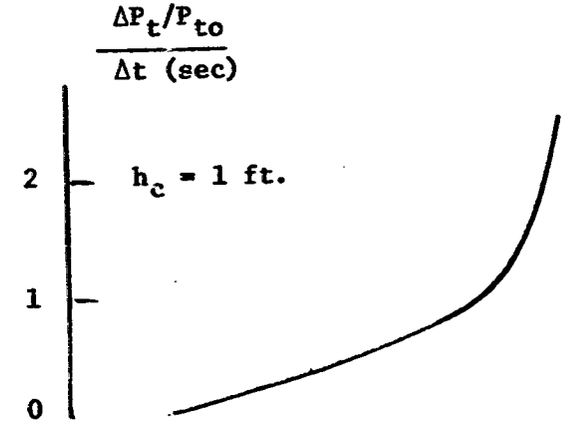

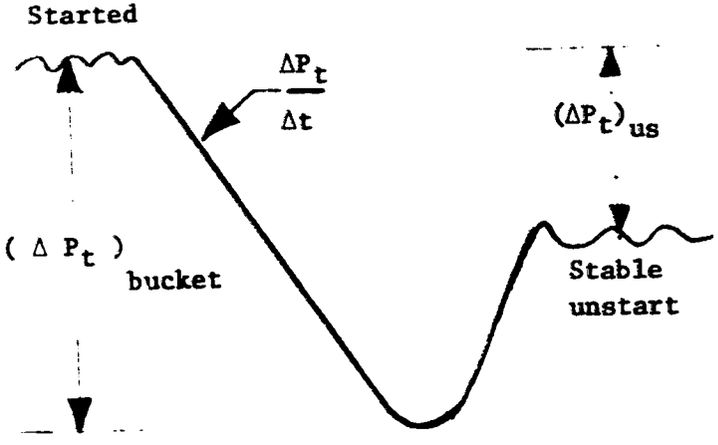

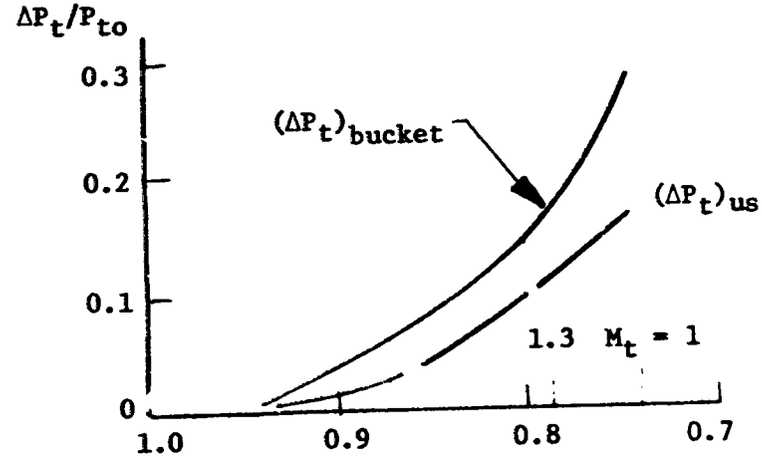

FIGURE 15. SELF-RESTARTING INLET PARAMETERS

Patent No. 3, 417, 767

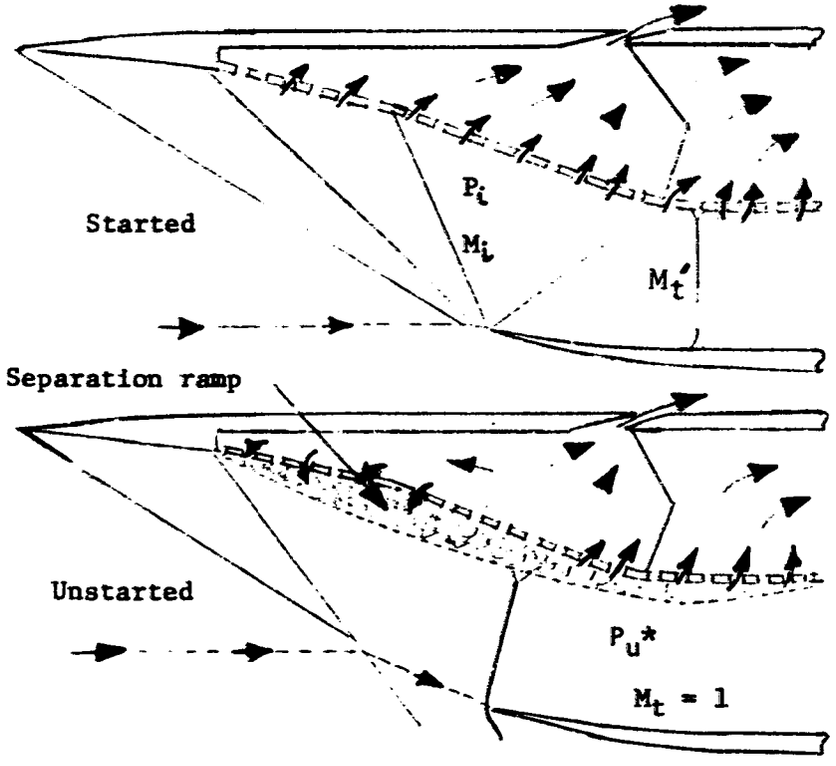

BLC Bleed Reversal and Separation Ramp Creates External Spillage and Reduces Internal Contraction

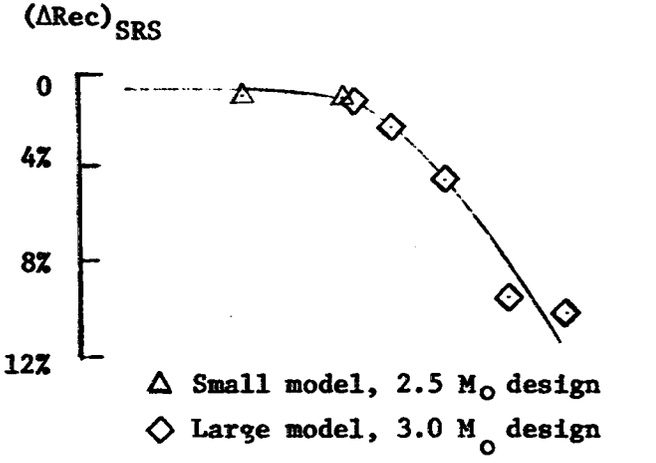

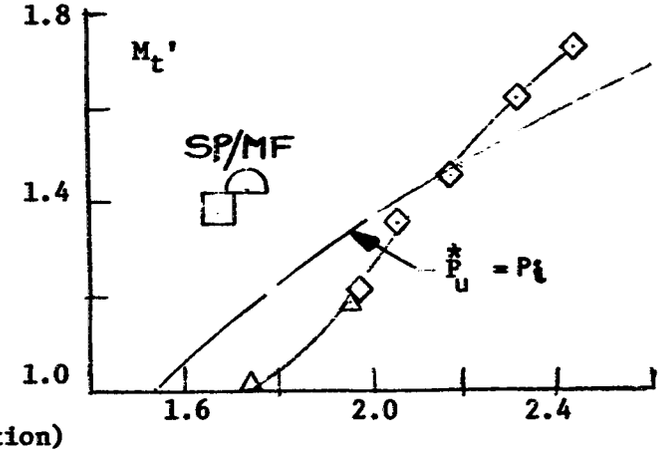

M_t' Mach Number at Throat (With Isentropic Internal Contraction)

P_u^* Sonic Throat Pressure, Unstarted Inlet

FIGURE 16. 2-D INLET, $M_d = 2.5$

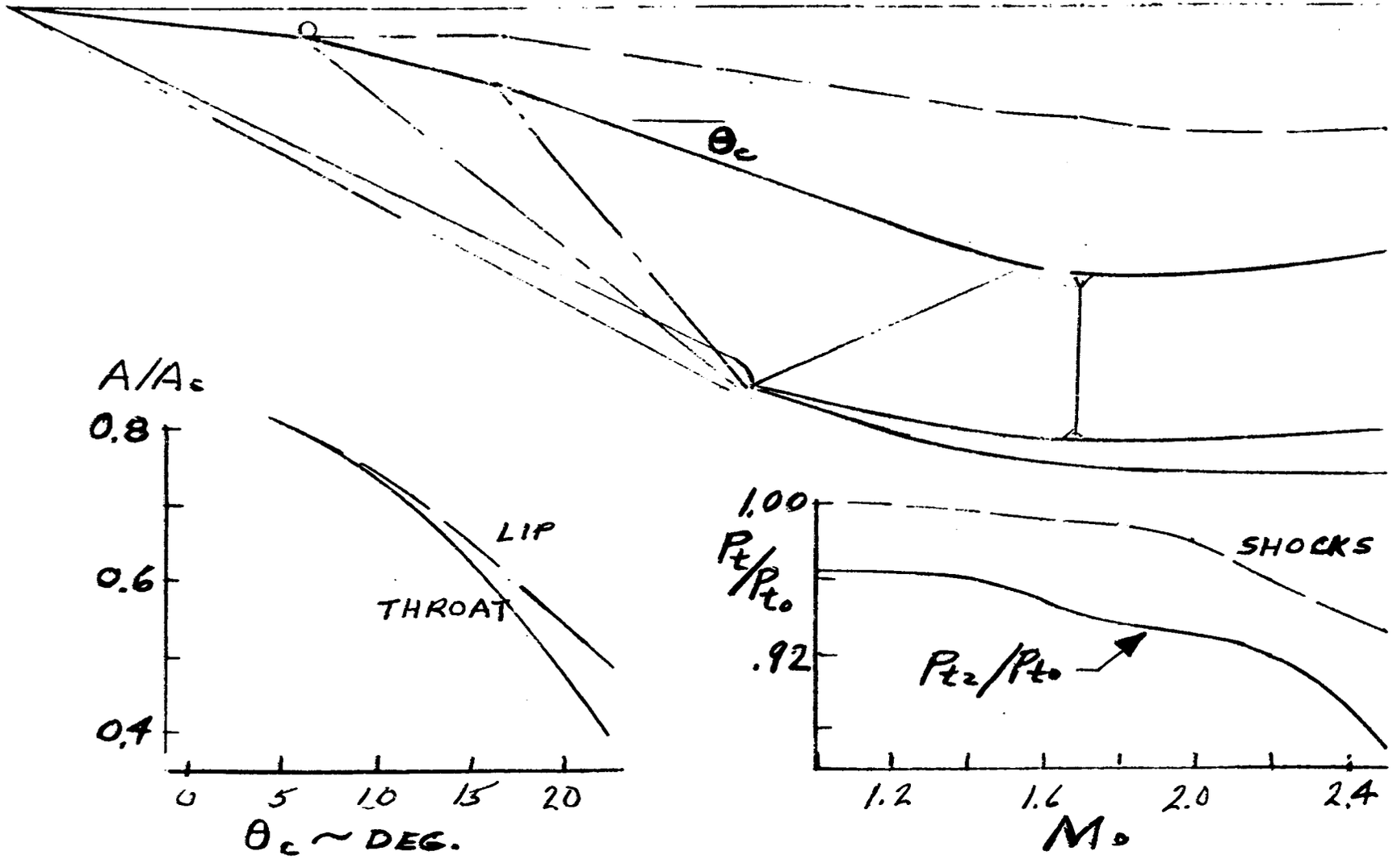

FIGURE 17. SEMI-CONE INLET, $M_d = 2.5$

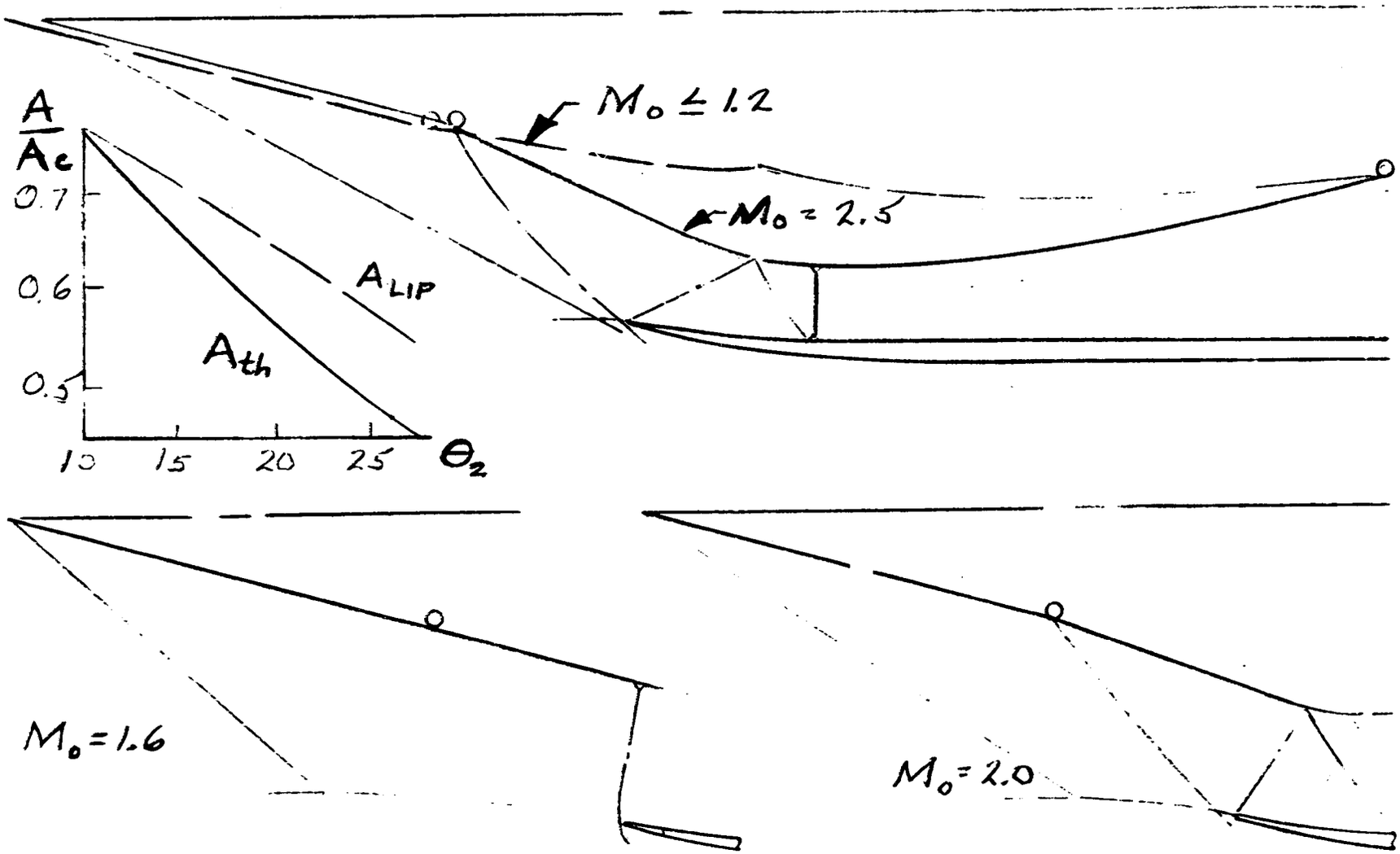

FIGURE 18 WING ROOT INLET PERFORMANCE , $M_d = 1.6$

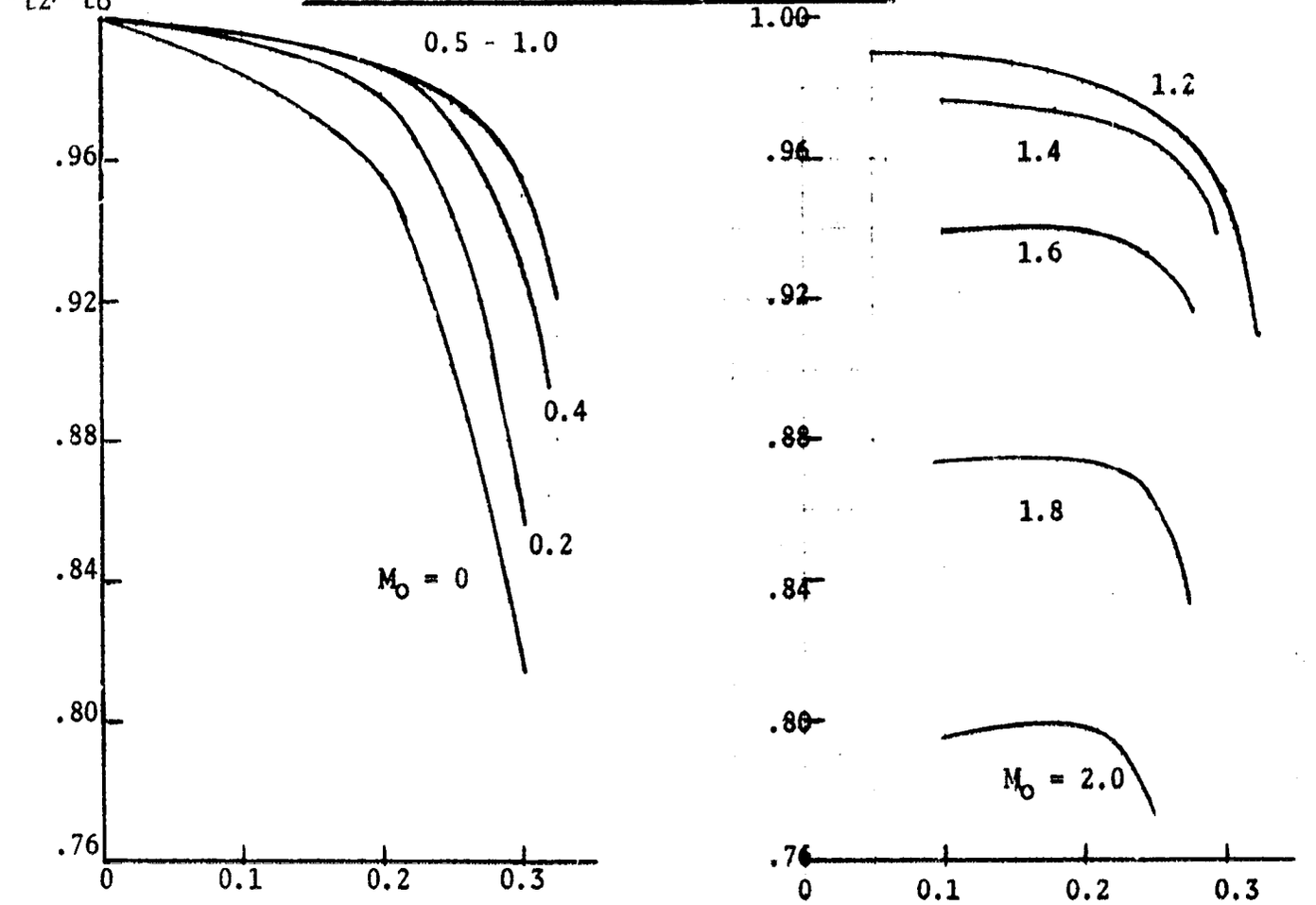

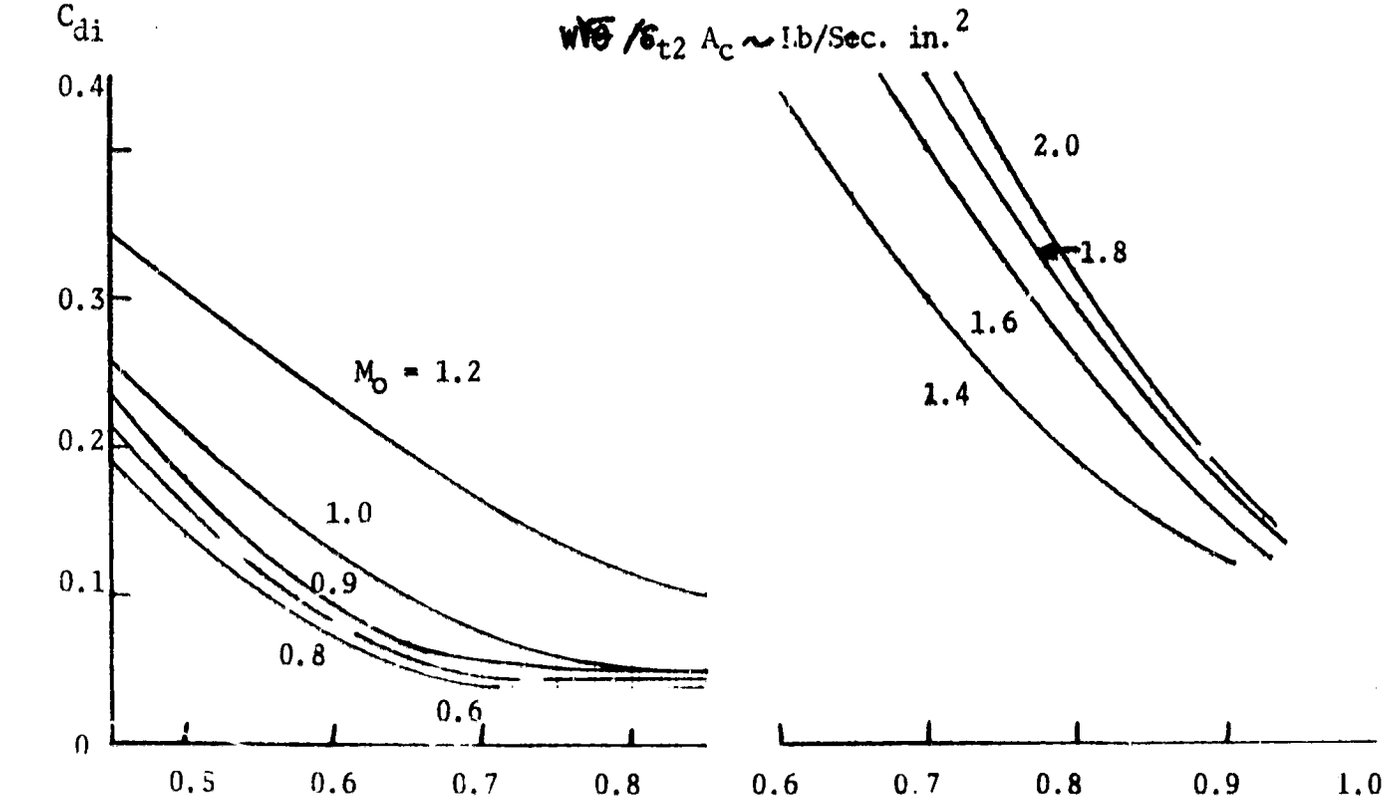

FIGURE 19. 2-D INLET, DESIGN MACH = 2.0

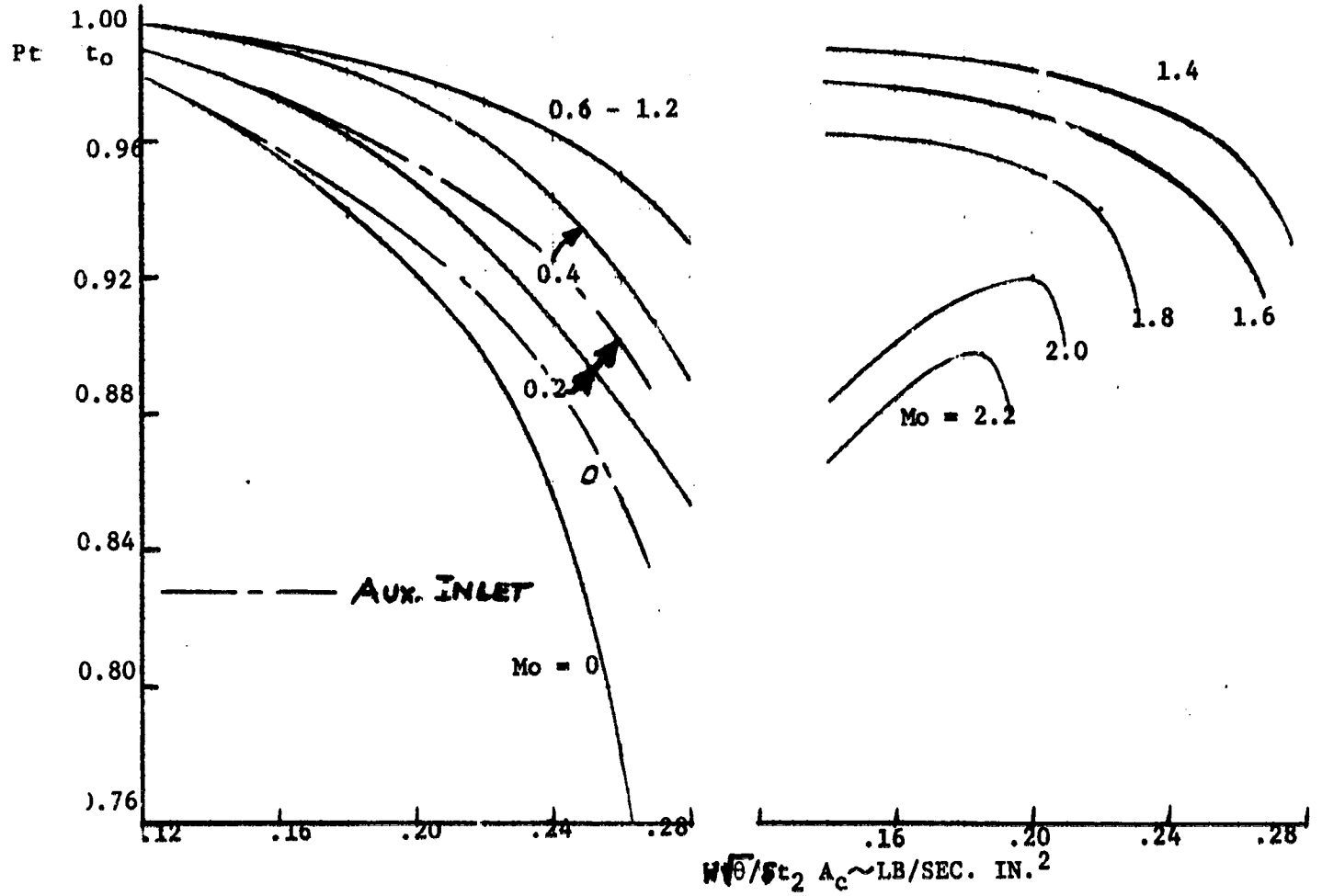

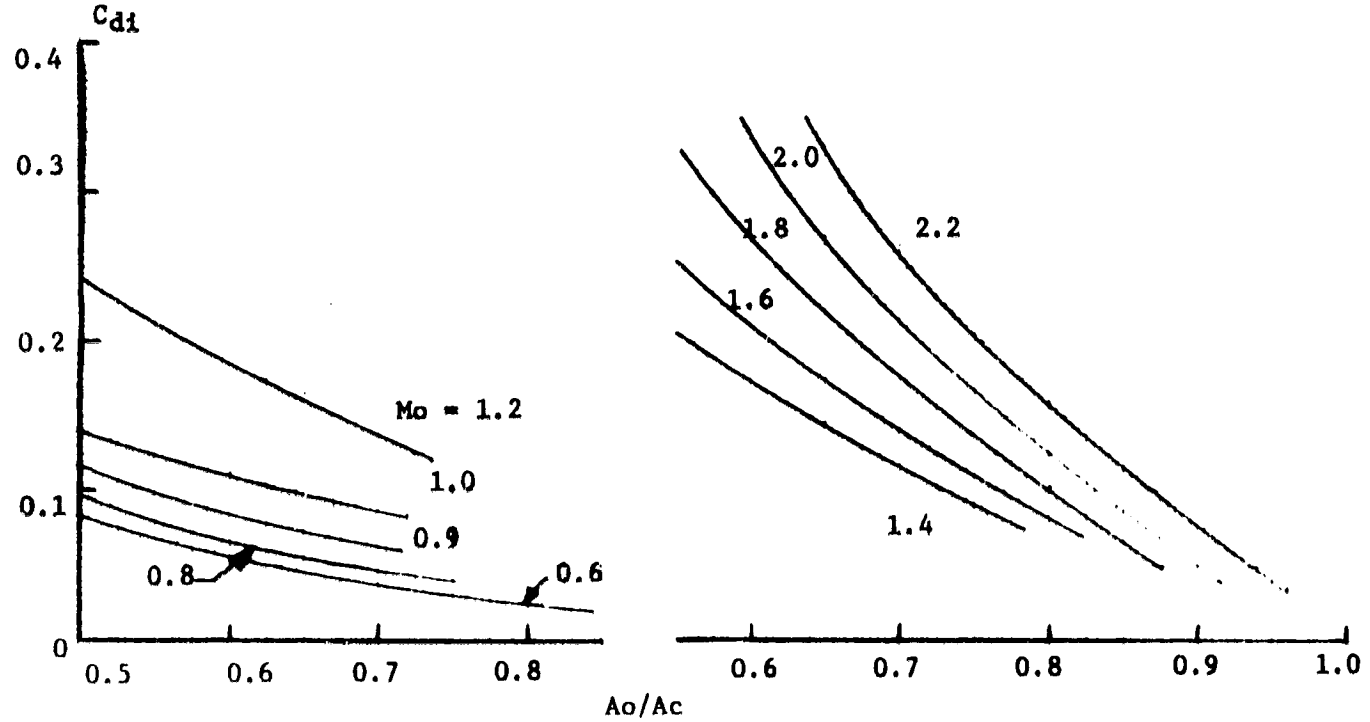

FIGURE 20. SEMI-CONE INLET, DESIGN MACH = 2.0

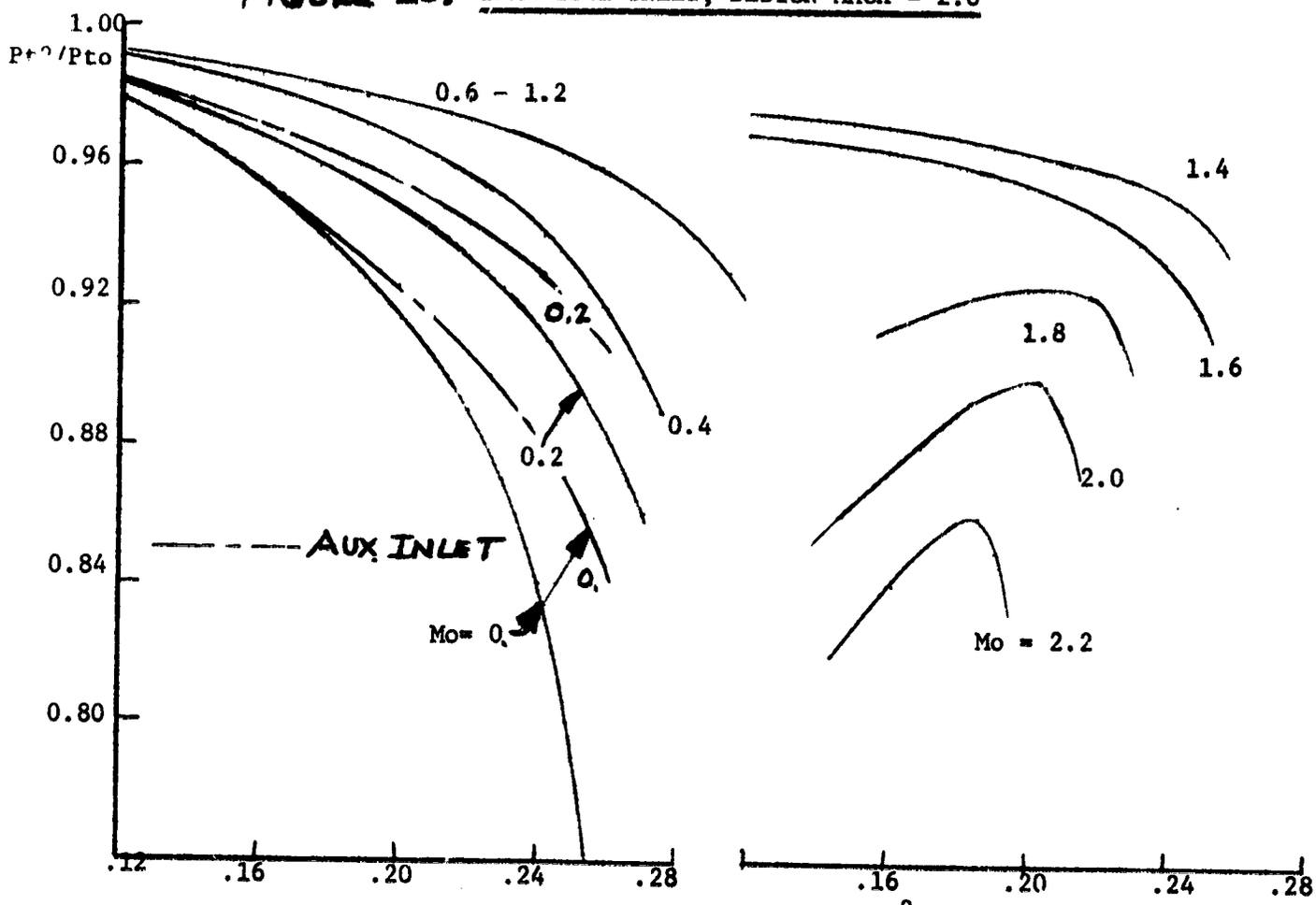

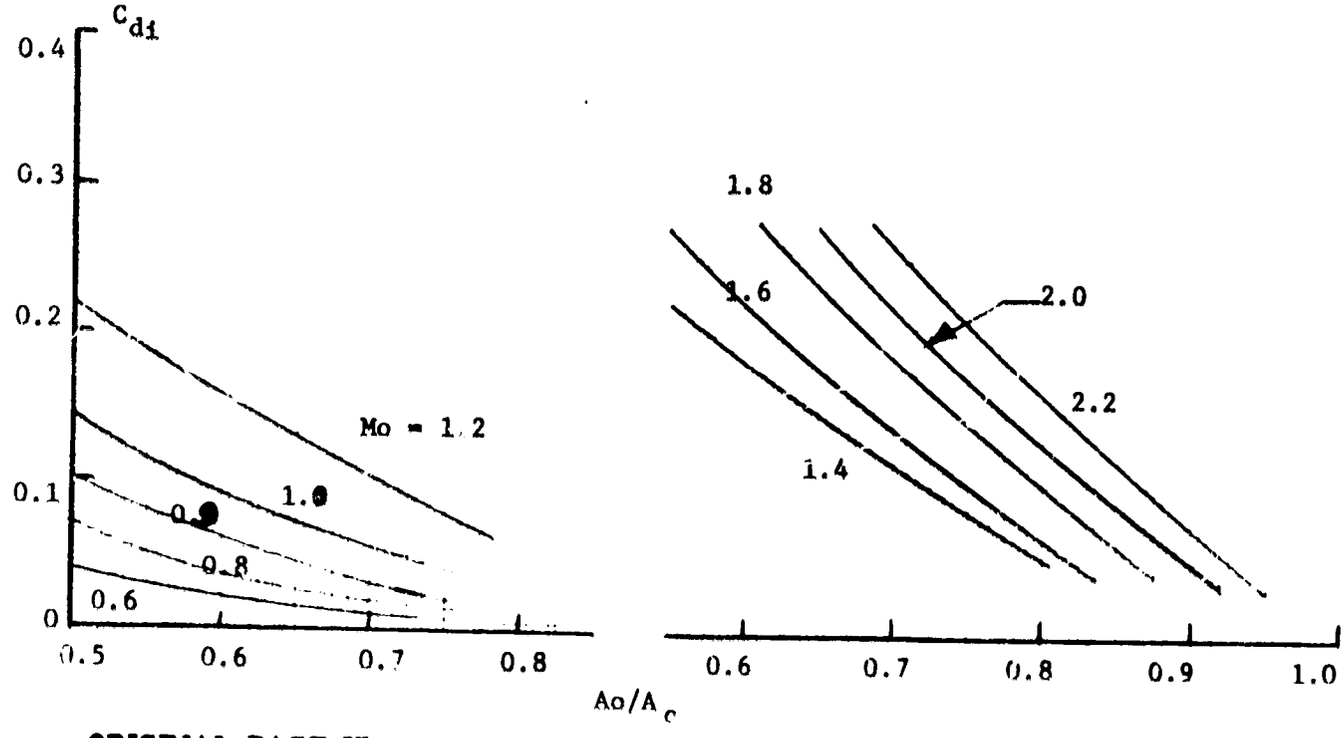

ORIGINAL PAGE IS
OF POOR QUALITY

FIGURE 21. 2-D INLET DATA, $M_d = 2.5$

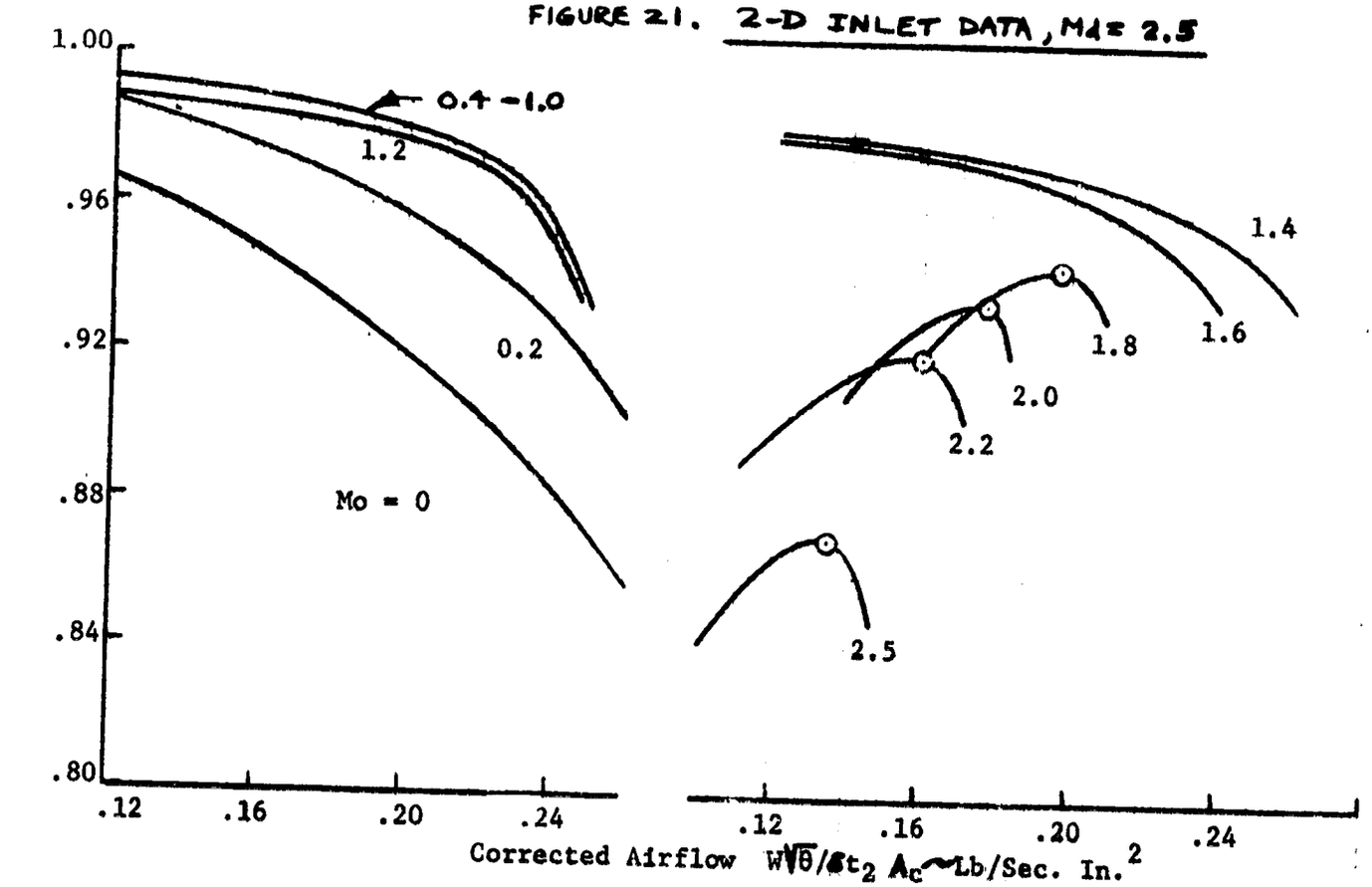

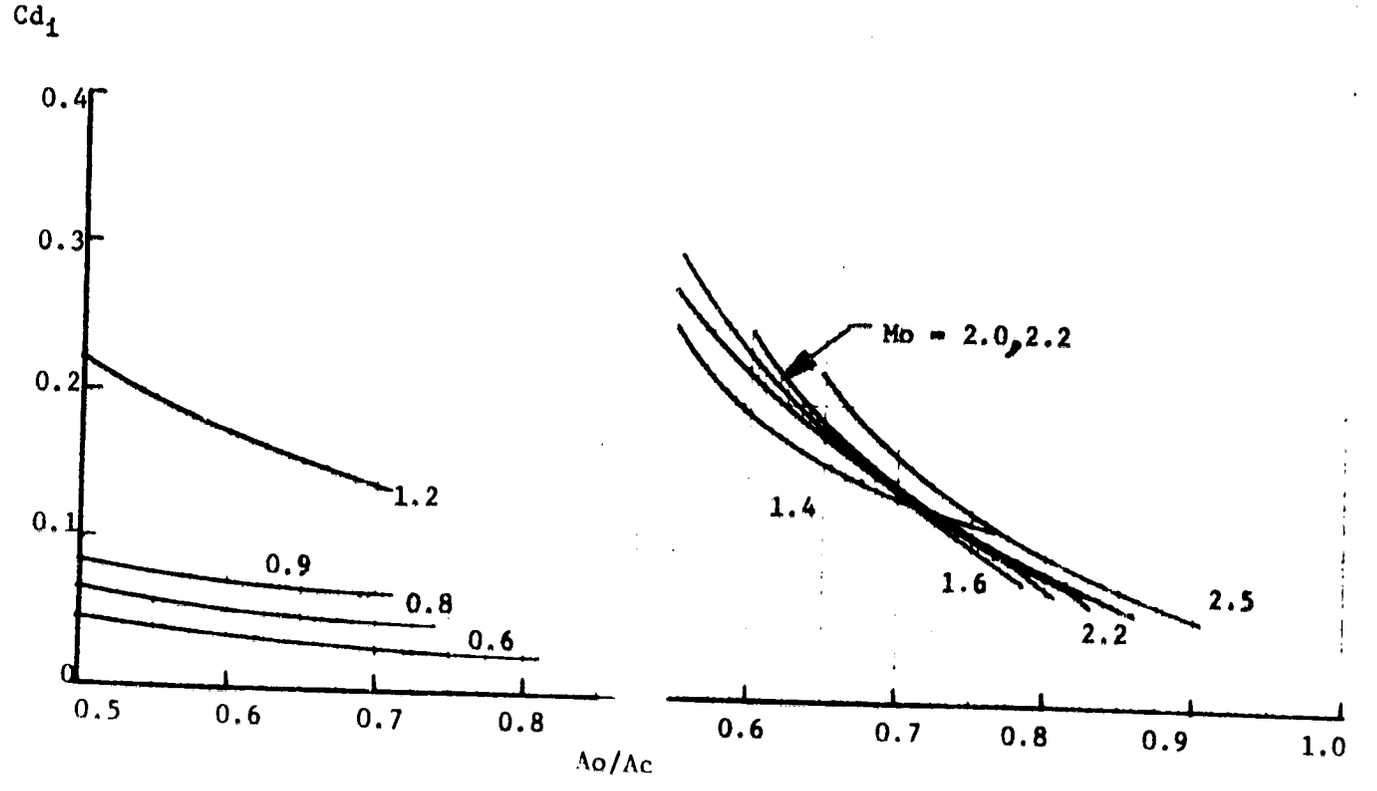

FIGURE 22. SEMI-CONE INLET, Md=2.5

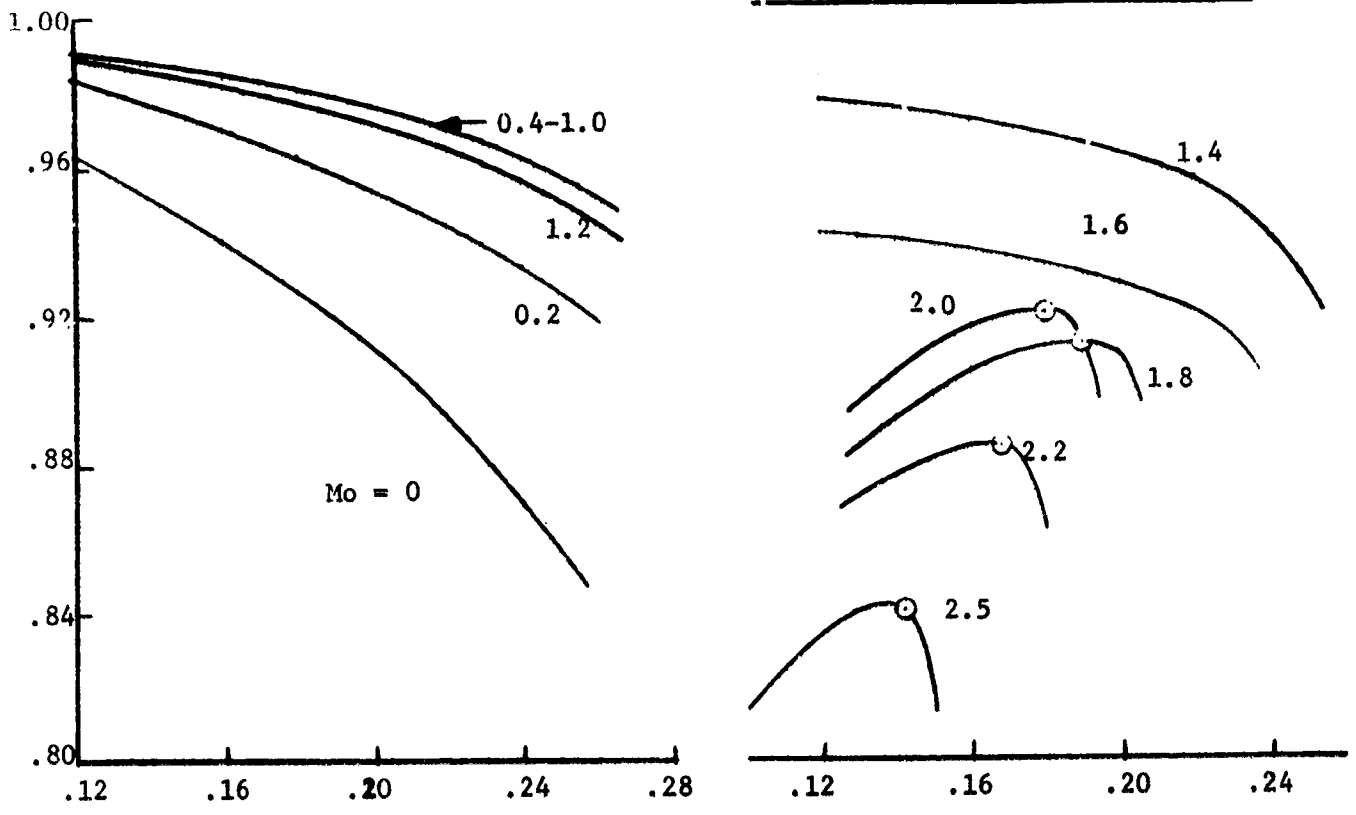

Corrected Airflow $W\sqrt{\theta}/\delta_{t2}$ A_c ~ Lb/Sec In^2

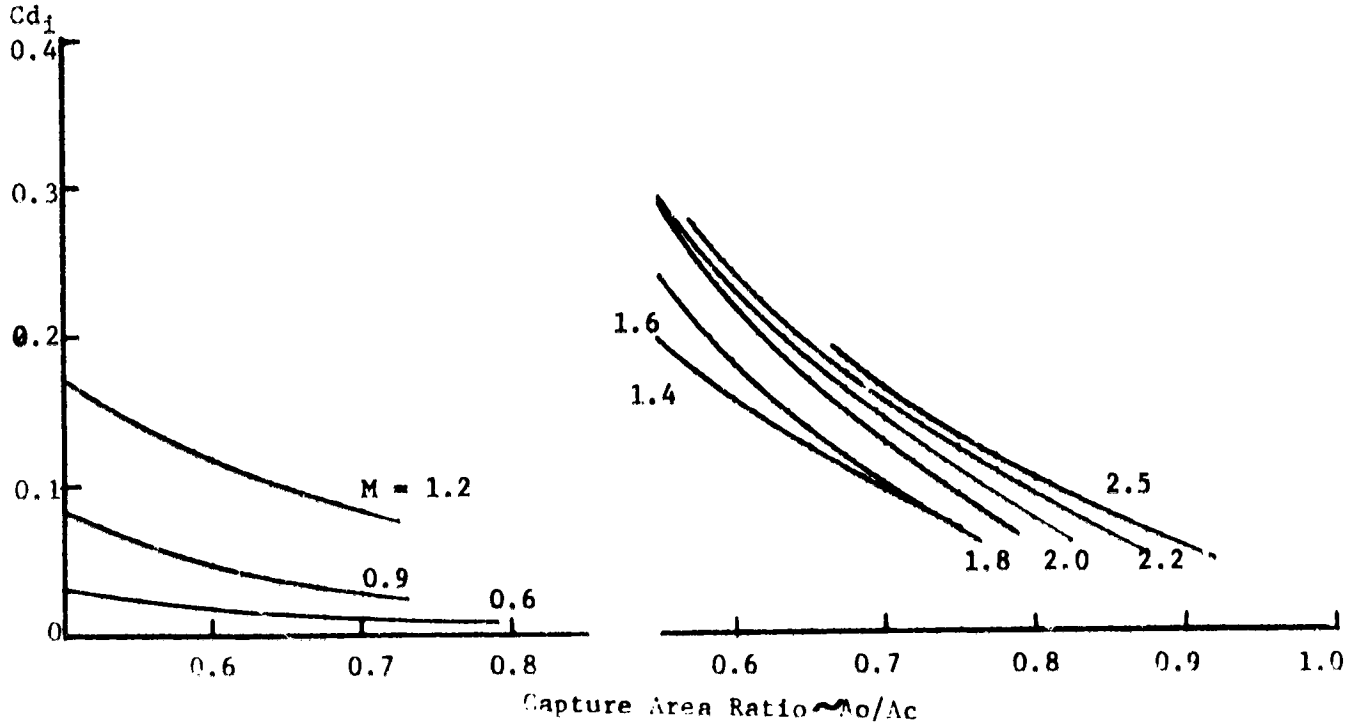

Capture Area Ratio ~ Ao/Ac

FIGURE 23. SP/MF DUCT EXIT PRESSURES

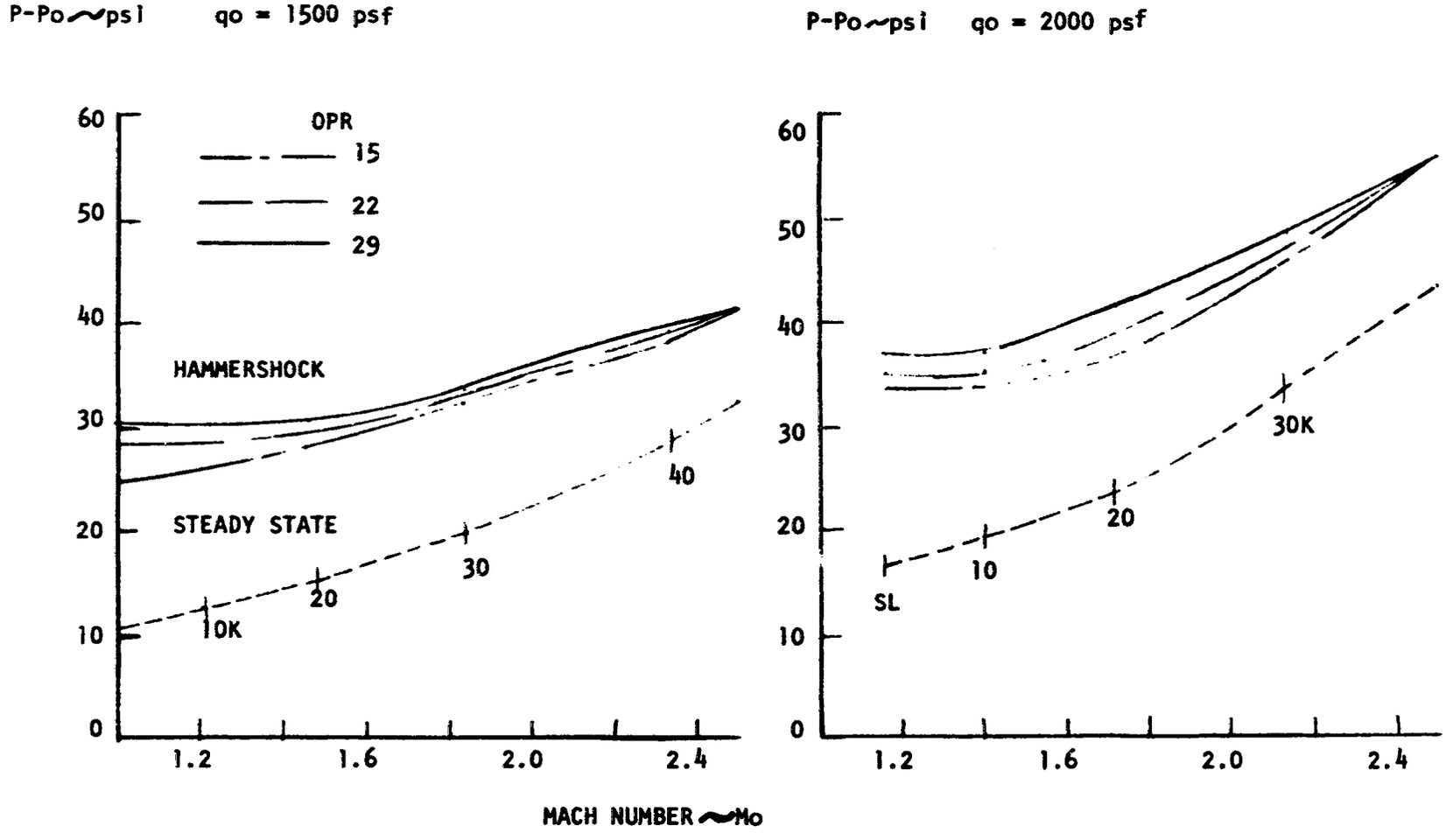

FIGURE 24. INLET COMPARISON, $M_1 = 2.5$, D 575-4

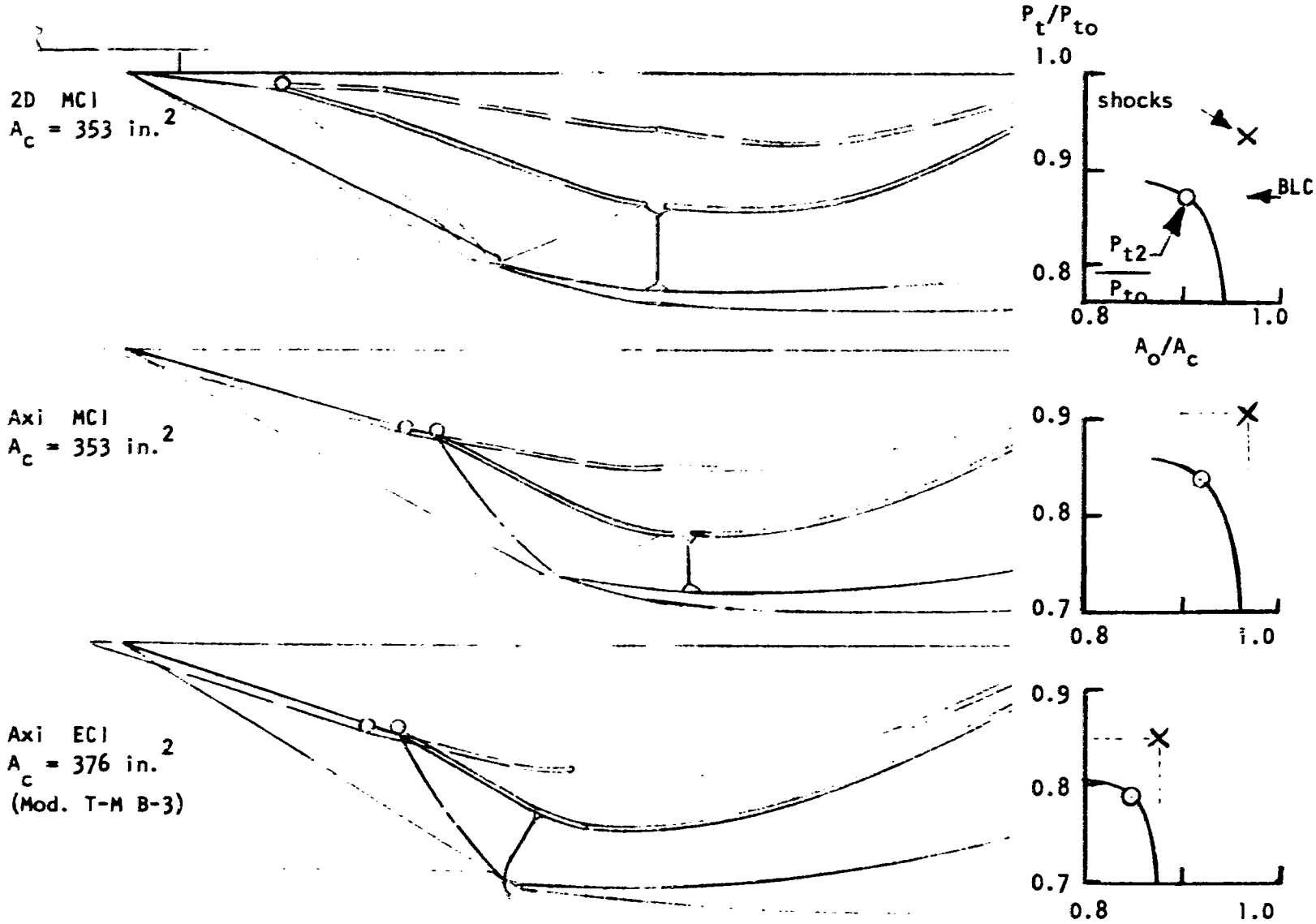

FIGURE 25, PW74 ENGINE/INLET PERFORMANCE COMPARISON

BPR = 0.2 OPR = 15 62.6% SIZE

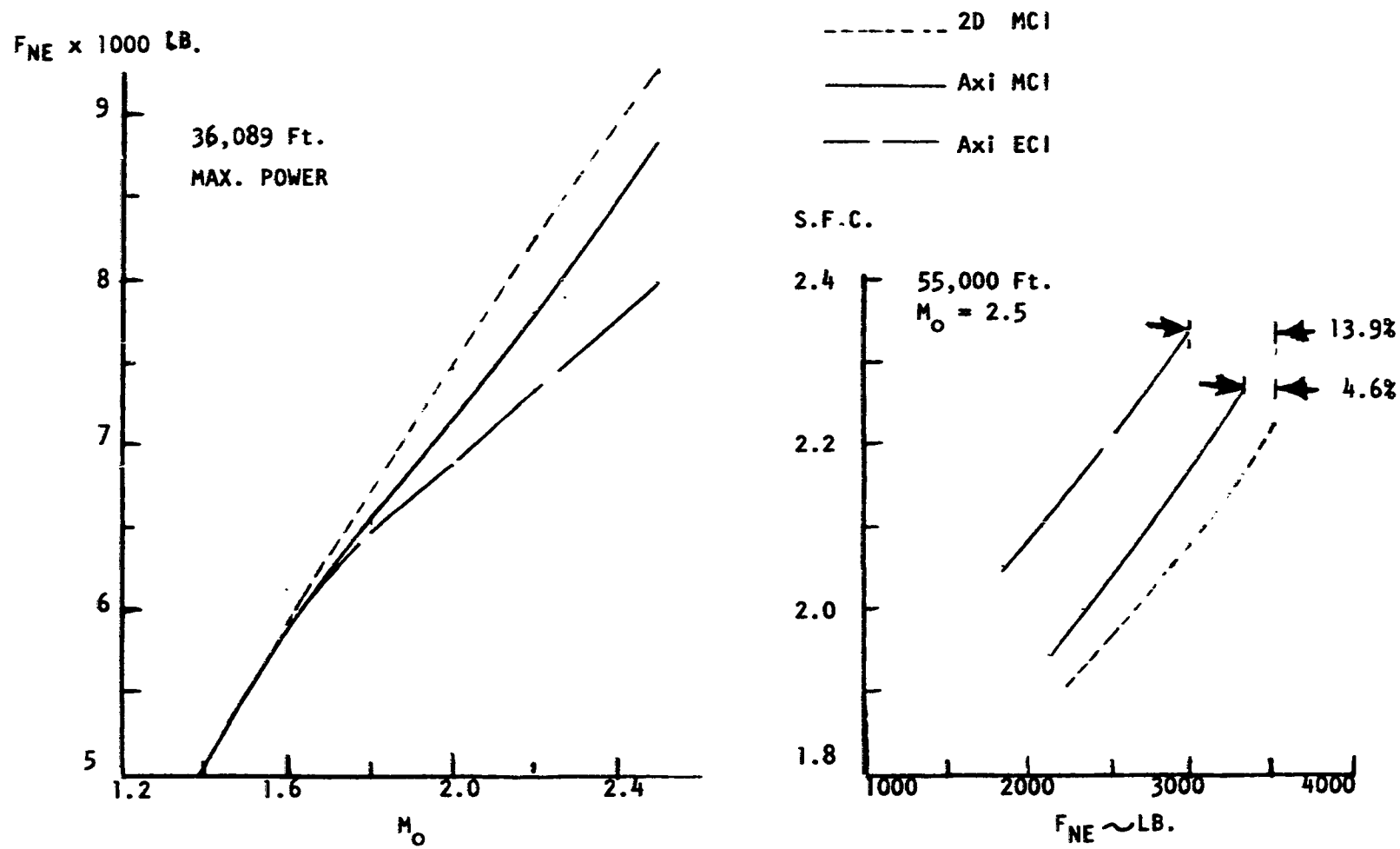

FIGURE 26. MISSION SENSITIVITY TO INLET PERFORMANCE

M_∞=2.5, SP/MF

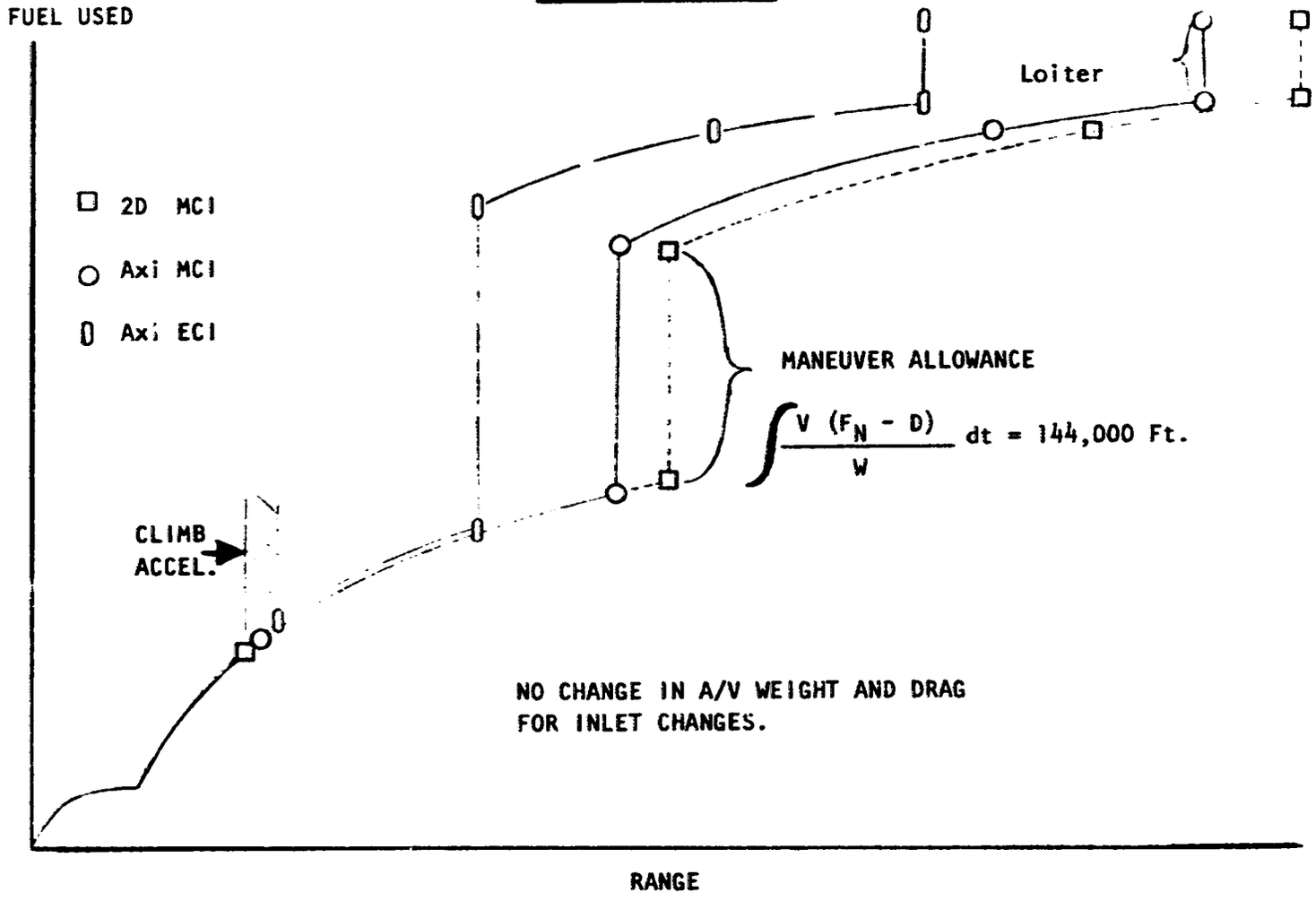

Section III

STABILITY AND CONTROL

LONGITUDINAL STABILITY

Preliminary longitudinal stability checks were made using both the RI Unified Vortex Lattice Program and the RI Unified Distributed Panel Program. A comparison of the two programs using the D575-1 configuration is shown on figure 27. It can be seen that the two methods agree at subsonic speeds where the Unified Vortex Lattice had been correlated with numerous wind tunnel data, but at supersonic speeds there is substantial disagreement. On figure 28 it can be seen that the area of disagreement is at the wing tip where the panel program estimated more load than the vortex lattice.

Because of the difference between the two methods, an investigation was made to determine which was more reliable at supersonic speeds. Figure 29 compares the two methods with wind tunnel data from reference 12 and an analytic solution from reference 13 for an arrow wing type configuration. Again it can be seen from this comparison that both methods predict the correct add load, but that the Unified Vortex Lattice program predicts an aerodynamic center location forward of that predicted by the Unified Distributed Panel program. The test data shows a variation of the aerodynamic center falling between the two methods, but the Unified Distributed Panel analytic method shows a much closer agreement. On the basis of this comparison and other similar comparisons for delta wings at supersonic speeds, it was decided that the Unified Distributed Panel program should be used during the remainder of the study.

The planform sensitivity study as shown on figure 30 was made. The planforms ranged from a two degrees subsonic trailing edge to a 10 degrees supersonic trailing edge as well as the effect of an unswept trailing edge inboard (trailing edge structural extension) to accommodate the engine and structure arrangement. The subsonic trailing edge configuration was chosen due to its smaller a.c. shift and higher lift curve slope. These data are shown on figure 31 and are all based on the same wing area moment reference. Figure 32 compares the span load distributions subsonically and supersonically for the selected planform. It can be seen from figure 33 the change in a.c. is due to the additional load carried on the trailing edge at supersonic speeds.

A low speed (M=0.16) wind tunnel test was run on a configuration similar to the D575-1 and the results are published in reference 21. The results of this test showed:

1. that the Unified Vortex Lattice program predicted the stability and control characteristics of this configuration

2. that approximately 50 percent of maximum vortex lift was attained

3. directional stability increased with increasing angle of attack

4. linear pitching moment characteristics up to approximately $C_L = 0.9$.

Analysis of the leading edge suction and correlation with other data indicated that the large sweep difference between inboard and outboard wing must be decreased. This will decrease the strength of the inboard vortex and increase the strength of the outboard vortex with a resultant linear pitching moment to a higher lift coefficient. The model is being modified to incorporate this change and will be tested in the near future.

An estimation of the balance of the D575-1 configuration showed that the CG was too far forward resulting in large trim requirements at certain Mach numbers as shown on figure 34. The planform modification discussed above which entailed moving the nose aft, changing the inboard blending, and changing the trailing edge sweep results in substantially improved characteristics. This coupled with moving the engine nacelle package (for wave drag reasons) results in the configuration shown on figure 35 (D575-1 revised) and the characteristics shown in table IV and figures 34 and 35.

DYNAMIC STABILITY

A preliminary aerodynamic characteristics study was accomplished for the advanced supercruiser vehicle utilizing the six degree of freedom of motion analytical program. The equations mechanized were those of a rigid aircraft, with the time history solution requiring engine performance, inertias, static and dynamic aerodynamic coefficients, and airplane weight. The static aerodynamic coefficients utilized in this study were those characteristics obtained from a low Reynolds number wind tunnel test performed in NAAL (7 x 11 foot atmospheric test facility). The dynamic derivatives were obtained by use of an in-house computer program. The nomenclature used in the dynamic stability computer program is found in table V. Basically, the test data was used "as is" except that the moment data was referenced to 17.5 percent of the mean aerodynamic chord (canard in). All time histories were started from a trimmed condition at five degrees angle of attack.

Investigation of pitch up to 7.5 degrees with the canard in and canard out time histories, runs 1A and 1B (figures 36 and 37, respectively), indicated that the aircraft has good pitch stability. Pitch ups through 13 degrees angle of attack were also performed with the canard in, figure 38. An analysis of the time histories leading up to this run indicated that the aircraft is quite sensitive in pitch above an angle of attack of 14 degrees. The static pitching moment data also show this to be true, i.e., unstable pitching moment above $\alpha = 12.5$ degrees.

An analysis of the time histories produced to date indicate that it would be desirable to have greater pitch stability above an angle of attack of 12 degrees than exhibited by the wind tunnel data, in order to have improved handling qualities in pitch at high angles of attack. An investigation will be performed at the higher angles of attack where the aerodynamic data reflects this increase in pitch stability. This new aerodynamic data will be obtained from a future wind tunnel test using the redesigned configuration (i.e., D575-2A).

Time history run 1B (figure 37) was rerun as run 4 (figure 39) with yaw/roll control, outboard flaps (4,5,6) deflected, plus roll recovery input, inboard flaps (1,2,3) deflected, being utilized during the pitch up. This run demonstrated good initial recovery in roll and yaw.

Time history run 5 (figure 40) is a yaw/roll doublet performed by use of the outboard flaps. This time history demonstrated that 30 degrees of roll angle can be achieved in one second at an angle of attack of 7.5 degrees. Run 6 (figure 41) indicated that 30 degrees of roll in one second could also be obtained by use of the inboard flaps. Additional runs are planned at higher angles of attack, with roll and pitch recovery, to study roll control in greater detail.

Ananalysis of the static data indicates that the inboard rolling surfaces have adverse yaw associated with roll input, while the outboard yawing surfaces exhibited adverse roll for yawing moment input. Upon analyzing the time histories where the flaps were deflected for positive roll input, it was noted that negative rolling motion actually developed. This result was due to the positive β generated during the run, associated with the roll/yaw control input, and its effect on the negative C_{ℓ_β} term. This above result is demonstrated by run 6 (figure 41) which also exhibited a favorable roll/yaw motion during the maneuver. Because of the previously mentioned problem, extremely poor roll recovery existed once the vehicle rolled through 90 degrees.

An attempt was made to sideslip the aircraft through 10 degrees of β with the wings level. This run was unsatisfactory in that the aircraft sideslipped through 10 degrees but also rolled through 10 degrees. This attempted sideslip run indicated that 10 degrees of β can be achieved but not with the wings level; some roll angle ($\phi \approx 10$ degrees) might have to be accepted.

Additional analyses were performed in determining how to improve and correct the rolling motion produced when partial roll control was introduced, and to yield improved roll recovery. Roll control in conjunction with correct yaw control inputs improved the situation in that a favorable roll/yaw motion existed and the vehicle rolled in the direction of the roll input, but poor roll recovery still prevailed for this case. The yaw input was utilized to yield the correct sign on sideslip (β) so that $C_{\ell_\beta} \times \beta$ had the correct sense during the attempted roll maneuver.

It was noticed that the roll recovery problem existed in an angle of attack region (0 through 10 degrees) where $C_{n_\beta}/C_{\ell_\beta}$ was approximately -0.03. This relationship is extremely small when compared to existing aircraft, which have an average value of $C_{n_\beta}/C_{\ell_\beta}$ of approximately -1.50 over an angle of attack range of 0 degrees to 10 degrees. An investigation was performed utilizing the six degrees of freedom program where C_{n_β} and C_{ℓ_β} were varied to determine the lower bound of the ratio $C_{n_\beta}/C_{\ell_\beta}$ which would yield favorable roll recovery for this vehicle. The analysis showed that a value of -0.465 or less (more negative) would be appropriate. Through use of the Unified Vortex Lattice Program and utilizing the new configuration described on figure 35, it was determined that the previously mentioned level of $C_{n_\beta}/C_{\ell_\beta}$ could be obtained by the addition of negative wing dihedral to the basic planform, figure 42.

A low speed wind tunnel investigation has been run to evaluate the static longitudinal and lateral-directional characteristics of these new wing designs in conjunction with the new vehicle planform. The preliminary results of this test are shown in reference 22.

FIGURE 27. A.C. AND LIFT CURVE SLOPE VERSUS MACH NUMBER, D 575-1

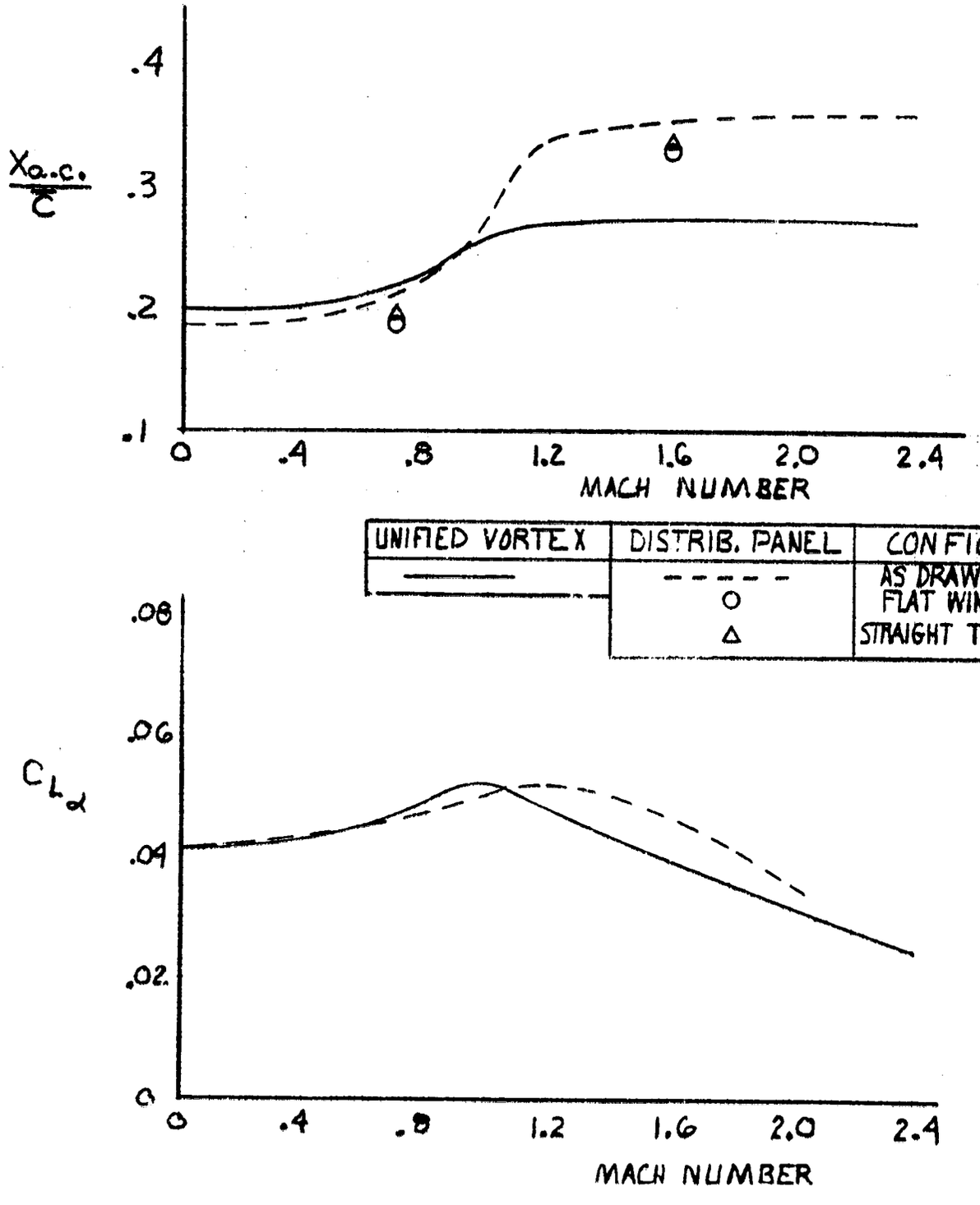

FIGURE 28. LOCAL LIFT AND WING LOADING VERSES SPAN , D575-1

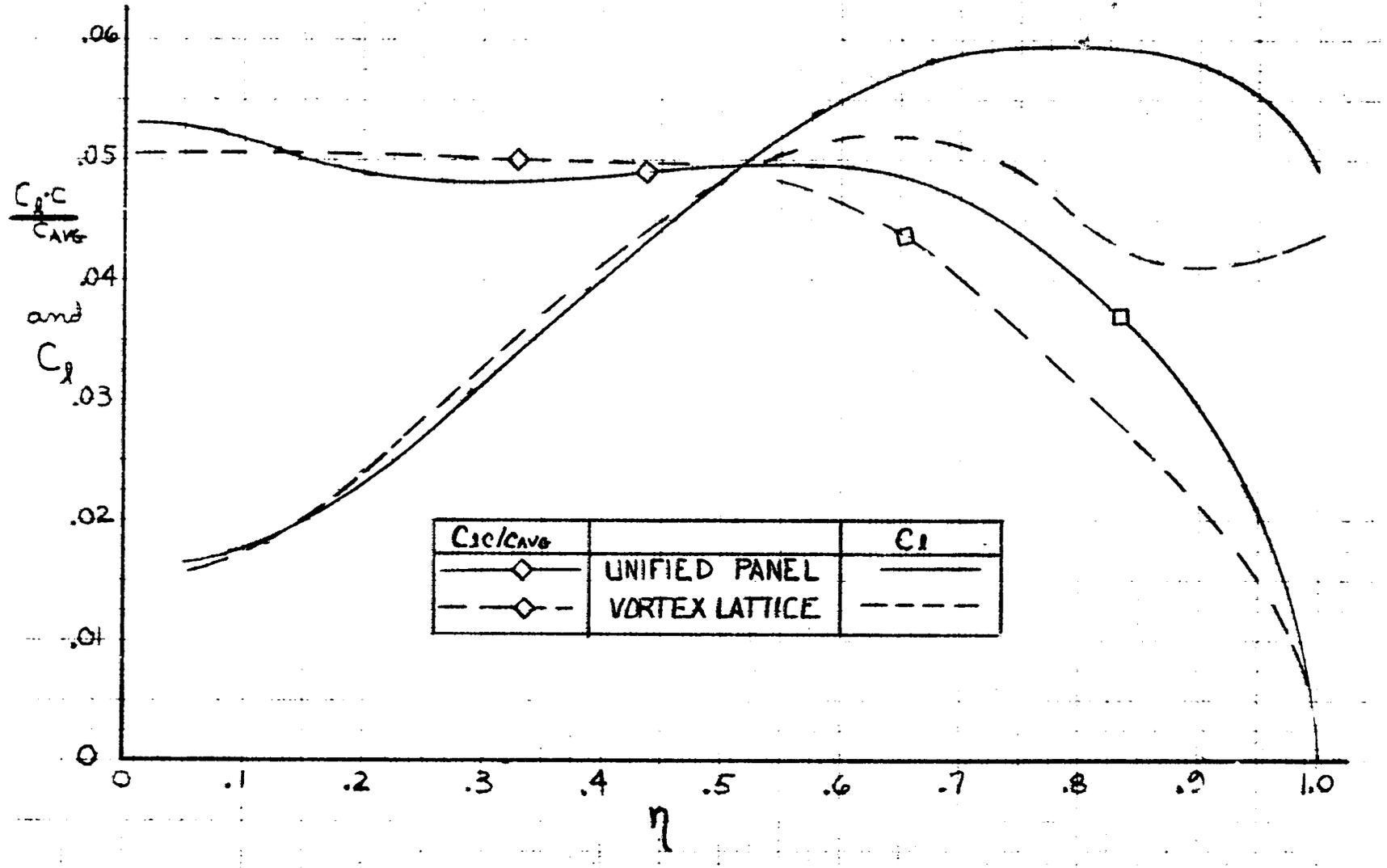

FIGURE 29. VARIATION OF C_{L_α} AND AERODYNAMIC CENTER WITH MACH NUMBER FOR ARROW WING AR = 1.6

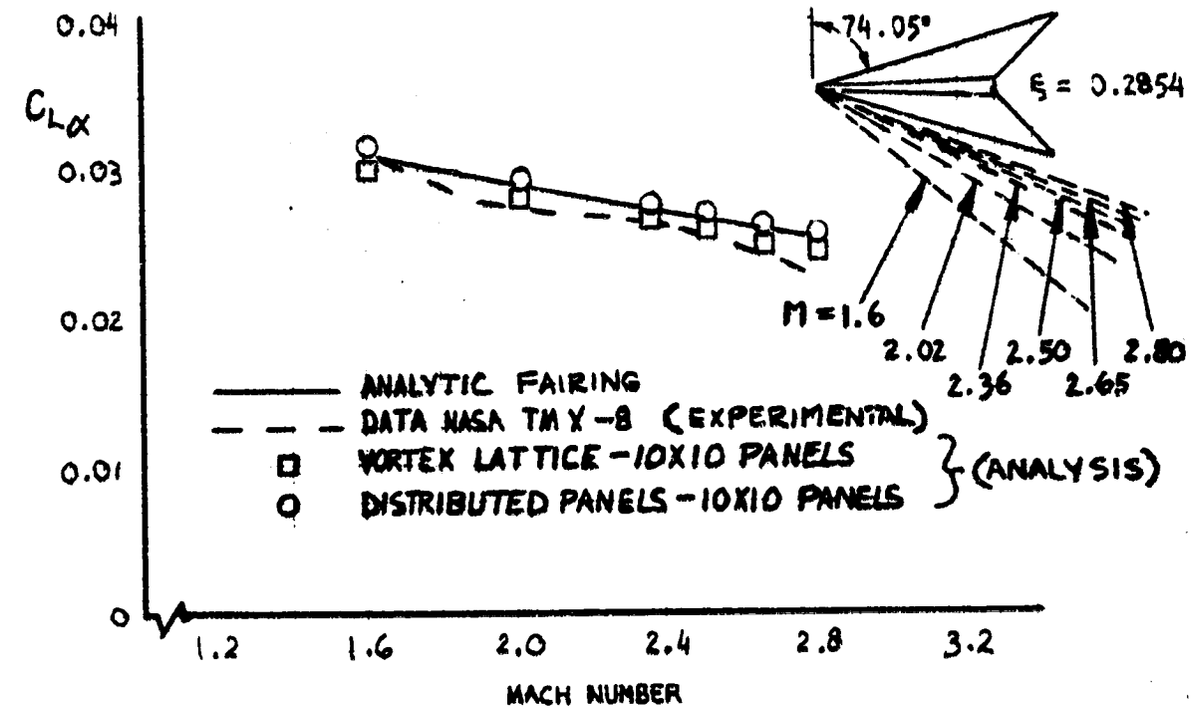

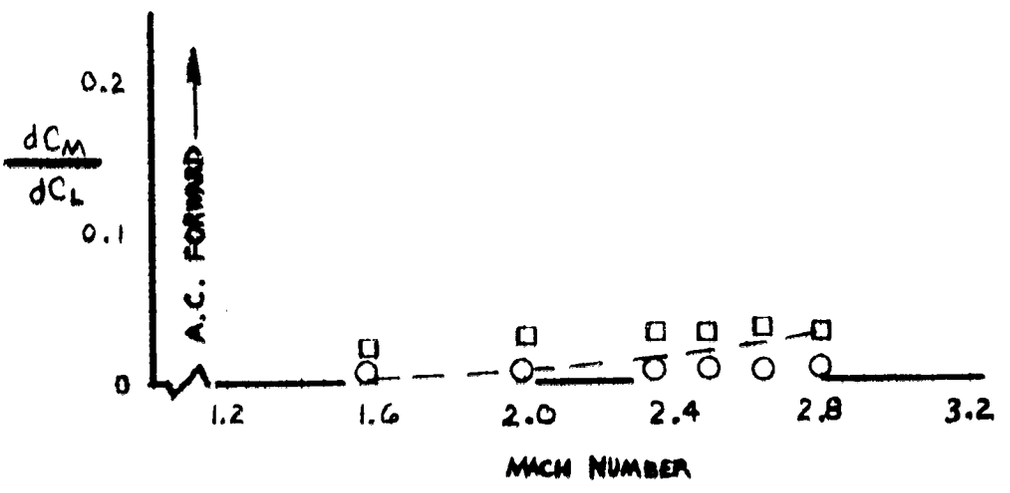

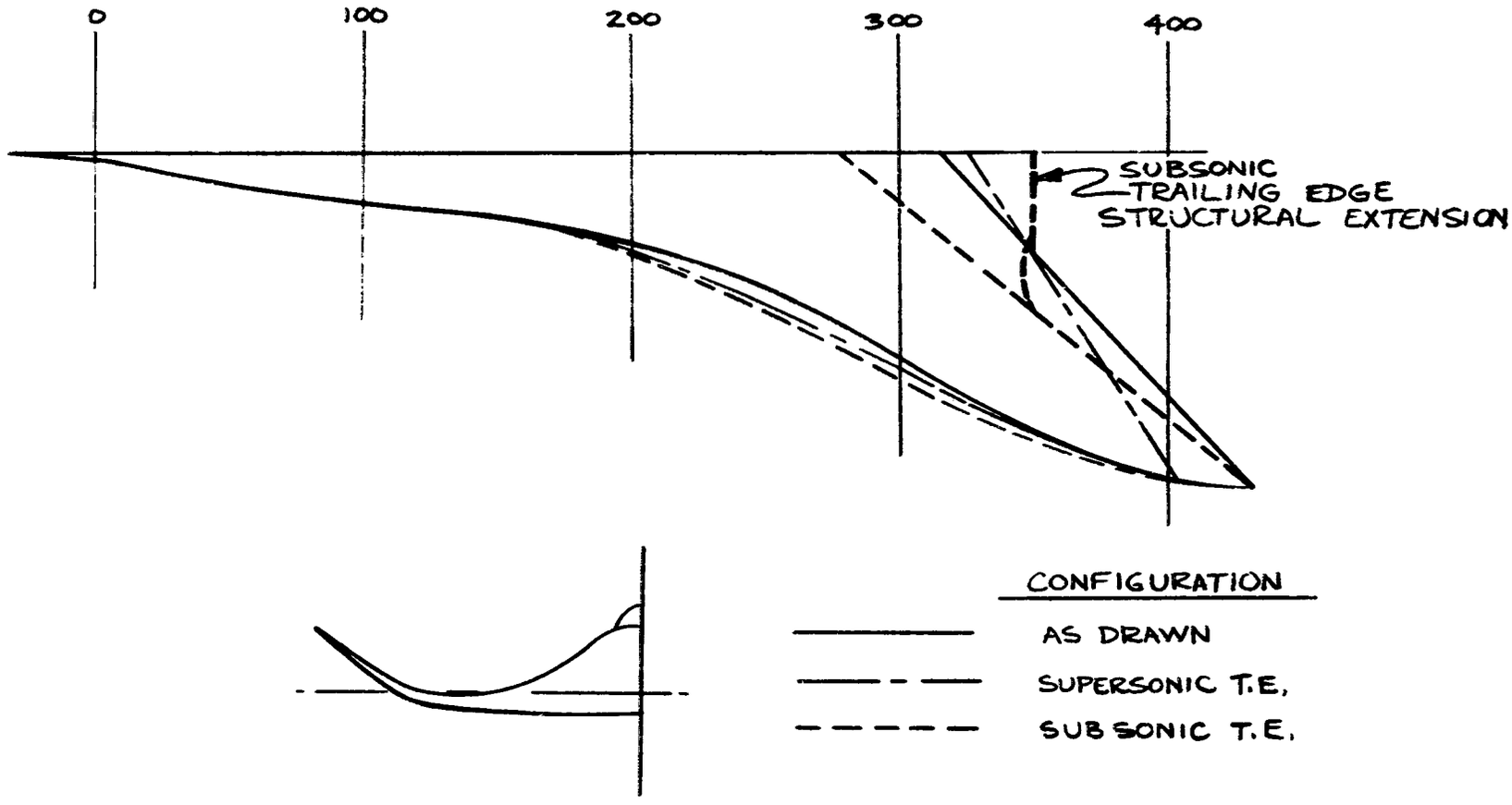

FIGURE 30. WING STUDY GEOMETRY VARIATIONS

FIGURE 31. A.C. AND LIFT CURVE SLOPE VERSUS MACH NUMBER, WING STUDY

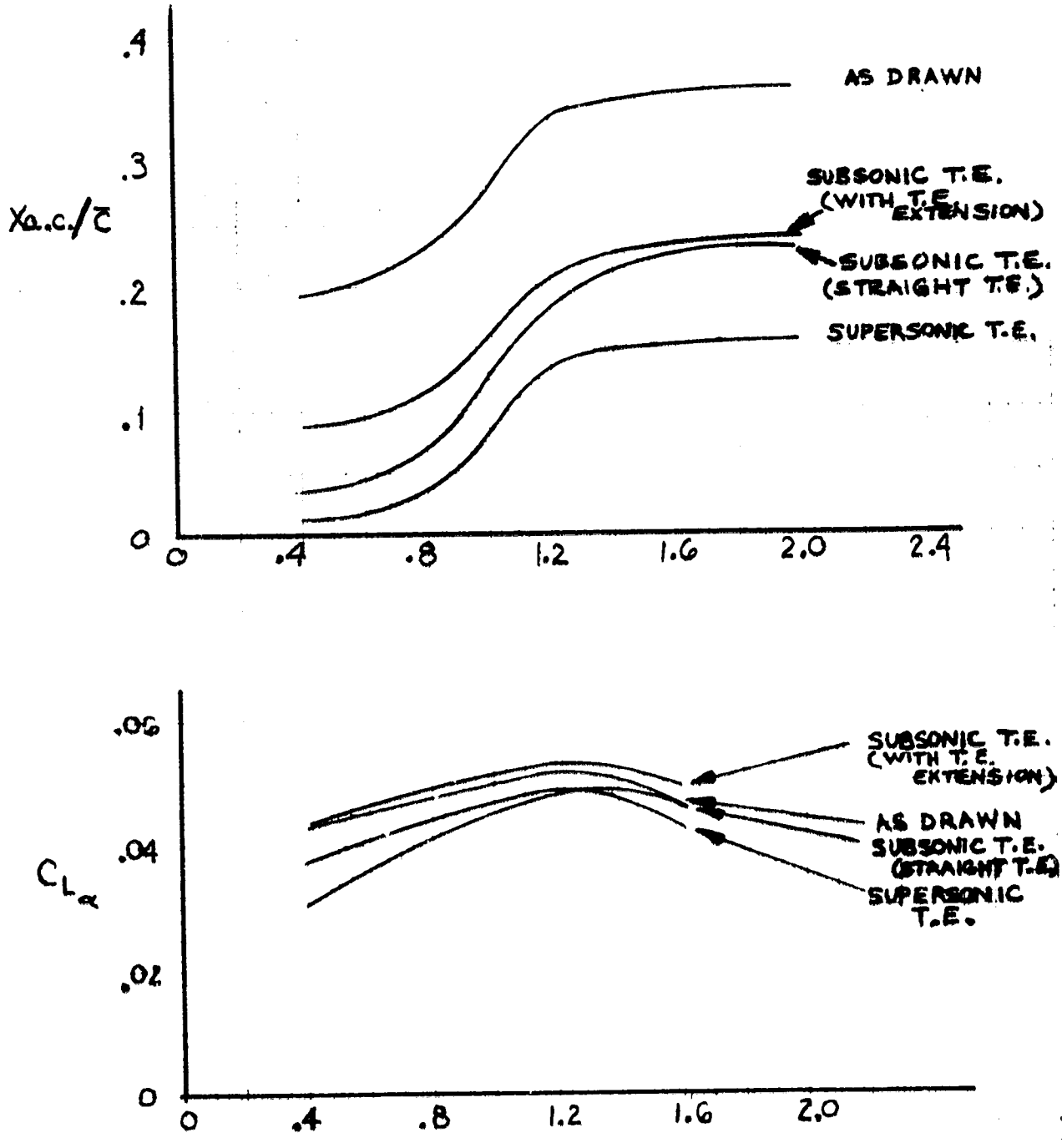

FIGURE 32. C.P. AND WING LOADING VERSUS SPAN WING STUDY

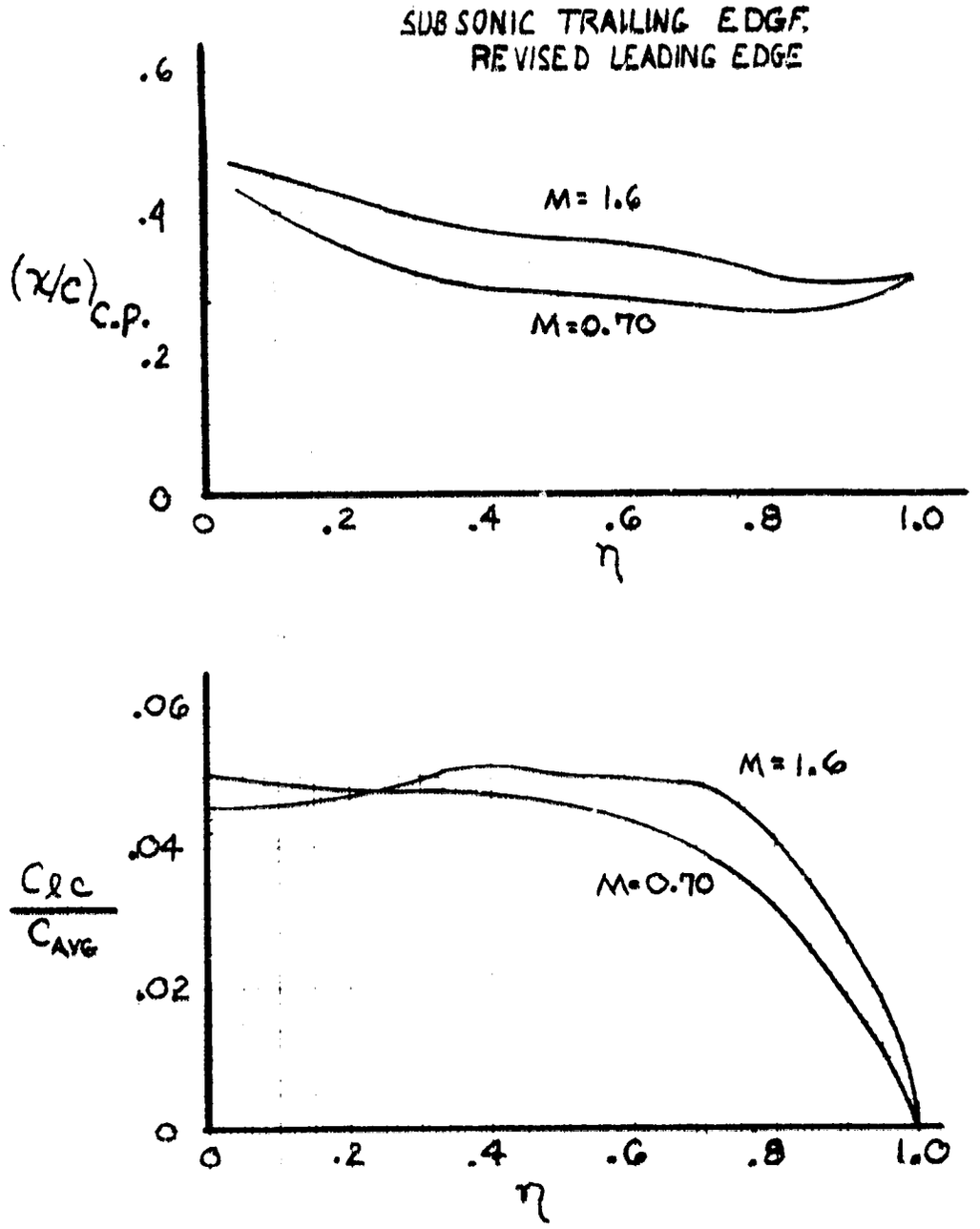

FIGURE 33. $C_{P_{NET}}$ VERSUS x/c, WING STUDY

SUBSONIC TRAILING EDGE

REVISED LEADING EDGE

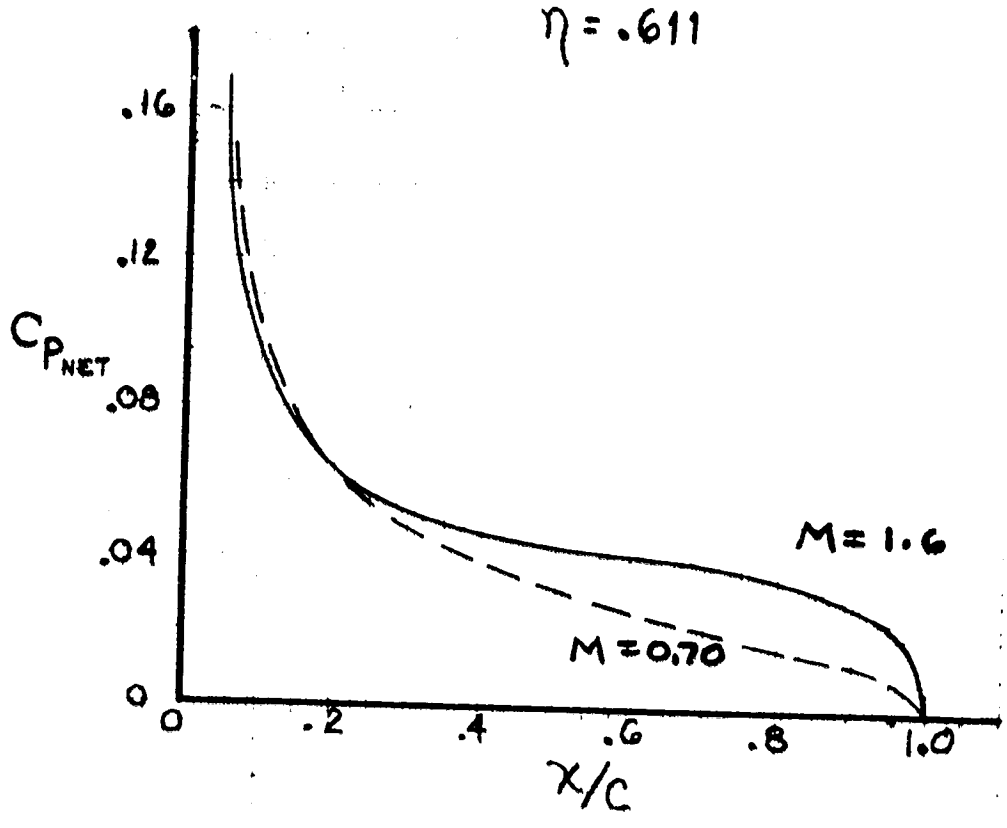

FIGURE 34. VARIATION OF LONGITUDINAL STABILITY WITH MACH NUMBER, D575-1

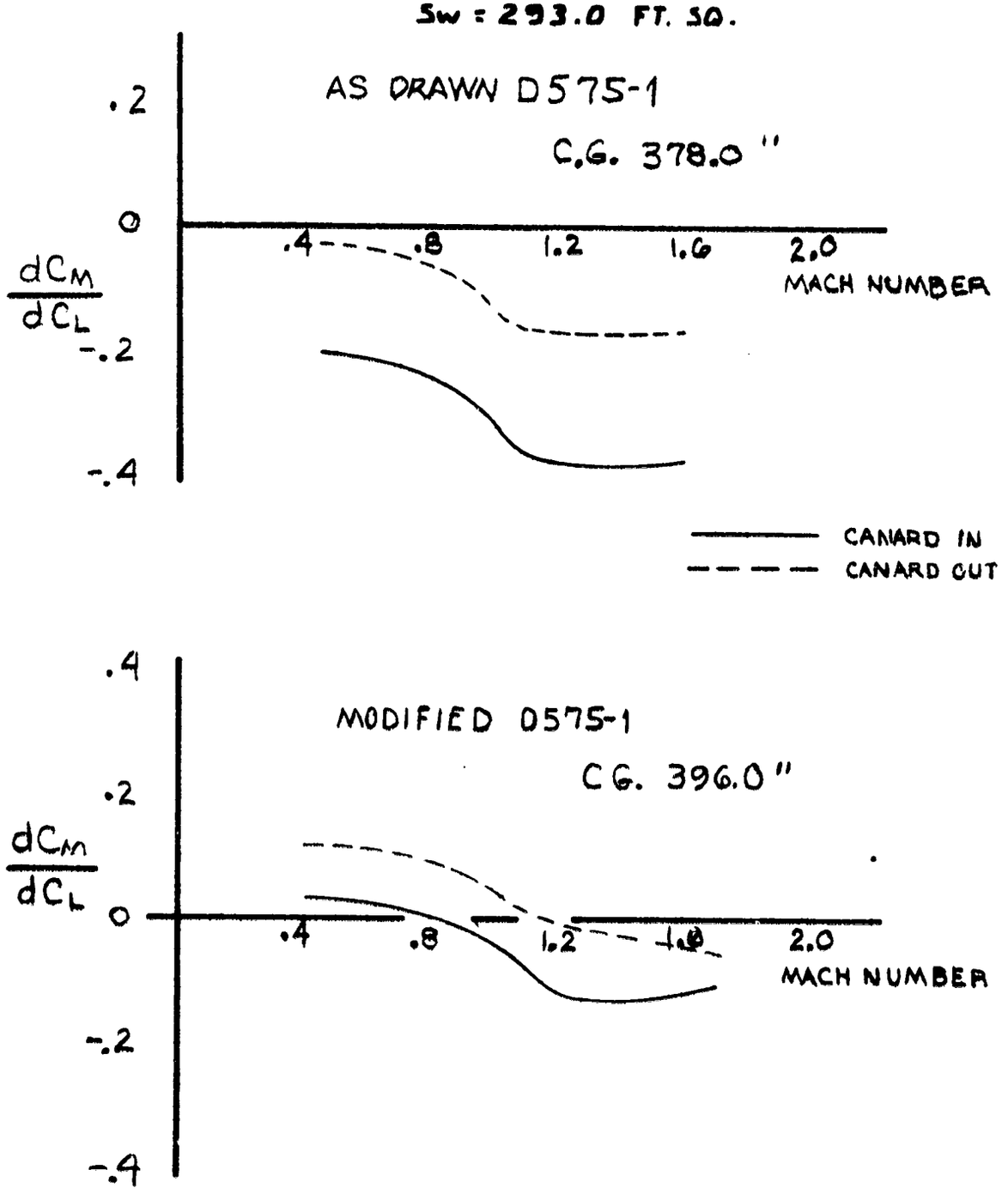

TABLE IV. WEIGHT SUMMARY, D575-1 REVISED

	WT.	C.G.		MOMENT		
TOTAL STRUCTURE	(7150)			(2753100)		
WING GROUP - COMPOSITE	2670	455				
TAIL GROUP - HORIZONTAL COMPOSITE	120	245				
- VERTICAL						
BODY GROUP - COMPOSITE	2130	300				
ALIGHTING GEAR GROUP - MAIN	680	380				
- AUXILIARY	160	240				
SURFACE CONTROLS	750	363				
ENGINE SECTION OR NACELLE GROUP COMPOSITE	640	470				
PROPULSION GROUP	(2690)			(1304900)		
ENGINE (AS INSTALLED)	1100	495				
ACCESSORY GEAR BOXES & DRIVES	100	470				
AIR INDUCTION SYSTEM INCL IN ENG. SEC.						
EXHAUST SYSTEM	850	540				
COOLING & DRAIN PROVISIONS	10	495				
LUBRICATING SYSTEM	20	495				
FUEL SYSTEM	530	395				
ENGINE CONTROLS	40	260				
STARTING SYSTEM	40	495				
PROPELLER INSTALLATION						
FIXED EQUIPMENT	2725			(928885)		
INSTRUMENTS	190	235				
HYDRAULIC & PNEUMATIC GROUP	340	416				
ELECTRICAL GROUP	445	377				
ELECTRONICS GROUP	580	215				
ARMAMENT PROVISIONS	670	459				
FURNISHINGS	270	230				
AIR CONDITIONING EQUIPMENT	220	350				
PHOTOGRAPHIC						
AUXILIARY GEAR	10	370				
TOTAL WEIGHT EMPTY	12565	396.89		(4986885)		
CREW	215	207				
FUEL						
INTERNAL	5100	395				
TRAPPED	75	395				
OIL	30	495				
ENGINE						
TRAPPED						
ARMAMENT GUN (M-61)	255	398				
AMMO (300 RDS)	170	395				
2-MADMAN MISSILES	960	366				
EQUIPMENT GUN CAMERA	5	190				
N_2	10	380				
O_2	25	235				
TOTAL USEFUL LOAD	6845	384.82		(2634105)		
TAKE OFF GROSS WEIGHT	19410	392.63		7620990		
FLIGHT DESIGN GROSS WEIGHT						
LANDING DESIGN GROSS WEIGHT						

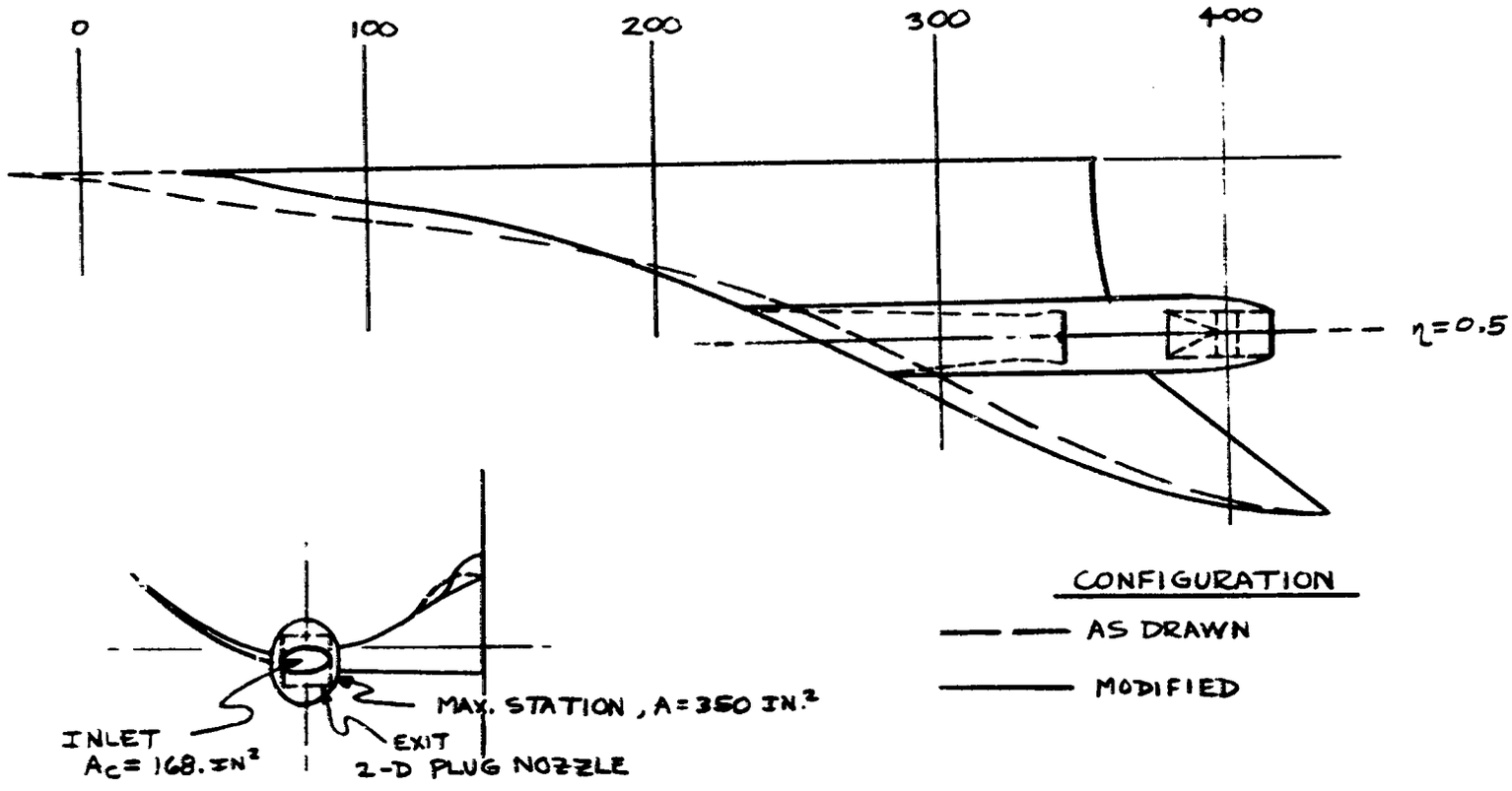

FIGURE 35. WING STUDY MODIFIED CONFIGURATION

Table V

NOMENCLATURE FOR TIME HISTORY RUNS

ALP-DEG	Angle of Attack, Deg. (Positive Up)
THETA	Euler Pitch Angle, Deg. (Positive Up)
PHI	Euler Roll Angle, Deg. (Positive Right)
PSI	Euler Azimuth Angle, Deg. (Positive Right)
GAMMADEG	Flight Path Angle of C.G., Deg.
BETA-DEG.	Sideslip, Deg.
ALT	Altitude, Ft.
VTOT	Resultant Velocity Along Flight Path, Ft/Sec
P-BODY	Roll Rate, Deg/Sec, Positive Clockwise
Q-BODY	Pitch Rate, Deg/Sec, Positive Up
R-BODY	Yaw Rate, Deg/Sec, Positive Clockwise
Q_o	Dynamic Pressure, Lbs/Ft^2
F-THRUST	Engine Thrust, Lbs
NZ(G's)	Load Factor Along Z-Axis, - F_Z/W
Canard Loc.	0.0 is in, 1.0 is full out
DFL(123) DFR(123)	Left Hand Inboard Flap, Positive Down Right Hand Inboard Flap, Positive Down
DFL(456) DFR(456)	Left Hand Outboard Flap, Positive Down Right Hand Outboard Flap, Positive Down

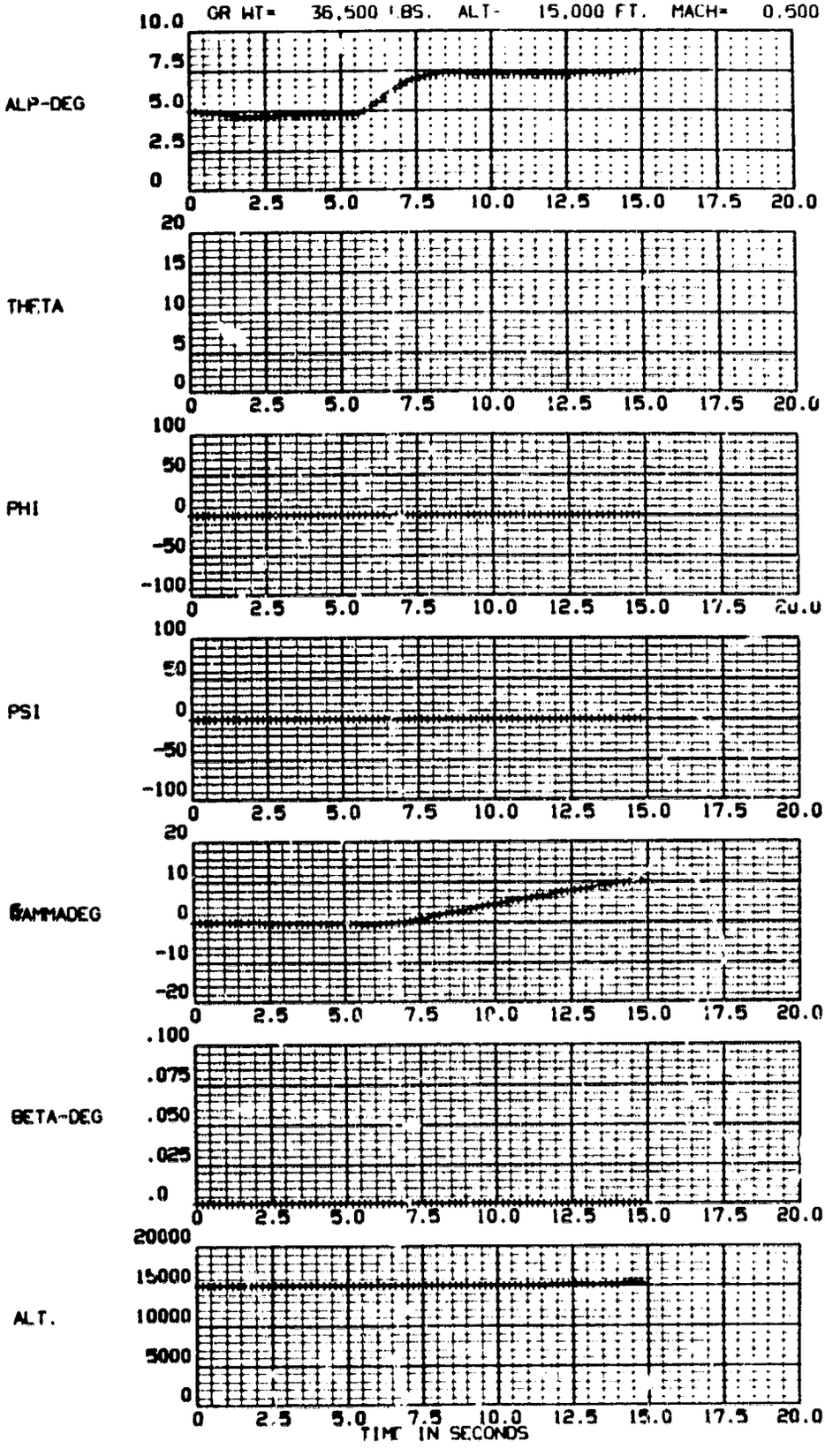

Figure 36a. Time History Results, Run 1a.

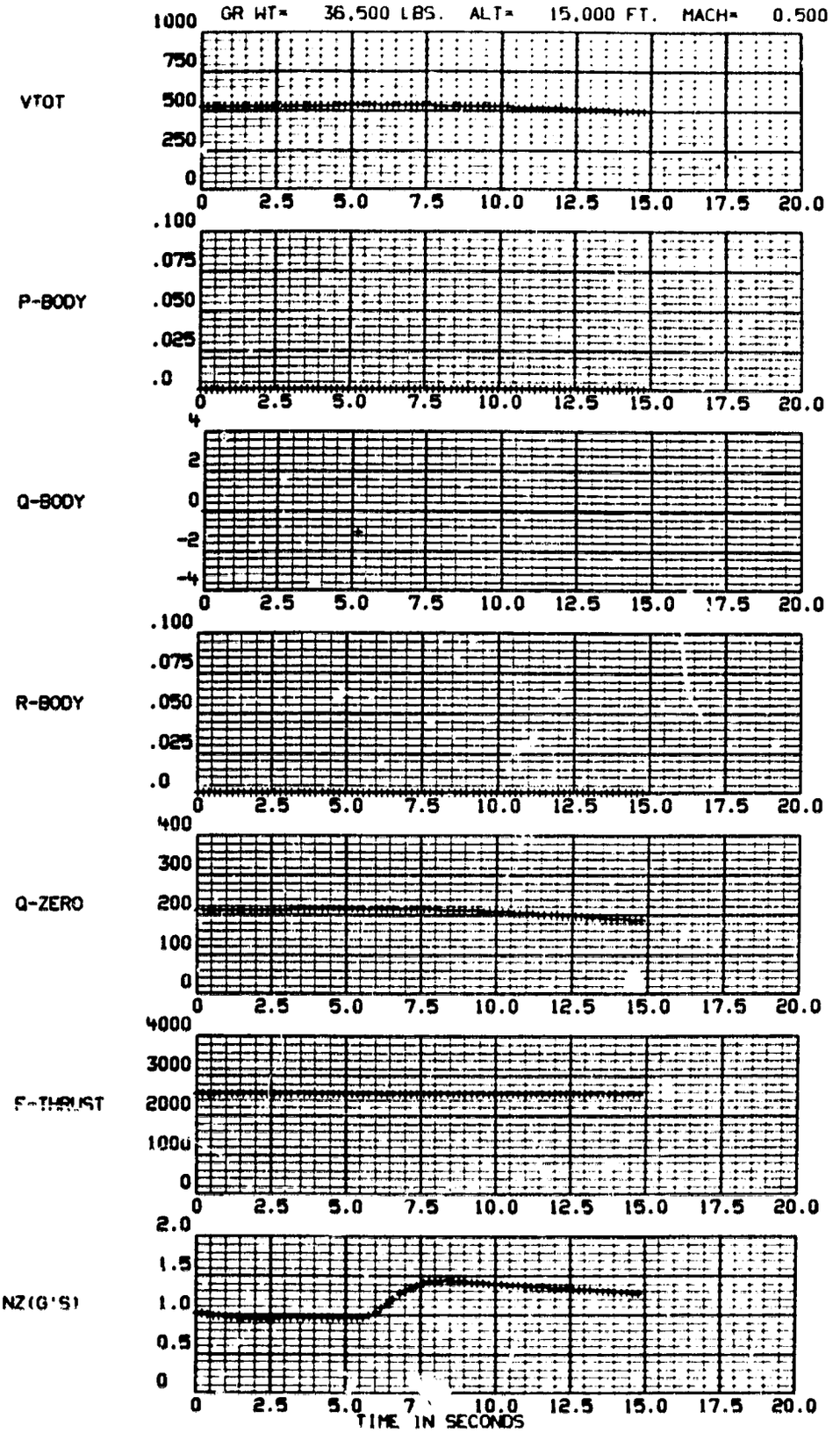

Figure 36b. Time History Results, Run 1a.

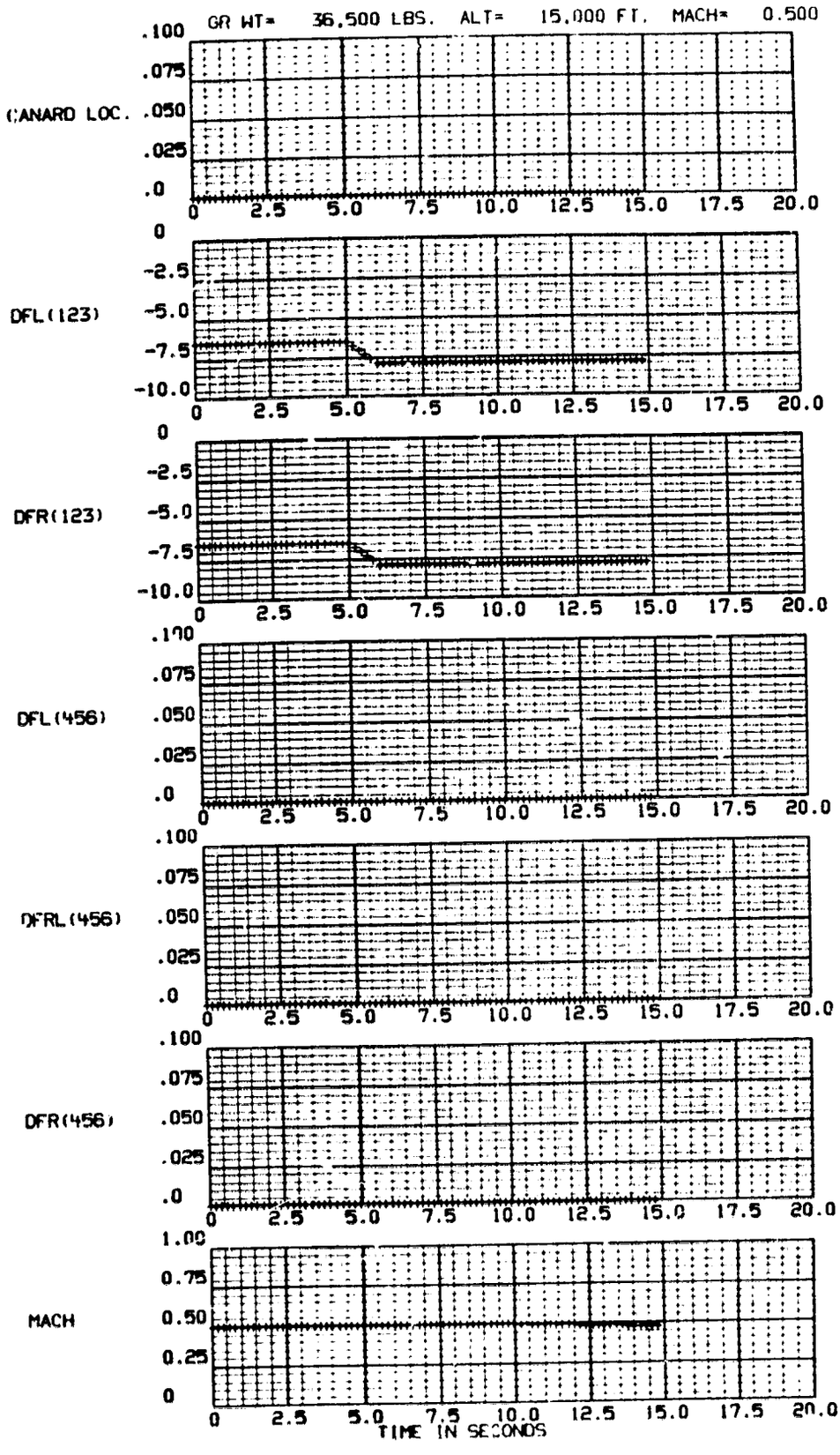

RUN 1a

Figure 36c. Time History Results, Run 1a.

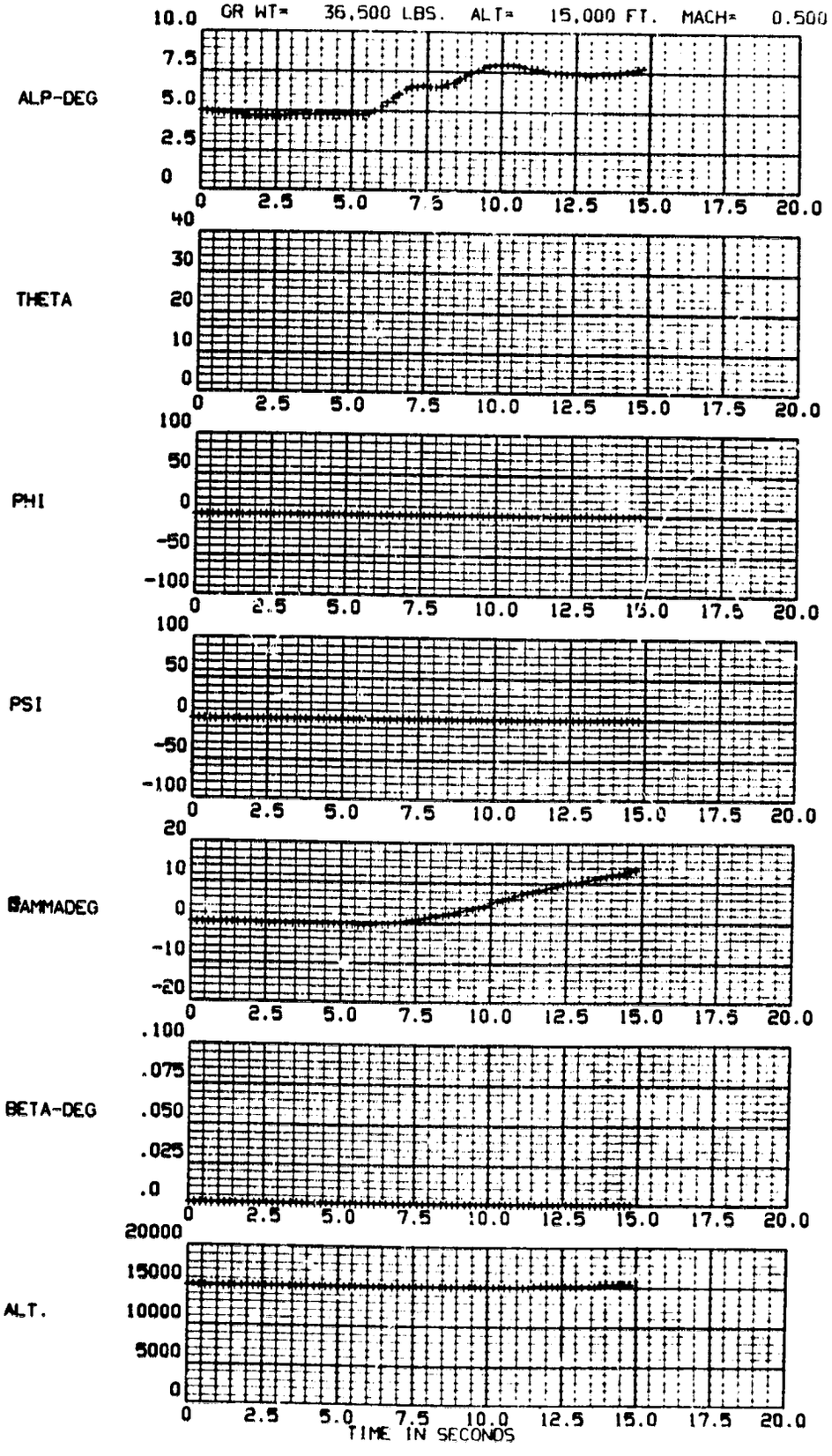

Figure 37a. Time History Results, Run 1b.

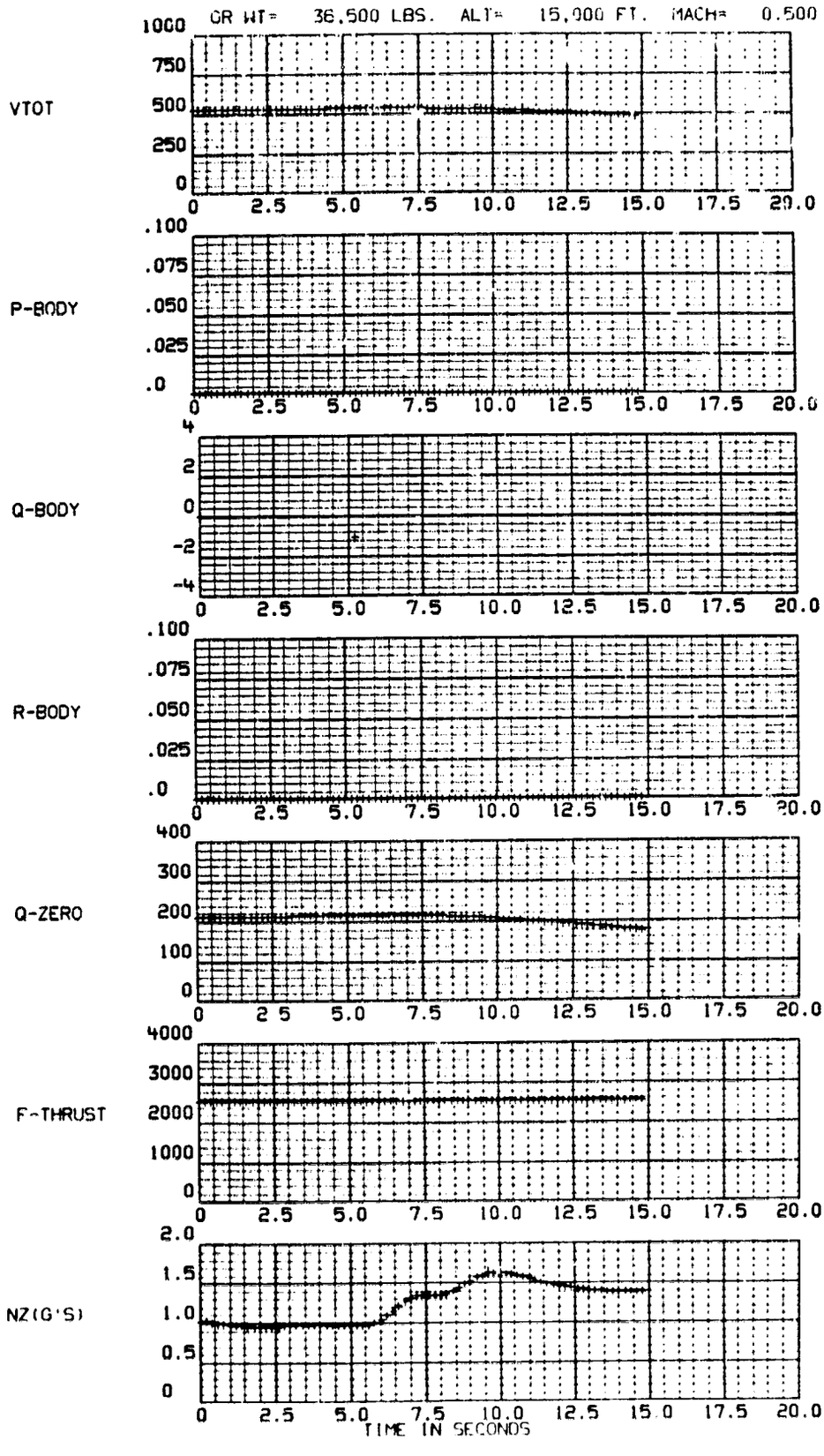

Figure 37b. Time History Results, Run 1b.

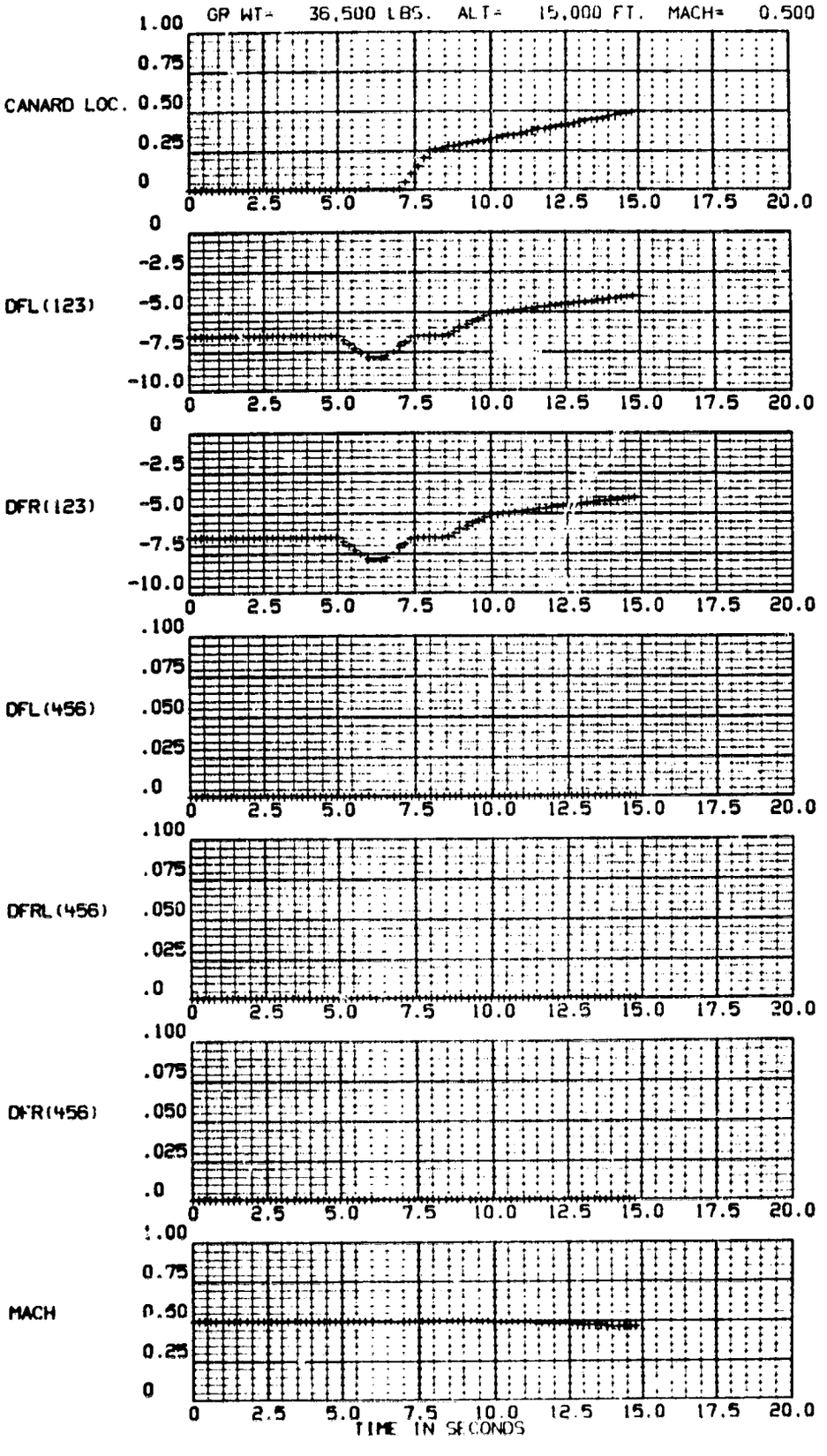

Figure 37c. Time History Results, Run 1b.

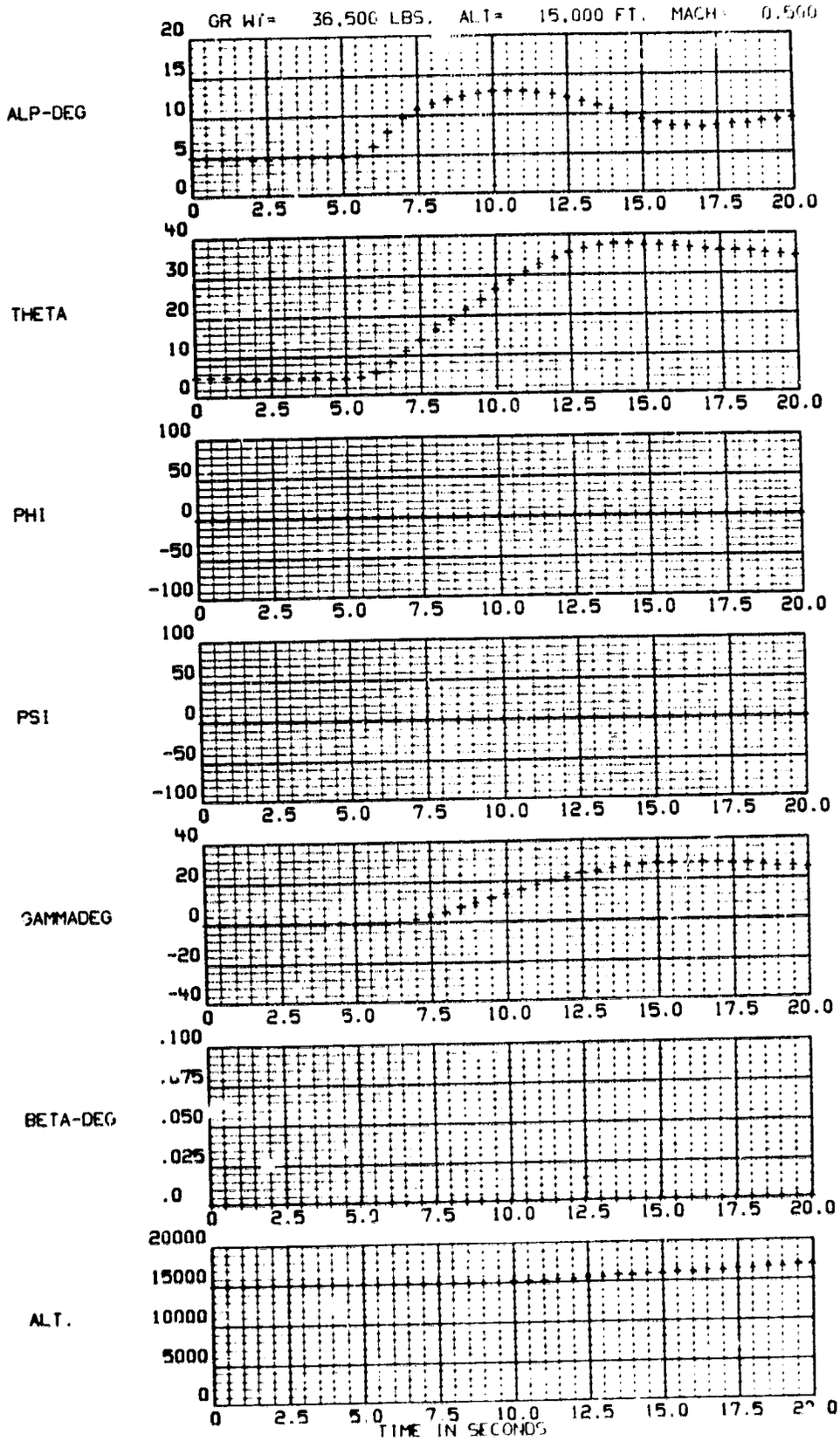

Figure 38a. Time History Results, Run 2.

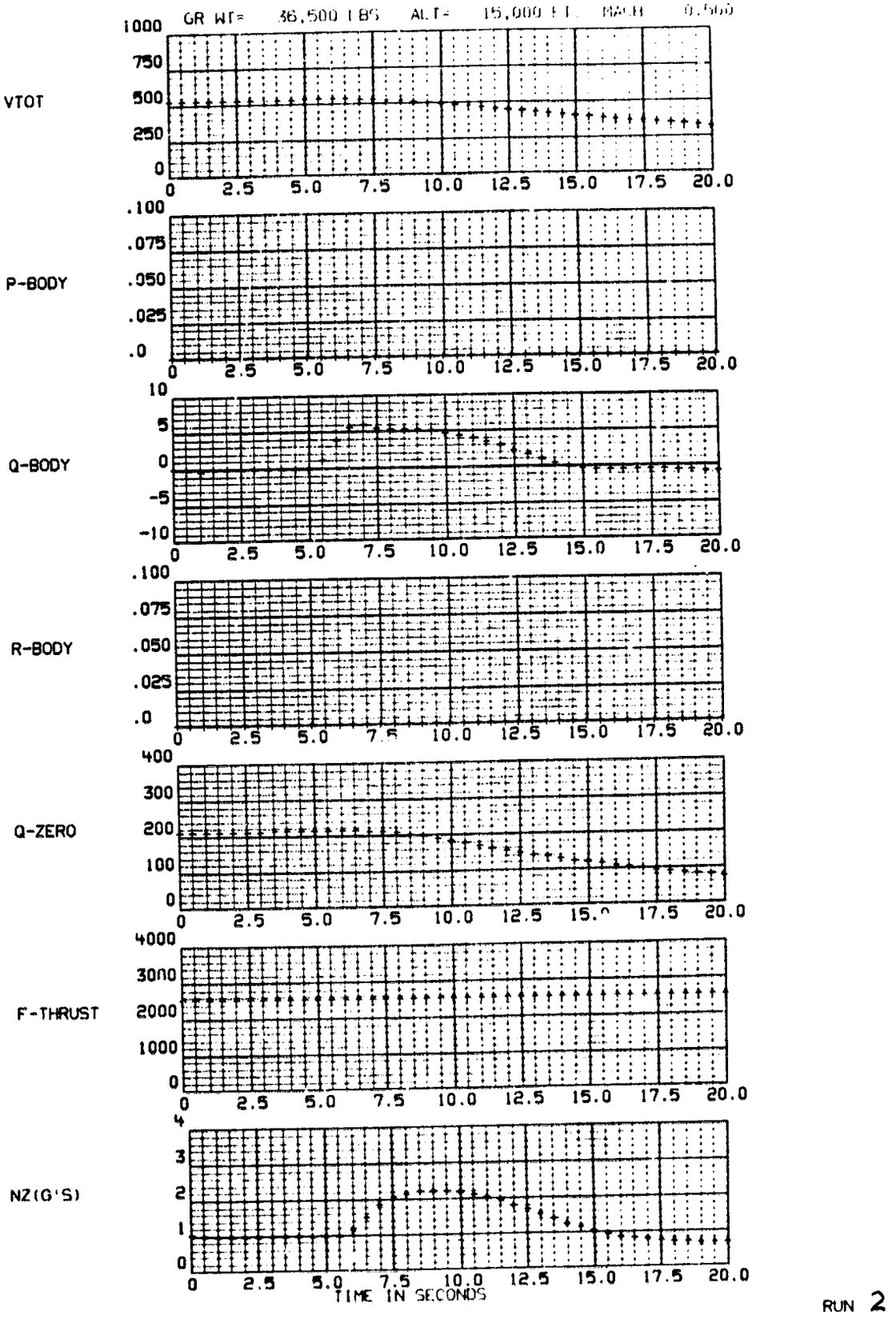

Figure 38b. Time History Results, Run 2.

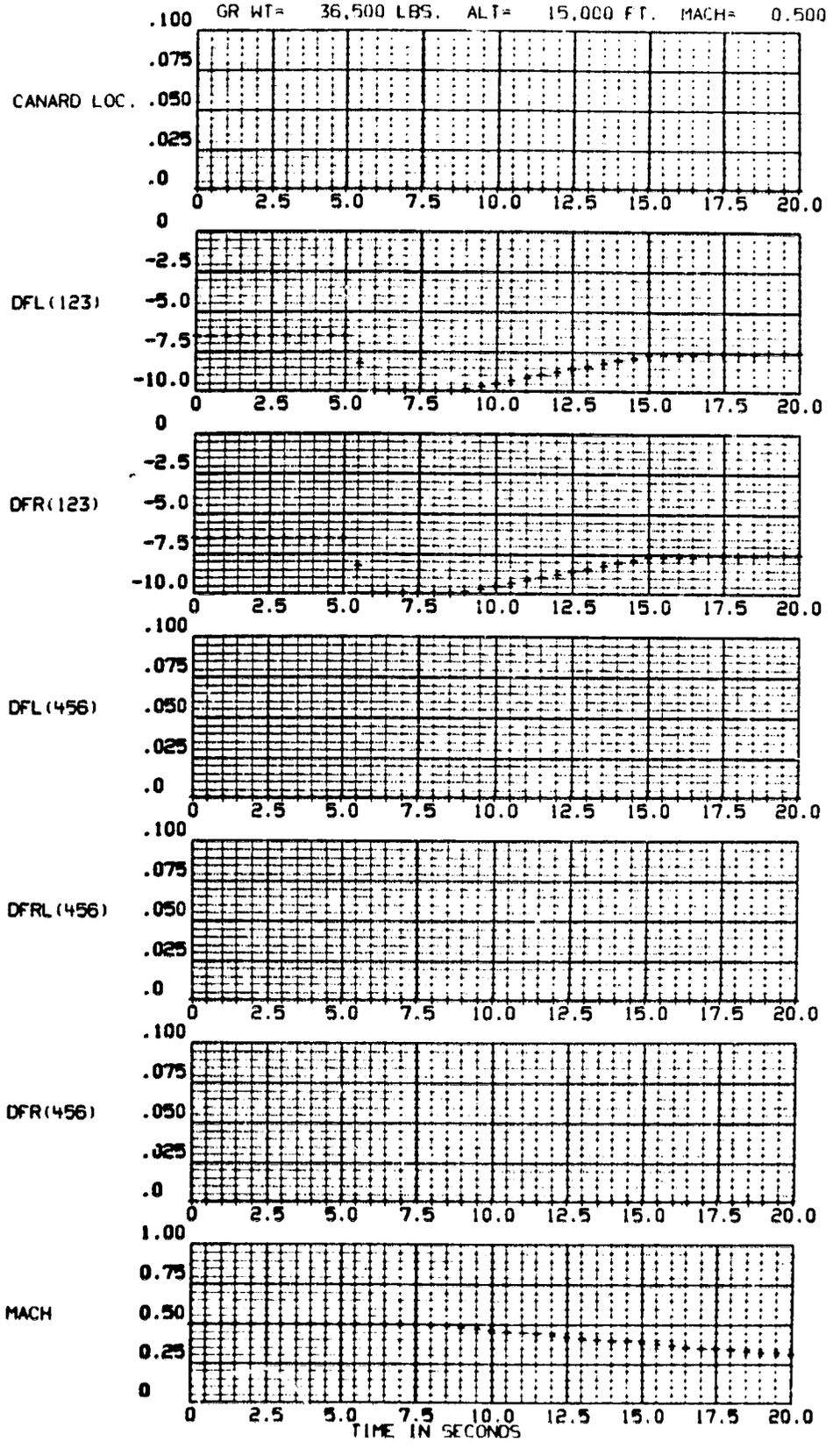

Figure 38c. Time History Results, Run 2.

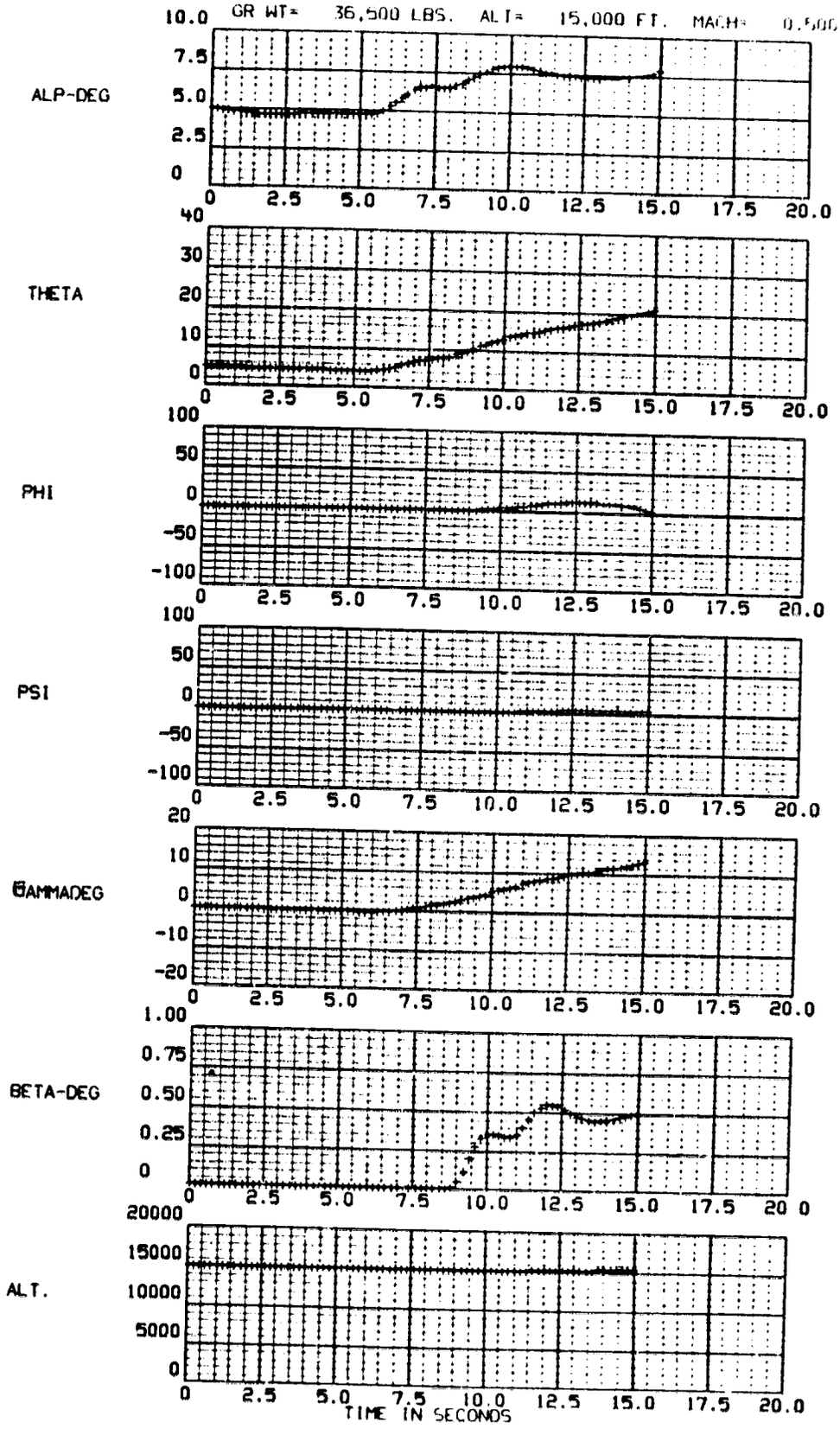

Figure 39a. Time History Results, Run 4.

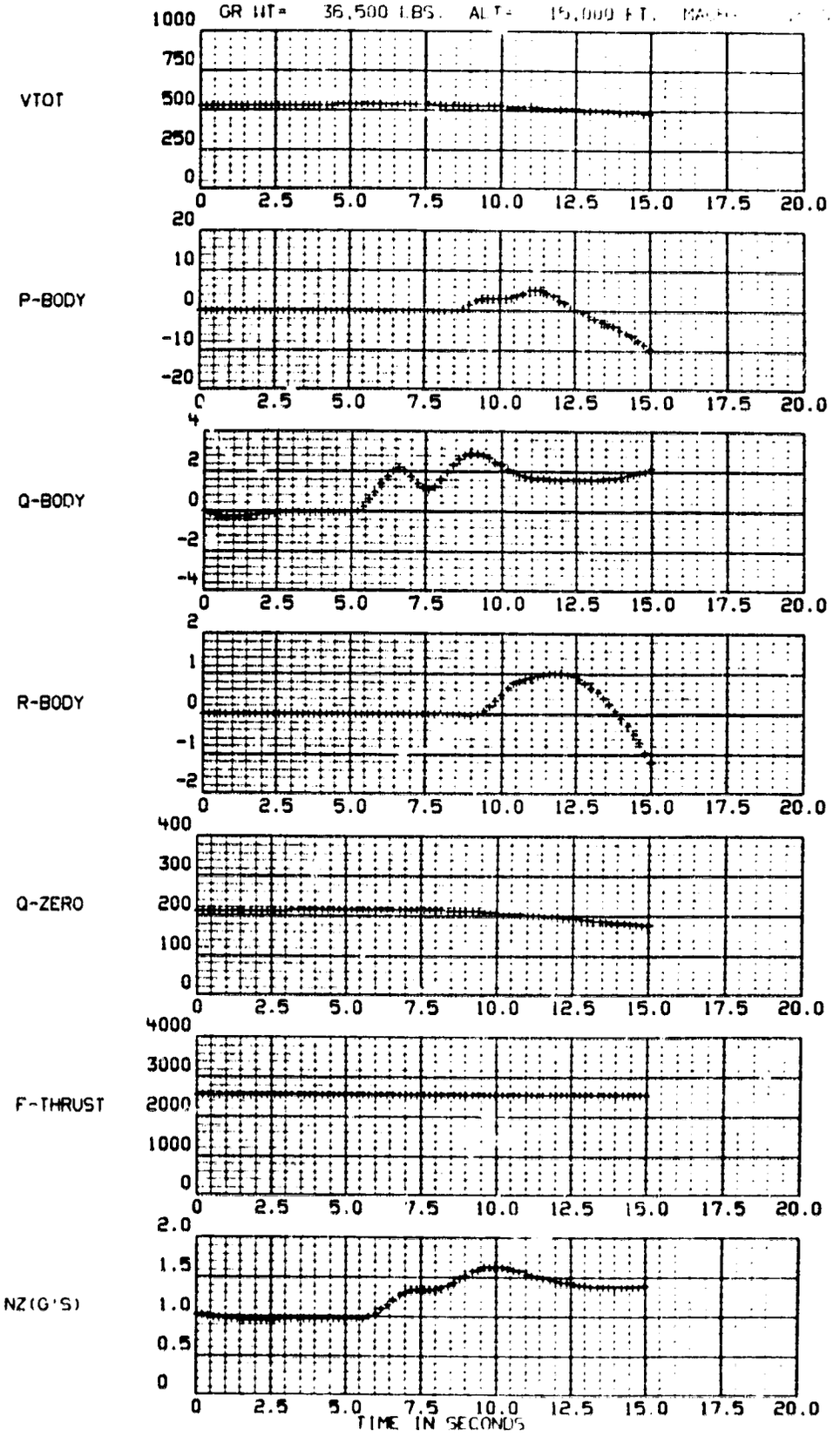

Figure 39b. Time History Results, Run 4.

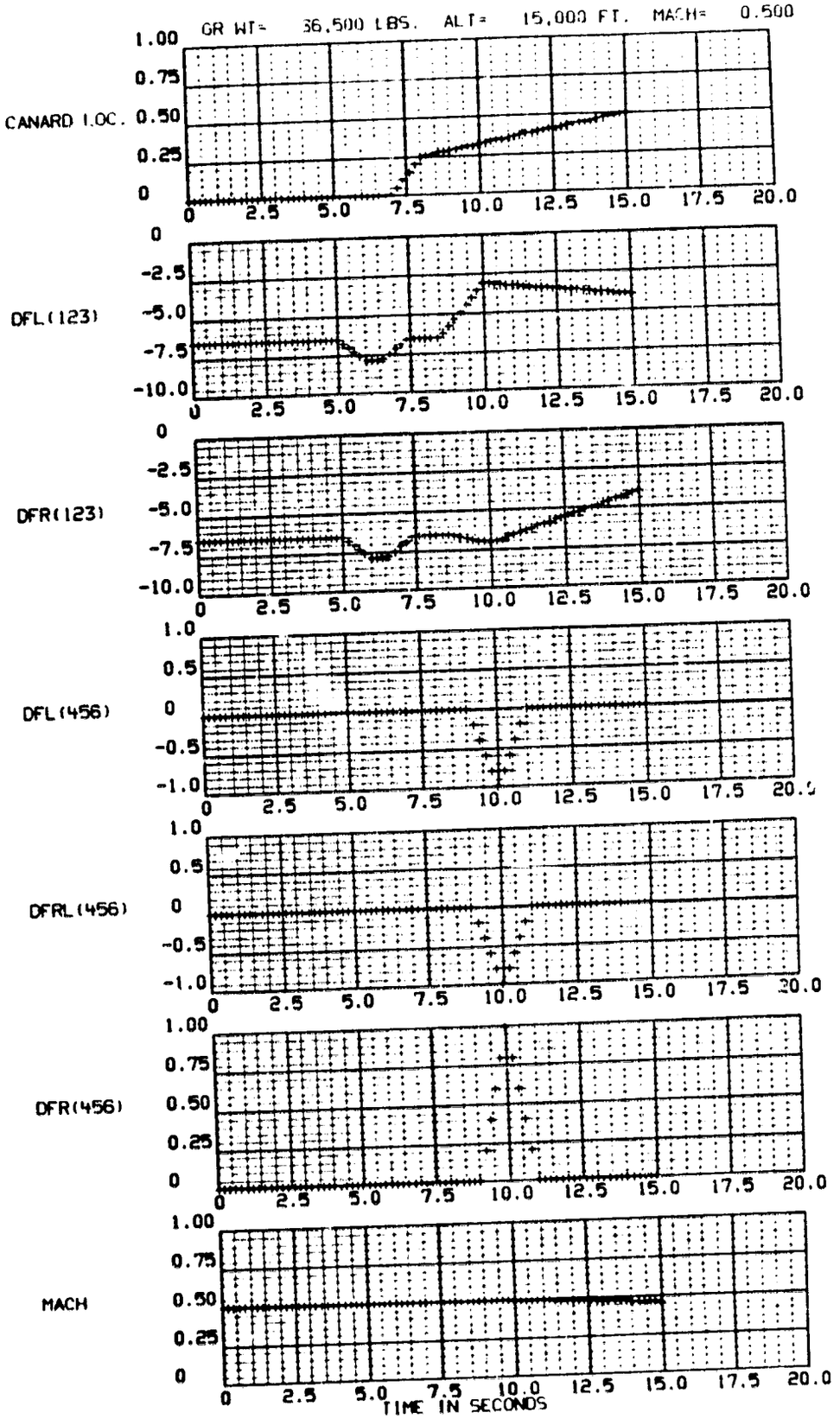

Figure 39c. Time History Results, Run 4.

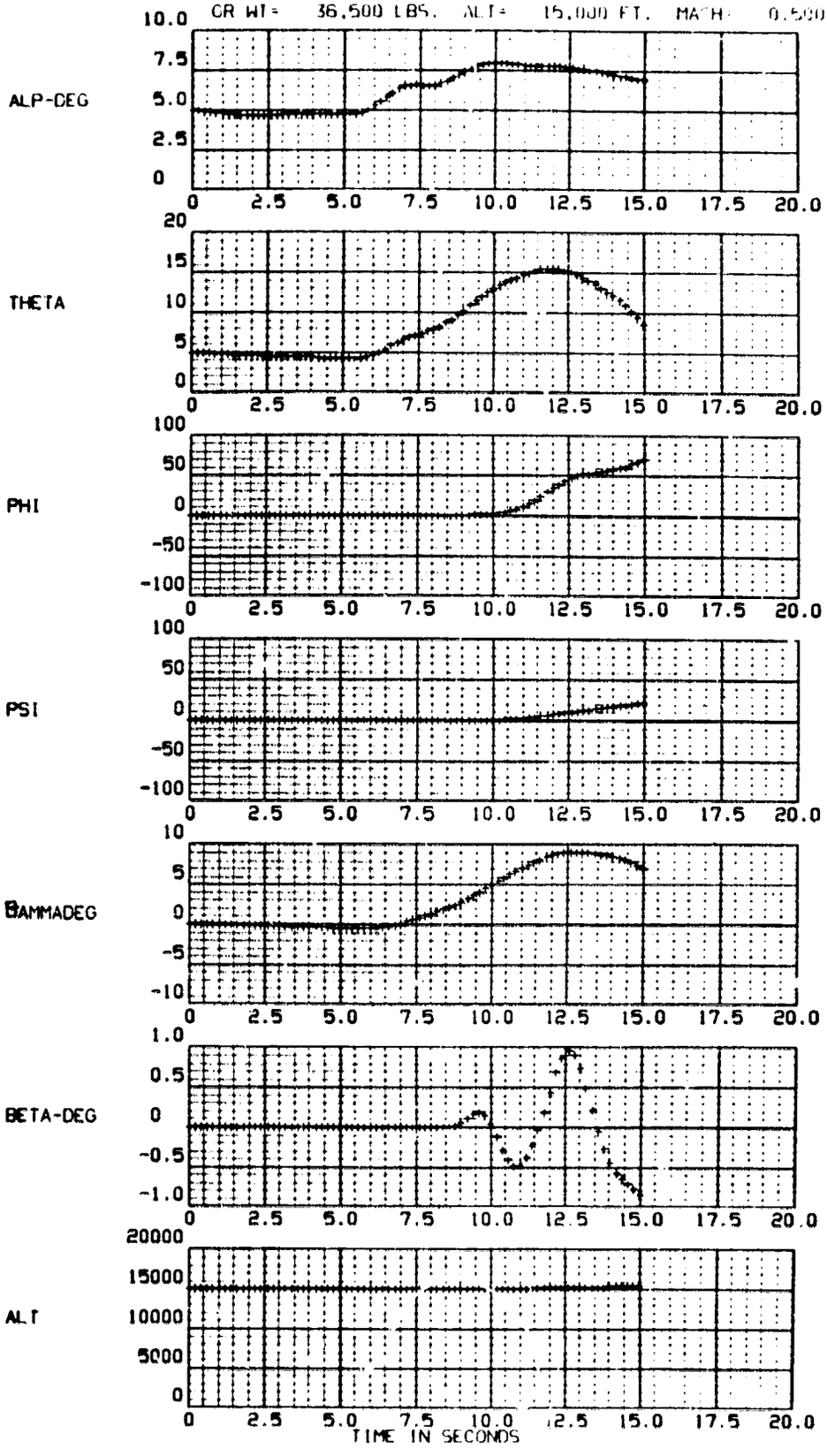

Figure 40a. Time History Results, Run 5.

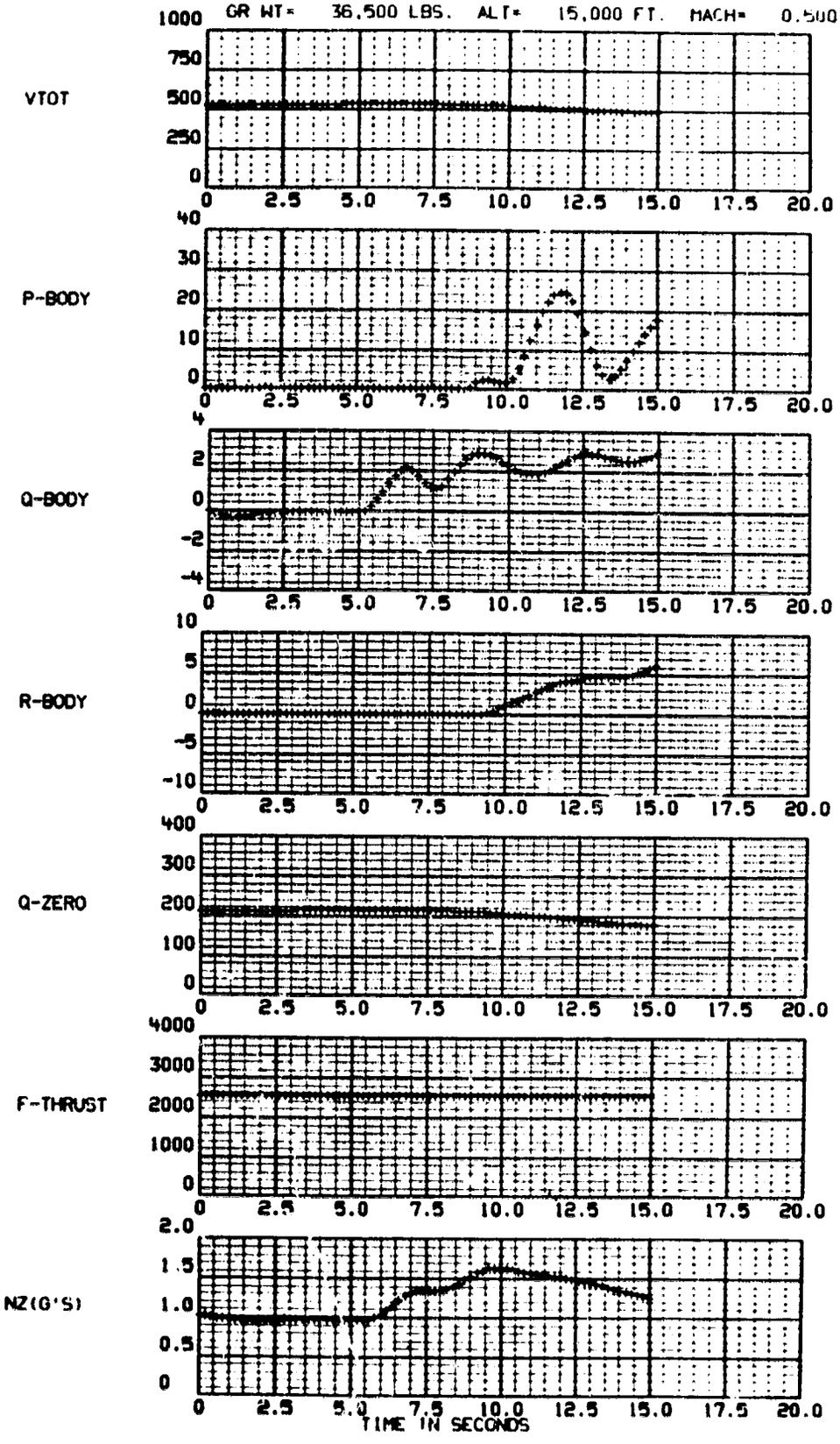

Figure 40b. Time History Results, Run 5.

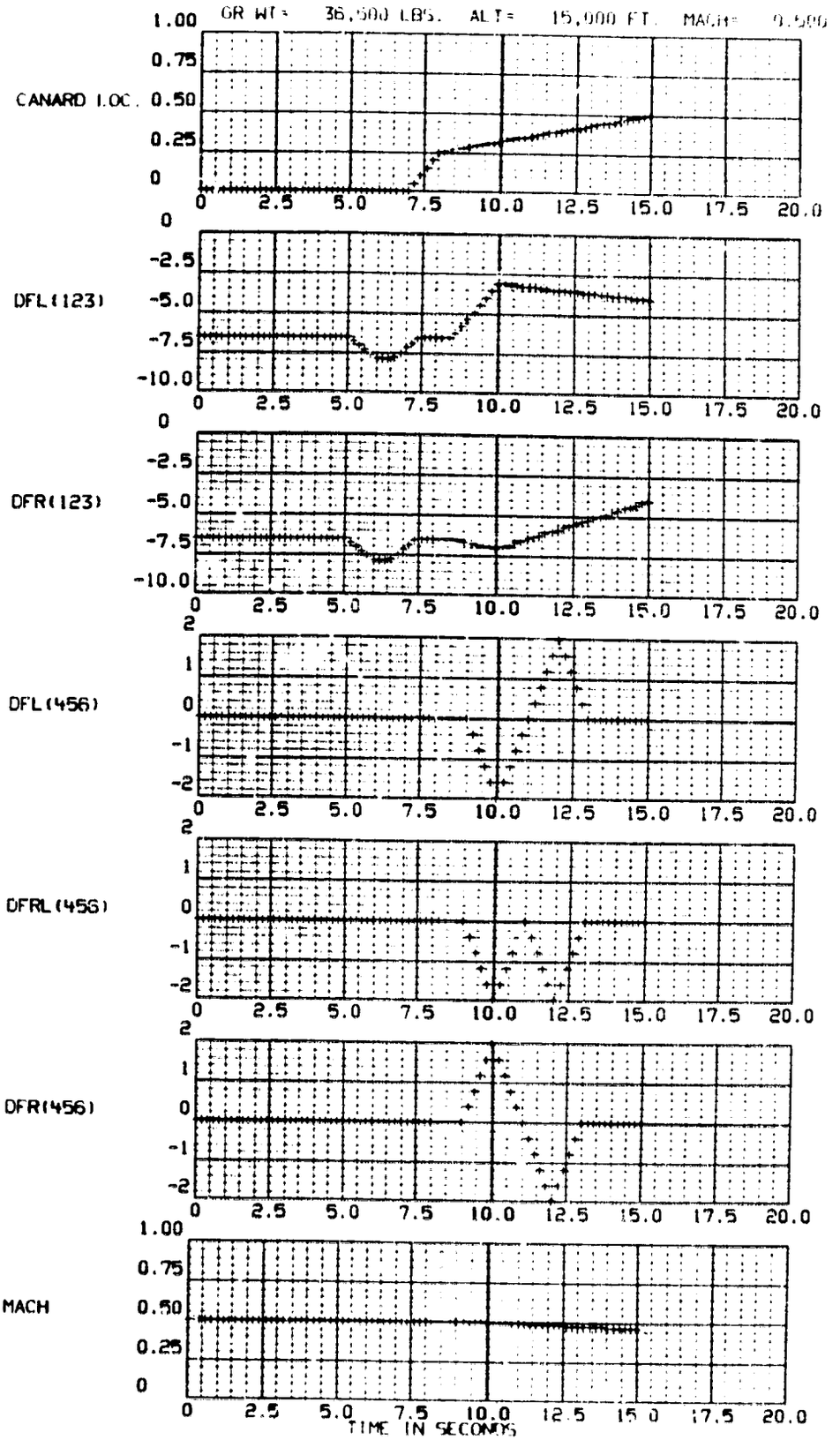

RUN 5

Figure 40c. Time History Results, Run 5.

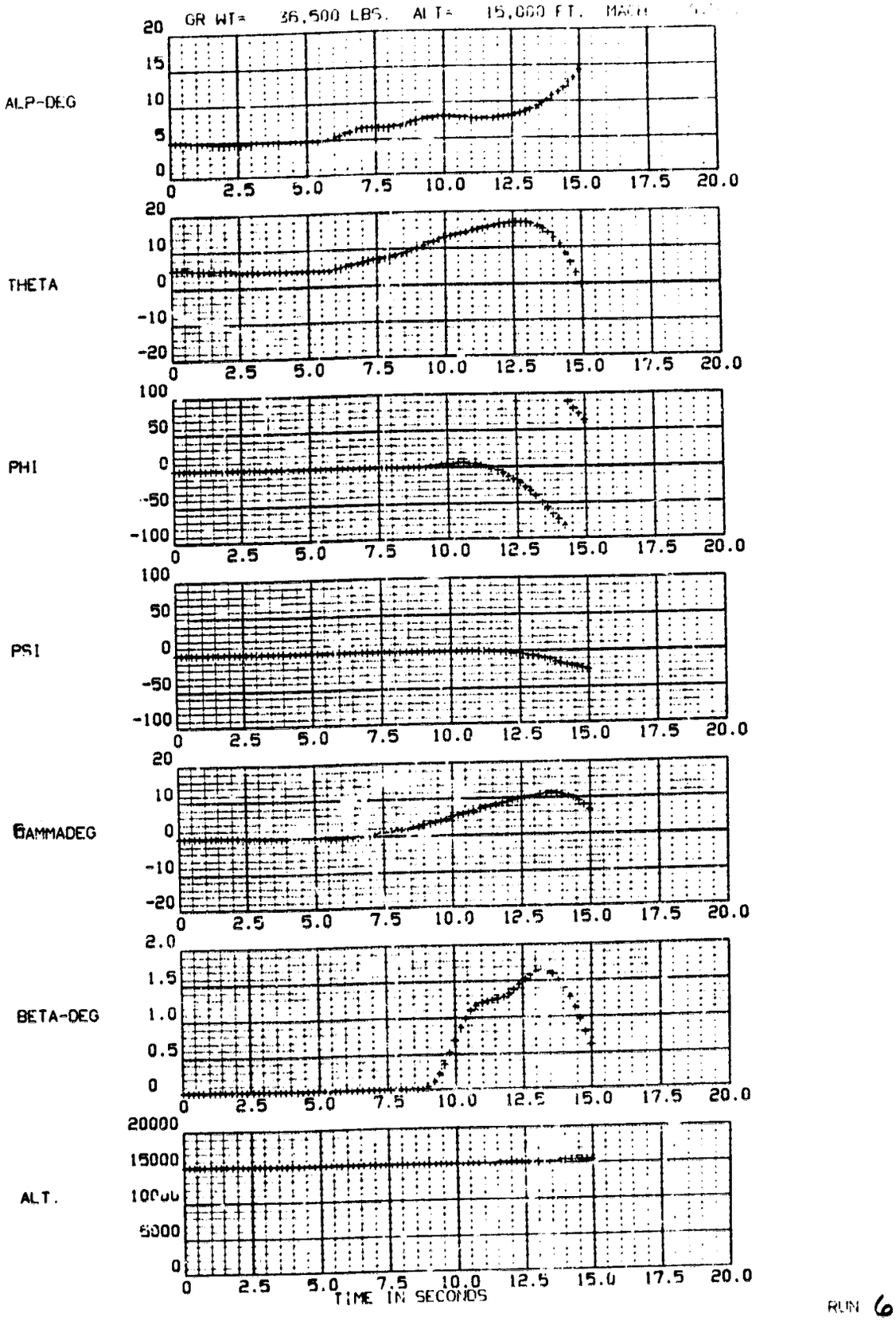

Figure 41a. Time History Results, Run 6.

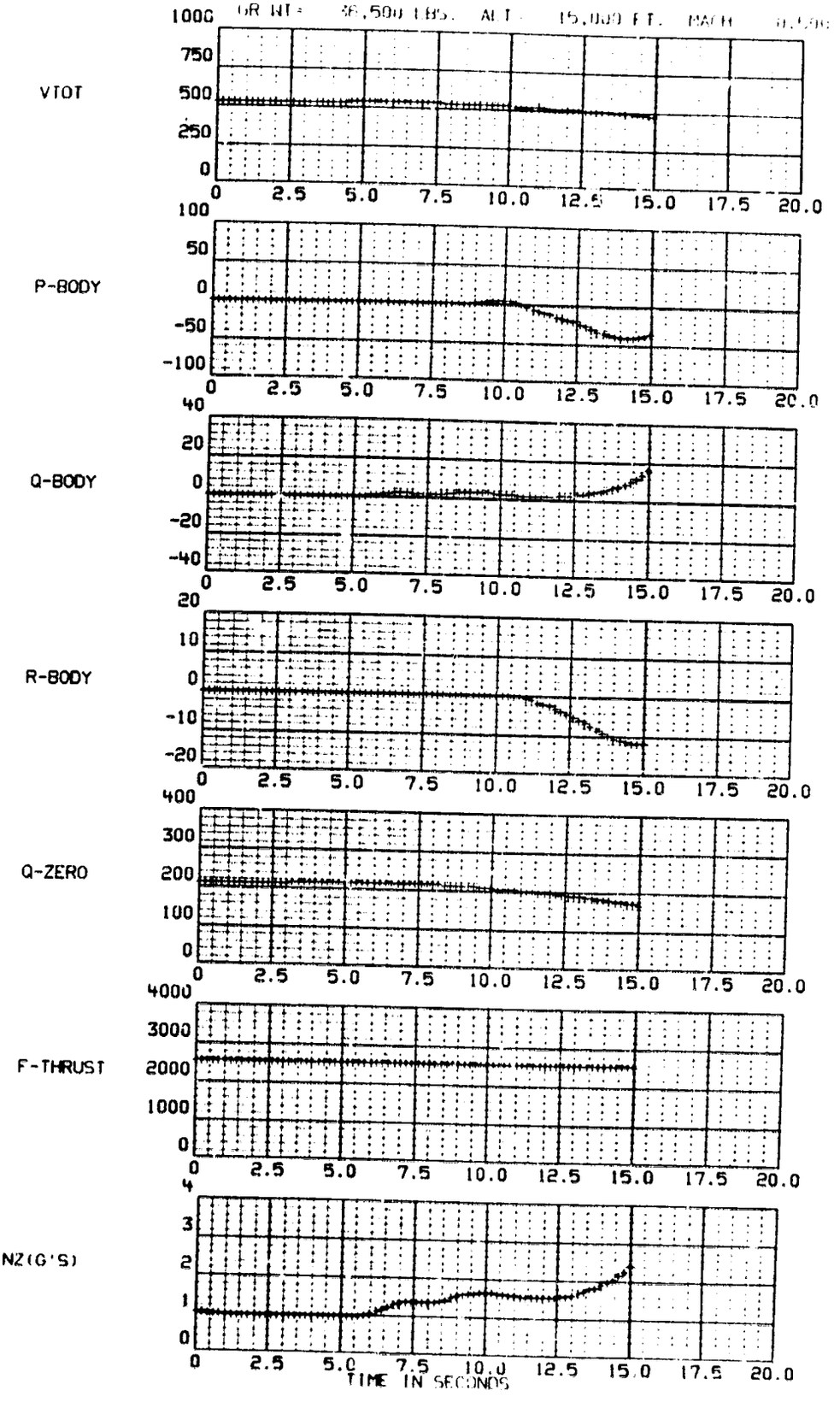

RUN 6

Figure 41b. Time History Results, Run 6.

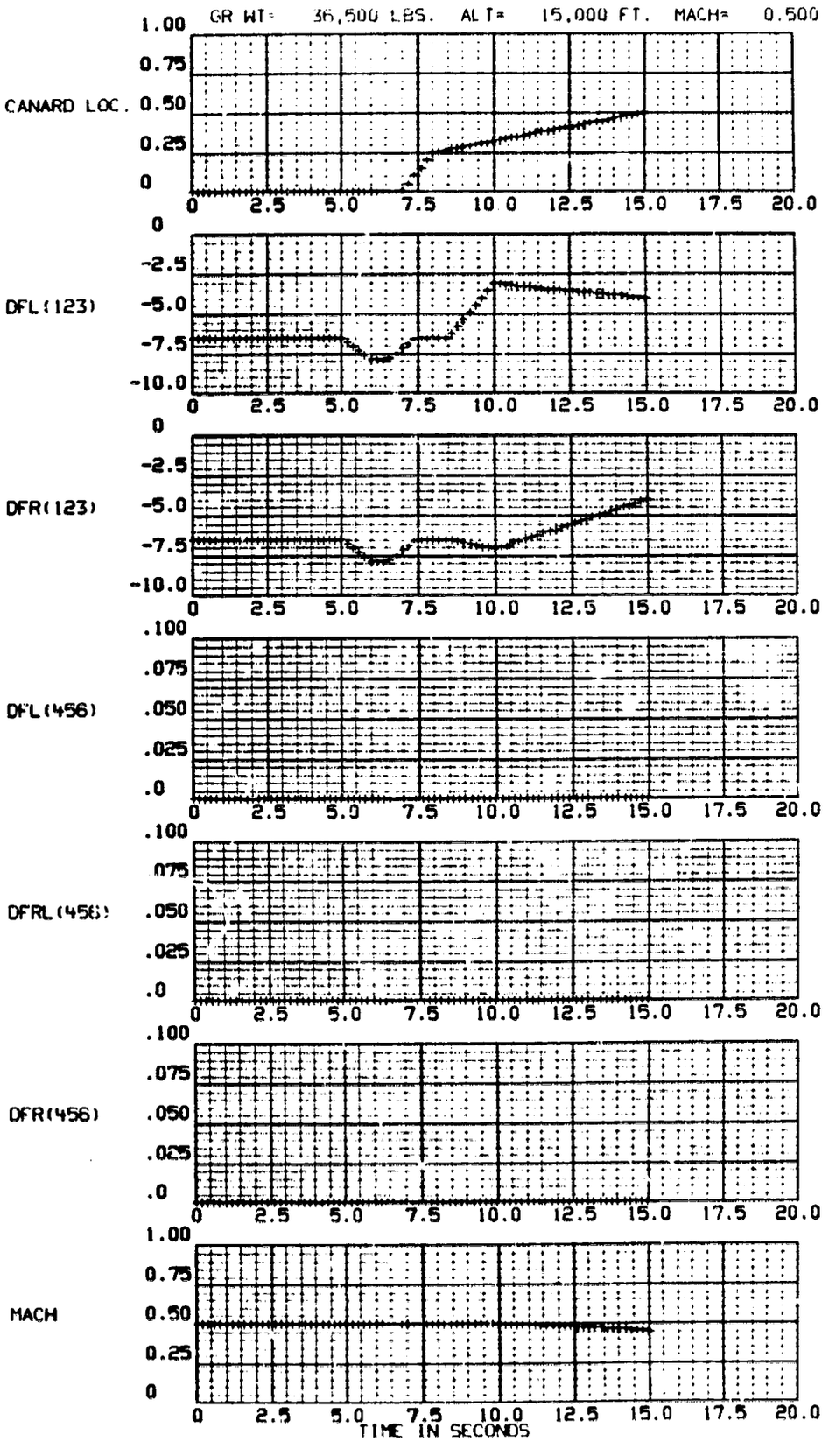

Figure 41c. Time History Results, Run 6.

FIGURE 42. SP/MF-MODIFIED GEOMETRY

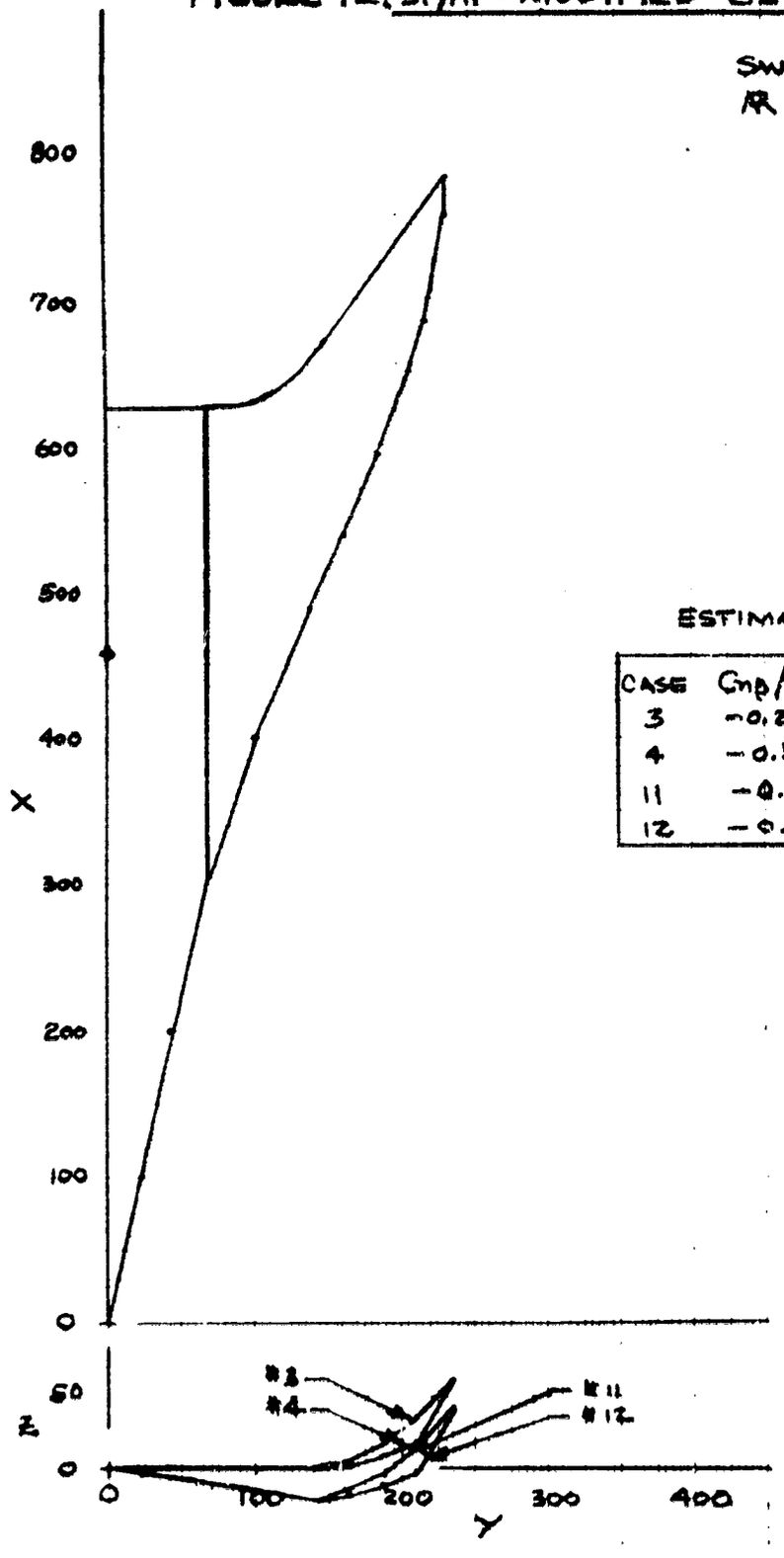

ESTIMATE

CASE	C_{np}/C_{l_β} (W. FUS.)	
3	-0.287	BASE
4	-0.567	MOD.
11	-0.311	BASE $\beta = -1$
12	-0.817	MOD. $\beta = -1$

Section IV

AERODYNAMIC DESIGN

The objectives of the detailed design procedure were to define the twist, camber and thickness distributions to obtain minimum potential form drag and viscous form drag at the design Mach number and lift coefficient.

The planform shape and wing volume defined for the basepoint configurations provided the inputs to the detailed design efforts, figures 43 through 45. The optimum twist and camber were obtained for the design lift coefficient under trimmed conditions and additionally satisfied constraints to produce mild camber shapes. The wing thickness distribution and the canopy and nacelle area distributions were optimized for minimum vehicle wave drag.

CAMBER AND TWIST

The camber and twist distributions were obtained at the design point for each configuration, D575-2A, -3, -4. The design lift coefficient and CG for each configuration are shown in table VI. For the design C_L the principal constraints involved were that the center of pressure of the basic load act at the CG and that the camber shapes produced exceptable pressure distributions such that viscous form drag would be minimized.

The optimized camber and twist distributions were computed with the Nonplanar Unified Distributed Panel Wing-Body Program. For a given planform, Mach number and C_L, the program computes the optimum twist and camber for minimum vortex and zero suction drag. The additional constraints available are: specification of the aerodynamic center and/or the spanwise variation of the center of pressure location.

The twist and camber were optimized for zero rather than 100 percent suction drag because of the following considerations. The twist and camber resulting from the supersonic optimization for zero suction drag, when analyzed will produce a 100 percent suction drag polar which is approximately tangent to the zero suction drag polar at the design condition. However, the supersonic optimization for 100 percent suction drag results in a twist and camber distribution that, when analyzed for zero suction drag, produces a drag polar which is not tangent at the design point. The difference between the zero and 100 percent suction drag may be of sufficient magnitude so that any loss of leading edge suction, which will always occur, will result in a substantial penalty.

For each configuration, M=1.6, 2.0, 2.5, the twist and camber were optimized for several combinations of the available constraints. These were (1) no constraint on the aerodynamic center (2) aerodynamic center at the CG and (3) trimmed condition with a specified spanwise variation of center of pressure. For the third case the spanwise distribution of center of pressure was constrained to that of the additional load. The camber shapes produced by the first two optimizations were essentially identical. For the

third case, the addition of the spanwise center of pressure constraint produced milder camber shapes with, of course, a small increase in drag. These camber shapes were those finally selected because, in comparison with those produced by the first two optimizations, (1) the milder adverse pressure distributions near the trailing edge were more acceptable with regard to viscous form drag (2) the possibility of large variations in center of pressure at off-design conditions was minimized and (3) the drag penalty was not substantial.

The final twist and camber distributions for the three configurations are shown on figures 46 through 54.

WING THICKNESS

To obtain minimum vehicle wave drag the volume distribution of each configuration was optimized with the Wave Drag Optimization Program. The total configuration volume was retained and critical sections were constrained to the minimum required area.

The Wave Drag Optimization Program determines optimum configuration geometry to minimize wave drag due to thickness. One or more components may be optimized simultaneously, or the components may be optimized sequentially. In the latter procedure a component which has been optimized may be saved within the program and the optimized geometry used in subsequent optimizations of the other components.

The configuration components are classed as either planar or nonplanar bodies. The nonplanar component is optimized with respect to cross sectional area distribution. One or more sections may be constrained to a given area. For planar components both the spanwise and chordwise thickness distributions may be optimized. Constraints may be applied at any particular point by specifying the local thickness, t/2c.

The configurations were modelled as follows. The inboard blended wing-fuselage was treated as a planar component defined initially by a series of airfoils with the same section profile but a variable spanwise thickness distribution. The wing outboard of the nacelle was defined similarly. The canopy was defined as the volume above the wing section. In this manner the fraction of the total volume attributed to the canopy was minimized. Each nacelle was modelled as two semi-elliptical bodies positioned above and below the wing. Thus, the wing thickness distribution was continuous across the span. It was necessary to follow this procedure for the D575-3 and -4 configurations since the semi-conical inlet is located below the wing and the nacelle is not symmetrical with respect to the wing chord plane. The D575-2A configuration has an elliptical leading edge inlet and the nacelle is symmetric relative to the wing chord plane. For this configuration (-2A) the final optimized thickness distributions were obtained with the above procedure. In addition, for the -2A the optimization was obtained with an alternative representation of the nacelle. The nacelle was treated as a single body and the wing was broken at the inboard and outboard junctures. The optimization produced a drag level that was identical to that obtained with the formerly described procedure of maintaining a continuous wing thickness distribution across the span.

For each configuration the components were optimized sequentially: canopy, nacelle and then all planar components. This procedure proved to be the most effective for these configurations. The nonplanar components were modelled so that they contributed only a small fraction of the total volume.

After the optimized canopy and nacelle geometry was determined the optimized components were saved within the program. Then all planar components were optimized simultaneously. In the process constraints were added where required to maintain minimum thickness levels for structural considerations. Constraints were added to produce acceptable chordwise thickness distributions. Specifically, positive curvature was maintained in the regions forward of the maximum thickness for all airfoil sections to minimize viscous form drag. The wing thickness distributions are shown on figures 55 through 57 for the three configurations. The optimized area distributions for the canopy and nacelle are shown on figures 58 through 60.

NACELLE LOCATION

The optimum placement of the nacelles depends upon several factors: stability and control, armament placement, inlet operation and wave drag. An examination of the effect on wave drag due to thickness was made for several alternate nacelle positions. The primary location, and that for which all detailed design and analysis was based on, is shown on figure 61 The outboard edge of the nacelle is located at 60 percent semispan for all configurations.

Wave drag was computed for the D575-2A for an alternate nacelle location, figure 61. The nacelle was moved inboard so that the thrust axis was at $\eta = .23$. The optimization procedure described previously was repeated for the alternate configuration. A new wing thickness distribution resulted but the total wave drag was the same as the basic configuration. A comparison of the optimized spanwise distribution of maximum wing thickness is shown on figure 61 for both nacelle locations.

For the D575-3 configuration two alternate nacelle locations were analyzed. The nacelle was first moved inboard so that the thrust axis was at $\eta = .34$. The total wave drag remained the same for this location. The nacelle was then moved forward 70 inches so that the distance from the leading edge to the inlet was the same as that for the basic configuration. The total wave drag for this position was 18 percent higher than the level for the basic configuration analysis.

ANALYSIS

At the design Mach number and for off design supersonic conditions, each configuration, as defined by the optimized twist, camber and thickness distributions, was analyzed with the Total Pressure Drag Program, reference 12. Total pressure drag polars for zero and 100 percent leading edge suction were obtained for each configuration. Also, wave drag due to thickness only was obtained as a function of Mach number.

The Total Pressure Drag Program computes wave drag due to lift and thickness, vortex drag and the interference between lift and volume. The pressure distribution for the basic and additional loads are required inputs and were obtained from the Non Planar Distributed Panel Program.

Drag polars for zero and 100 percent leading edge suction for the three configurations are shown on figures 62 through 64 at the design condition. The approximate tangency of the zero and 100 percent suction polars at the design C_L is verified. For each configuration, polars corresponding to 50 percent leading edge suction were constructed at the design condition and for off-design supersonic operating conditions. The values of C_{LK}, C_{DK} and induced drag factor $K = (C_{D_i} - C_{DK})/(C_L - C_{LK})^2$ are shown for each configuration on figures 65 through 70. These induced drag factors are compared with the theoretical values for delta and arrow wings on figure 71.

The basic wave drag level due to thickness for each optimized configuration is shown on figures 72 to 74 . As noted on the figures, optimizing the geometry for the cruise condition alone did not result in substantial wave drag penalties at off-design conditions.

To determine performance for transonic conditions, the three configurations were analyzed with the Non Planar Distributed Panel Wing-Body Program at M=.9. The optimized twist, camber and wing thickness distributions were used in the analysis. From these results, drag polars for zero leading edge suction were available. 100 percent suction polars were obtained by evaluating the wing efficiency factor e.

Configuration	e
D575-2A	1.1735
-3	1.1711
-4	1.1694

From the results of the Non Planar Distributed Panel Program the lift curve slope and lift at $\alpha = 0$ were obtained for each configuration as a function of Mach number. These results are shown on figures 75 to 77.

An analysis of the isobar pattern was made for transonic operating conditions for the D575-3 configuration for M=.9, C_L = .118, the isobars are shown on figure 78 relative to the actual wing chord plane. As noted on figure 78 , swept isobars have been maintained as required to minimize shock losses and to obtain a high drag divergence Mach number. For the condition shown in figure 78 , M_{DD} was estimated to be 0.95. The nacelle does not substantially affect the isobar pattern, except for a region near the inboard juncture where locally the isobar sweep is reduced.

Estimates of skin friction drag were made for the three configurations. Skin friction drag coefficient for the cruise condition at 45,000 ft and at M=.6, 25,000 ft are shown in table VII.

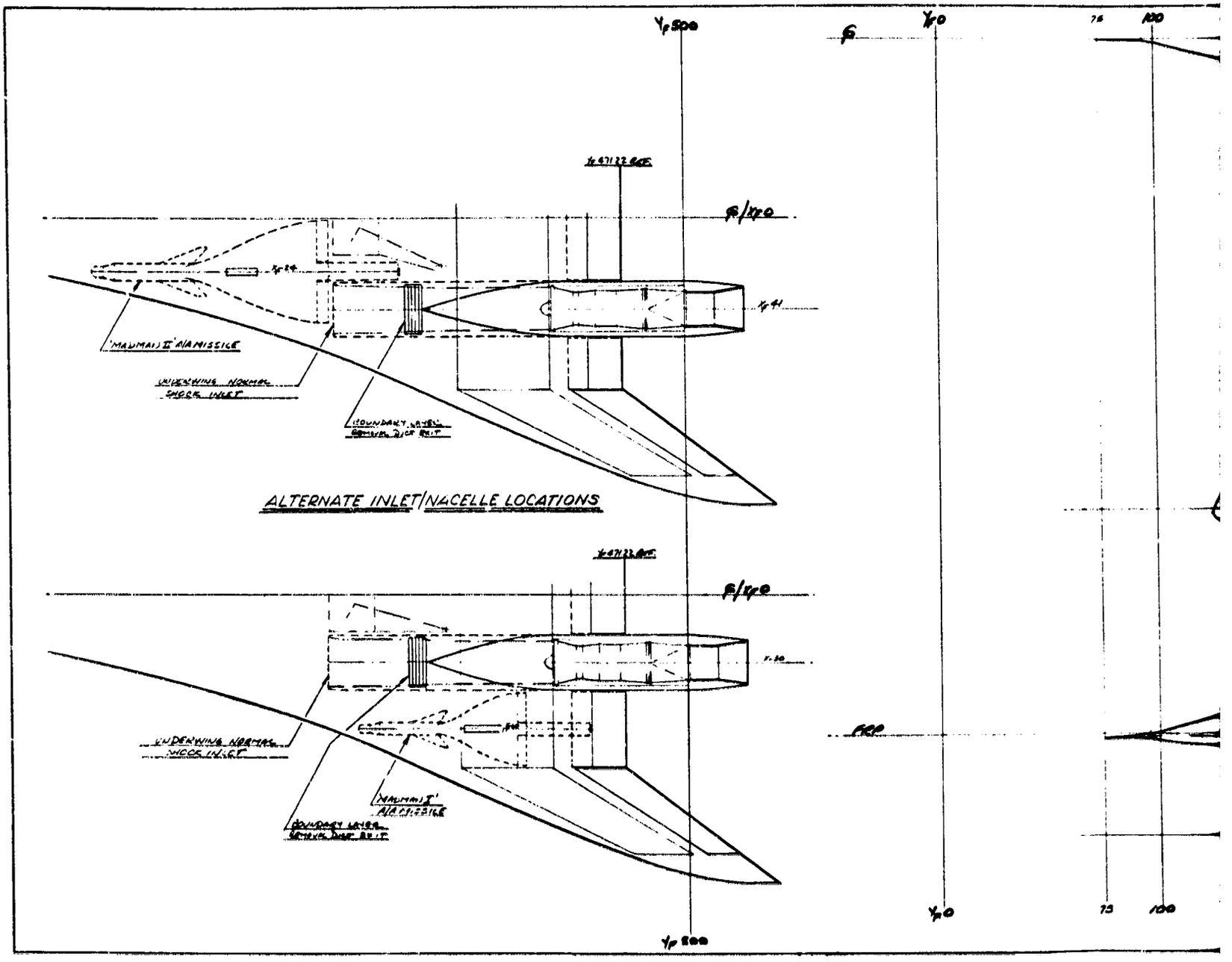

FOLDOUT FRAME

1

ORIGINAL PAGE IS
OF POOR QUALITY

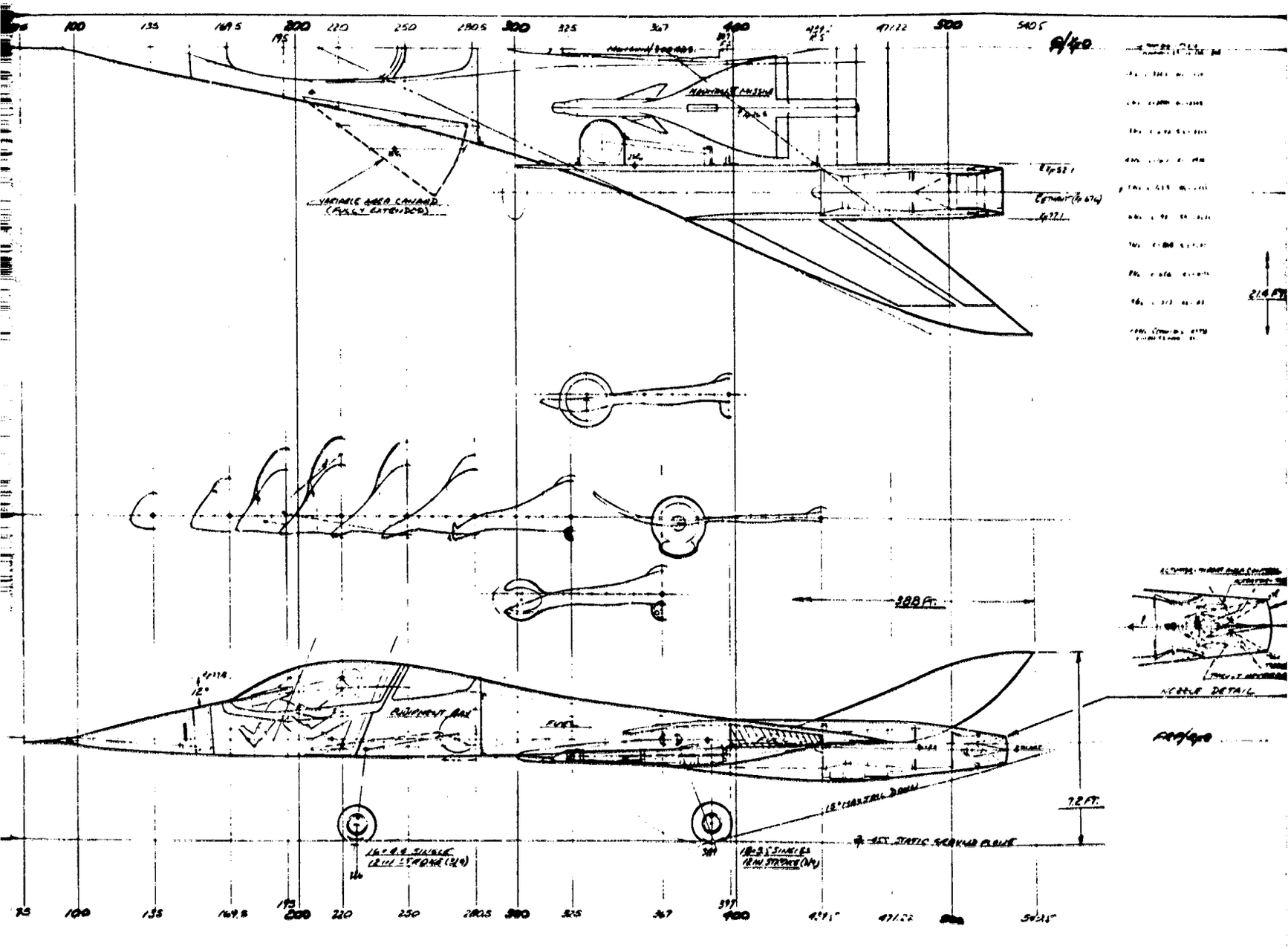

FOLDOUT FRAME

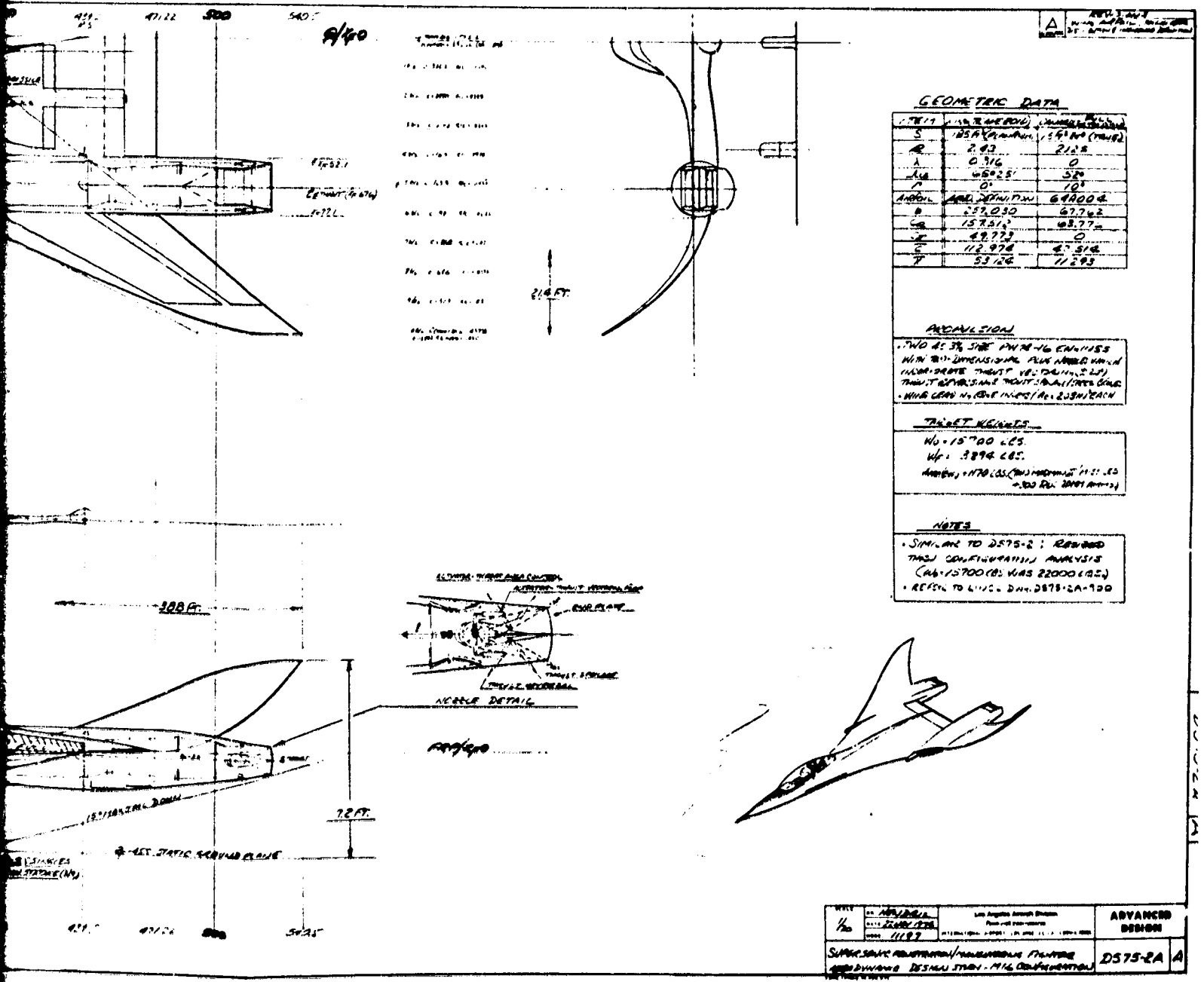

Figure 43. Configuration Layout SP/MF, D575-2A

FOLDOUT FRAME

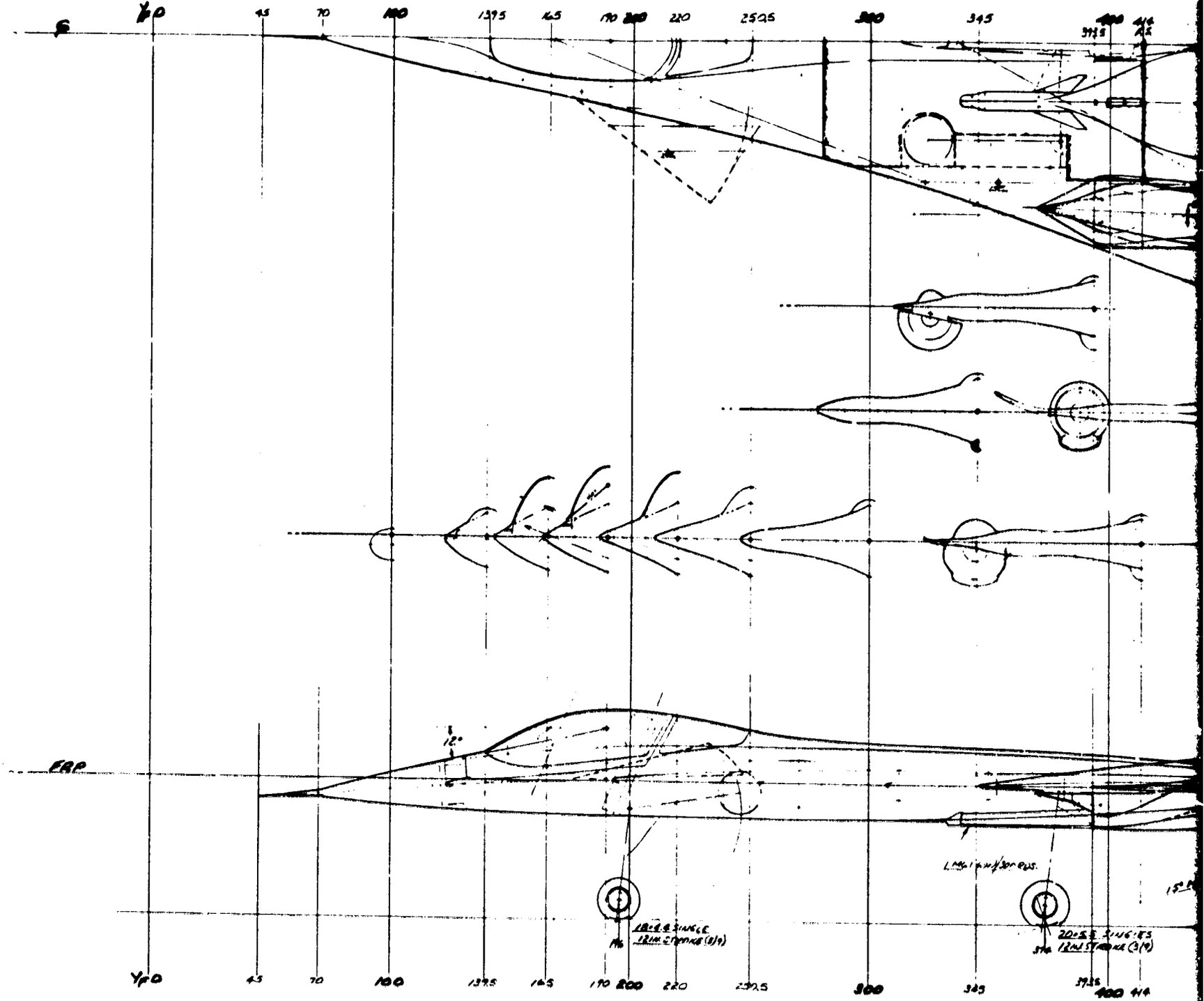

FOLDOUT FRAME

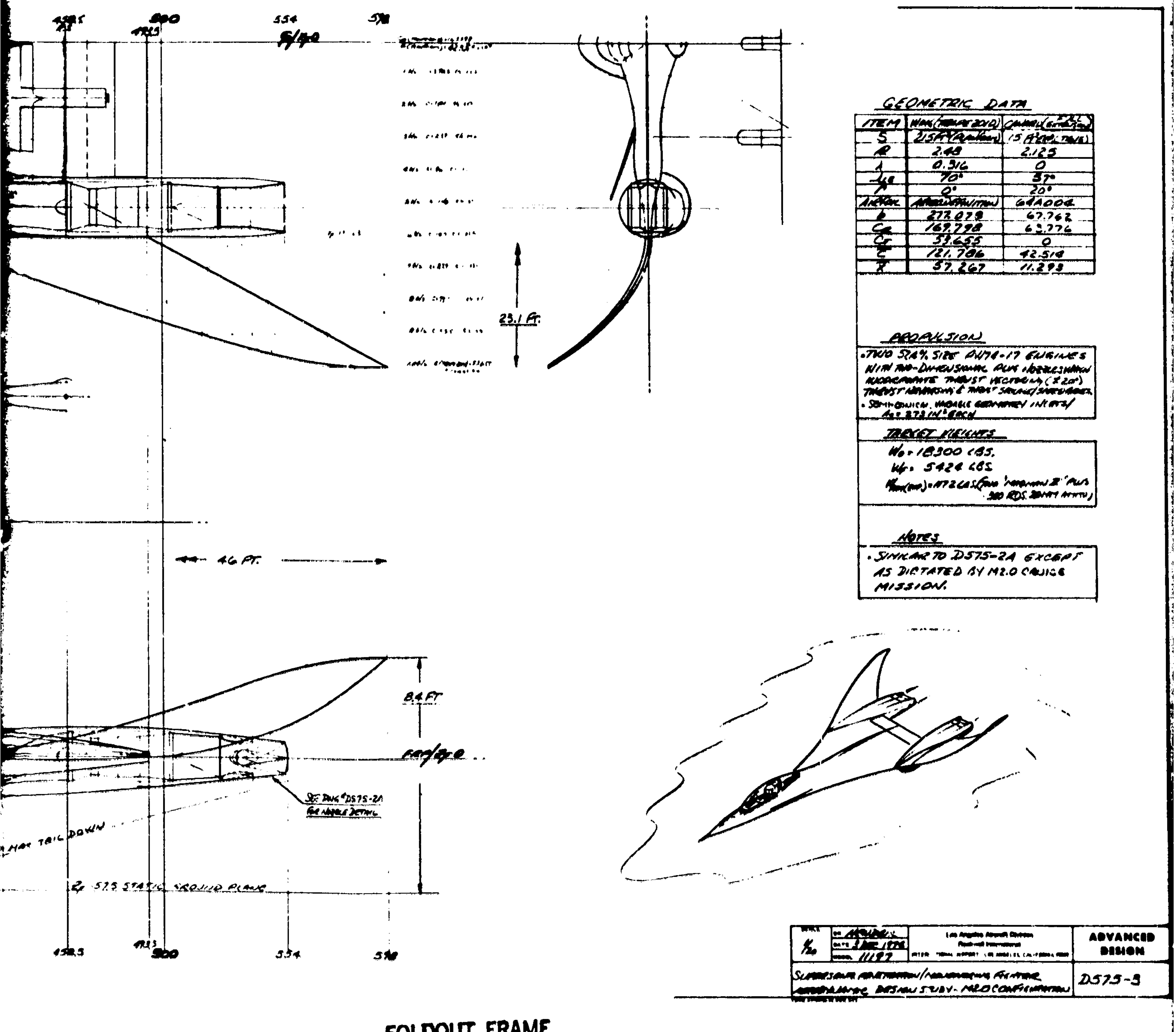

FOLDOUT FRAME

Figure . Configuration Layout-
SP/MF, D575-3

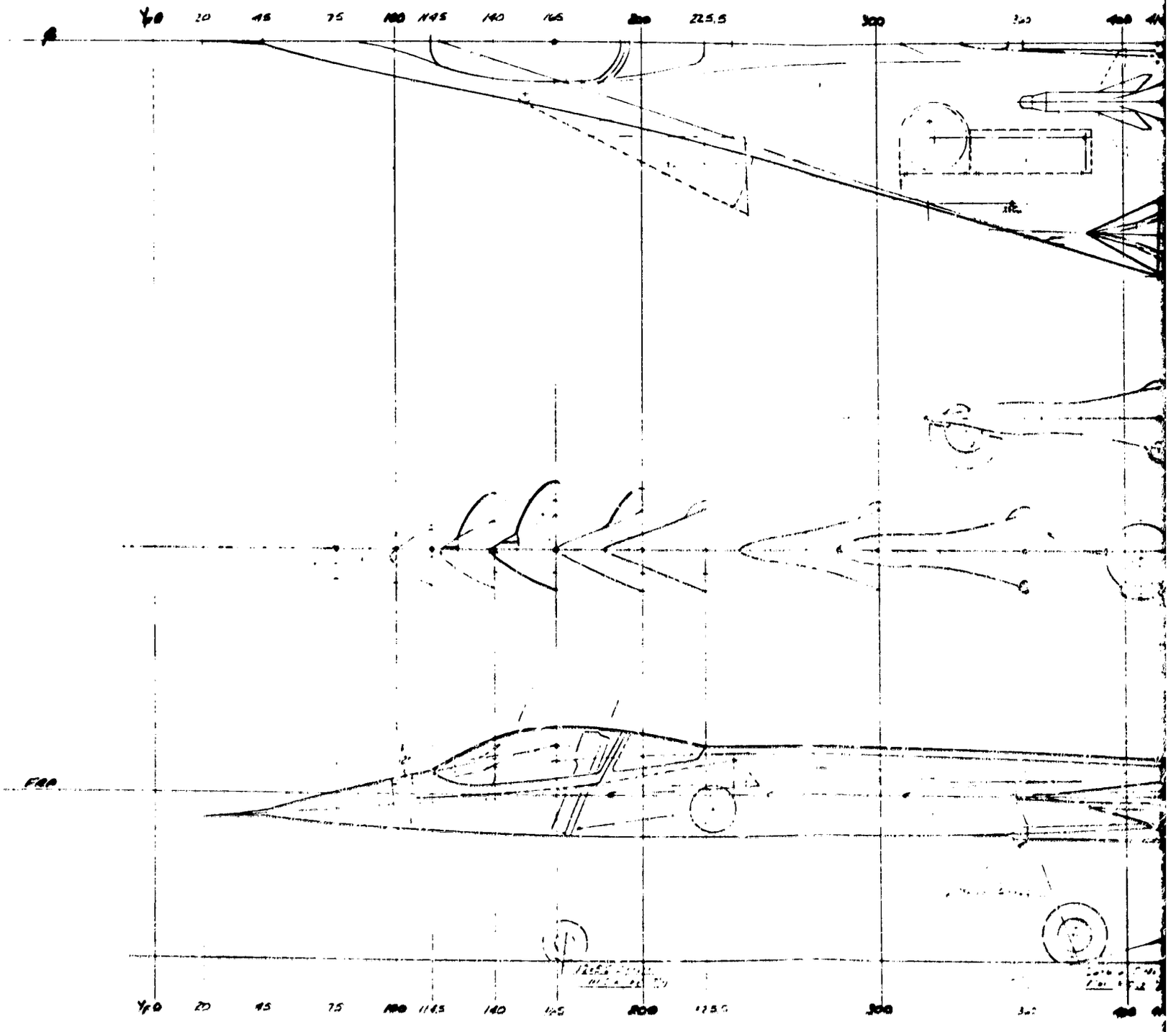

FOLDOUT FRAME

1

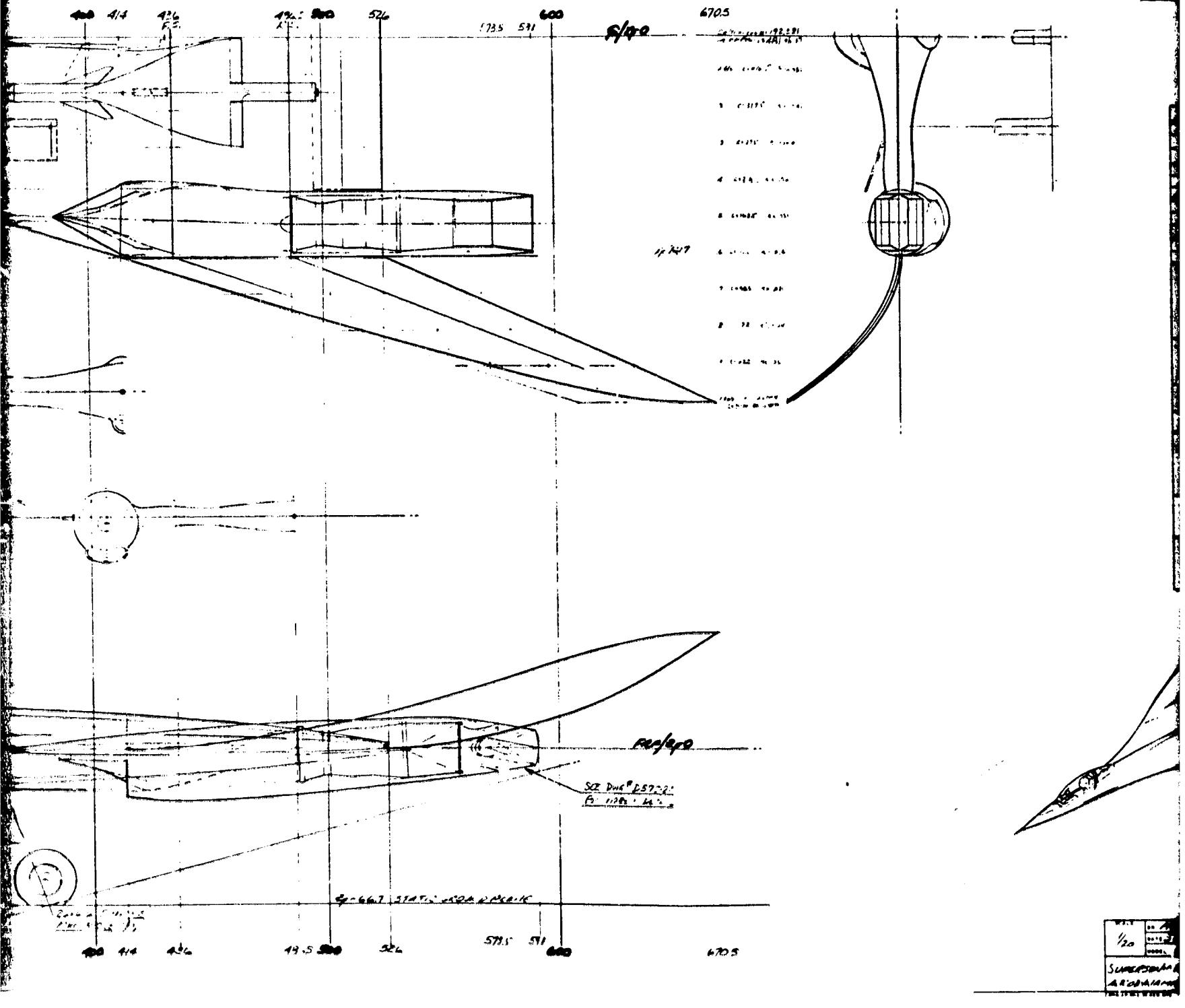

FOLDOUT FRAME

2

Figure

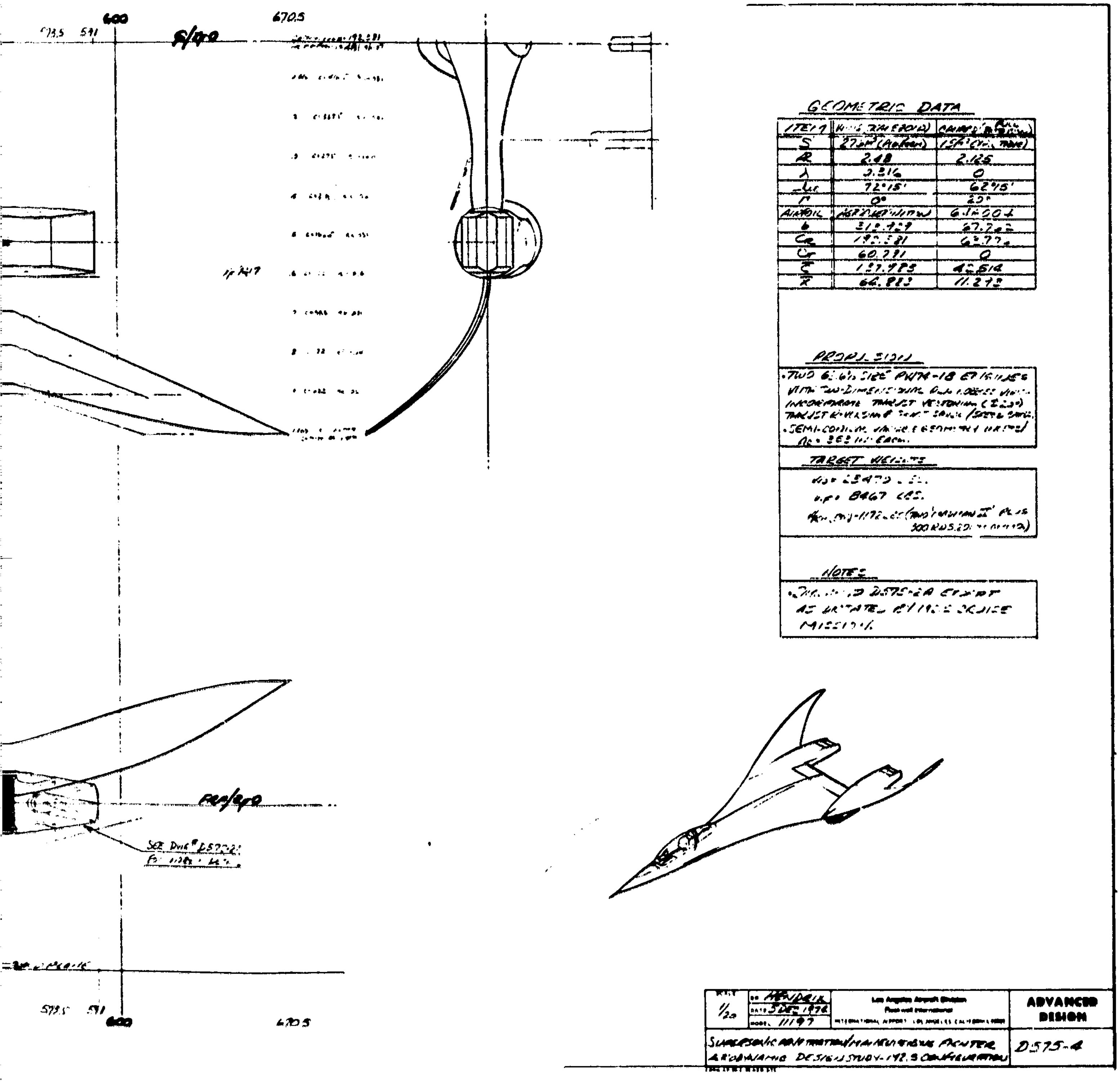

Figure 45. Configuration Layout-SP/MF, D575-4

FOLDOUT FRAME

FOLDOUT FRAME

TABLE VI, CRUISE DESIGN PARAMETERS

Configuration	D575-2A	-3	-4
Cruise Mach Number	1.6	2.0	2.5
Cruise C_L	.179	.117	.085
C.G. (Sta. in.)	270.	385.	405.

TABLE VII, SKIN FRICTION DRAG

Configuration	D575-2A	-3	-4
S_{wet}/S_{ref}	3.70	3.95	3.74
45,000 ft.	M 1.6 C_{DP} .00777	2.0 .00718	2.5 00574
25,000 ft.	M .6 C_{DP} .01033	.6 .01111	.6 .01021

FIGURE 46. SPANWISE TWIST DISTRIBUTION OPTIMIZED AT M=1.6, D575-2A

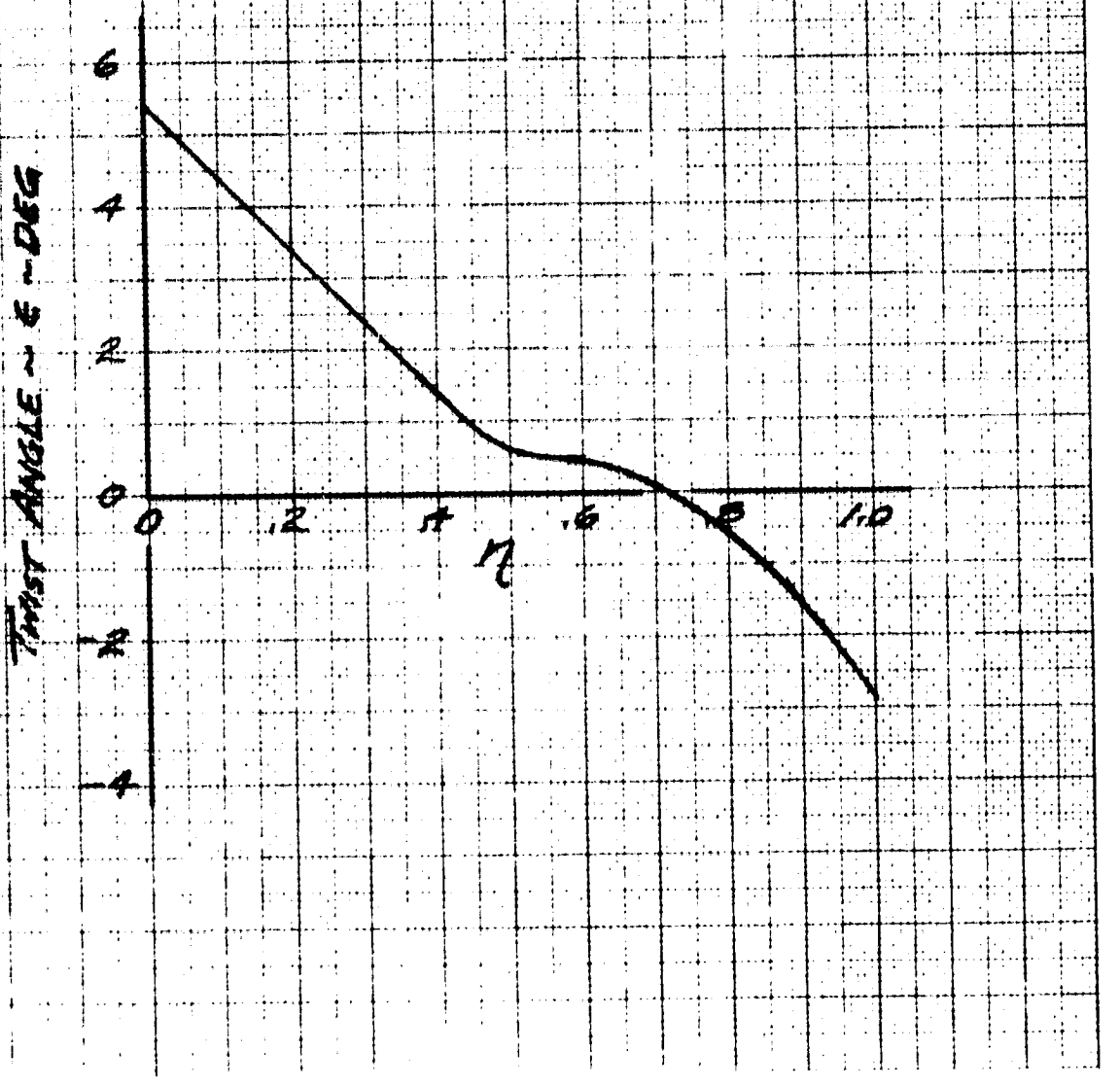

D575-3

S_{REF} = 215 FT²

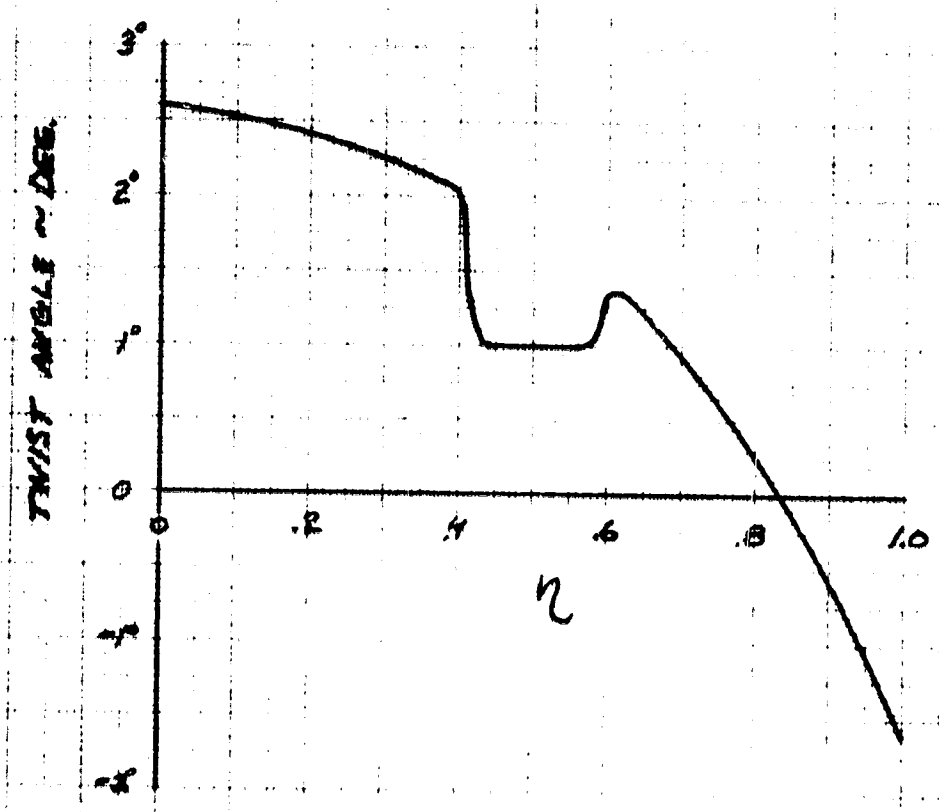

FIGURE 47. SPANWISE TWIST DISTRIBUTION OPTIMIZED AT M=2.0, D575-3

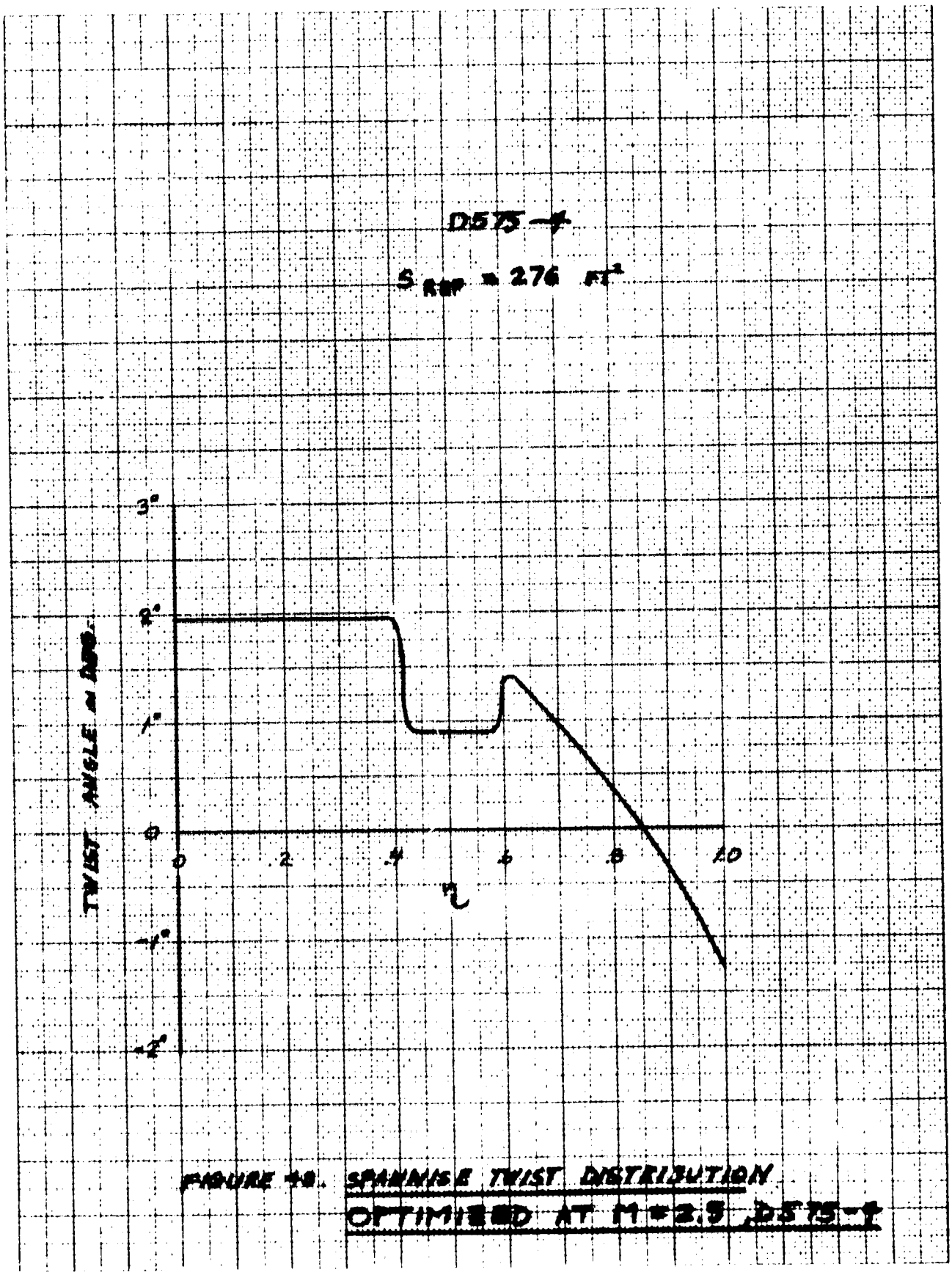

FIGURE 40. SPANWISE TWIST DISTRIBUTION OPTIMISED AT M = 2.5, D575-4

FIGURE 49. OPTIMIZED CAMBER AT M = 1.6
INBOARD SPANWISE STATIONS, D575-2A

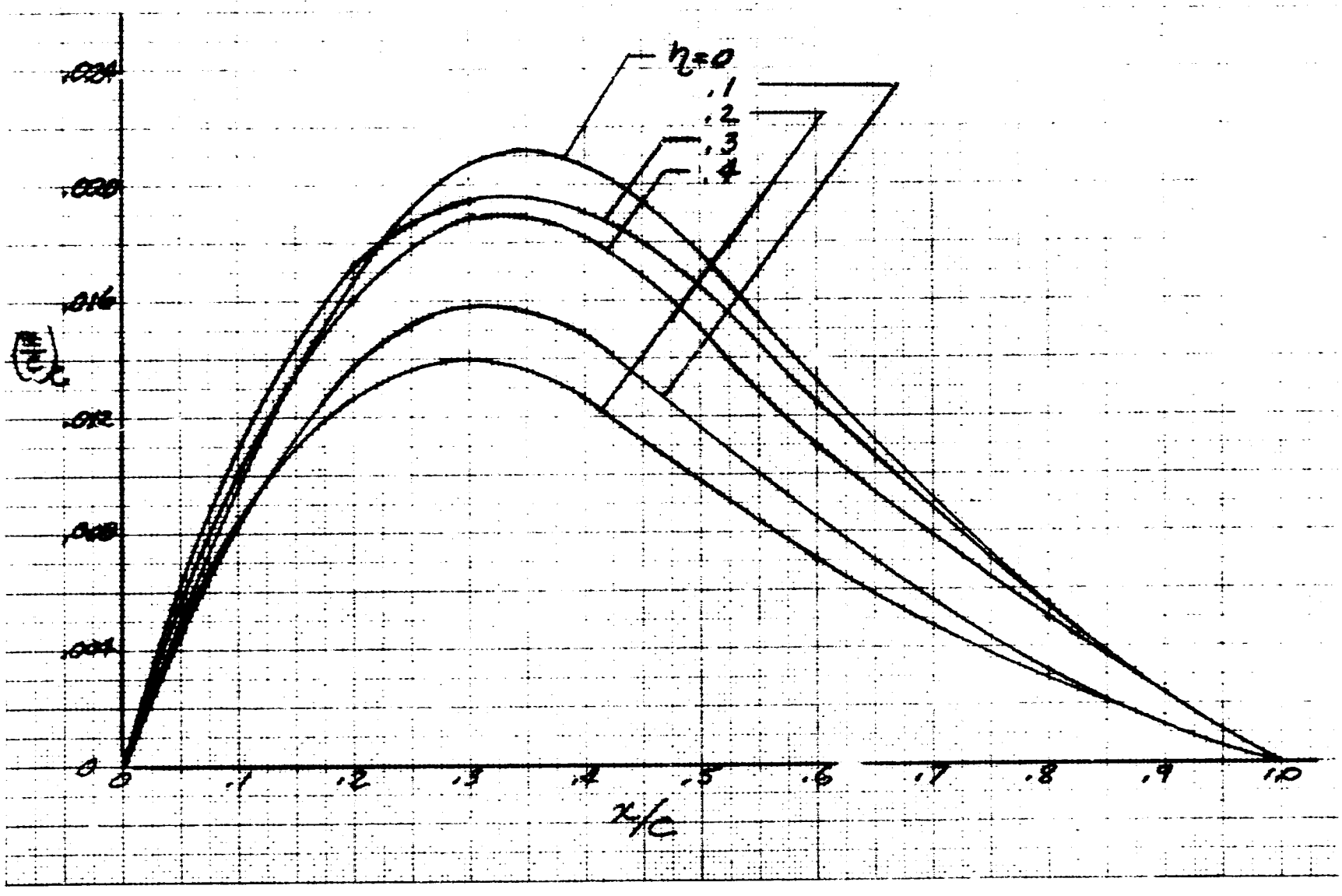

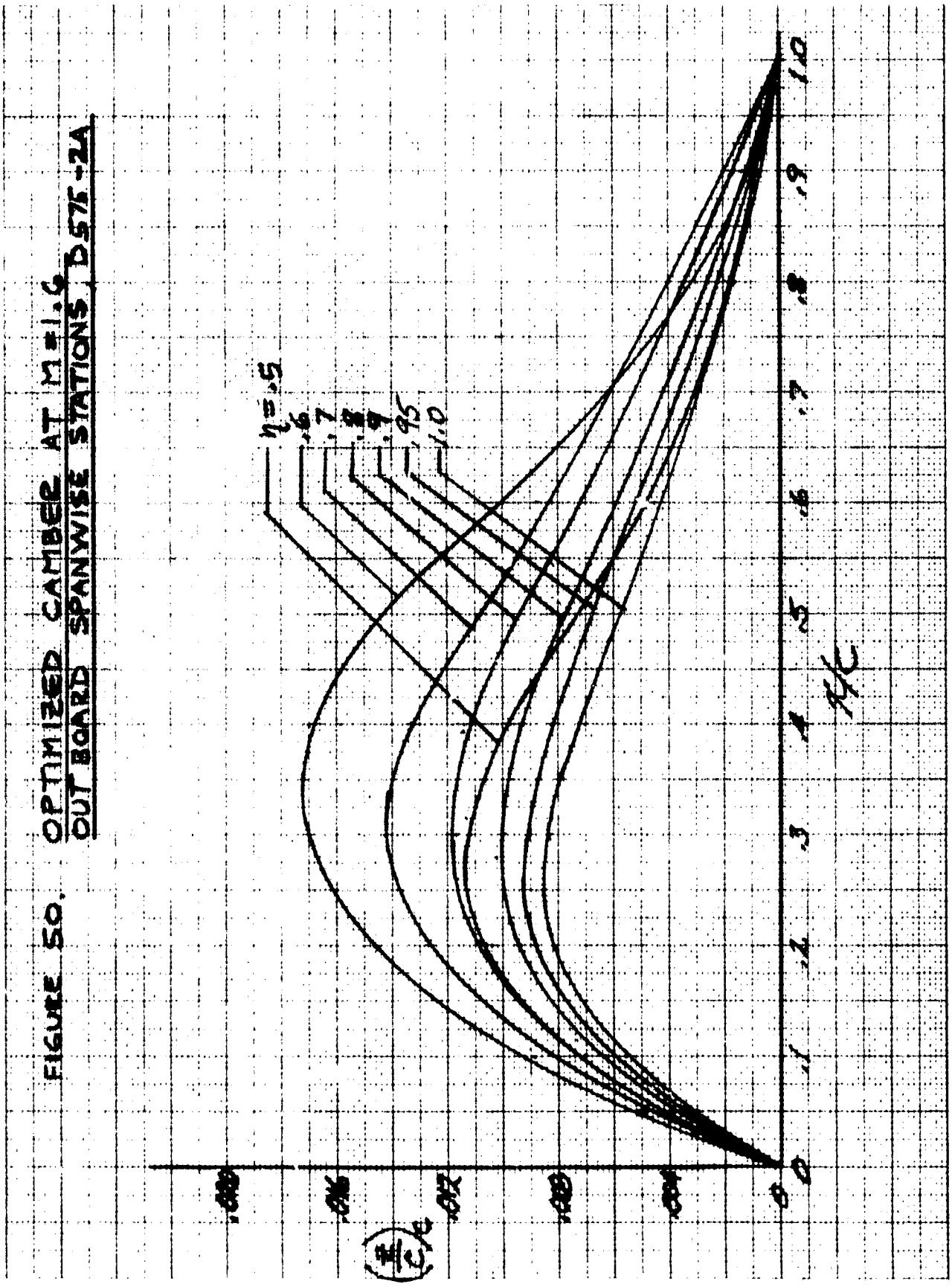

FIGURE 50. OPTIMIZED CAMBER AT M=1.6
OUT BOARD SPANWISE STATIONS, D575-2A

FIGURE 51. OPTIMIZED CAMBER AT M=2.0
INBOARD SPANWISE STATIONS, D 575→

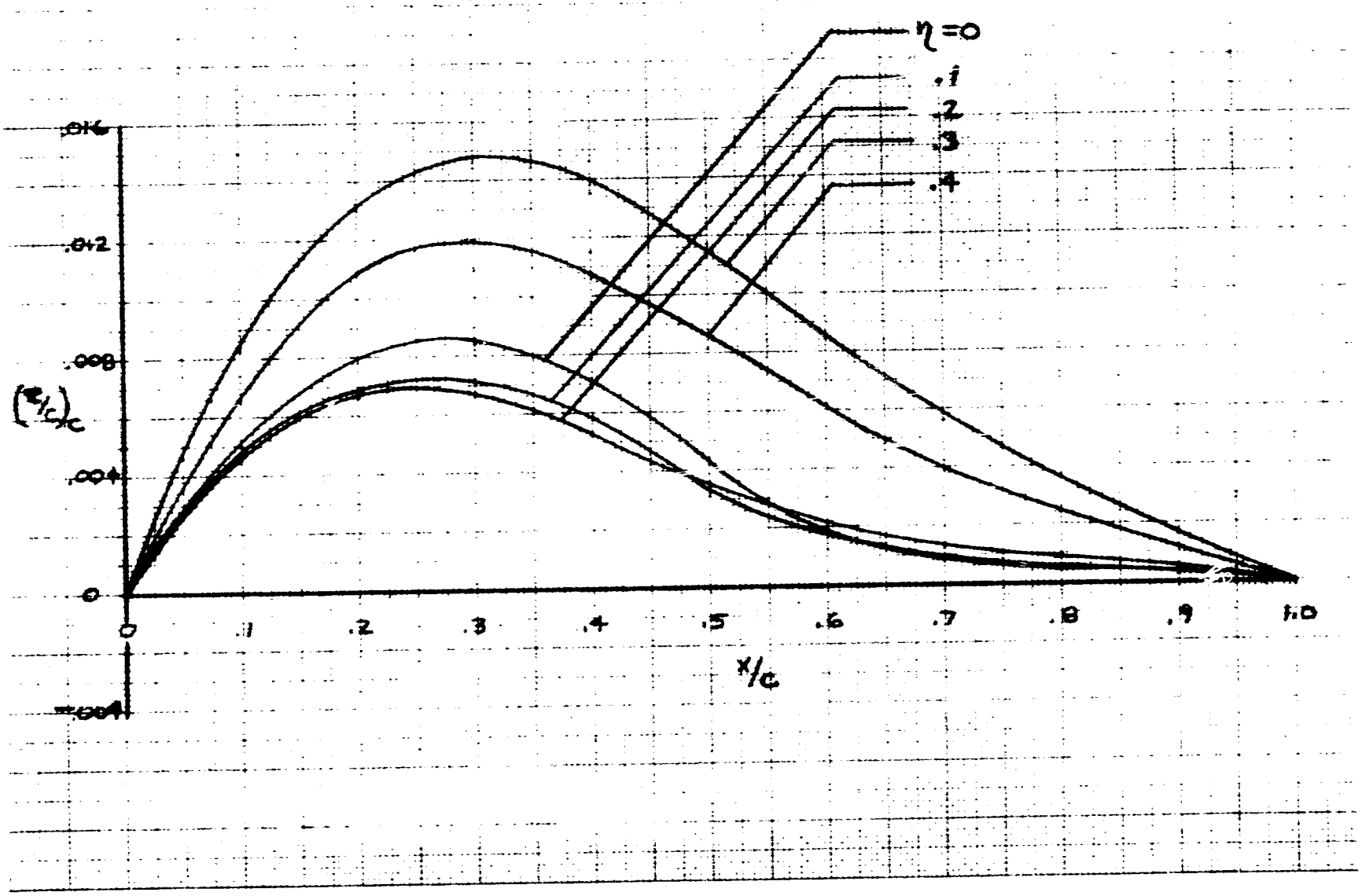

FIGURE 52. OPTIMIZED CAMBER AT M = 2.0
OUTBOARD SPANWISE STATIONS, DS75-3

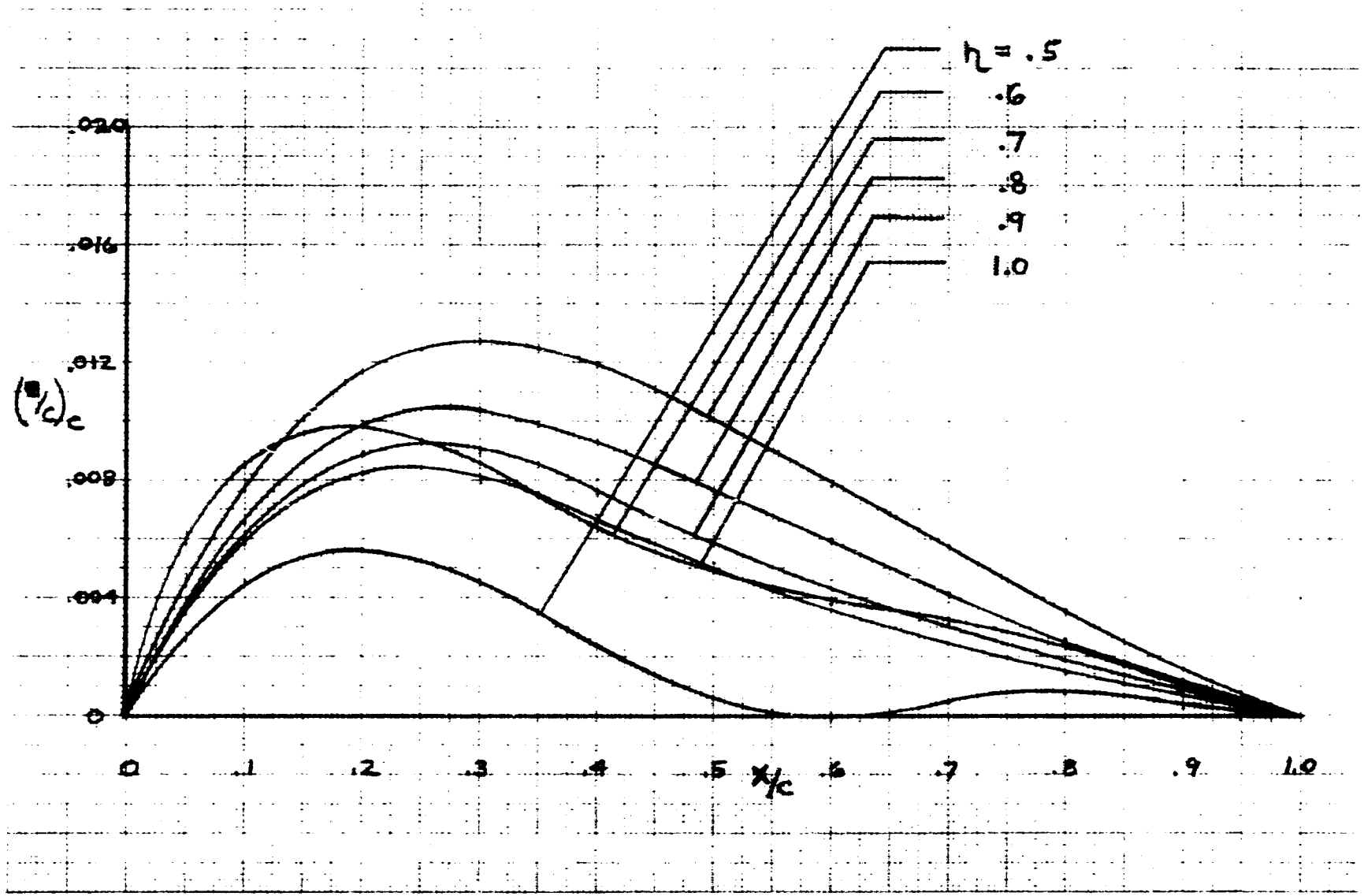

FIGURE 53. OPTIMIZED CAMBER AT M = 2.5
INBOARD SPANWISE STATIONS, DS75 -4

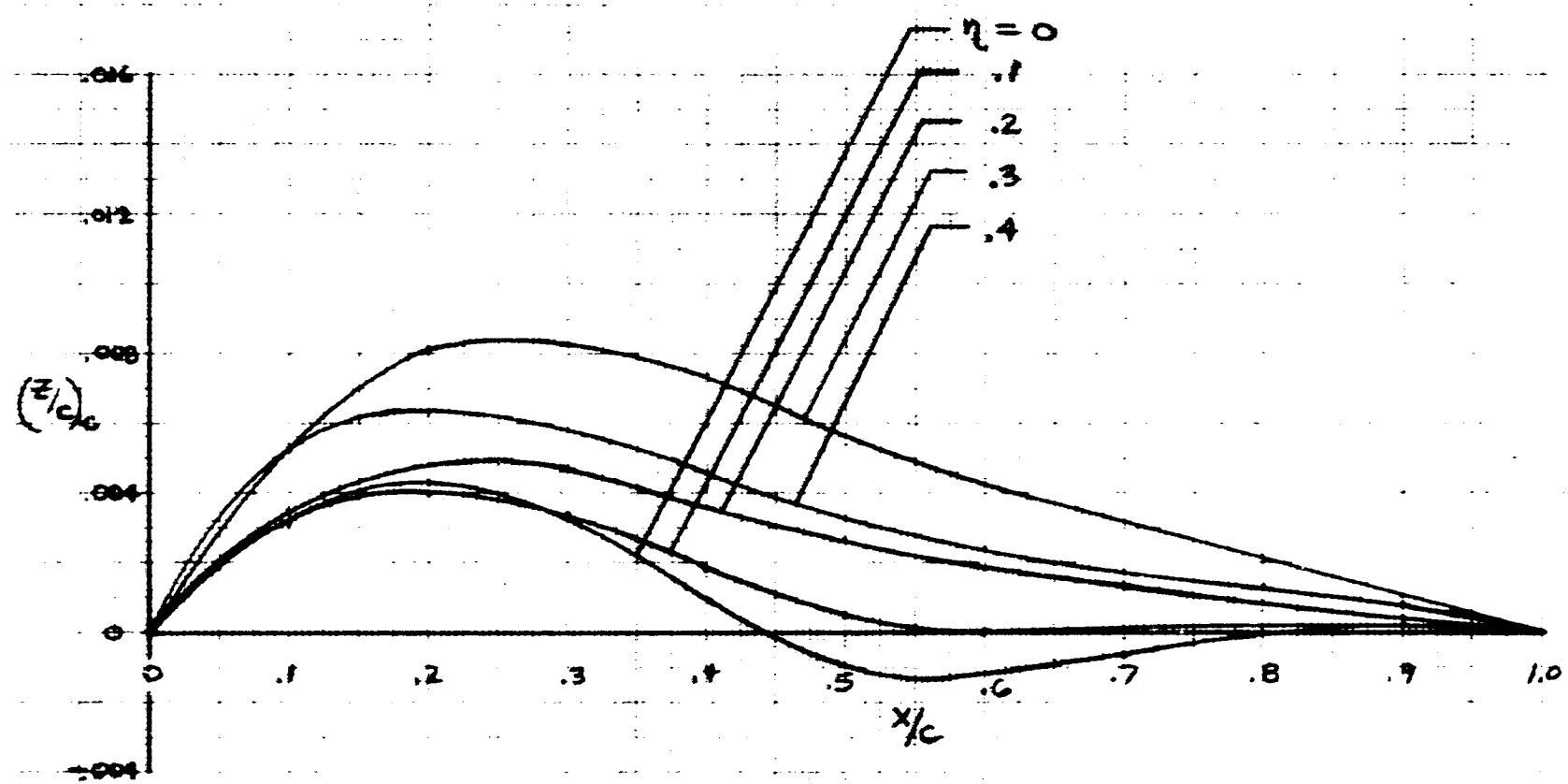

FIGURE 54. OPTIMIZED CAMBER AT M = 2.5
OUTBOARD SPANWISE STATIONS, D575-4

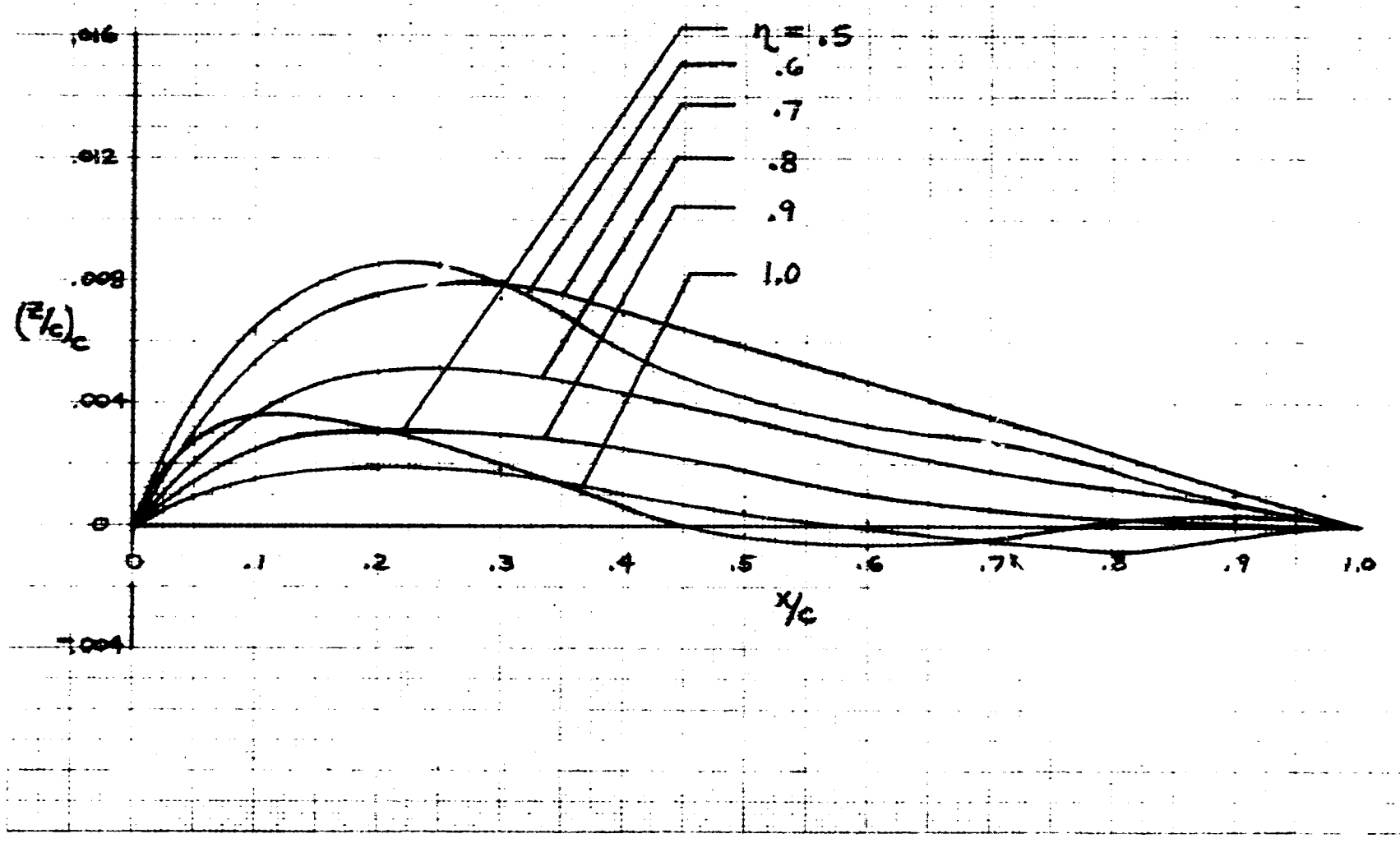

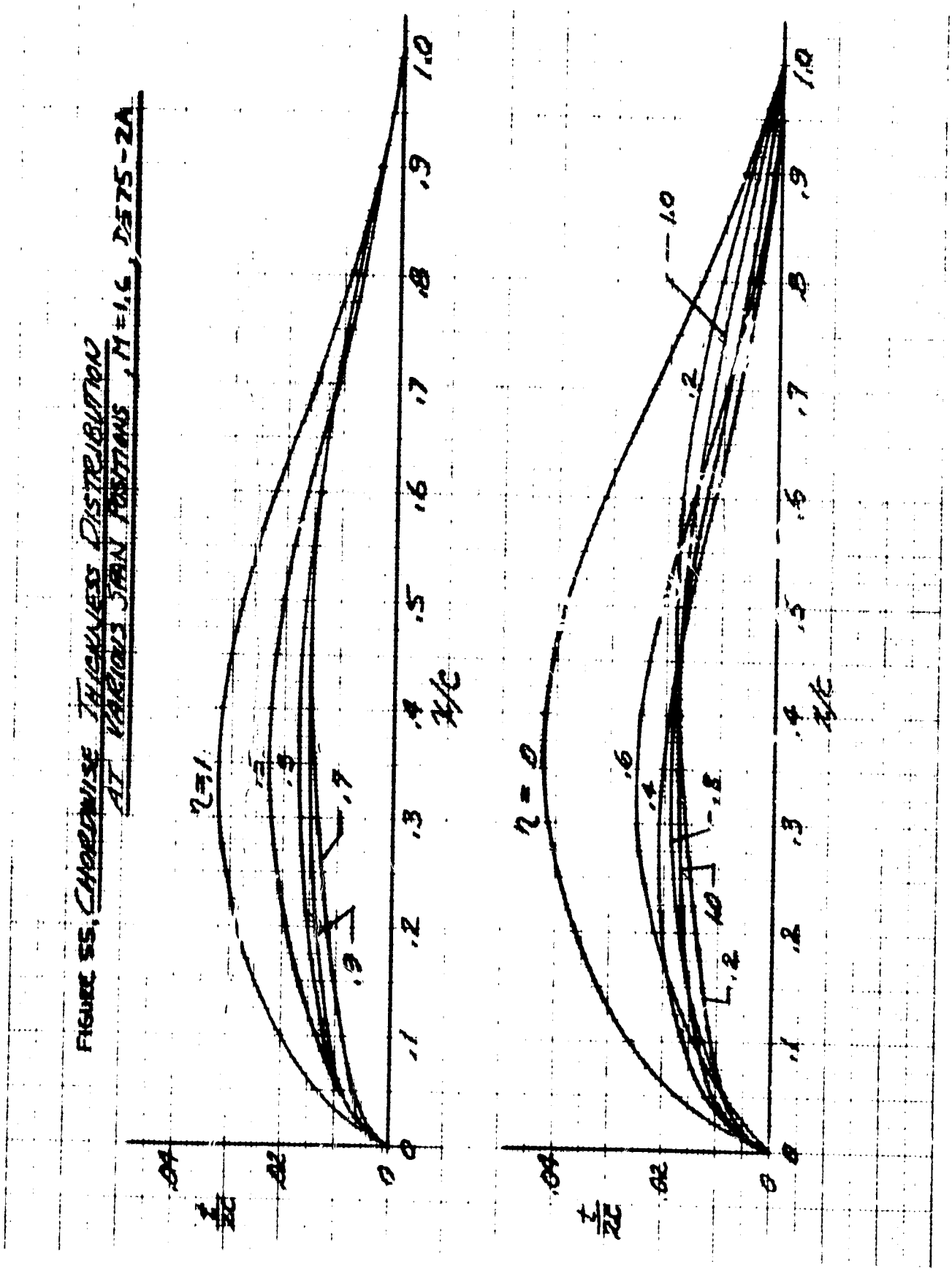

FIGURE 55. CHORDWISE THICKNESS DISTRIBUTION AT VARIOUS SPAN POSITIONS, M=1.6, DZ75-2A

FIGURE 56. CHORDWISE THICKNESS DISTRIBUTION AT VARIOUS SPAN POSITIONS, M = 2.0, DS 7% -3

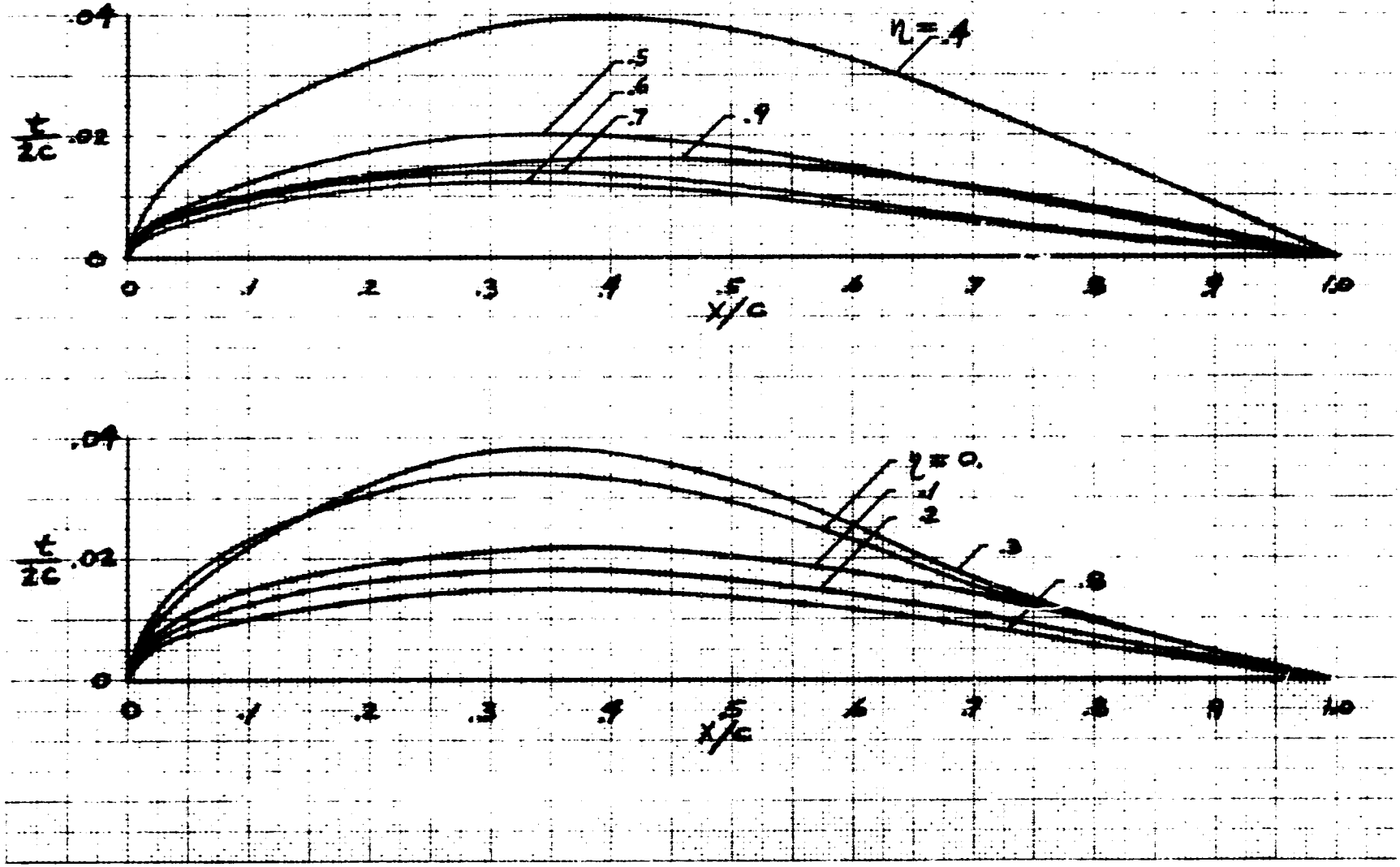

FIGURE 57. CHORDWISE THICKNESS DISTRIBUTION AT VARIOUS SPANWISE POSITIONS, M=2.5, D575-4

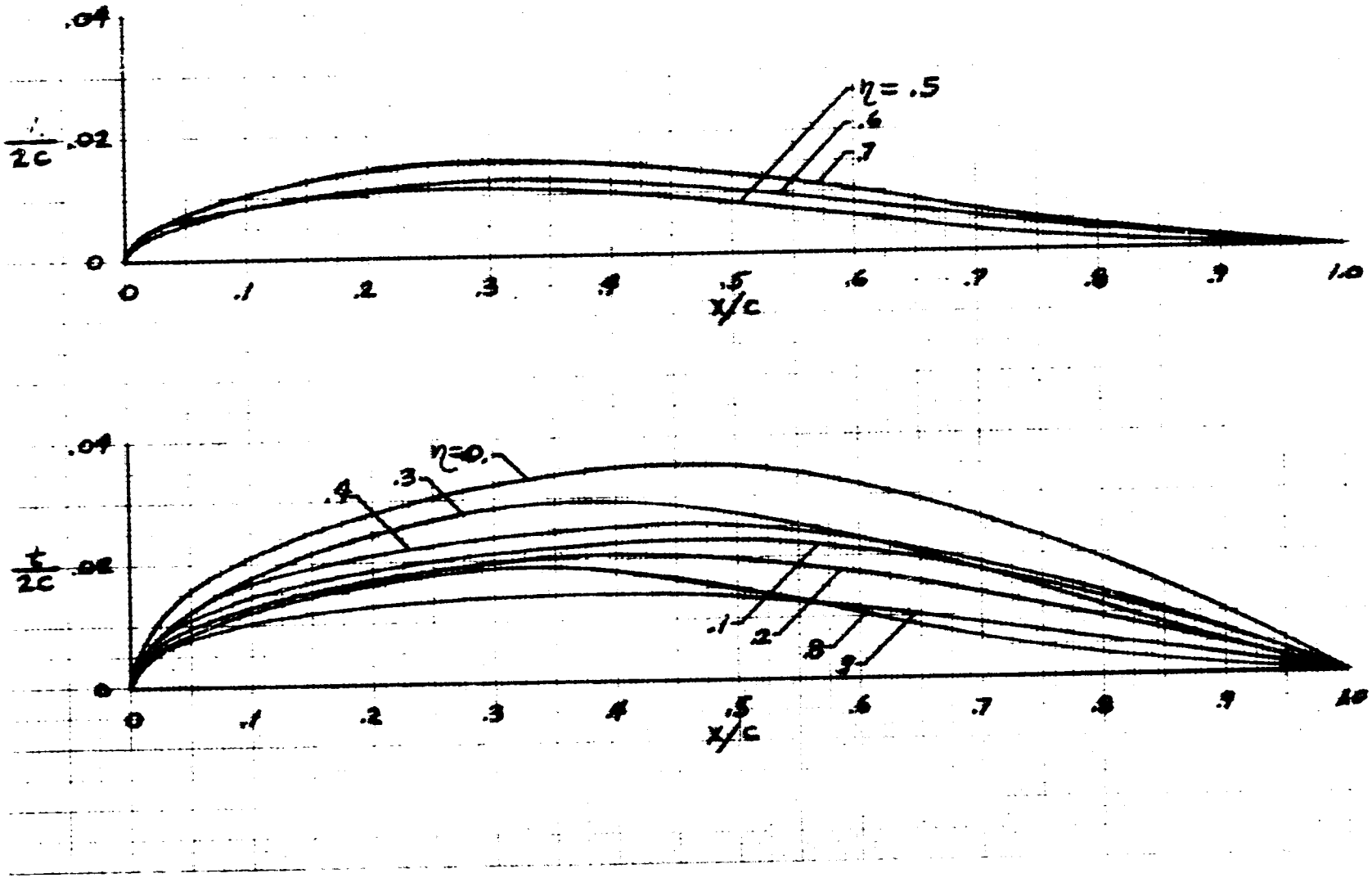

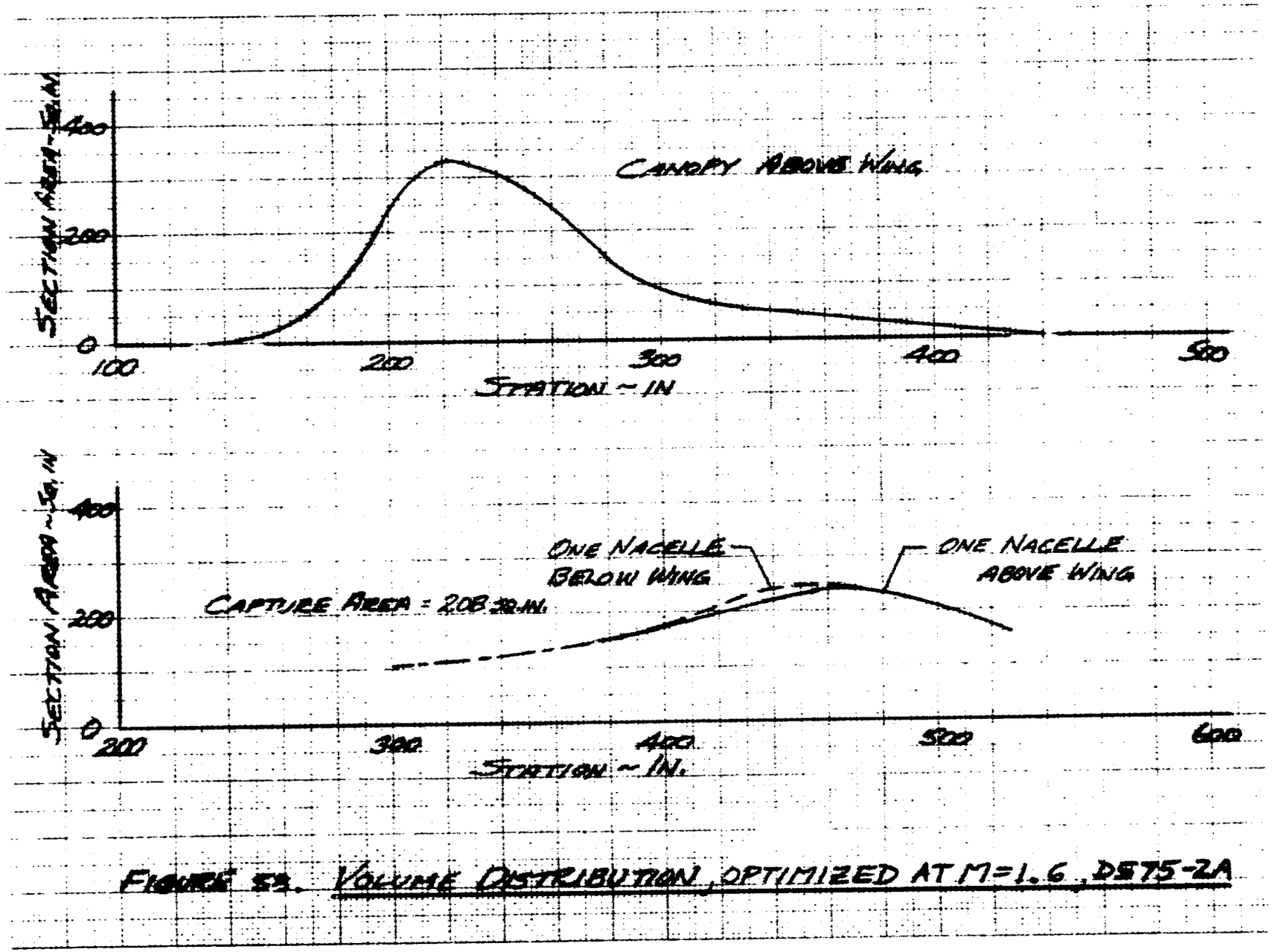

FIGURE 52. VOLUME DISTRIBUTION, OPTIMIZED AT M=1.6, D575-2A

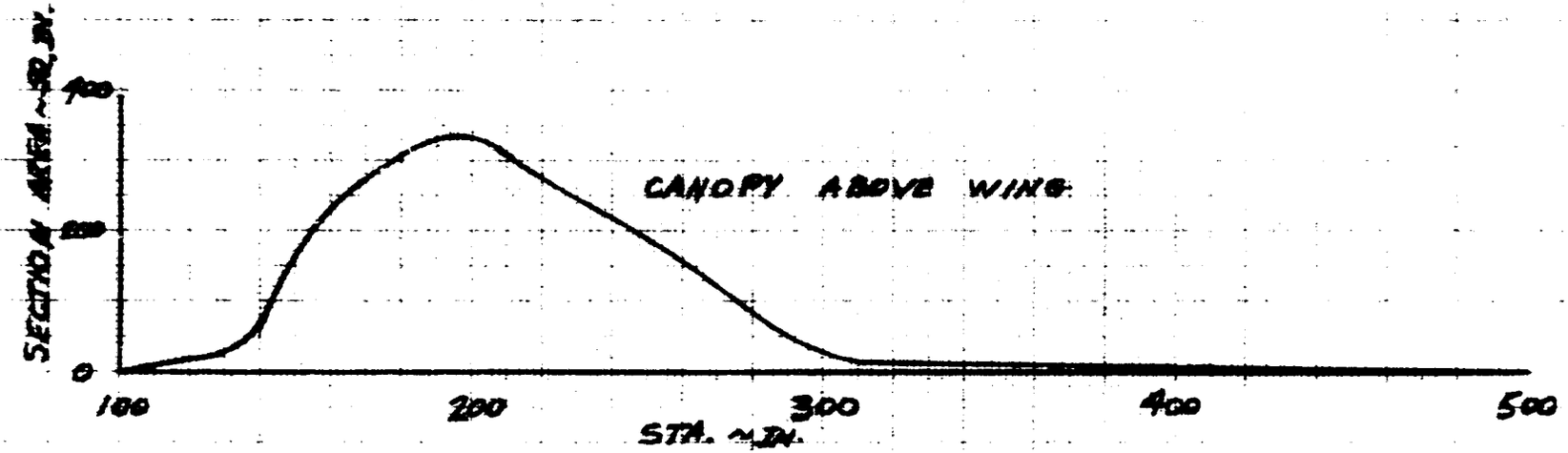

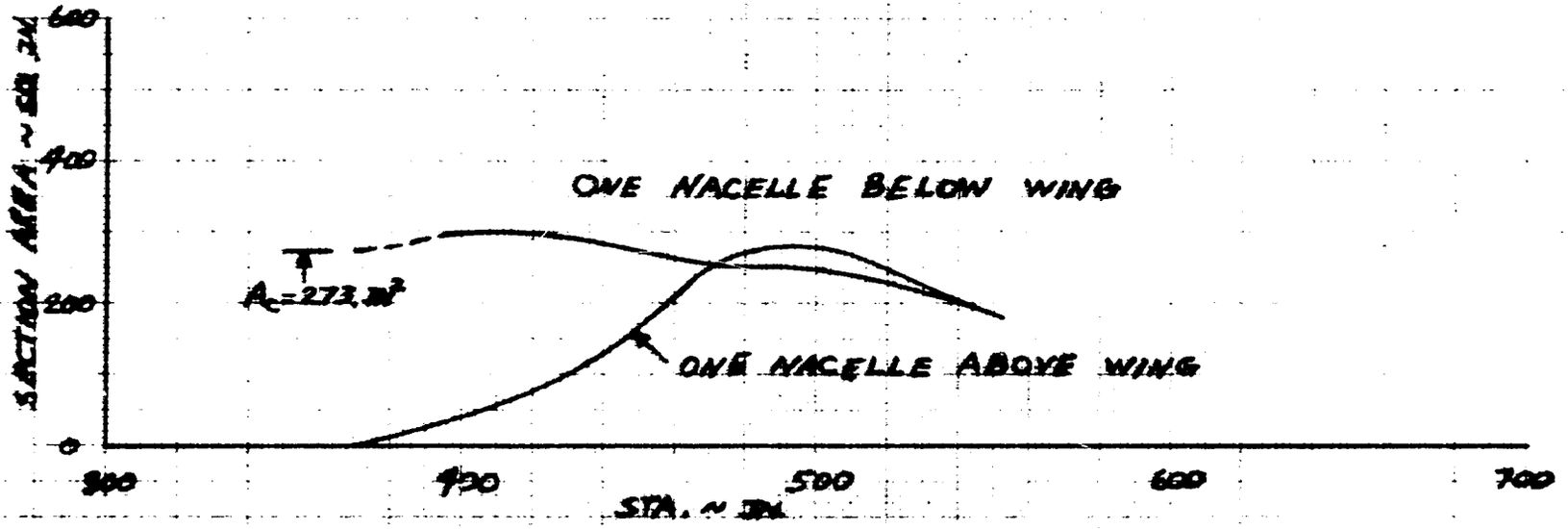

FIGURE 59. VOLUME DISTRIBUTION, OPTIMIZED AT M = 2.0, DS 75-3

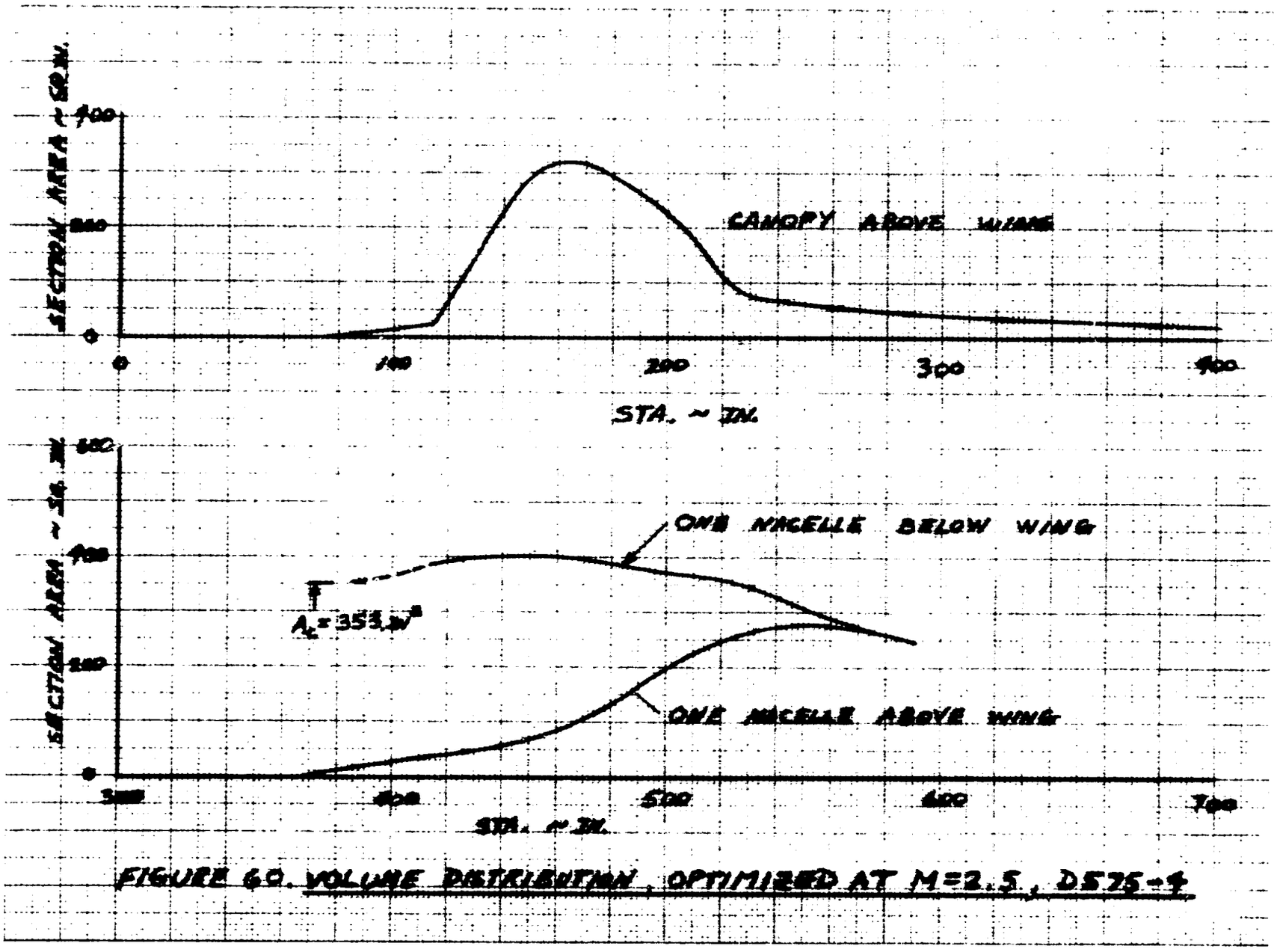

FIGURE 60. VOLUME DISTRIBUTION, OPTIMIZED AT M=2.5, D575-4

D575-2A

S_{REF} = 185 FT^2

OPTIMIZED AT M=1.6

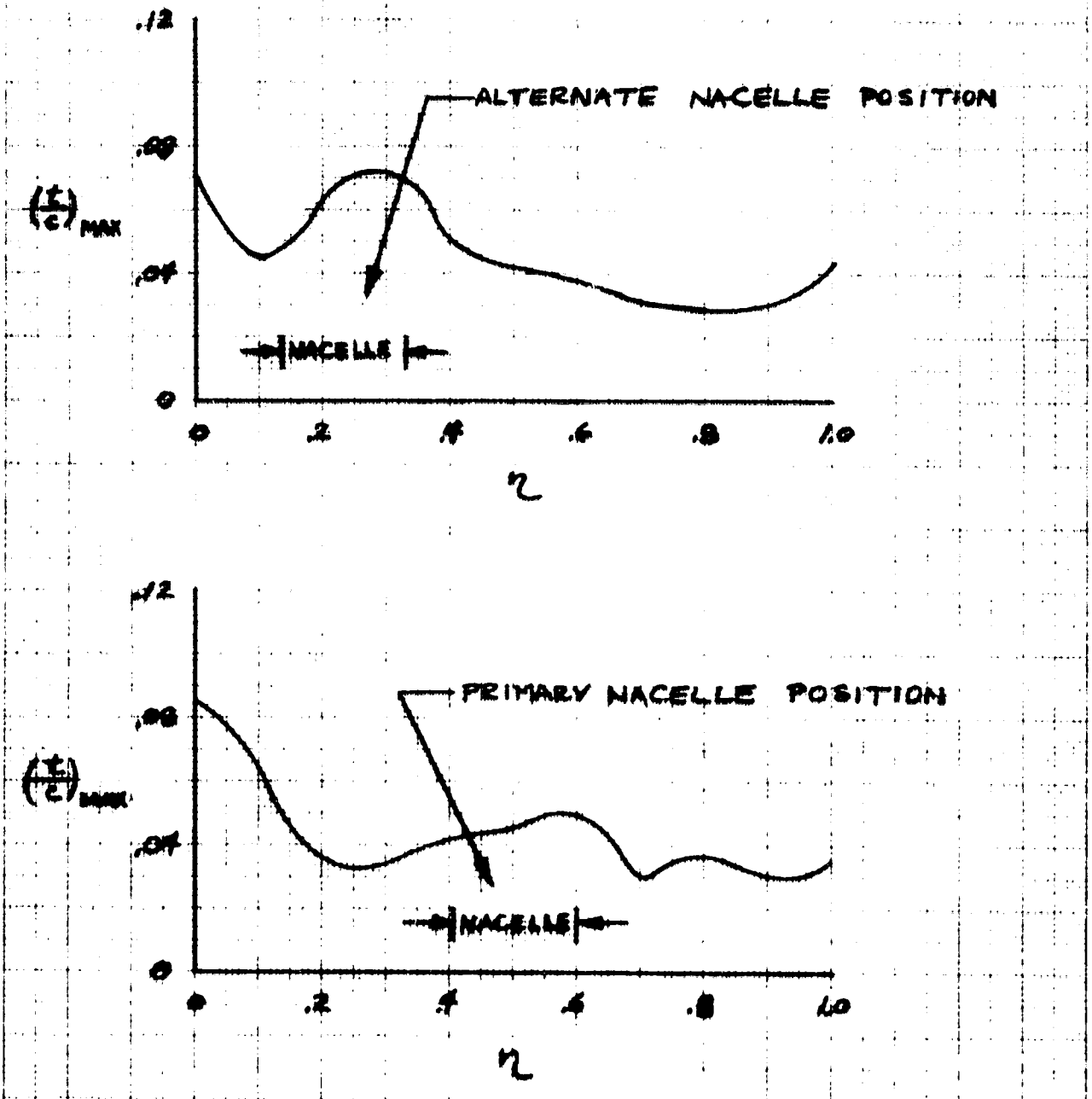

FIGURE 61. EFFECT OF NACELLE LOCATION ON WING THICKNESS DISTRIBUTION, DESIGN

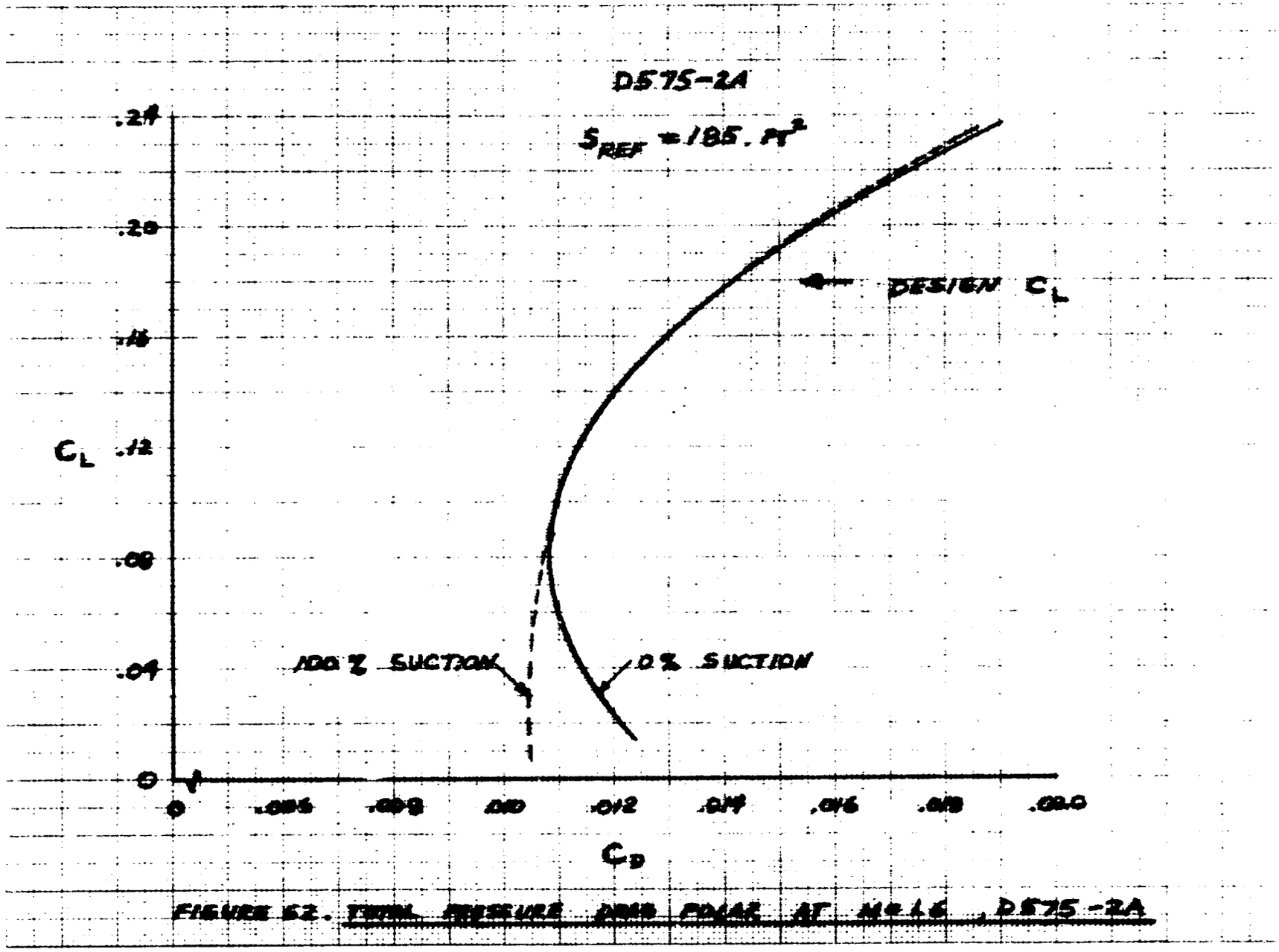

FIGURE 52. TYPICAL PRESSURE DRAG POLAR AT M=1.6, D575-2A

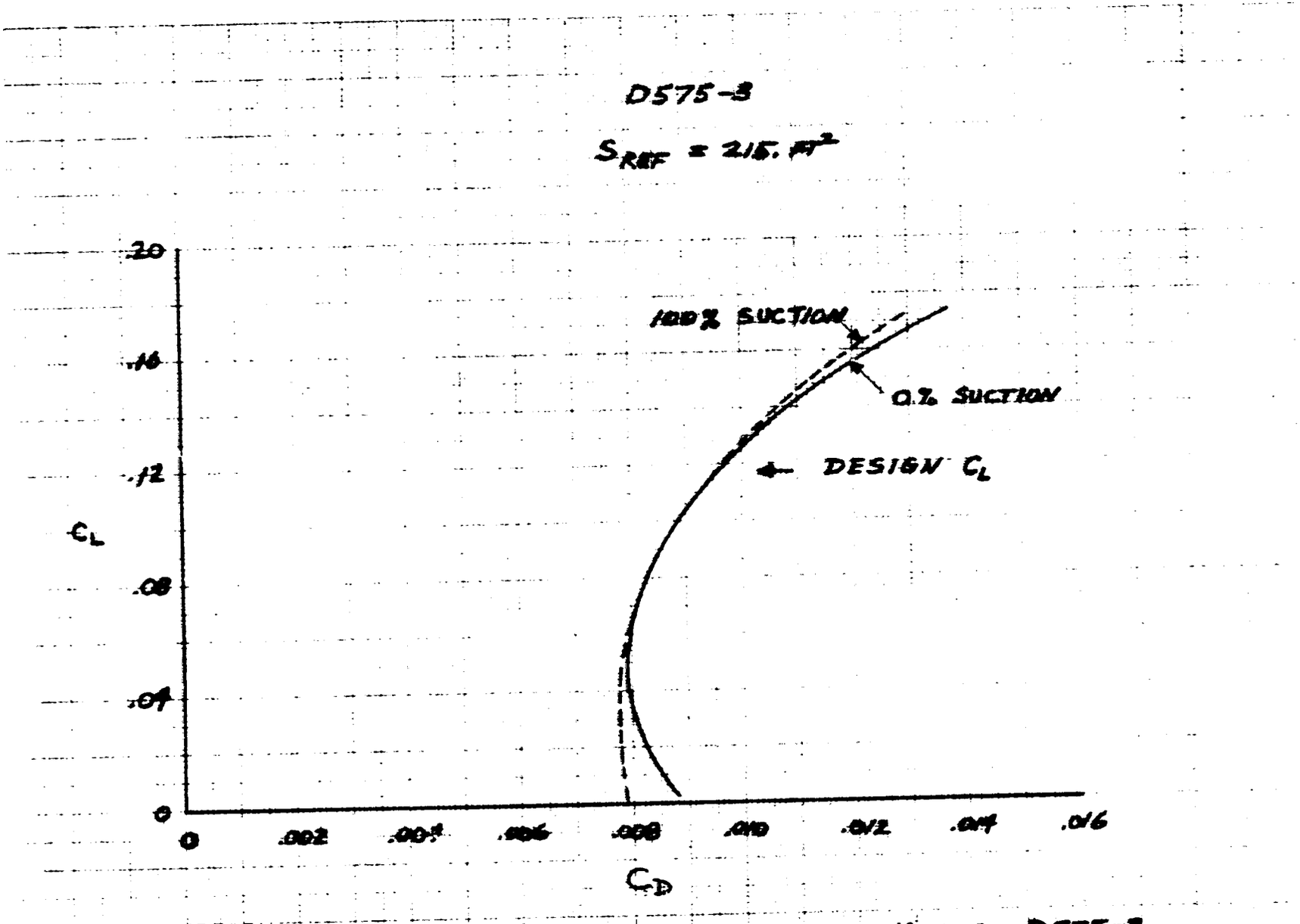

FIGURE 63. TOTAL PRESSURE DRAG POLAR AT M=2.0, D575-3.

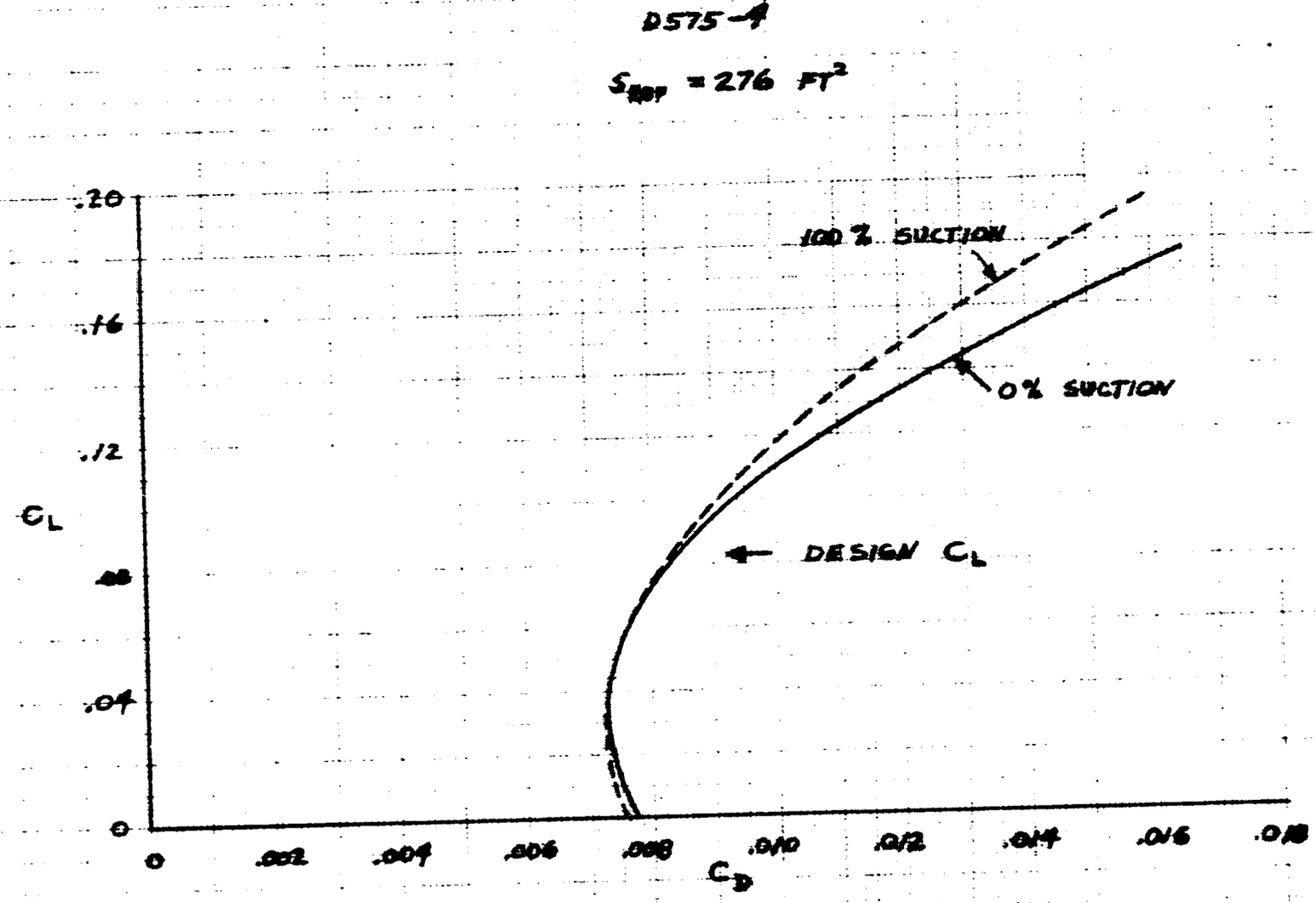

FIGURE 64. TOTAL PRESSURE DRAG POLAR AT M=2.5, D575-4

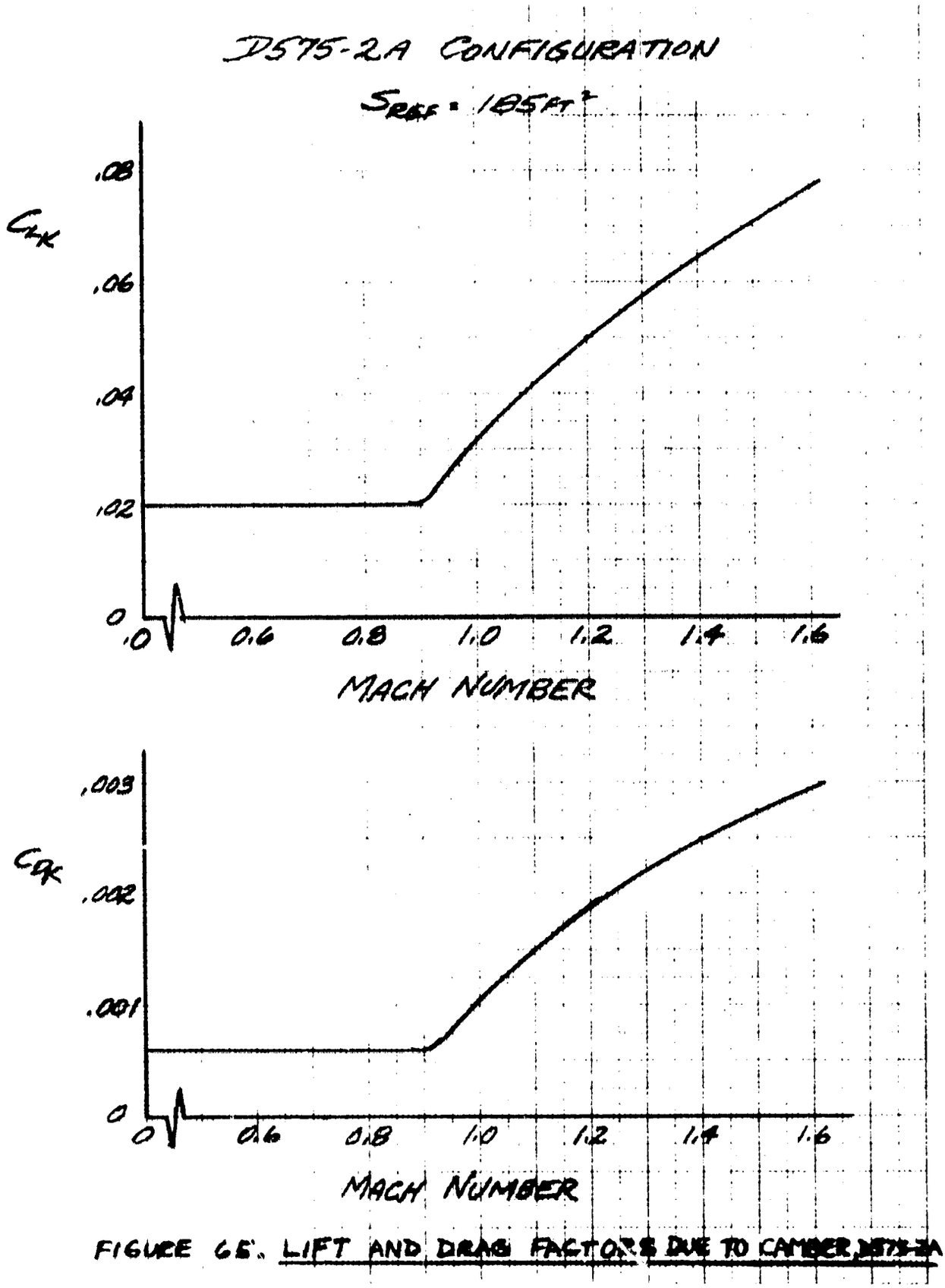

FIGURE 65. LIFT AND DRAG FACTORS DUE TO CAMBER, D575-2A

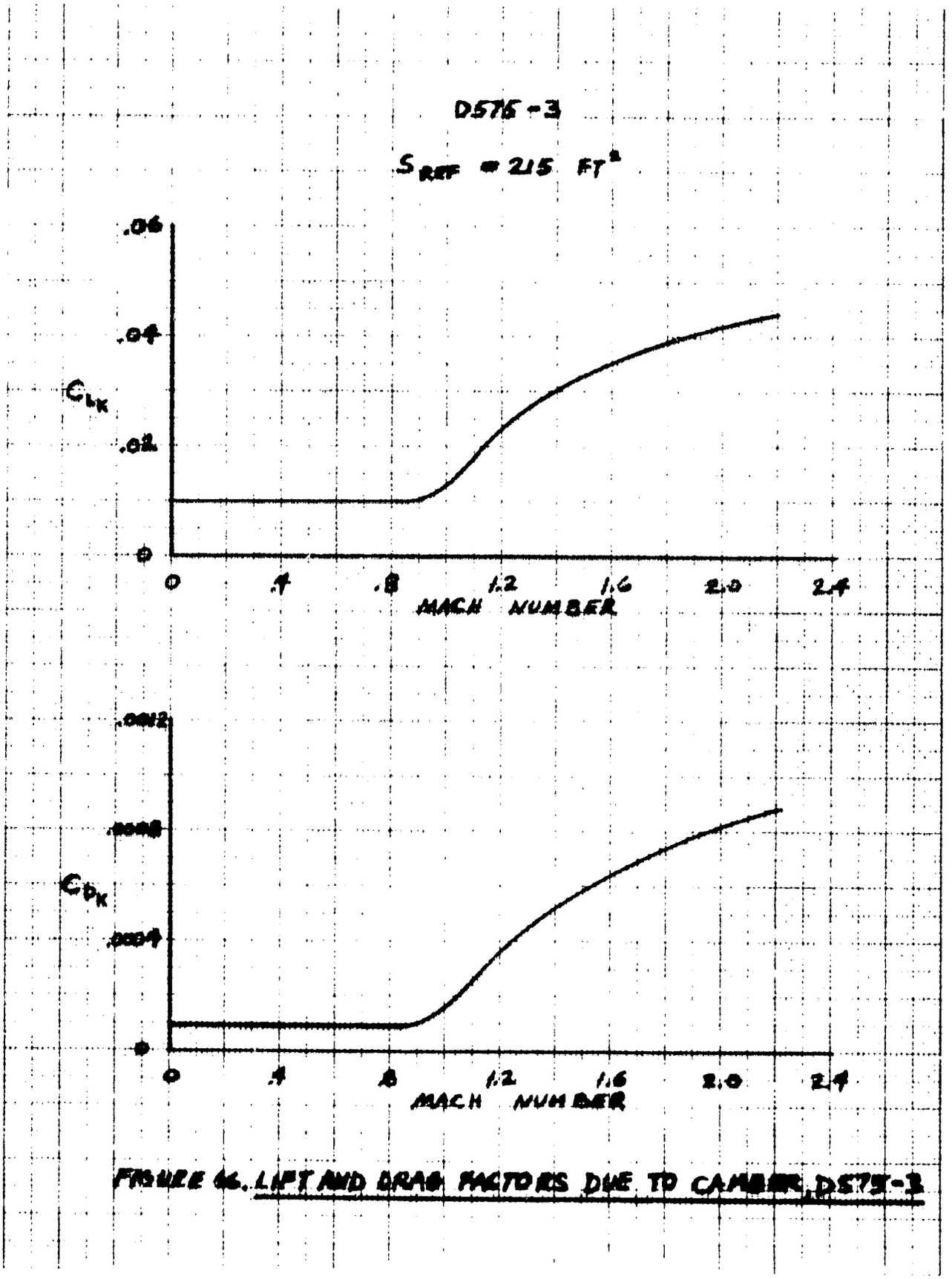

FIGURE 66. LIFT AND DRAG FACTORS DUE TO CAMBER, D575-3

D575-4

S_{REF} = 276 FT^2

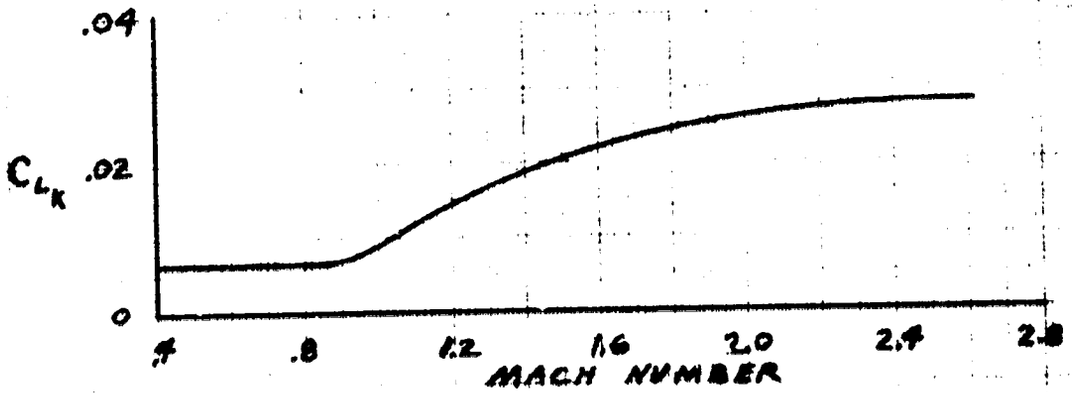

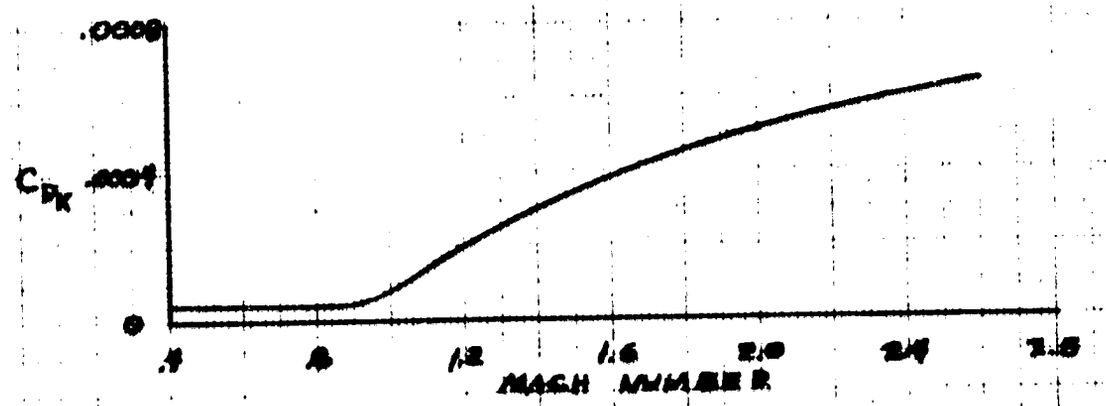

FIGURE 67. LIFT AND DRAG FACTORS DUE TO CAMBER, D575-4

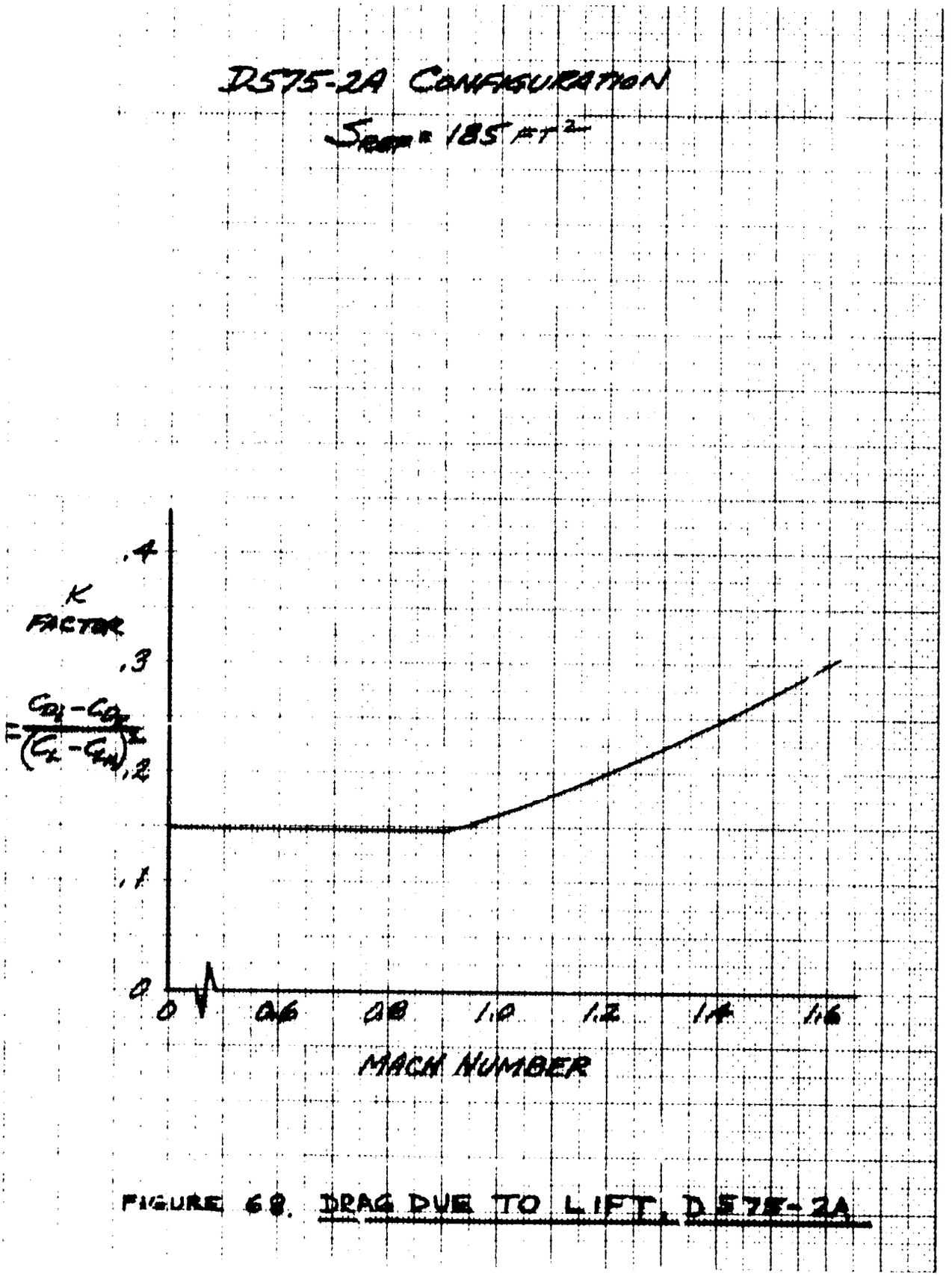

FIGURE 68. DRAG DUE TO LIFT, D575-2A

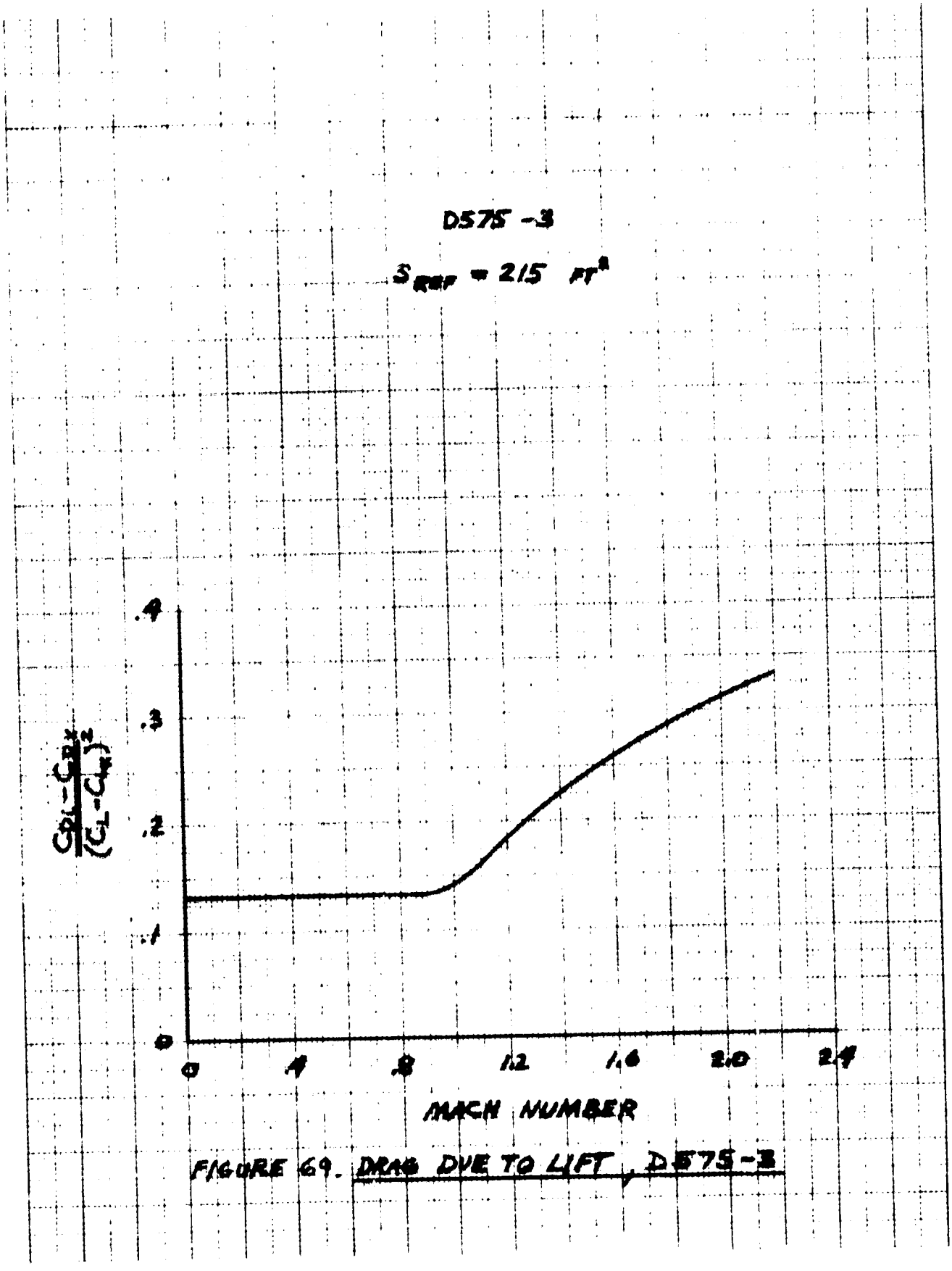

FIGURE 69. DRAG DUE TO LIFT, D575-3

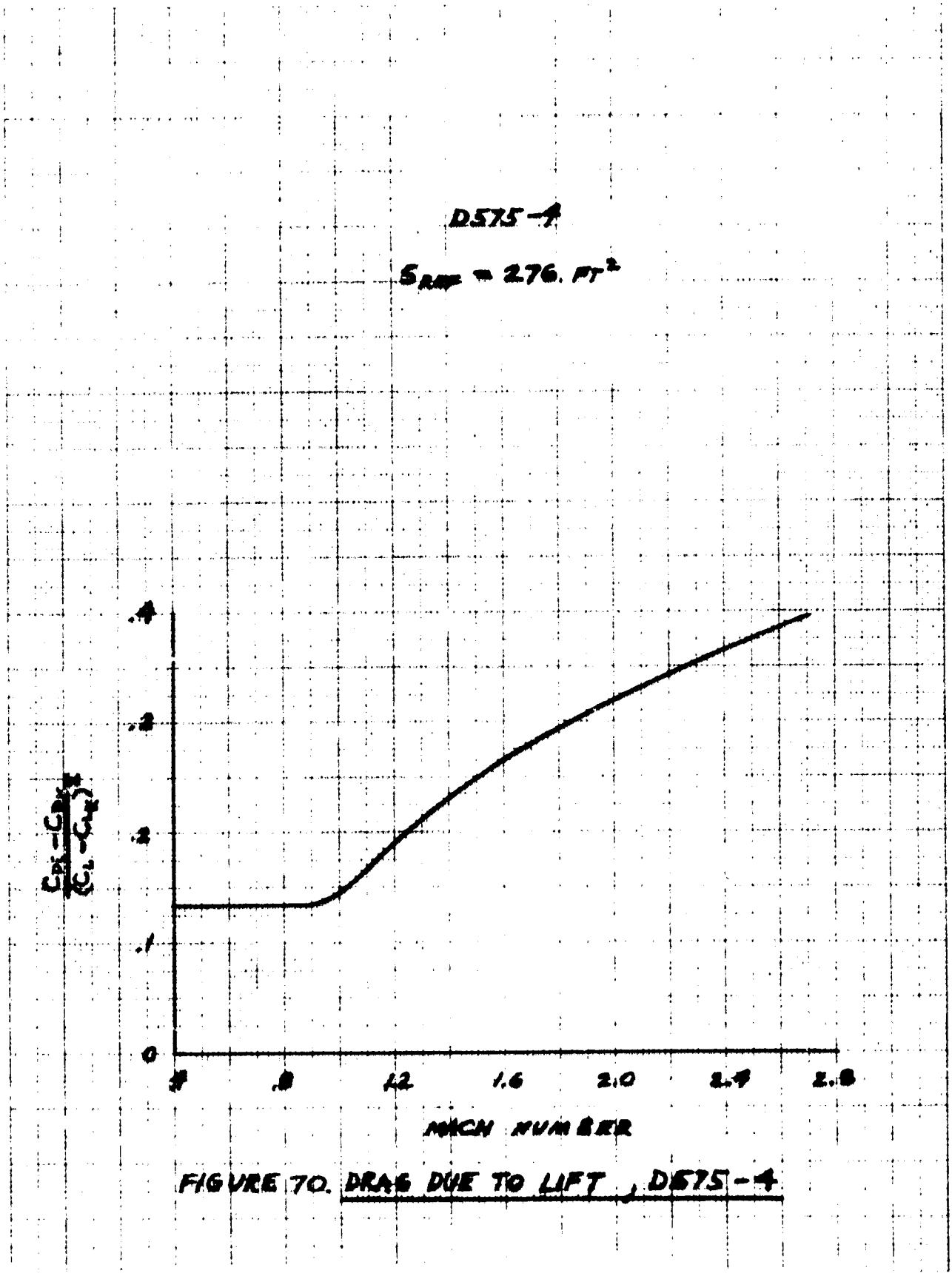

FIGURE 70. DRAG DUE TO LIFT, D575-4

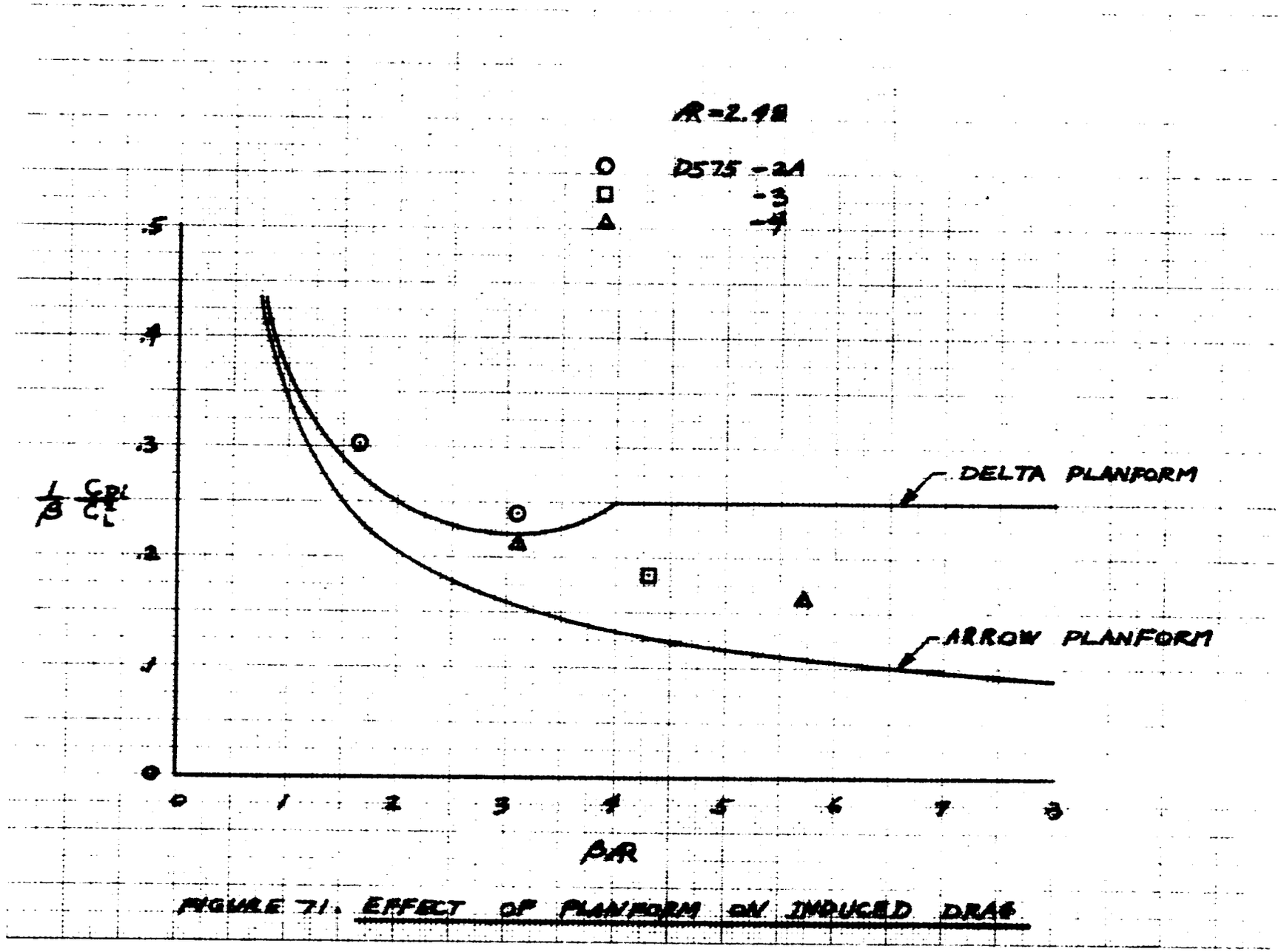

FIGURE 71. EFFECT OF PLANFORM ON INDUCED DRAG

FIGURE 72. WAVE DRAG VERSUS MACH NUMBER

D S75-2A

$S_{REF.} = 185. Ft$

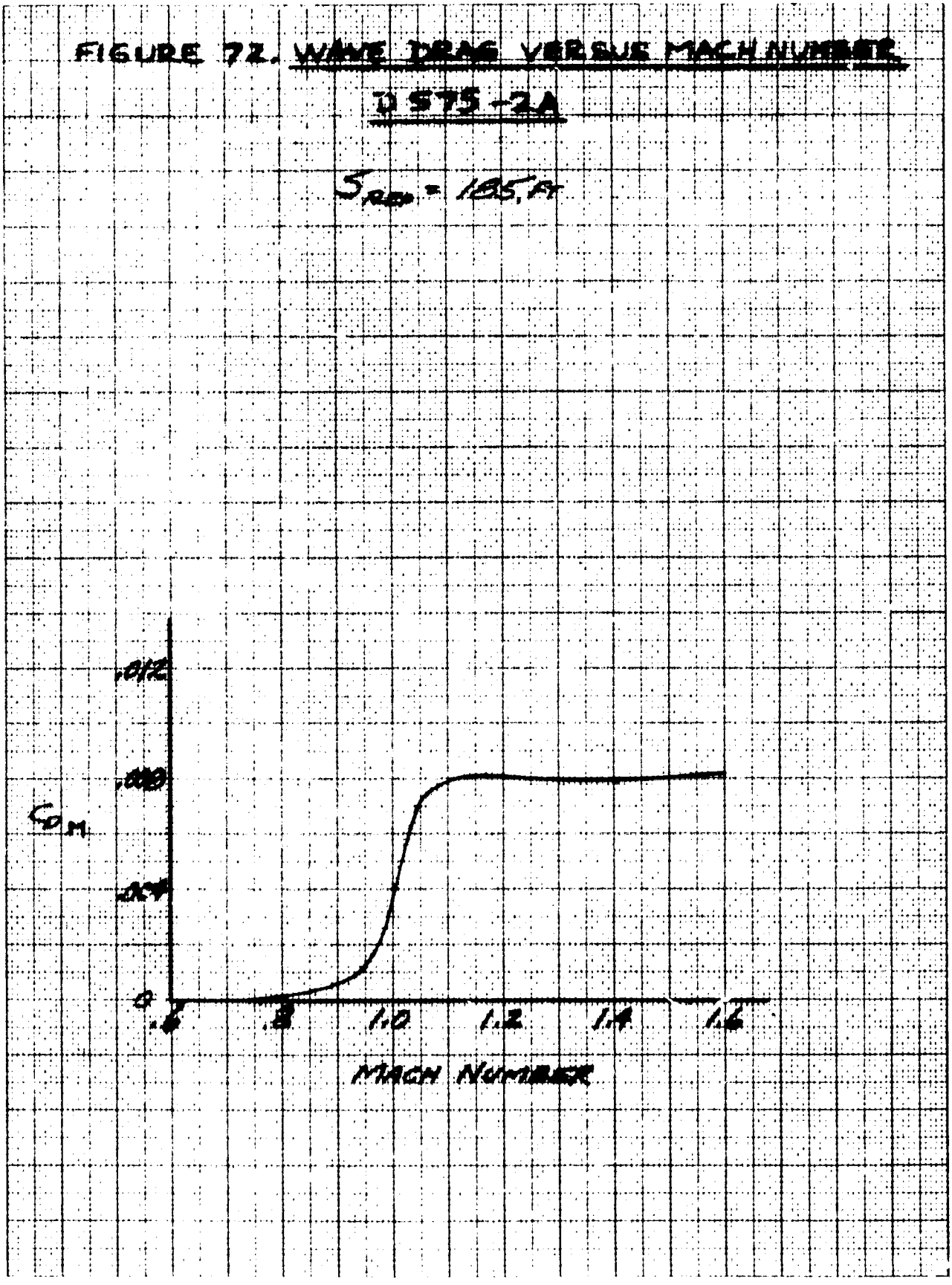

FIGURE 73. WAVE DRAG VERSUS MACH NUMBER

D 575-3

$S_{REF} = 215. FT^2$

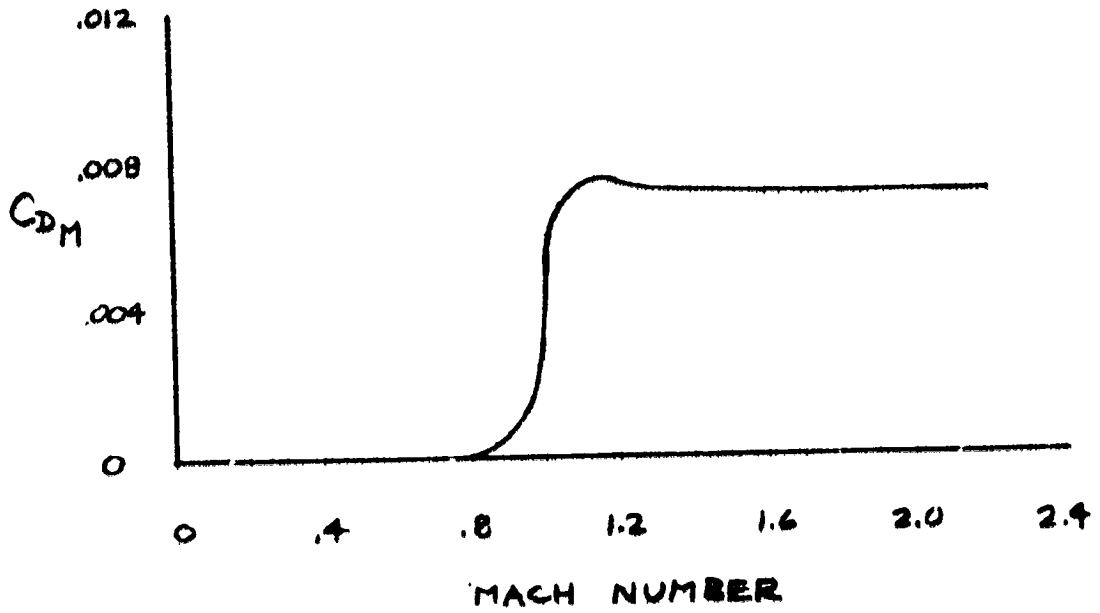

FIGURE 74. WAVE DRAG VERSUS MACH NUMBER

D575 -4

S_{REF} = 276. FT^2

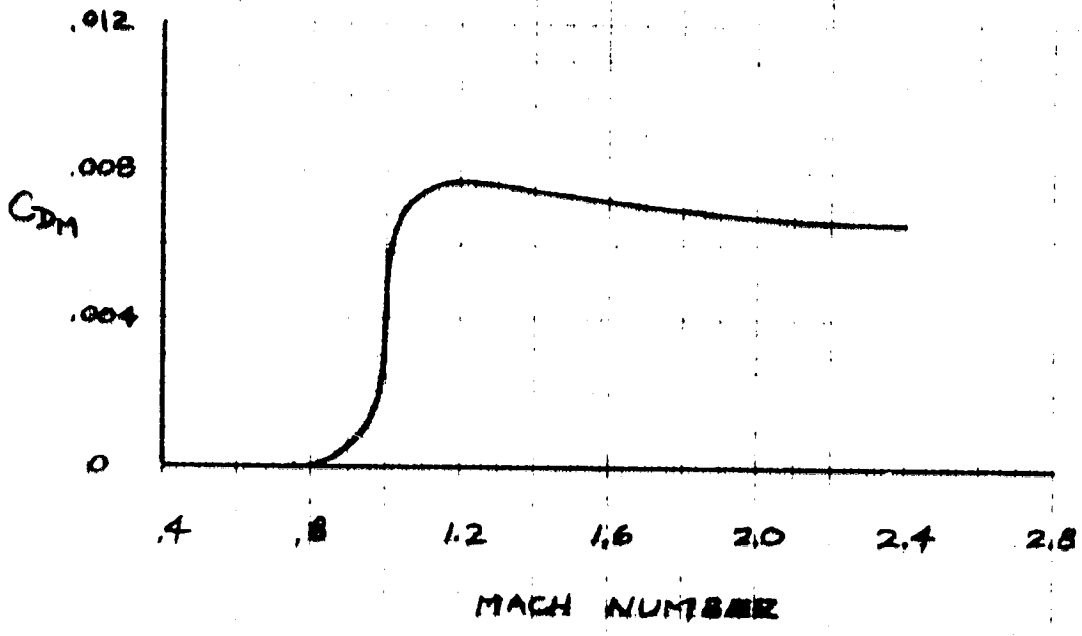

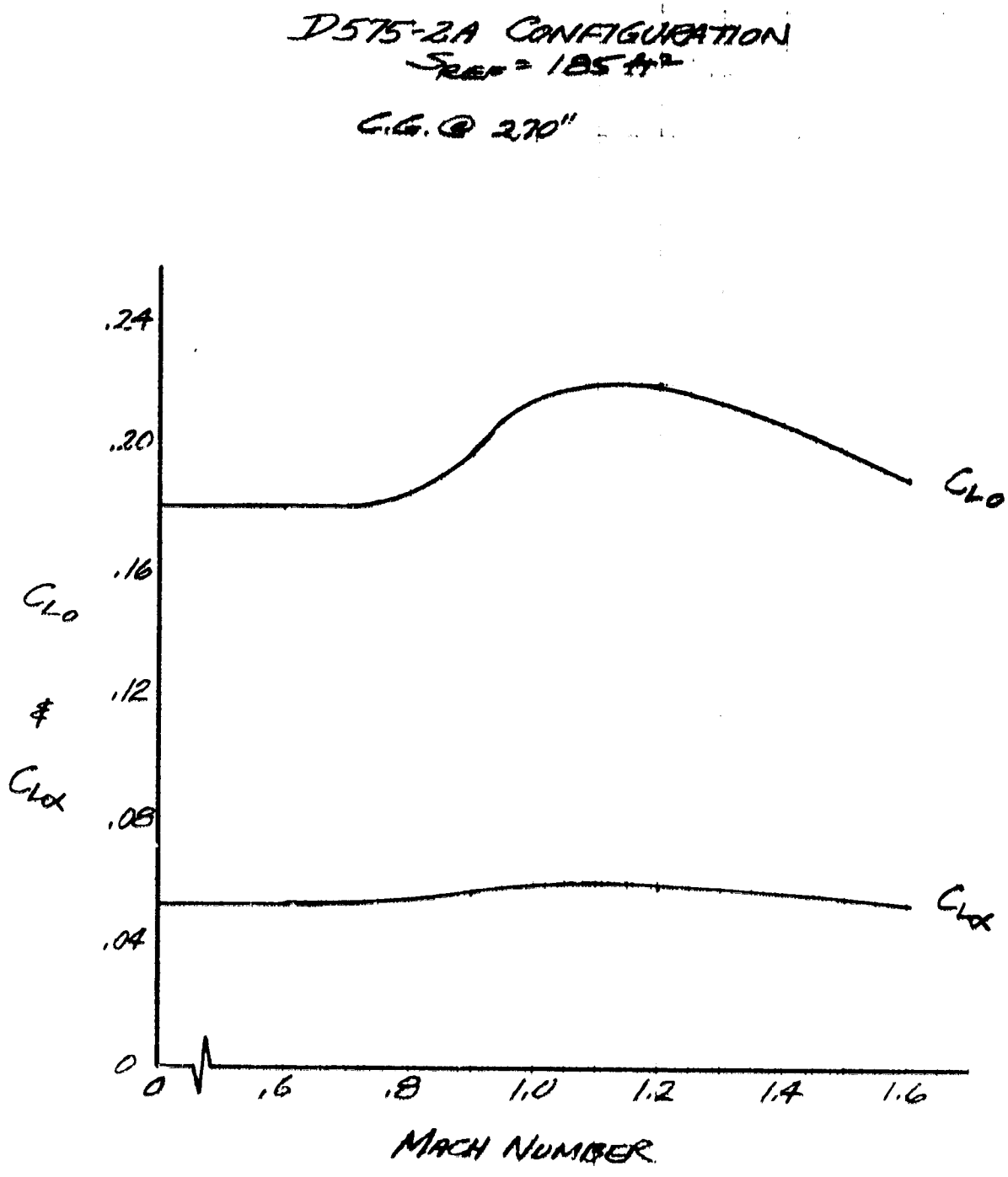

FIGURE 75. LIFT CURVE SLOPE AND LIFT AT $\alpha_C = 0°$ VERSUS MACH NUMBER, D575-2A

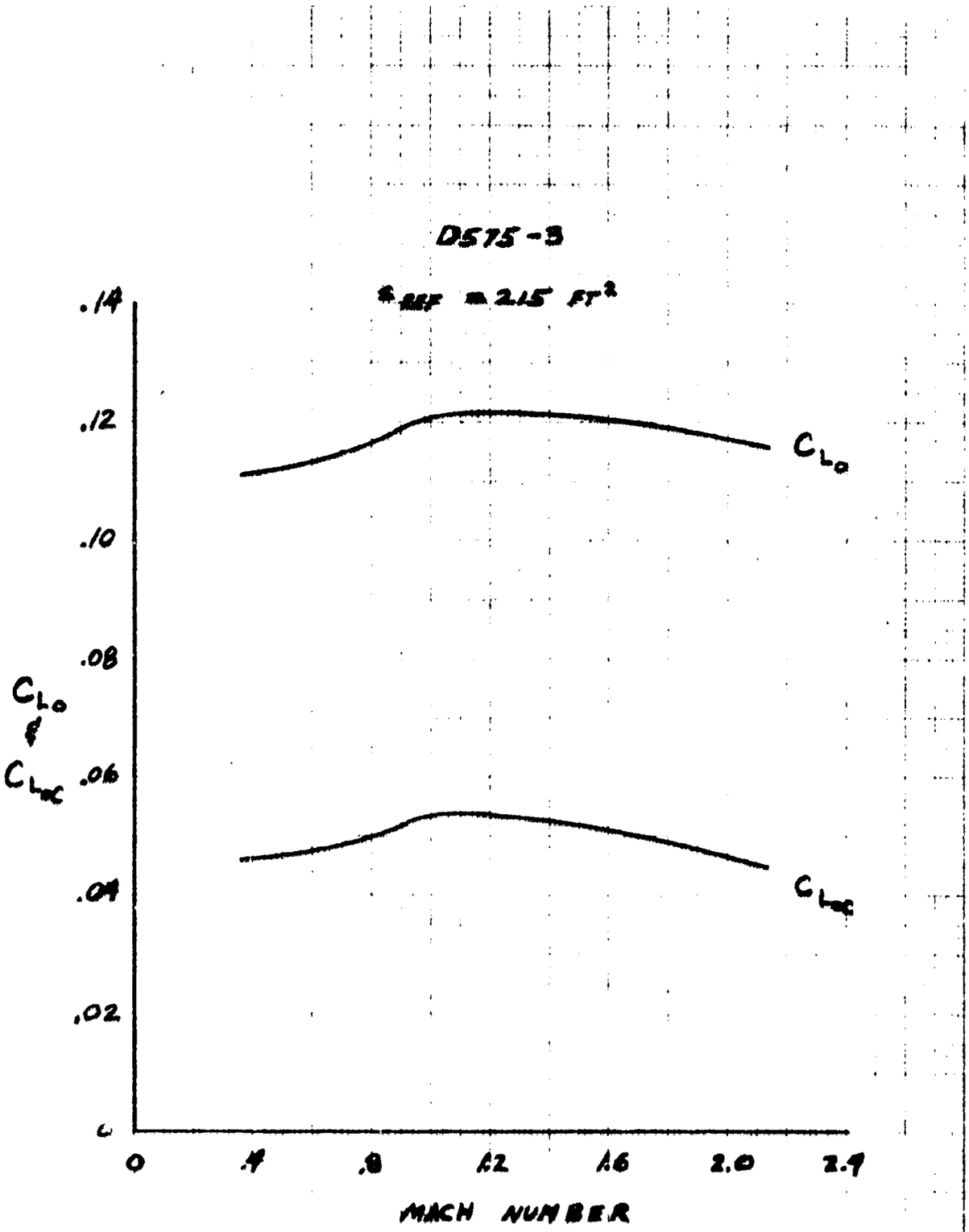

FIGURE 76. LIFT CURVE SLOPE AND LIFT AT $\alpha=0°$ VERSUS MACH NUMBER, D575-3

D575-4

$S_{REF} = 276. FT^2$

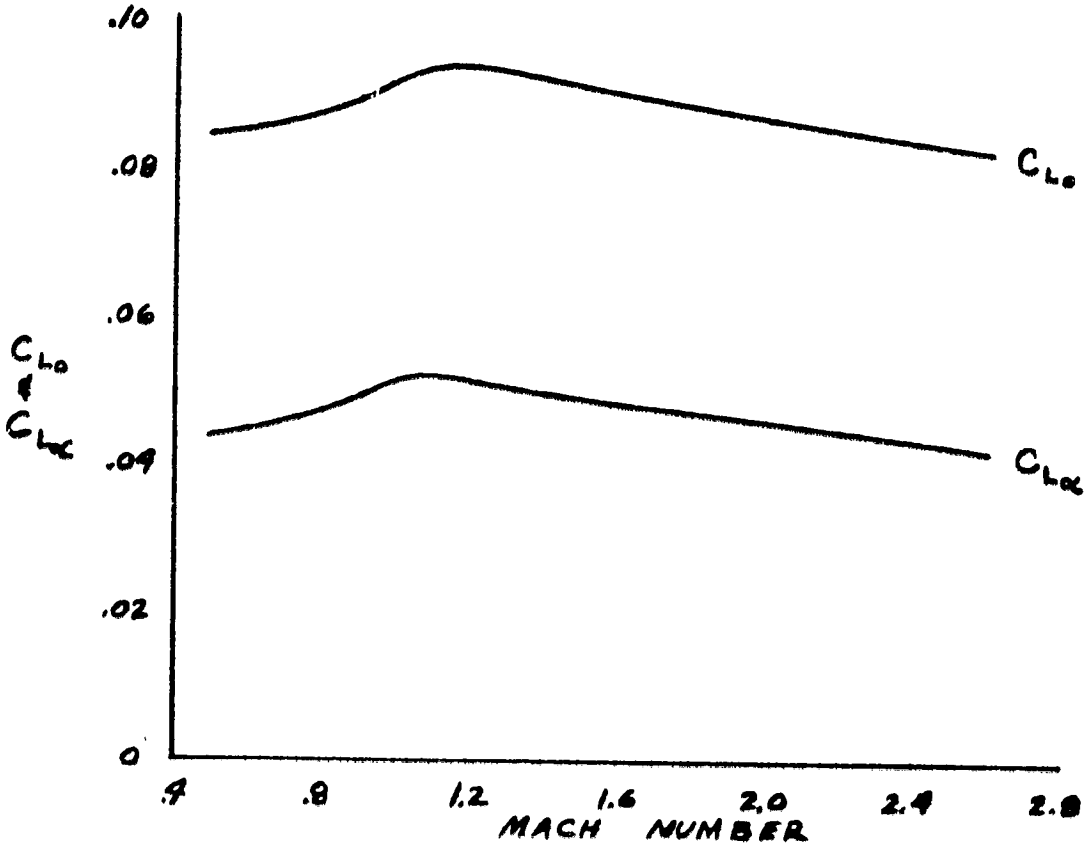

FIGURE 77. LIFT CURVE SLOPE AND LIFT AT $\alpha=0°$ VERSUS MACH NUMBER, D575-4

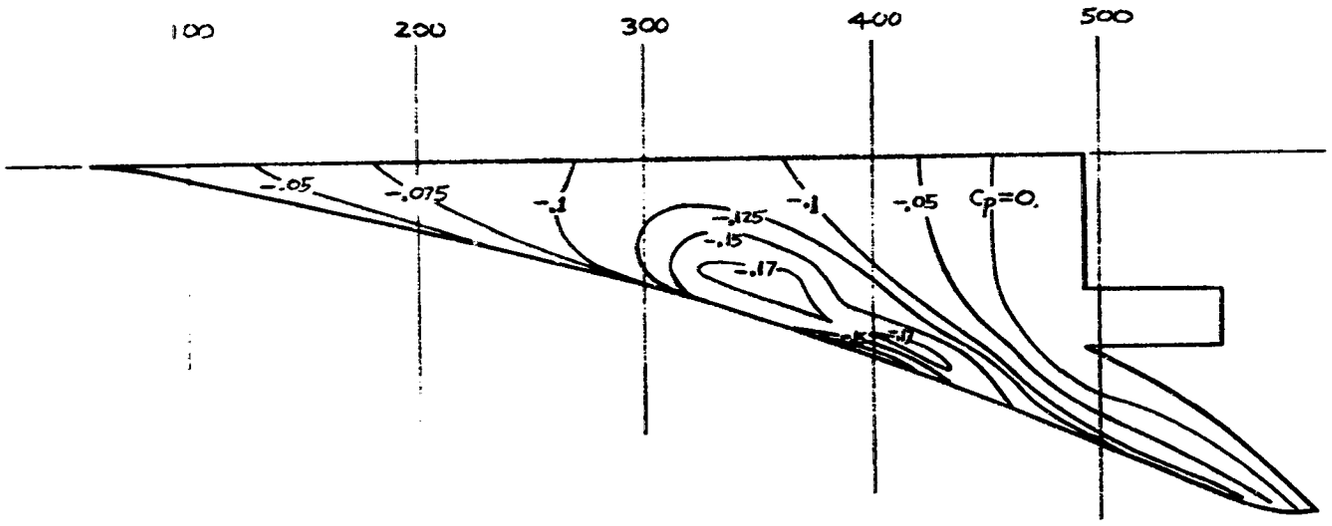

FIGURE 78. ISOBAR PATTERN FOR D575-3 AT M=.9 , C_L= .118

Lateral-directional stability is a function of lift per unit angle of attack and the center of pressure. It can be seen on figures 31 and 32 (pages 54 and 55, respectively) that for these planforms the lowest lift as well as the most forward center of pressure occurs at low speed. Experimental tests on planforms similar to these have shown that nonlinearity of pitching moment versus lift coefficient is more pronounced at low Mach numbers. For the above reasons the stability and control characteristics were investigated at low speed.

Experimental test data obtained by Rockwell International on similar configurations (references 21 and 22) have been correlated with the stability and control derivatives predicted by the Unified Vortex Lattice Program. These results showed excellent correlation in the low to moderate lift coefficient range. These data also showed that the only parameters showing any appreciable nonlinearity was lift, pitching moment, yawing moment , and rolling moment while trailing edge effectiveness was essentially linear versus angle of attack.

Figure 79 shows the estimated stability and control characteristics of the D575-2A configuration and figure 80 shows them for the control surfaces. The nonlinear variations of C_{L_α}, C_L/C_m, C_{n_β}, and C_{ℓ_β} are shown on figures 83 through 85. These variations were obtained from the wind tunnel data of references 21 and 22. It can be seen from figure 81 that extending the canard results in an increase in lift at a given angle of attack. It can also be seen that trimming the configuration by trailing edge deflection results in an additional increase in lift at a given angle of attack. A similar estimate for the D575-1 is shown on figure 82. It can be seen for this configuration that extending the canard does not result in an increase in lift and that trimming results in a loss in lift in the intermediate angle of attack range. This is due to the stability of the airplane (dC_m/dC_L) and the nonlinearity of the pitching moment.

The D575-2A configuration has a two-dimensional plug nozzle on the engine which can be used for pitch or roll control. The maximum power gross thrust coefficient at M=0.6 and an altitude of 10,000 feet was used to compute the effectiveness parameters shown in figure 79. At 8 "g", 20,000 feet and 20 degrees deflection of the nozzle, 40 percent of the total unbalanced pitching moment is trimmed out by the nozzle, therefore assuring adequate control to the maximum airplane limits as well as a linear variation of trailing edge deflection versus angle of attack.

As discussed in section III the ratio of $C_{n_\beta}/C_{\ell_\beta}$ should be approximately -0.5 for favorable rolling performance. It can be seen from figure 79 that the D575-2A meets this criteria.

During the landing approach it is desirable to be able to roll the airplane 30 degrees in one second to compensate for gusts. In the landing approach power is applied to maintain 20 feet per second rate of descent. At this power setting, if the nozzles are deflected differentially 20 degrees the rolling moment input is $\Delta C_\ell = 0.033$. As shown in reference 21 this is sufficient to obtain 30 degrees roll in one second.

D575-2A CONFIGURATION

M=0.6

All coefficients are per degree

$C_{L_\alpha} = .0516$

$dC_m/dC_L = .011$

$C_{L_{\delta e}} = .0259$

$C_{m_{\delta e}} = .0156$

$C_{L_{\delta_{THRUST}}} = .003$

$C_{m_{\delta_{THRUST}}} = .004$

$\Delta C_{Y_{\beta_W}} = -.0038$

$\Delta C_{n_{\beta_W}} = .0016$

$\Delta C_{\ell_{\beta_W}} = -.0024$

$\Delta C_{Y_{\beta_F}} = -.0006$

$\Delta C_{n_{\beta_F}} = -.0006$

$\Delta C_{\ell_{\beta_F}} = 0.0$

$\Delta C_{Y_{\beta_{NAC}}} = -.0012$

$\Delta C_{n_{\beta_{NAC}}} = .0001$

$\Delta C_{\ell_{\beta_{NAC}}} = 0.0$

$C_{Y_\beta} = -.0056$

$C_{n_\beta} = .0011$

$C_{\ell_\beta} = -.0024$

$C_{Y_p} = -.0051$

$C_{n_p} = .0020$

$C_{\ell_p} = -.0043$

$C_{Y_{\delta a_{1,2}}} = -.0018$

$C_{n_{\delta a_{1,2}}} = .0008$

$C_{\ell_{\delta a_{1,2}}} = -.0024$

$C_{Y_{\delta r_3}} = -.0011$

$C_{n_{\delta r_3}} = .0006$

$C_{\ell_{\delta r_3}} = -.0006$

$C_{Y_{\delta a_{1,2,3}}} = -.0029$

$C_{n_{\delta a_{1,2,3}}} = .0014$

$C_{\ell_{\delta a_{1,2,3}}} = -.0030$

$\Delta C_{n_{THRUST}} = 0.0$

$\Delta C_{\ell_{THRUST}} = .0016$

Figure 79. Estimated Stability and Control Characteristics of Configuration D575-2A

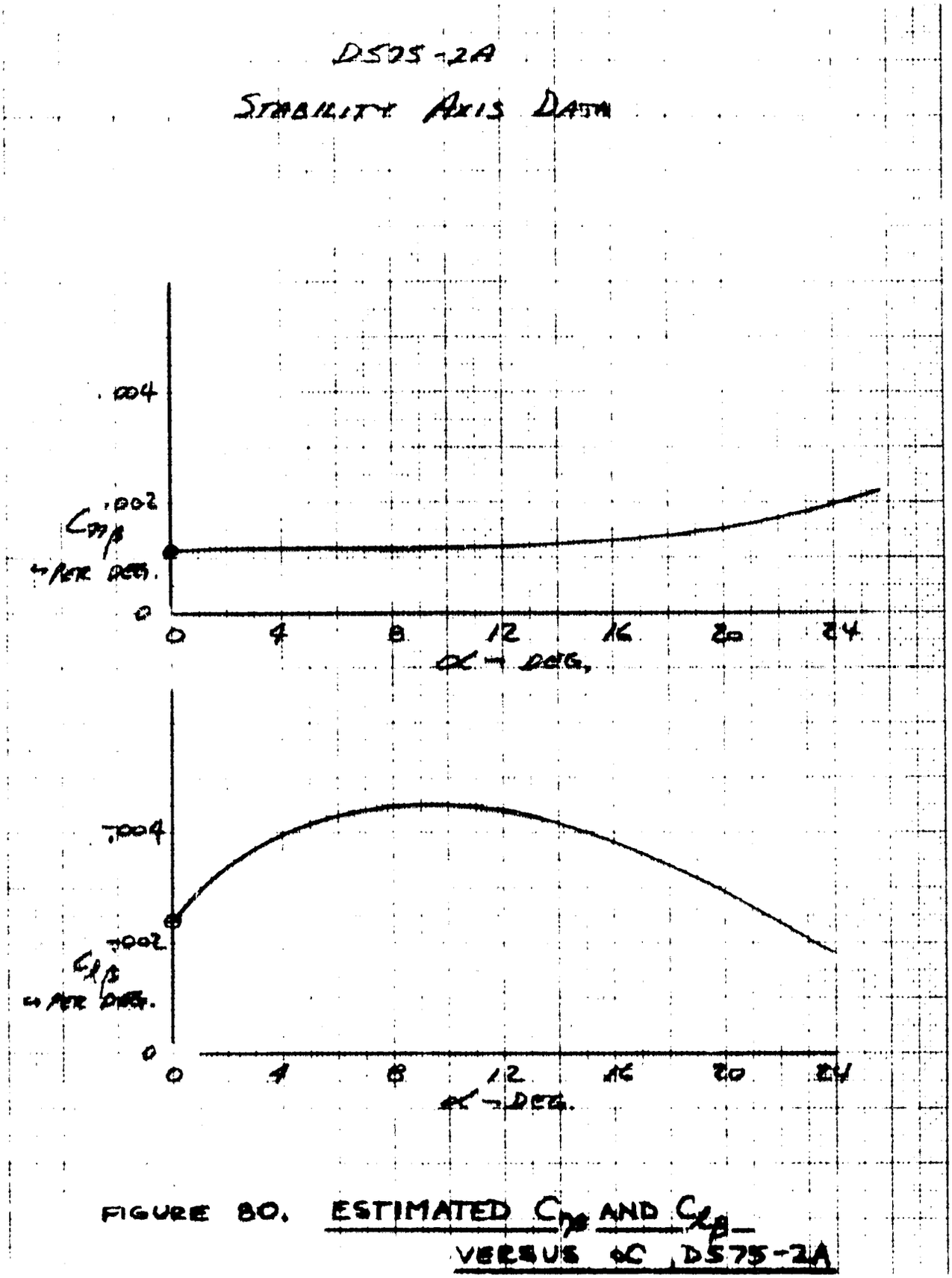

FIGURE 80. ESTIMATED C_{n_β} AND C_{l_β} VERSUS α, D575-2A

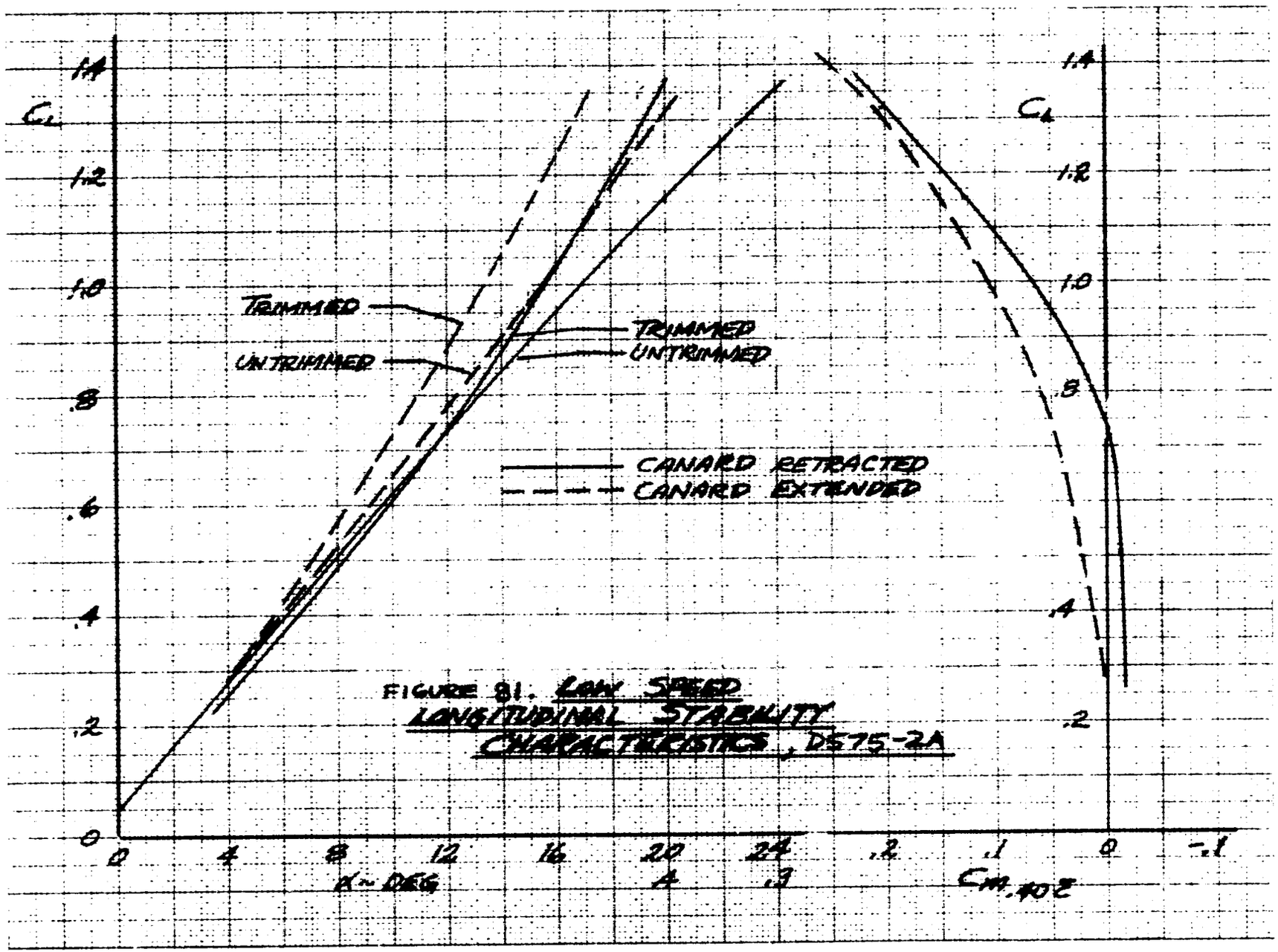

FIGURE 81. LOW SPEED LONGITUDINAL STABILITY CHARACTERISTICS, DS75-2A

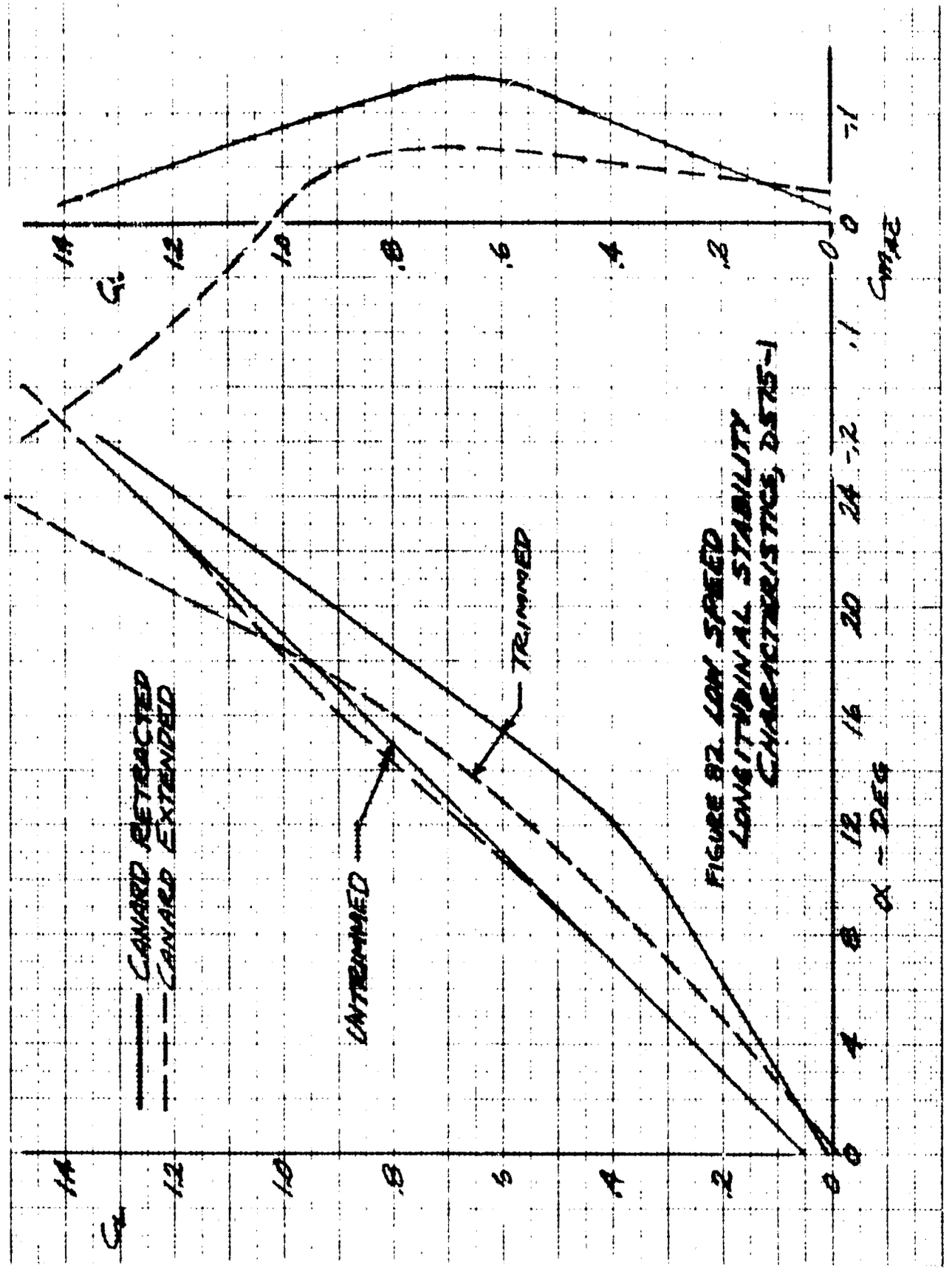

FIGURE 82. LOW SPEED LONGITUDINAL STABILITY CHARACTERISTICS, DSTS-1

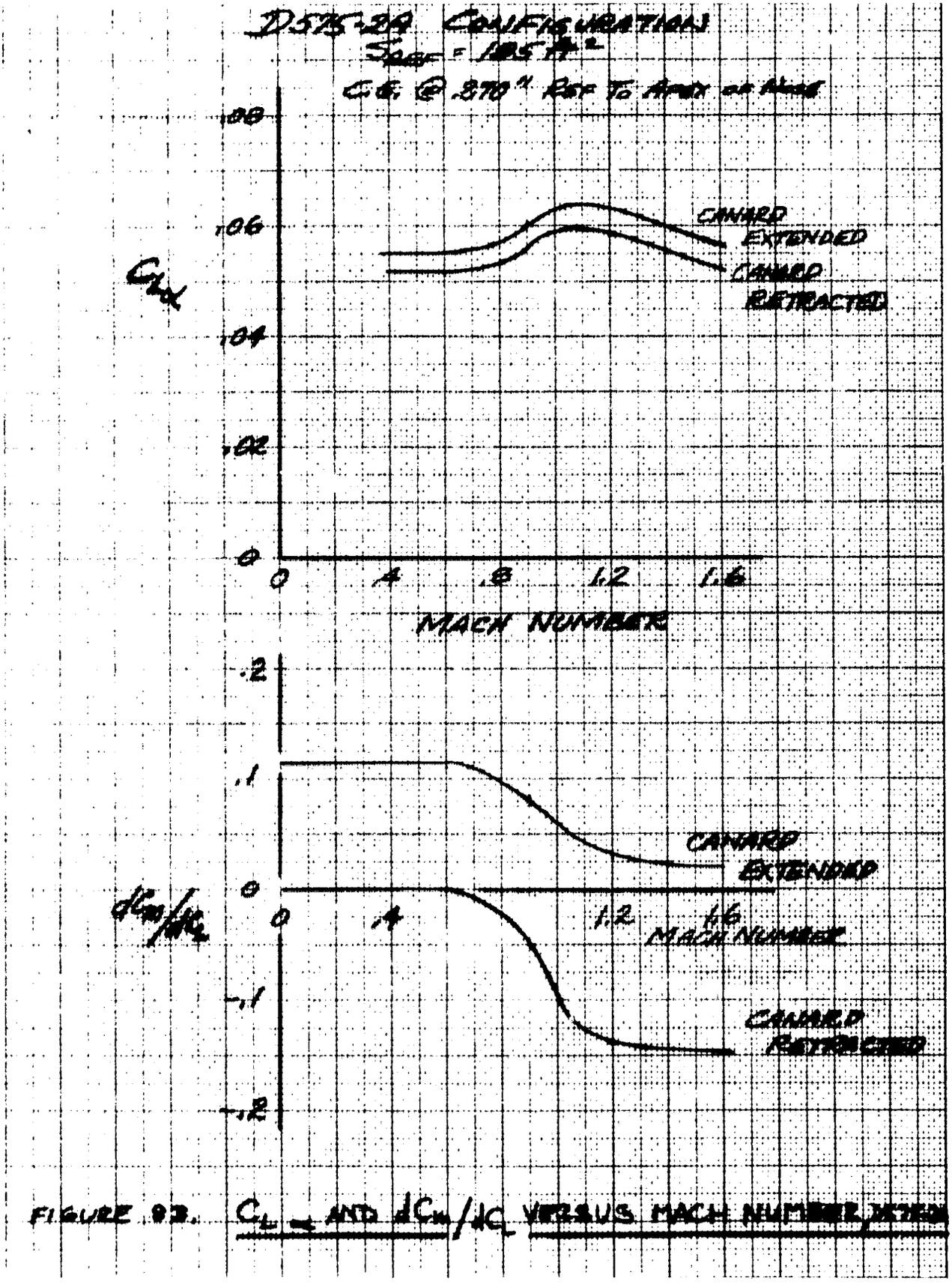

FIGURE 93. C_{L_α} AND dC_m/dC_L VERSUS MACH NUMBER, XCG=

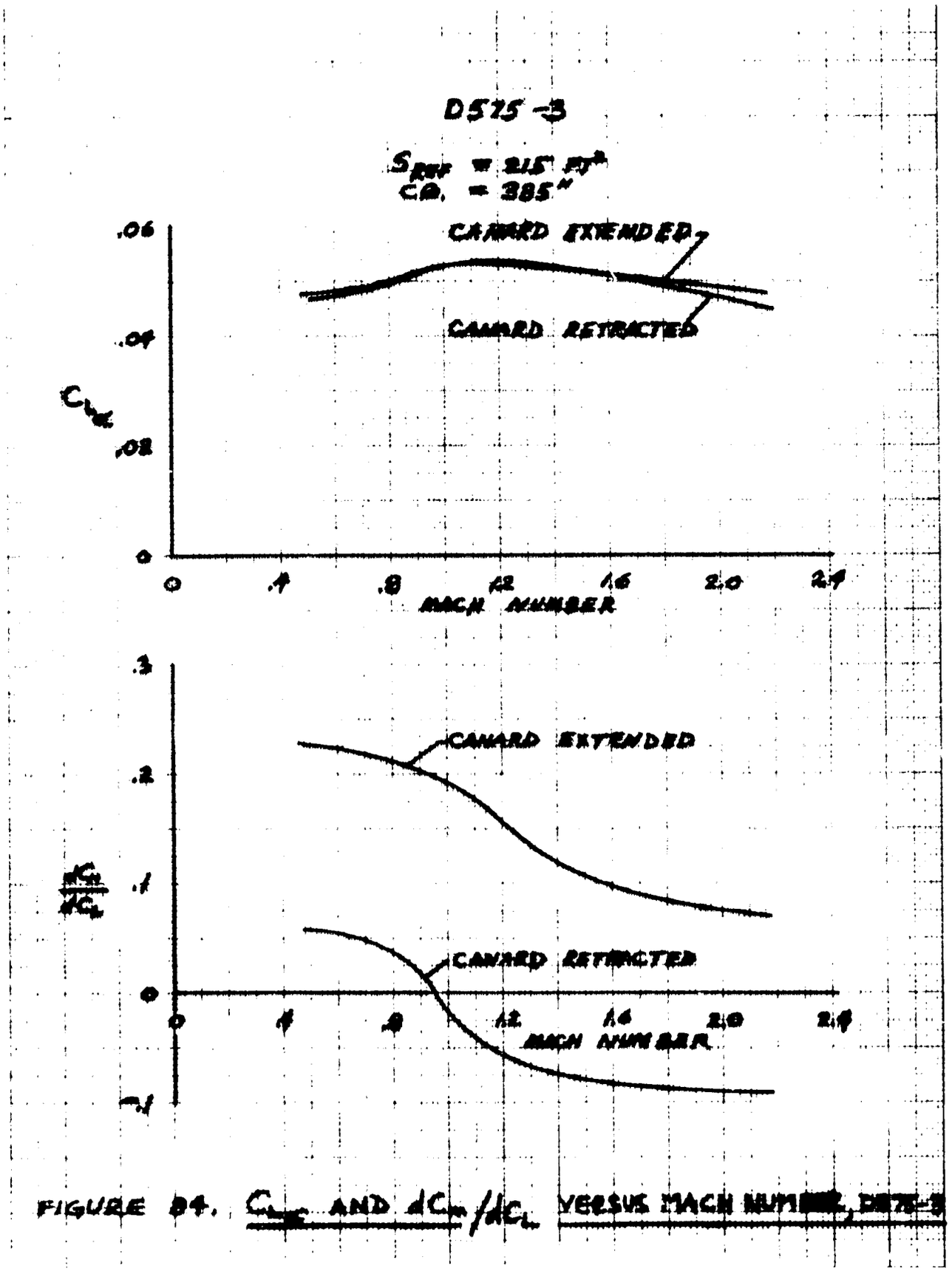

FIGURE 84. $C_{m_{\alpha}}$ AND dC_m/dC_L VERSUS MACH NUMBER, DATA-3

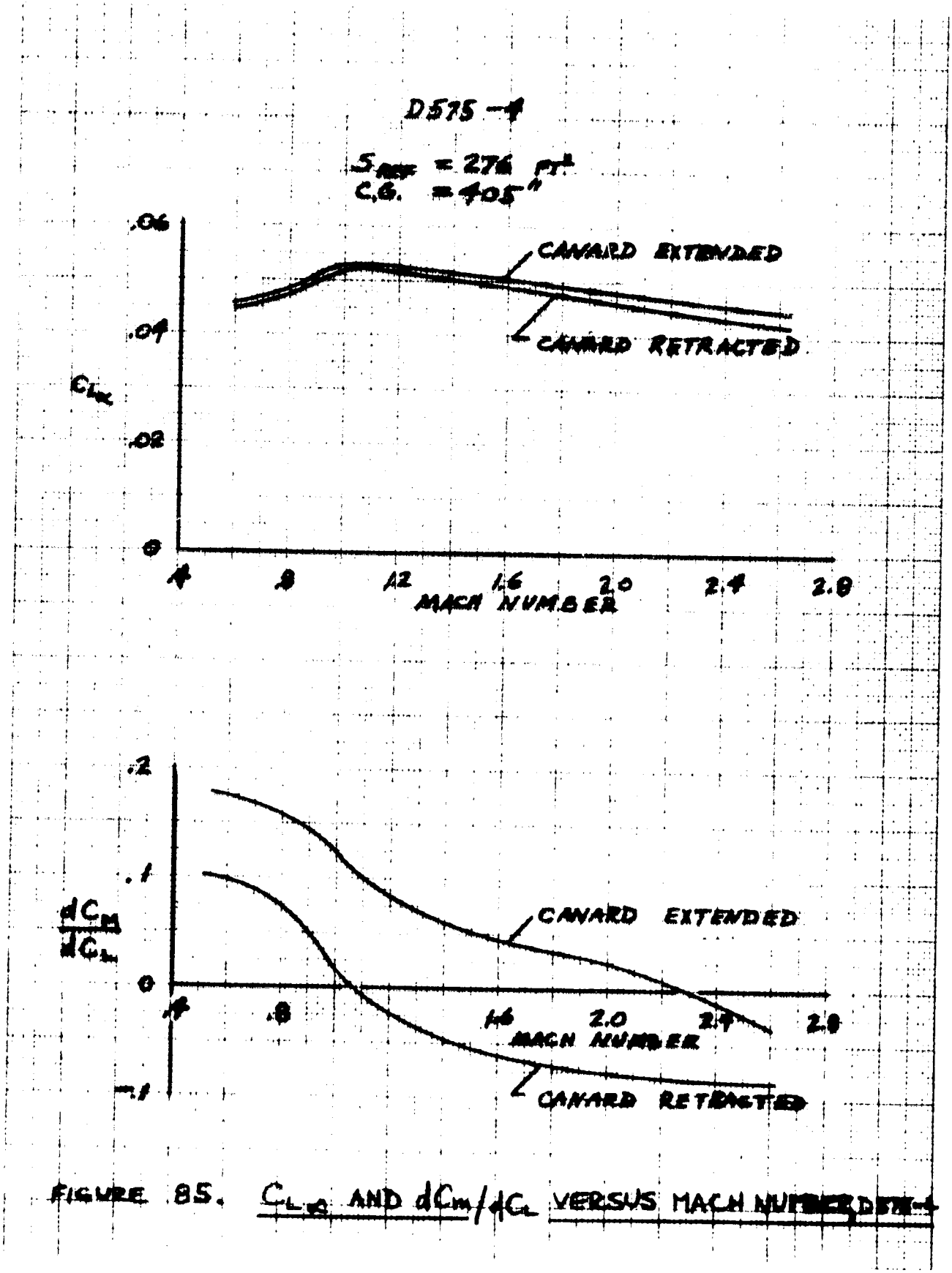

FIGURE 85. C_{L_α} AND dC_m/dC_L VERSUS MACH NUMBER, D575-4

Section V

STRUCTURAL ANALYSIS AND WEIGHT ESTIMATION

GENERAL

The structural analysis of the three maneuvering fighter configurations was performed using the Structural Weight Estimating Program (SWEEP) which was developed by the Los Angeles Aircraft Division of Rockwell International under contract with the Air Force System Command, Wright Patterson Air Force Base. SWEEP was developed to provide rational structural weight estimates and trend data for the conceptual and early preliminary design stage of an aircraft development.

The computer program, reference 15, which is referred to as SWEEP has a basic rigid airload routine, and a first order flutter stiffness approximation. It has capability of both a conventional metal and advanced composite structural synthesis for lifting surfaces and conventional metal structural synthesis for fuselage, nacelles, landing gear, and air induction structure. SWEEP includes two stand-alone programs that will evaluate the effects of flexible loads and a flutter optimization for lifting surfaces. The results of these two programs can be used in the basic program in lieu of the built-in routines at the option of the user. The SWEEP program capabilities are described briefly in references 16 and 17.

LOADS

The basic loads calculated for the structural analysis are rigid. Since these configurations do not fit the built-in aircraft model used by SWEEP, some adjustments had to be made in order to model it for the structural evaluation. The varying wing dihedral had to be made a planer one. The wing was unrolled into a common Z plane maintaining the same leading and trailing edge sweep angle. The resulting geometry was then evaluated and is as follows for the three configurations.

	D575-2A	D575-3	D575-4
Mach Number	1.6	2.0	2.5
S_w (sq. ft.)	194.36	225.76	290.07
AR	2.97	2.97	2.97
λ	.233	.233	.233
Λ_{LE}	65° 25'	70° 0'	72° 15'
C_R (in.)	157.512	169.798	192.381

The symmetrical maneuver loads were estimated at M_L for three altitudes, sea level, 20,000 feet and the maximum Mach number altitude. The speed profiles for the three aircraft are as shown in figure 86. One additional speed was checked and that was for Mach 0.9 at sea level. The SWEEP model for loads assumes that there is a separate lifting surface for trimming the aircraft. SWEEP was used as a tool for estimating centers of pressure for fuselage nose, canard, exposed wing, wing carryover lift and a portion of the wing planform outboard of the nacelle. It was assumed that the estimated center of pressure for the planform outboard of the nacelle would be the application point for the balancing trim load to give a total vehicle lift center of pressure equal to the aircraft center of gravity. A balanced airload system was then calculated for a one degree angle of attack and it was scaled up to give the proper vehicle load factor. The canard was assumed to be fully extended in the transonic region and fully closed at the supersonic speeds. The resulting airloads were used as the external vehicle airload in the SWEEP calculations. The lift distribution for the wing is assumed to be the same as that which results from a trapezoid wing at the given speeds ignoring any redistribution required for wing blending, or possible balancing twist and camber distributions. No gust, pitching, or yawing maneuver loads were checked.

The maximum takeoff gross weight (MTOWT) is defined with 1000 pounds of fuselage stores and 300 rounds of ammunition. This weight was also used for maximum taxi weight for landing gear loads since no alternate loadings are available at this point in time. The basic flight design gross weight (FDWT) is defined as the MTOWT less 50 percent internal fuel. The landing design gross weight (LDWT) is defined as MTOWT less 60 percent internal fuel. Based on the above definitions the following are the design weights used for the three configurations.

	D575-2A	D575-3	D575-4
MTOWT (lbs)	15060	18090	23985
FDWT (lbs)	13113	15378	19753
LDWT (lbs)	12723	14835	18906

The vertical load factors used to determine critical loads at FDWT are +7.33 and -3.0. The landing sink speeds are 6 ft/sec at MTOWT and 10 ft/sec at LDWT.

The wing critical loads are shown in figures 87 to 90. The loads are for the D575-2A configuration. The critical loads for the D575-3 and -4 configurations are shown on figures 91 through 98. SWEEP data for the D575-2A only will be shown in all the following plots, but the same type of data is available for all configurations. In all the structural evaluations it was found that the highest Mach number was the critical wing condition due to the higher temperature and material property degradation with temperature associated with this condition. The following temperatures were determined by the skin temperature routine of SWEEP.

ALTITUDE FT	MACH NO.	TEMPERATURE °F
0	0.9	135
0	1.006	153
20,000	1.484	165
23,800	1.7	198
33,750	2.1	249
42,500	2.6	380

Figure 99 shows a simple sketch of the wing planform for D575-2A without the curved leading edge. It shows that the wing was separated into outboard and inboard panels for structural analysis. The load reference axis for these two panels are defined in this figure and all wing stations are measured along these axis. The origin of the load axis is always at the intersection of the aircraft centerline with the axis.

MATERIAL PROPERTIES

The structure of the three configurations is primarily built of composite materials. The composite material used in the primary structure is graphite/epoxy except for the Mach 2.5 configuration. The temperature increased to outside the graphite/epoxy material range hence estimated data for graphite/polyimide was substituted. The properties used for these two materials in the SWEEP stress analysis are shown in figures 100 through 103. This data is based on the information presented in references 18 and 19. Only lifting surfaces can be stressed for composite material in the current version of SWEEP. The other structures such as fuselage, landing gear, nacelles and air induction ducts and ramps can only be analyzed for metal structure. The fuselage skins and frames are 2024-T851 aluminum alloy while the longerons are 7075-T6511 aluminum alloy. In the Mach 2.5 configuration these two materials were changed to 6AL-4V Titanium alloy. The material properties for metal comes from MIL-4DBK-5B.

WING

The wings have been analyzed as two distinct panels. The parting line between the inboard and outboard panels is the break in the trailing edge. The wing thickness ratio is defined in figure 104.

The outboard panel construction is graphite/epoxy skins and closeout spars with full depth aluminum honeycomb core. The core density is four pounds per cubic foot. The inboard panel is multi-spar-plate-skin construction made of graphite/epoxy. Figures 105 through 108 show the SWEEP required number of fiber plies for the upper and lower skin. The 45 degree plies shown are the sum of both plus and minus 45 degree requirements.

Figures 109 and 110 give the cover stresses while figures 111 and 112 have the wing stiffness data. In SWEEP the following criteria is used to obtain the number of plies

1. The zero degree fiber must be able to carry all the applied axial without failure.

2. The minimum number of plus and minus 45 degree fibers must carry the applied shear load without failure.

3. The 90 degree fibers are a constant fractional value of the zero degree fiber (25 percent in this case).

4. Panel instability is solved by adding increments of plus and minus 45 degree fibers until the panel is stable under axial load.

5. All layups are balanced and symmetrical and are spread homogeneously throughout the thickness.

Figures 107 and 108 have a set of ±45 degree fibers labeled flutter. This flutter increment (71 lbs) is a result of the basic SWEEP assumptions which only adds ±45 degree fibers to maintain panel instability. Panel instability is not a problem with full depth honeycomb construction. The shear load due to torque is low enough in the outboard panel so that only four ±45 degree fibers are needed for strength. The primary supplier of torsional stiffness of a torque box in composite design is the ±45 degree fibers. Hence, for a SWEEP designed full depth honeycomb surface some form of torsional stiffness criteria must be available to get a reasonable torsional stiffness capability into the torque box.

The SWEEP built-in lifting surface torsional stiffness requirements are based on a semi-empirical technique for predicting the stiffness required to prevent flutter. This technique has proved to be very useful for high and moderate aspect ratios. However, it has been found to give fair results for lower aspect ratio surfaces, with the exception of delta wings. This technique was also originally developed to handle only flutter at subsonic speeds. An extension has been developed for modifying the results to obtain stiffness predictions for flutter at transonic and supersonic speeds.

The SWEEP generated data which was used for stiffness requirements should be conservative based on data presented in reference 20. The conclusions of reference 20 were that the aft mounted engines will cause an increase in flutter speed over the required flutter speeds for bare wings. This increase is primarily due to a high ratio of engine mass to bare wing mass. The mode line (rotation point) follows the center of gravity and high mass ratio engines tend to remain fixed in space because of their greater inertia. The engine mass ratio of reference 20 is 1.23. The engine mass ratios for our three configurations are 1.9, 1.6 and 1.4 for the Mach 1.6, 2.0 and 2.5 vehicles, respectively.

FUSELAGE

The fuselages have been analyzed as metal construction. SWEEP does not have the capability at the present time to handle a composite fuselage. It has been assumed that if a metal fuselage is analyzed, then the composite fuselage weight could be arrived at by multiplying the metal component weights by composite to metal weight fractions. The fractions used for these configurations are as follows:

longerons	0.65
skins	0.75
frames	0.80

The fuselage is skin-frame-longeron construction. The materials which were used for the metal fuselage are 7075-T6511 aluminum alloys for longerons, 2024-T851 aluminum alloy for skins and minor frames, and 6AL-4V Titanium alloy for highly loaded support frames. All components are 6AL-4V titanium alloy for the Mach 2.5 configuration. The critical shear and bending moment are given in figures 113 and 114 . The resulting longeron areas and skin gages are given in figures 115 and 116. Most of the fuselage skin gages are set by panel flutter.

LANDING GEAR

The landing gear loads analysis of SWEEP follows the procedure outlined in MIL-A-008862A. The resulting loads for the Mach 1.6 configuration are shown in table VIII. Tables IX and X give the main and nose gear weight required to accommodate the loads of table VIII for the gear arrangement shown on the configuration drawing. The gear structure analysis is based on using a 240000 heat treat steel.

STRUCTURE GROUP WEIGHTS

The structural weights were obtained from the SWEEP analysis for each configuration. The composite structural weights for those items which were analyzed as a metal structure has been obtained by multiplying by a composite to metal weight fraction. The weight fractions based on local Rockwell studies are as follows:

Nacelle	0.85
Air induction ducts and variable inlets	0.85
Longerons (fuselage)	0.65
Skins (fuselage)	0.75
Frames (fuselage)	0.80

The leading and trailing edge structural weight for lifting surfaces in SWEEP are obtained by statistical equations which are a function of geometry, speed, and gross weight. The correlation for these equations are based on metal parts hence scaling weight factors which are based on local studies were used to arrive at composite structural weights. The scale factors are as follows:

Fixed leading edge structure	0.8
Leading edge camber devices	0.8
Fixed trailing edge structure	0.8
Trailing edge high lift devices	0.7

No structural weight increments have been included for aerodynamic tailoring of wing deflections.

PROPULSION GROUP WEIGHTS

The engine weight is based on scaling of Pratt-Whitney supplied parametric engine data. The remaining propulsion group weights are statistical. The fuel system weights are based on 0.10 lb of system for one lb of fuel. This is comparable to 0.09 for the F-5B, and 0.117 for the F-100A.

EQUIPMENT AND SUBSYSTEM GROUP WEIGHTS

The equipment and subsystem group weights are statistical estimates. The various functional group estimates are further subdivided for information on what has been included in the weights. The surface controls weight estimate was varied for these configurations but the rest of the groups were assumed to be constant between configurations. The weight breakdowns of the equipment and subsystem groups are shown below.

Surface Controls

Mach Number	1.6 Weight lbs	2.0 Weight lbs	2.5 Weight lbs
Cockpit controls	25	25	25
Fly-by-wire equipment	180	180	180
Wiring	40	40	40
Canard control	70	70	70
Leading edge controls	120	135	160
Trailing edge controls(incl. fuselage)	190	205	230
TOTALS	(625)	(655)	(705)

Instruments	(190 lbs)
Indicators	65
Transmitters and amplifiers	90
Installations	35
Hydraulic	(340 lbs)
Pumps	40
Reservoirs	40
Accumulators	20
Filters and valves	30
Plumbing and fluid	160
Emergency system	50
Electrical	(445 lbs)
Generators	170
Equipment	100
Distribution system	140
Lights and signal devices	35
Avionics	(580 lbs)
UHF	45
IFF	40
CADS	30
TACAN	60
ILS	15
Navigation	50
Fire control	340
Flight controls (included in surface controls)	
Armament Provisions	(670 lbs)
Gun provisions	
Drums	180
Feed, ejector, chutes, exit, conveyors	90
Starter, governor, trigger	65
Purging	20
Blast tubes and plates	30
Miscellaneous	55
Weapon control and release system	60
Launchers	100
Supports	70

Furnishing	(270 lbs)
Seat	165
Misc. accommodations	10
Oxygen system	25
Misc. equipment	30
Flooring and trim	10
Fire detection and emergency equip	30
Air Conditioning	(220 lbs)
Heat exchanger	30
Precooler	20
Water separator	5
Ducting and sealing	65
Controls and valves	90
Scoops	10

The weight summary for each configuration is given in tables XI, XII, and XIII. The center of gravity for each configuration is plotted against gross weight in figures 117, 118 and 119.

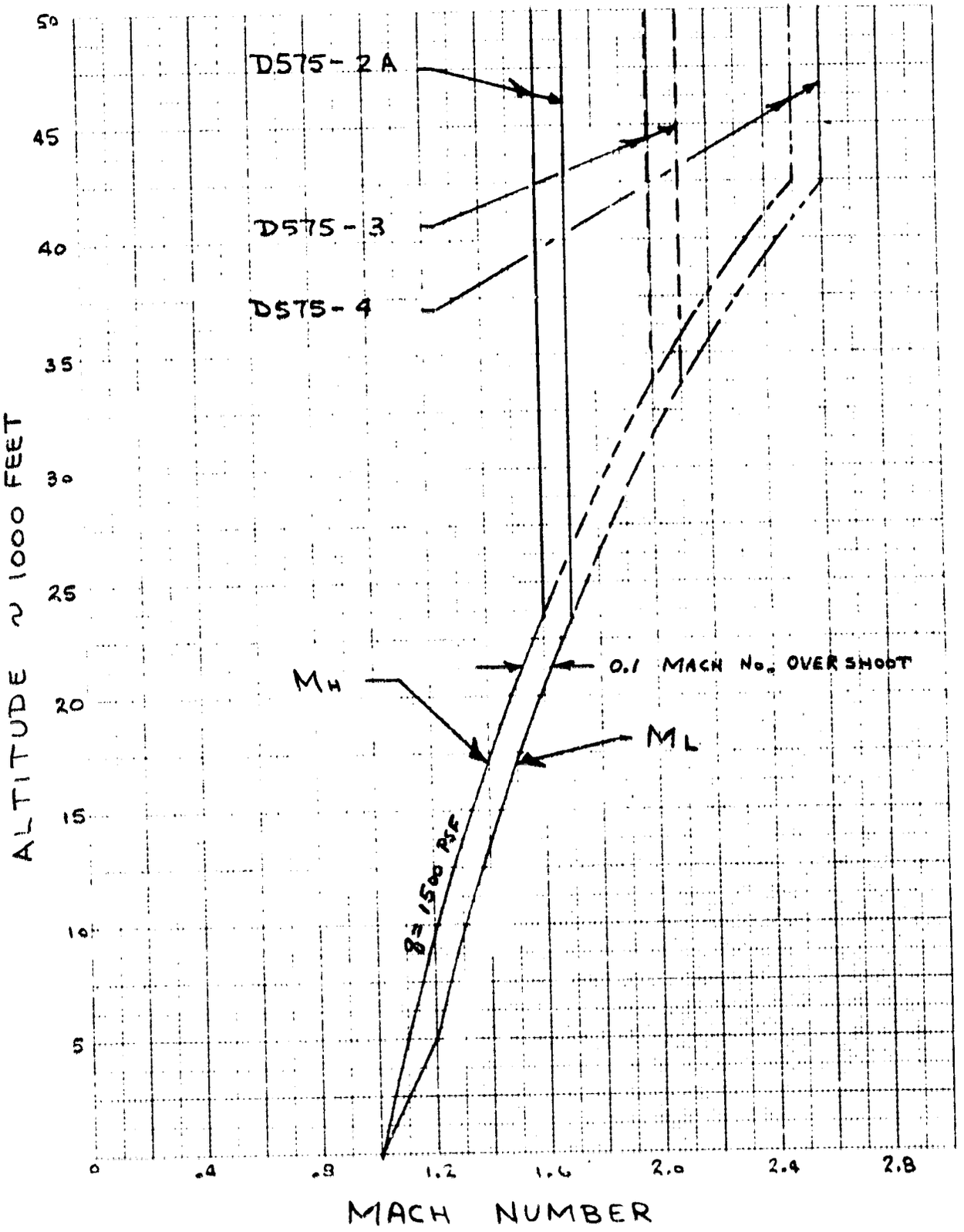

FIGURE 86. SPEED - ALTITUDE PROFILE

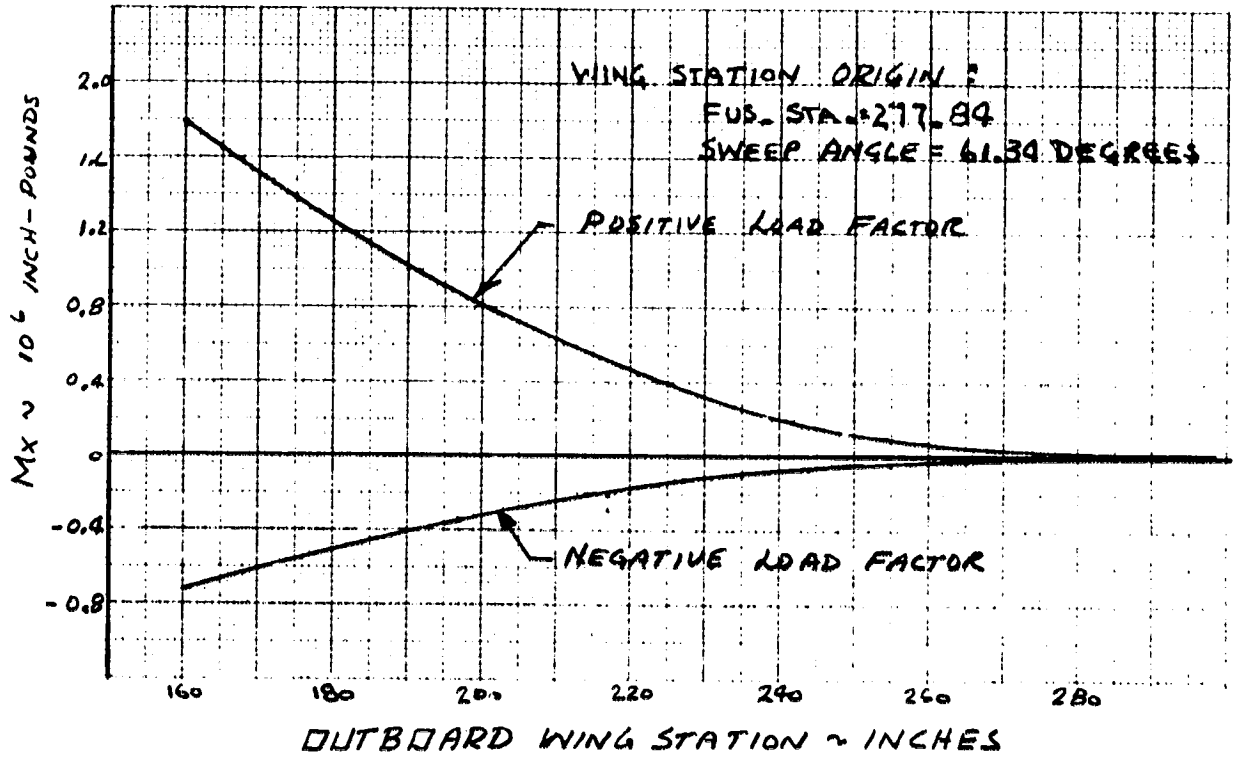

FIGURE 87. WING OUT BOARD PANEL ULTIMATE BENDING LOADS, (D575-2A)

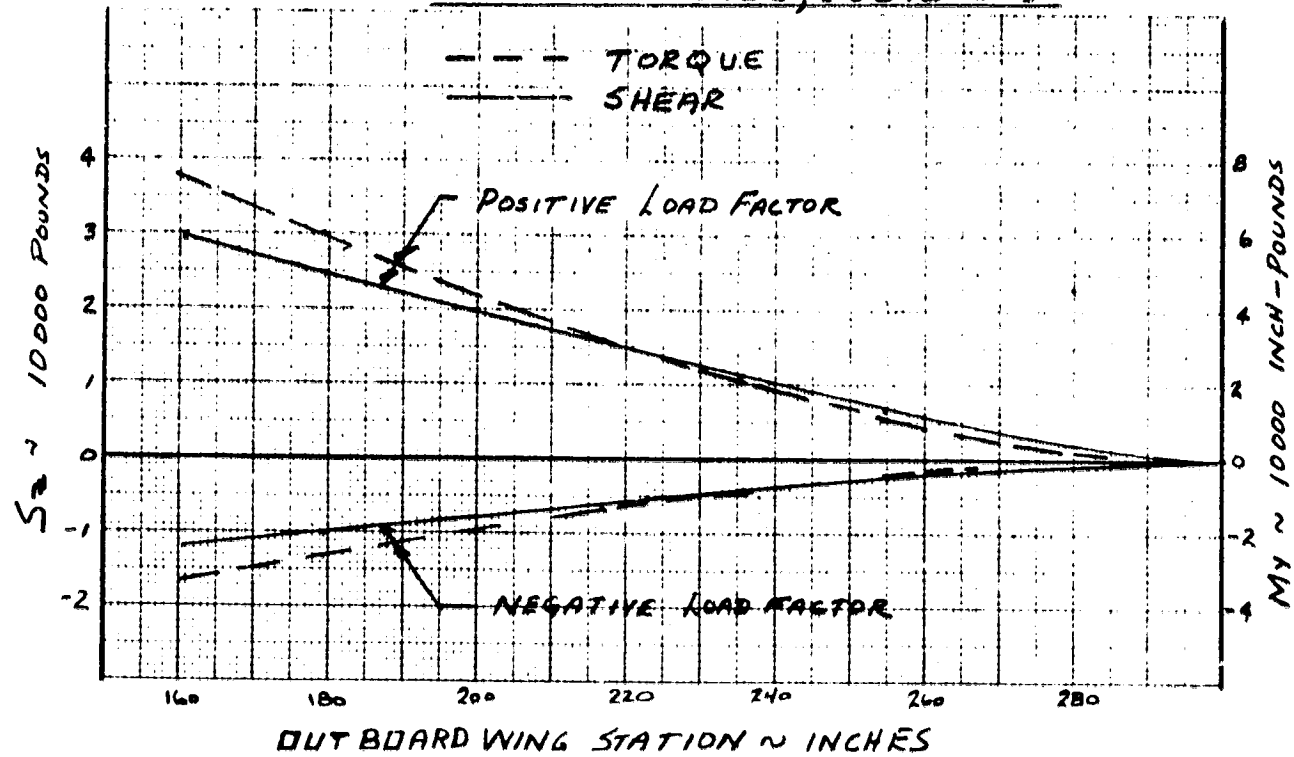

FIGURE 88. WING OUTBOARD PANEL ULTIMATE SHEAR AND TORQUE LOADS, (D575-2A)

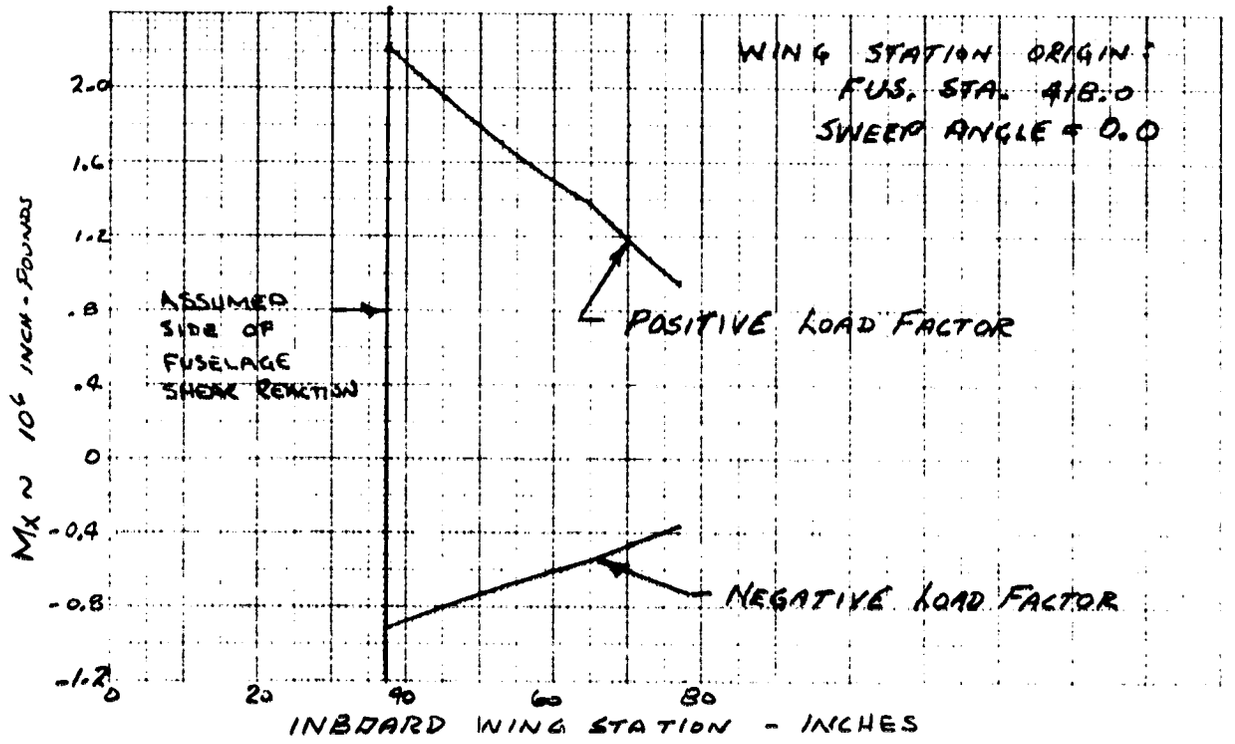

FIGURE 89. WING INBOARD PANEL ULTIMATE BENDING LOADS, (DS75-2A)

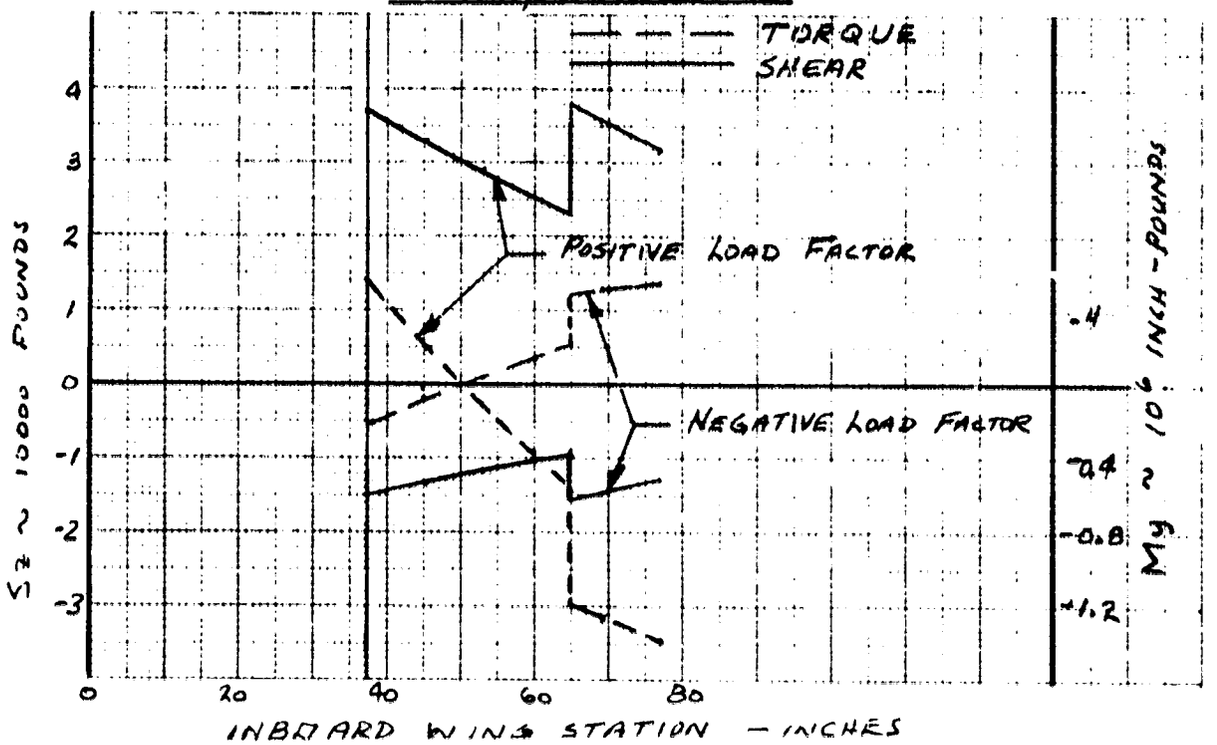

FIGURE 90. WING INBOARD PANEL ULTIMATE SHEAR AND TORQUE LOADS, (DS75-2A)

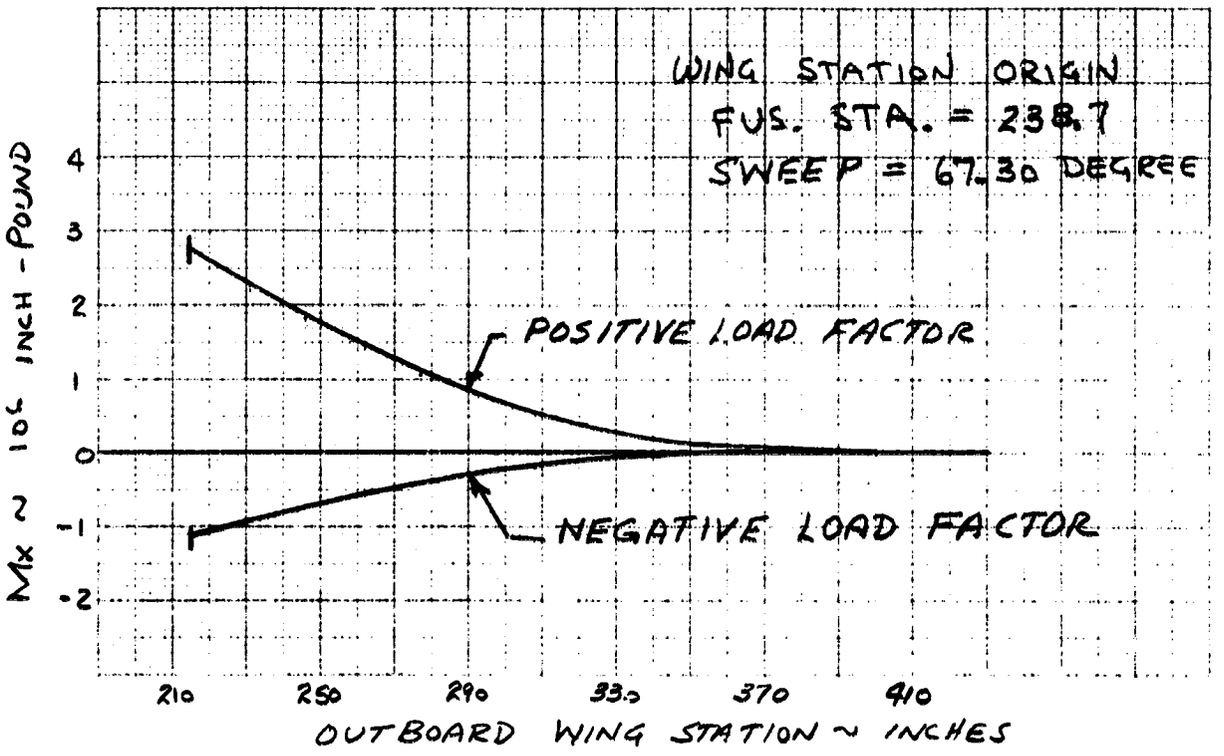

FIGURE 91. WING OUTBOARD PANEL ULTIMATE BENDING LOAD, (DS75-3)

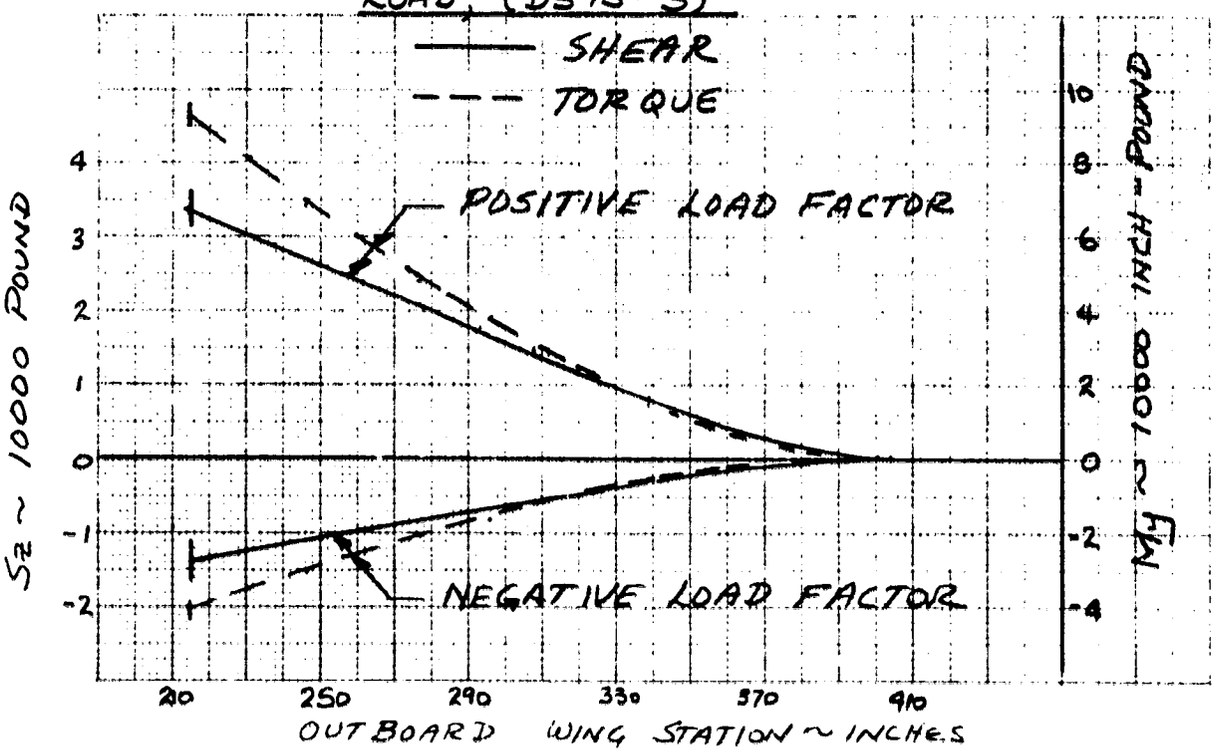

FIGURE 92. WING OUTBOARD PANEL ULTIMATE SHEAR AND TORQUE LOADS, (DS75-3)

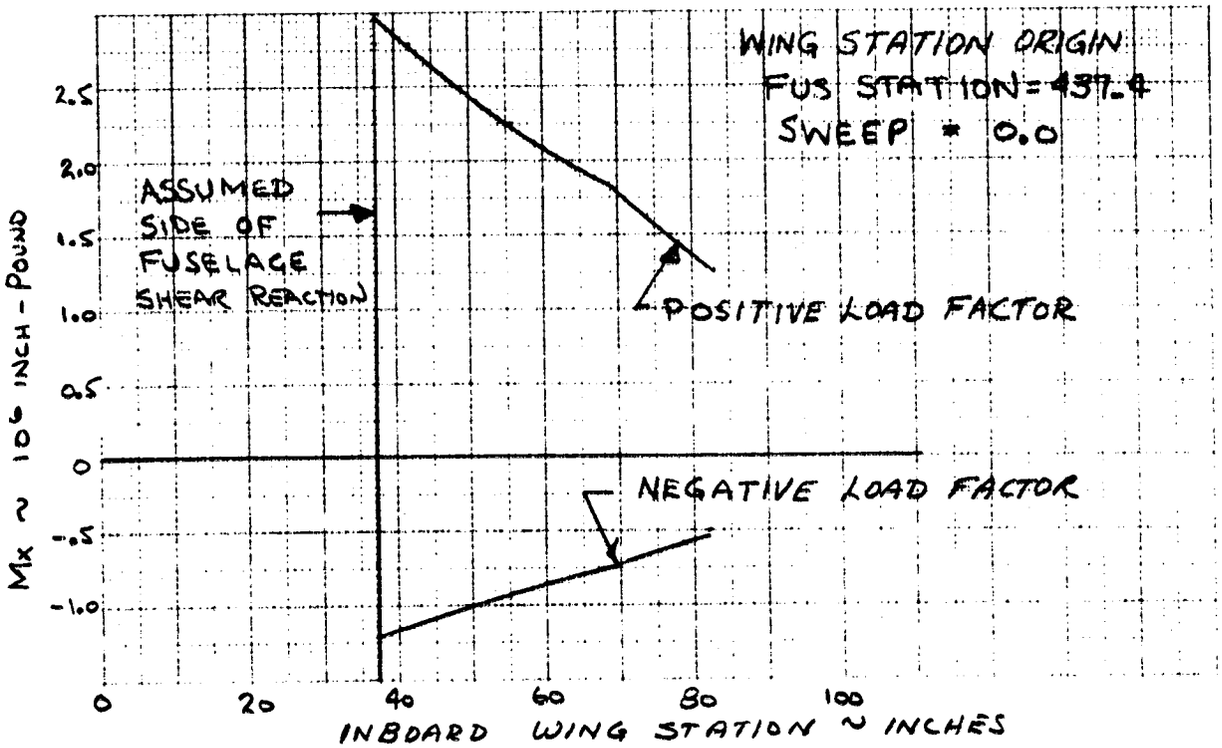

FIGURE 93. WING INBOARD PANEL ULTIMATE BENDING LOADS, (D575-3)

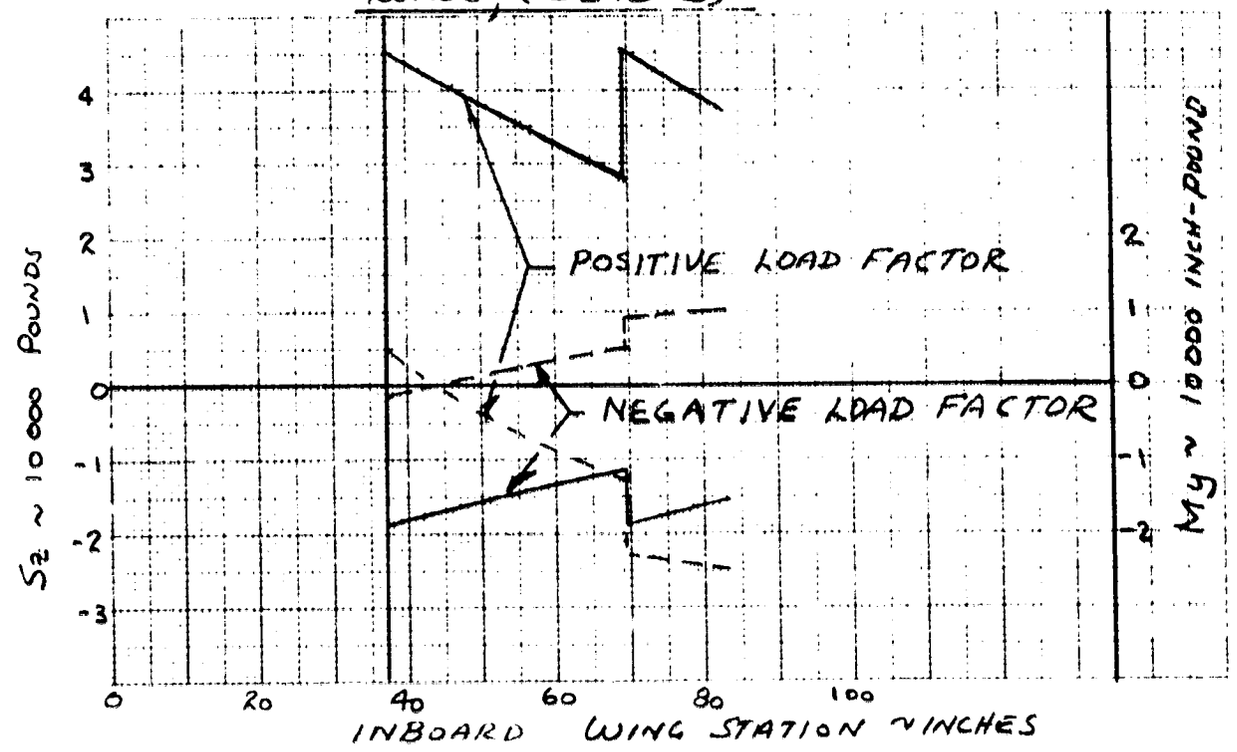

FIGURE 94. WING INBOARD PANEL ULTIMATE SHEAR AND TORQUE LOADS, (D575-3)

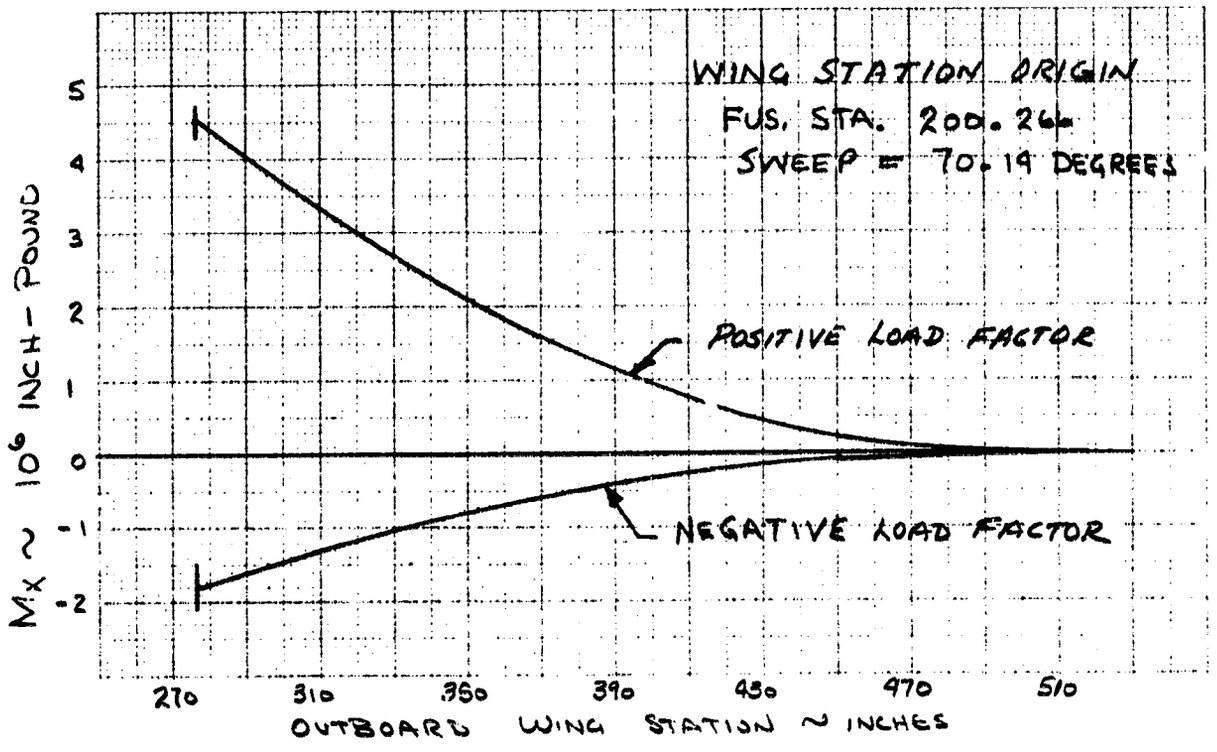

FIGURE 95. WING OUTBOARD PANEL ULTIMATE BENDING LOADS, (DSTS-4)

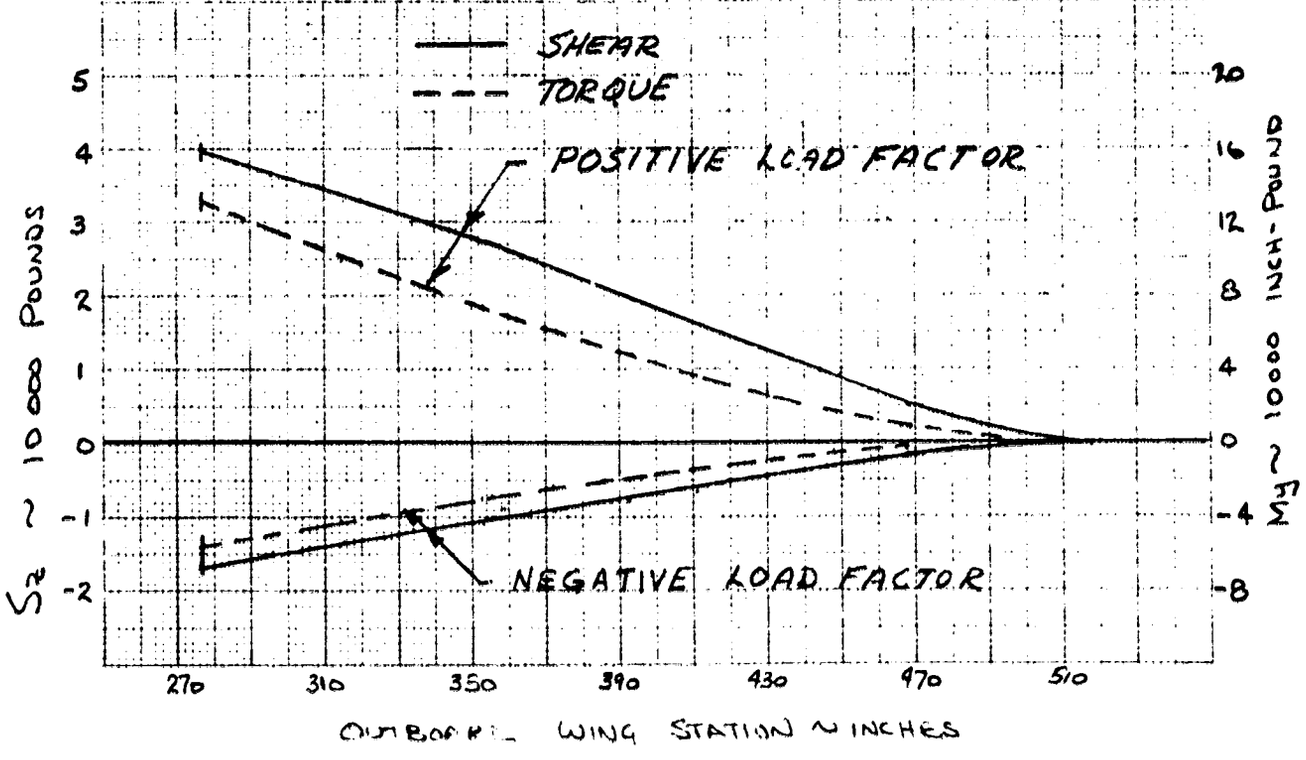

FIGURE 96. WING OUTBOARD PANEL ULTIMATE SHEAR AND TORQUE LOADS, (DSTS-4)

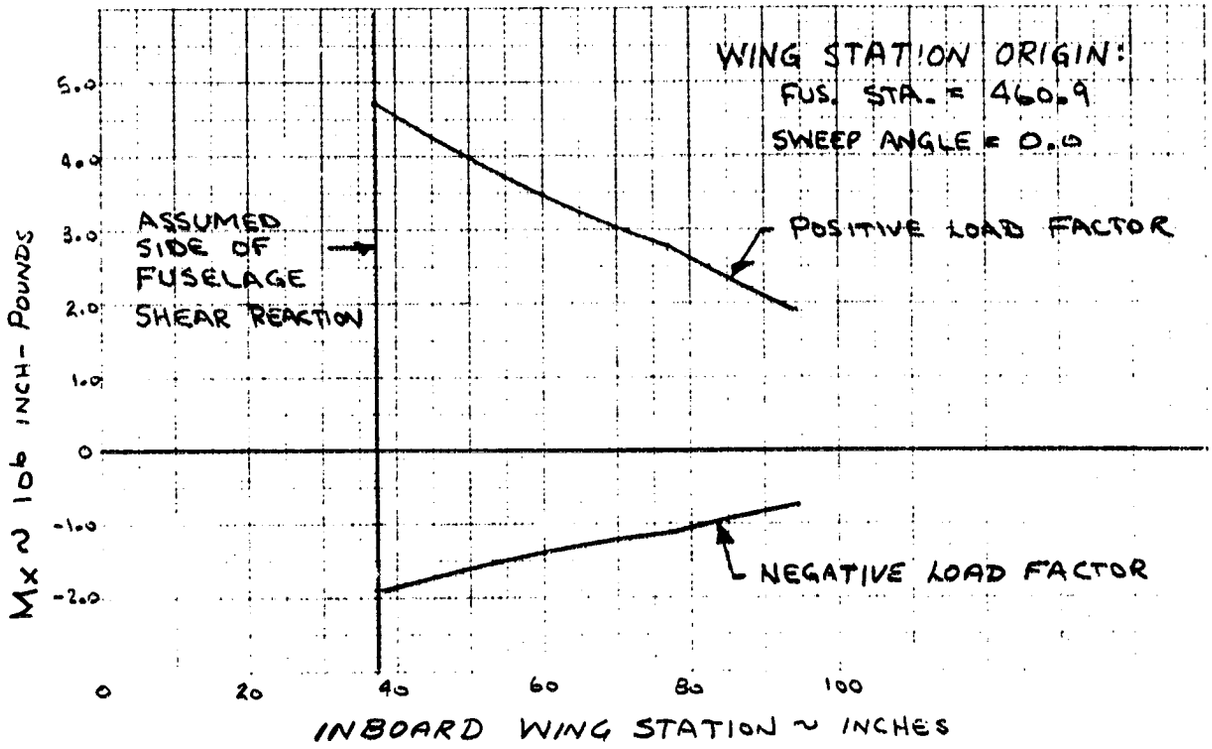

FIGURE 97. WING INBOARD PANEL ULTIMATE BENDING LOADS (DS75-4)

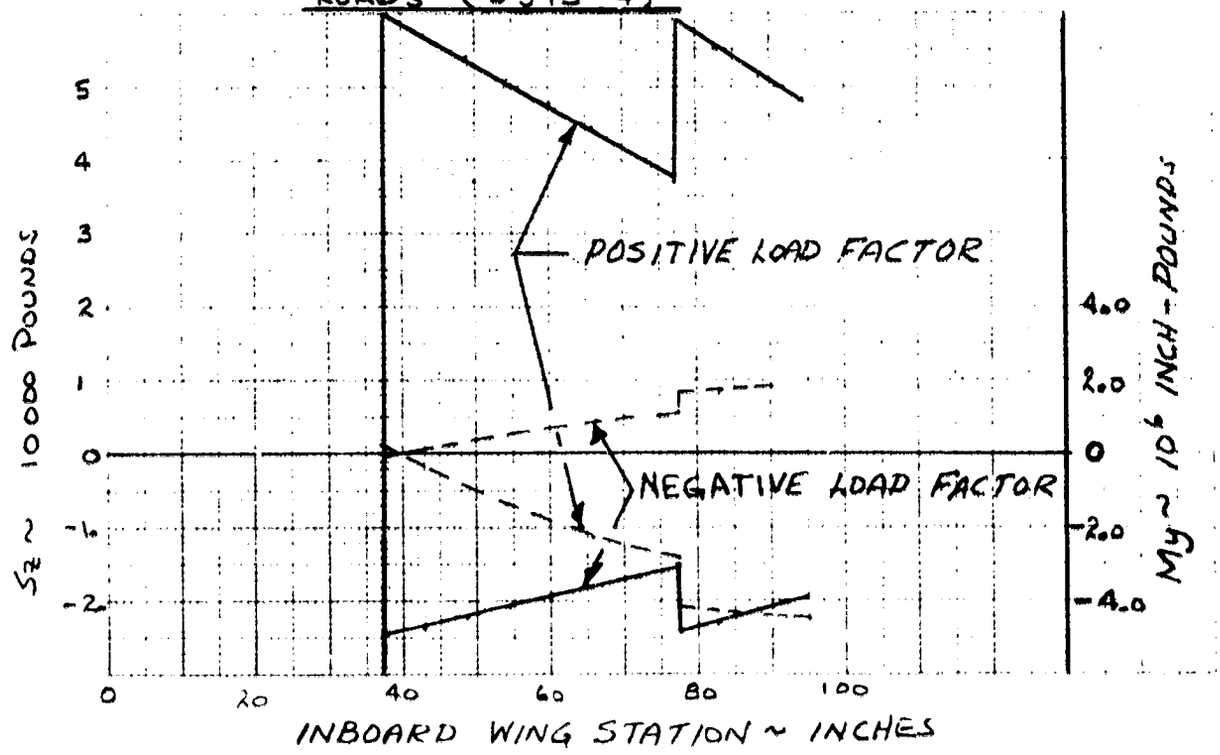

FIGURE 98. WING INBOARD PANEL ULTIMATE SHEAR AND TORQUE LOADS (DS75-4)

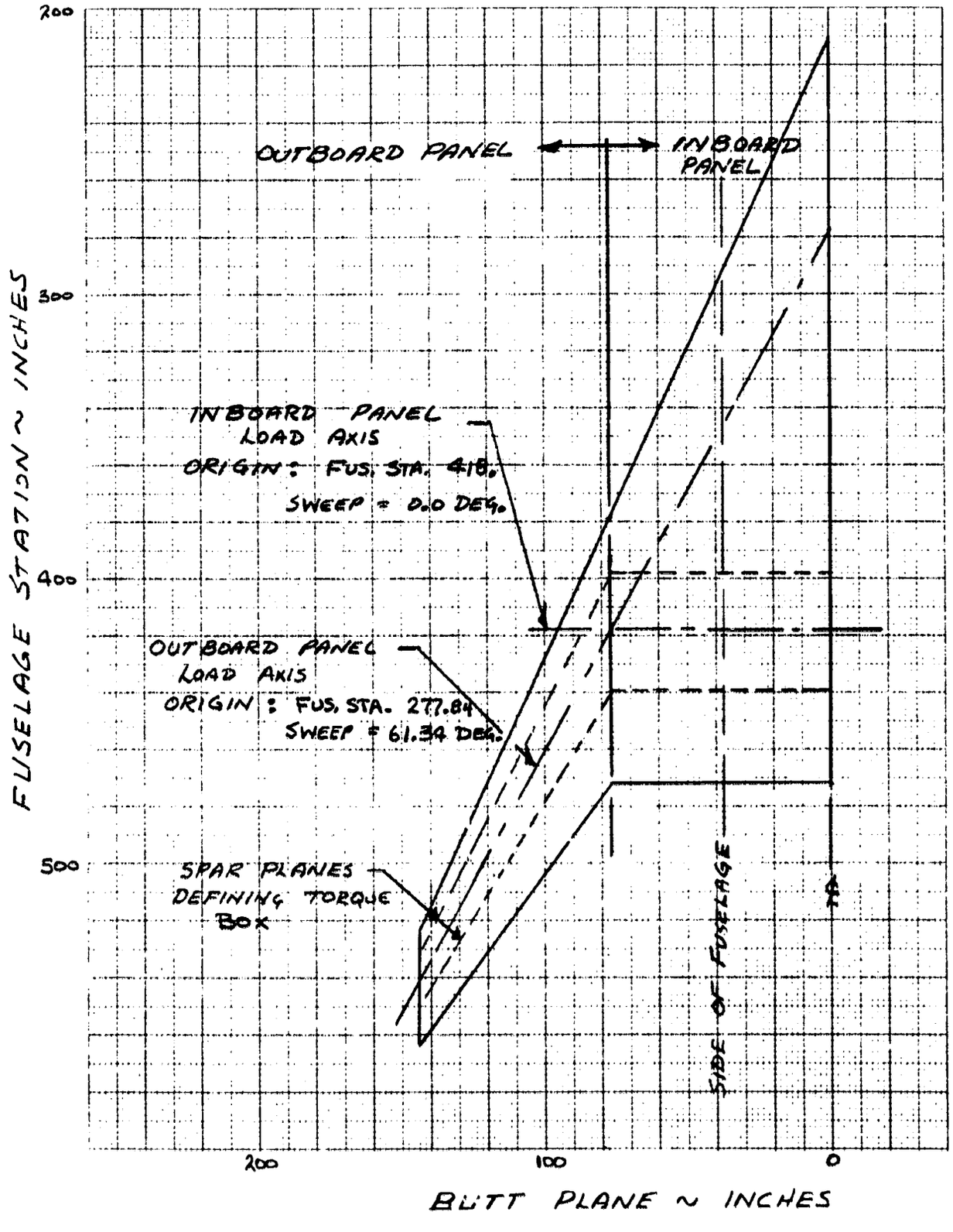

FIGURE 99. D575-2A LOAD AXIS IDENTIFICATION

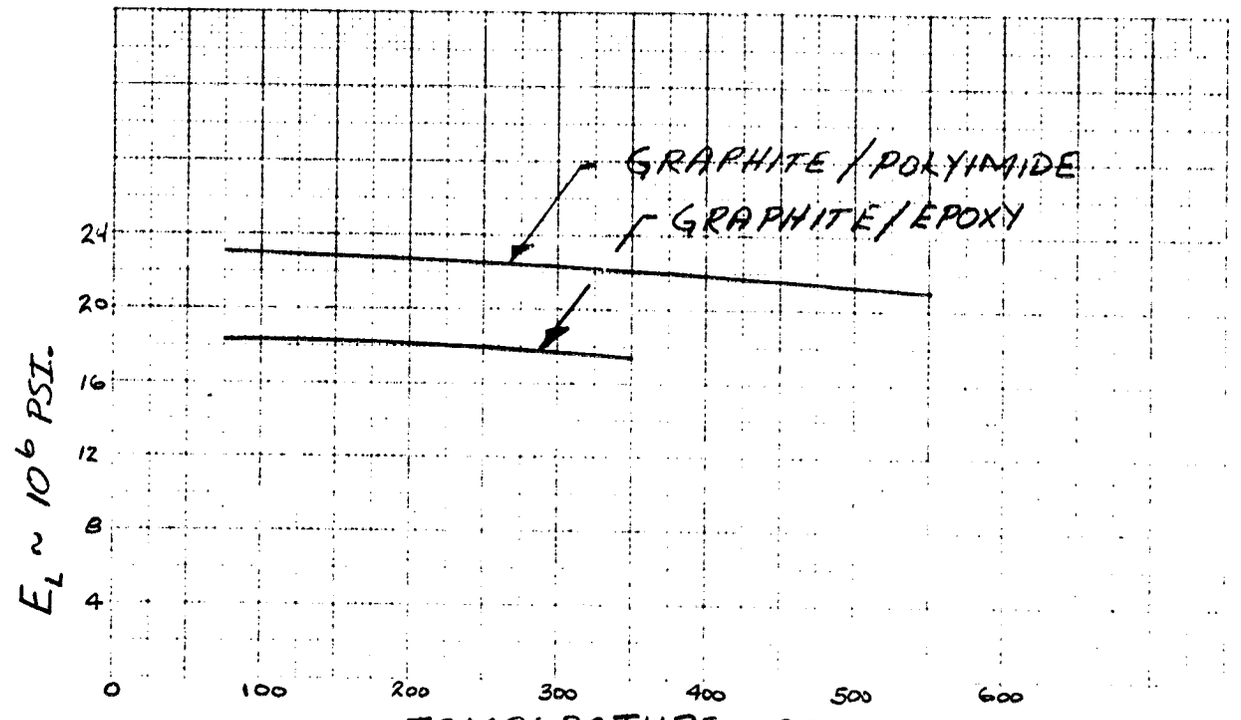

FIGURE 100. YOUNG'S MODULUS PARALLEL TO FILAMENT DIRECTION

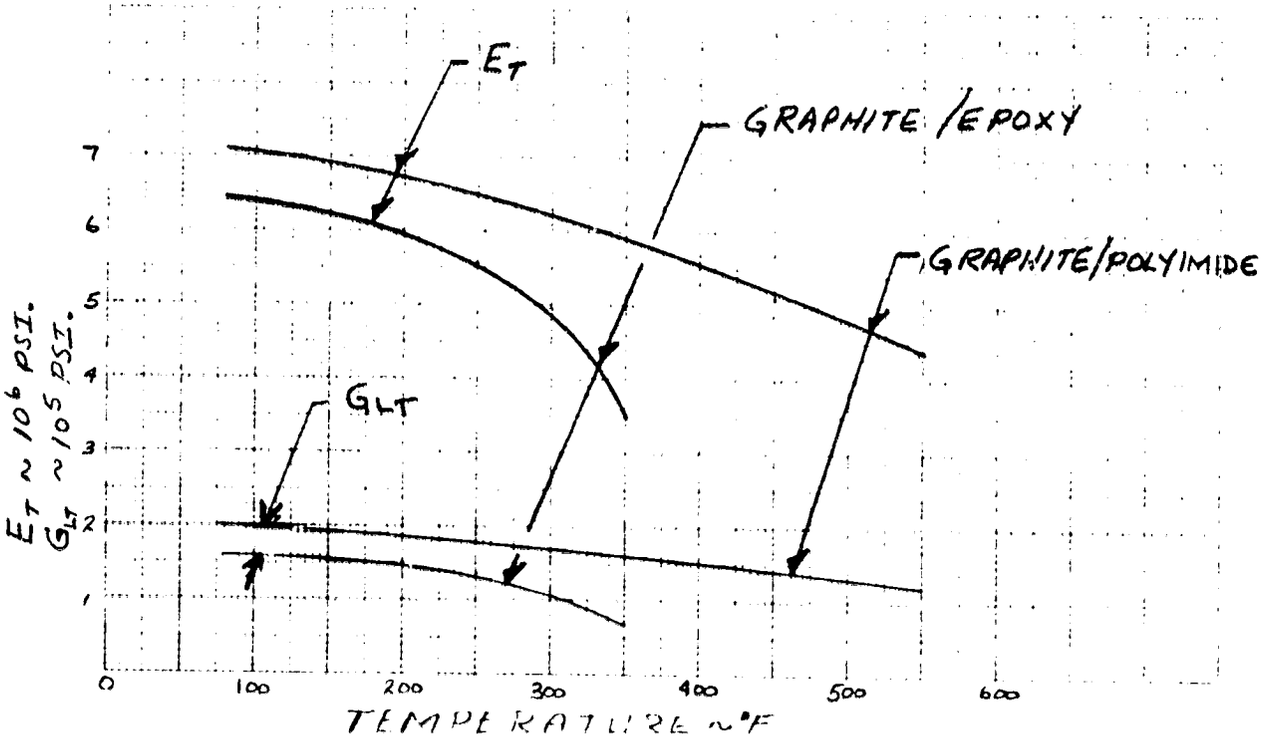

FIGURE 101. TRANSVERSE YOUNG'S AND SHEAR MODULUS OF FILAMENT

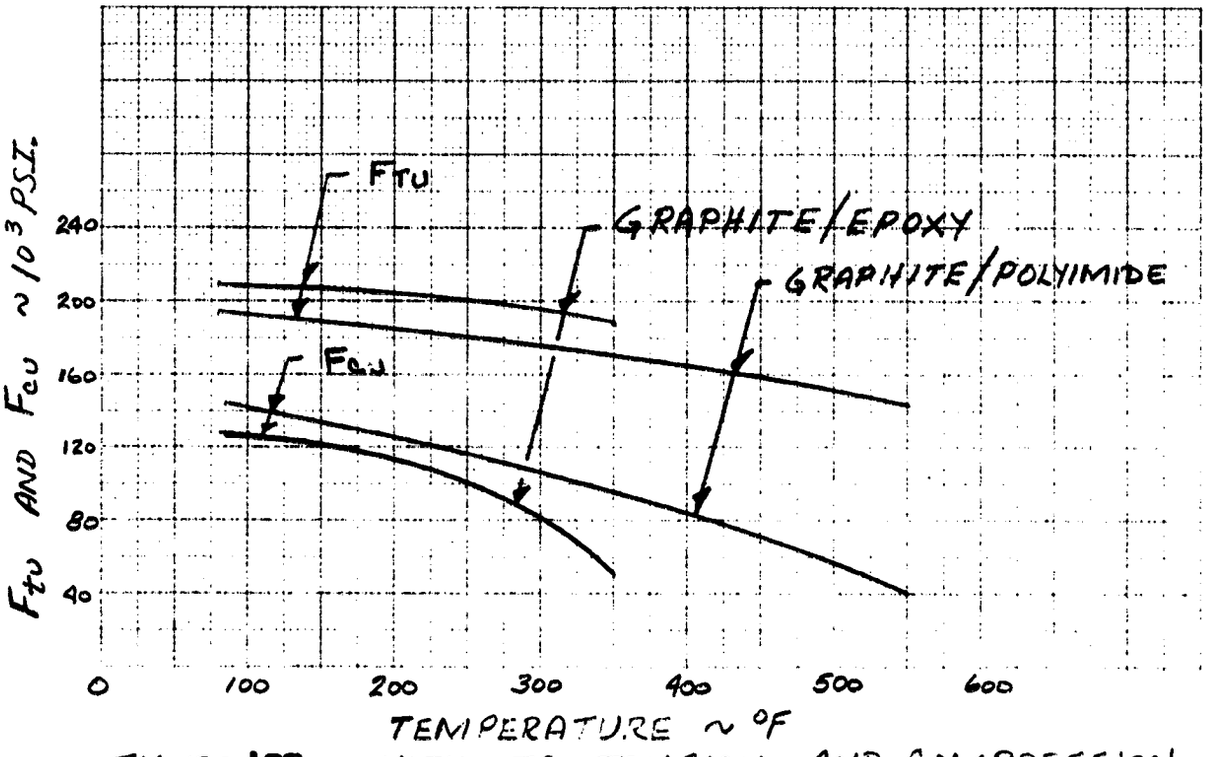

FIGURE 102. ULTIMATE TENSION AND COMPRESSION STRENGTH

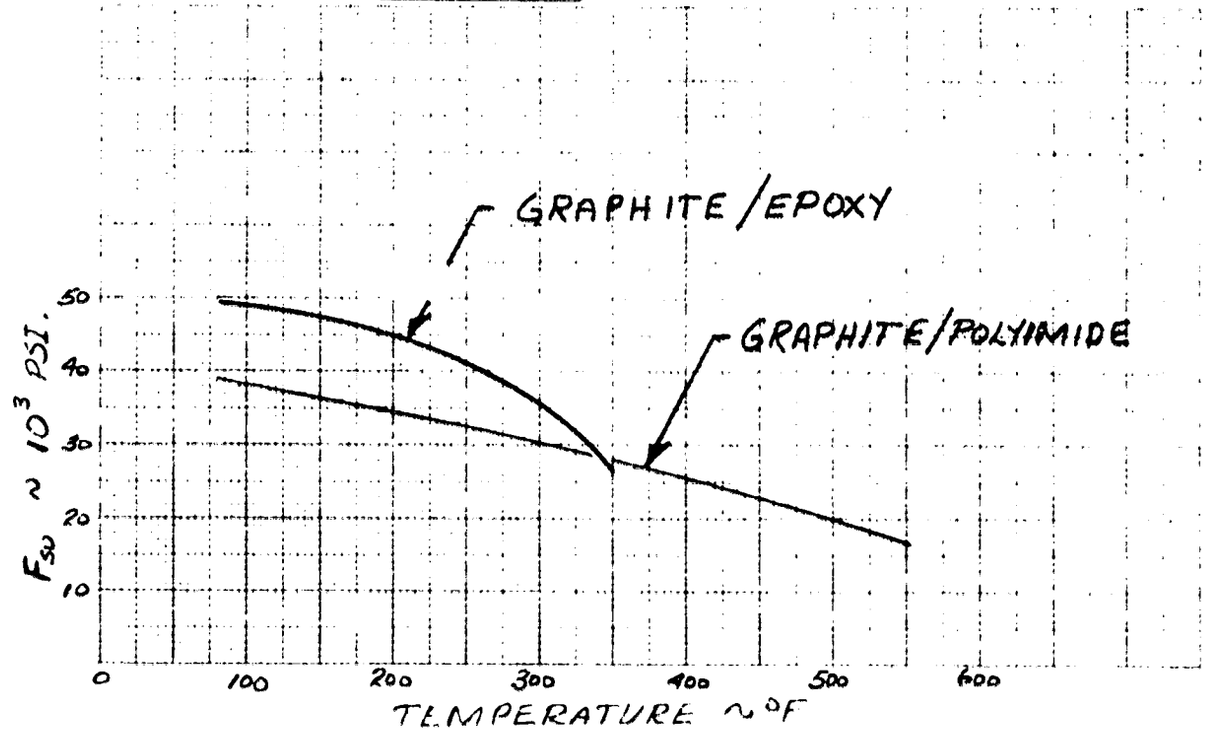

FIGURE 103. ULTIMATE SHEAR STRENGTH

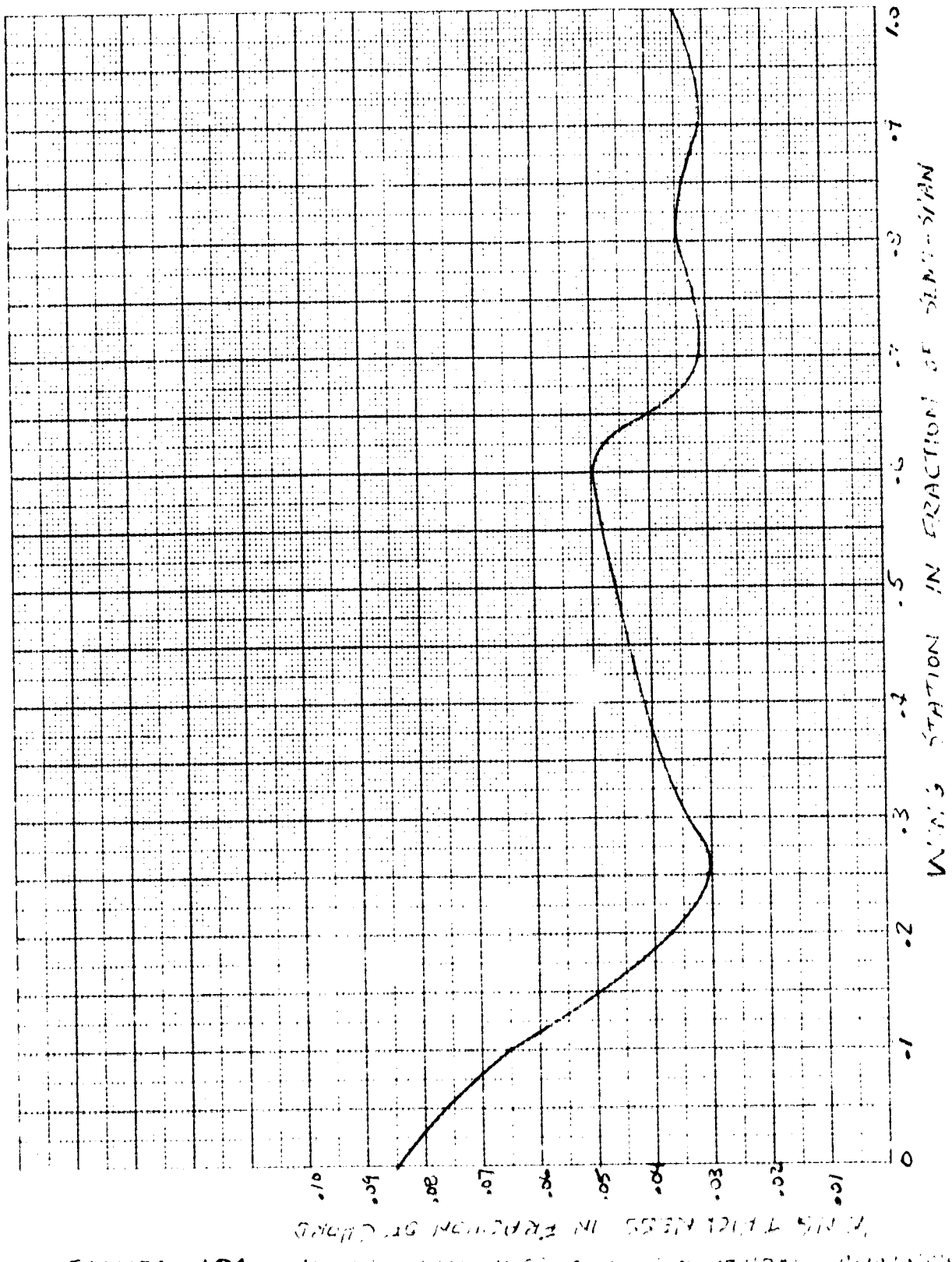

FIGURE 104.

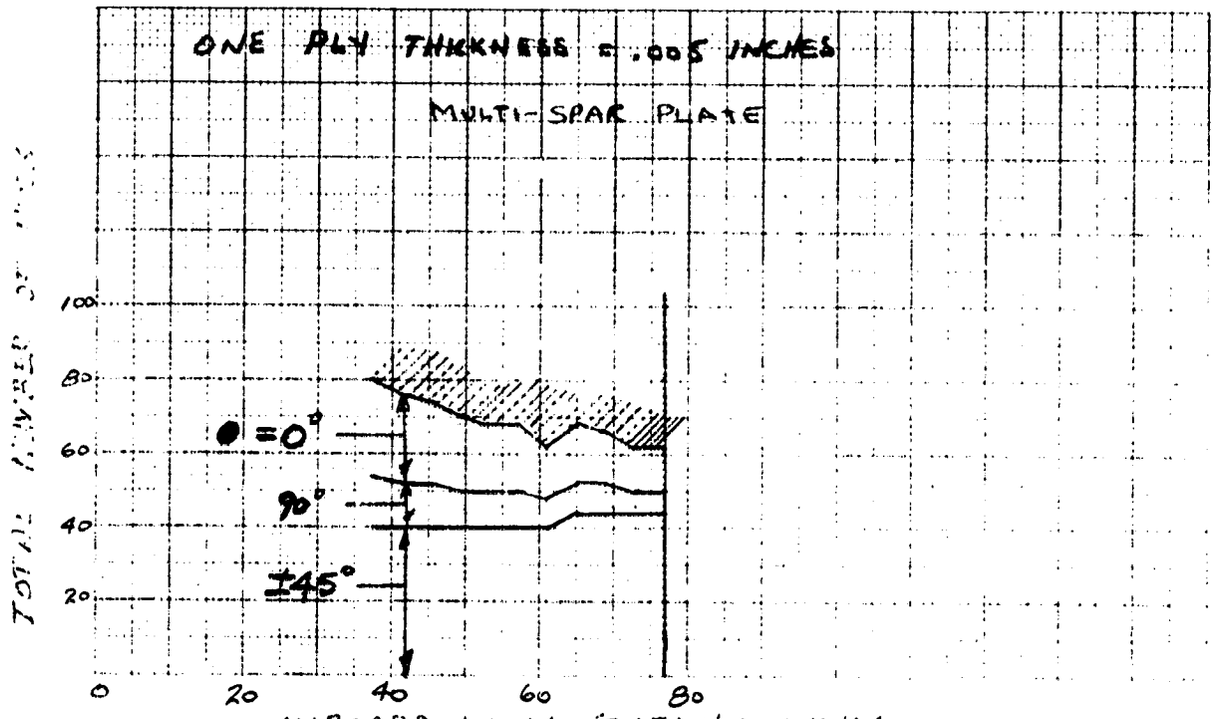

FIGURE 105. INBOARD WING PANEL UPPER COVER PLY BUILD-UP (DSIS-2A)

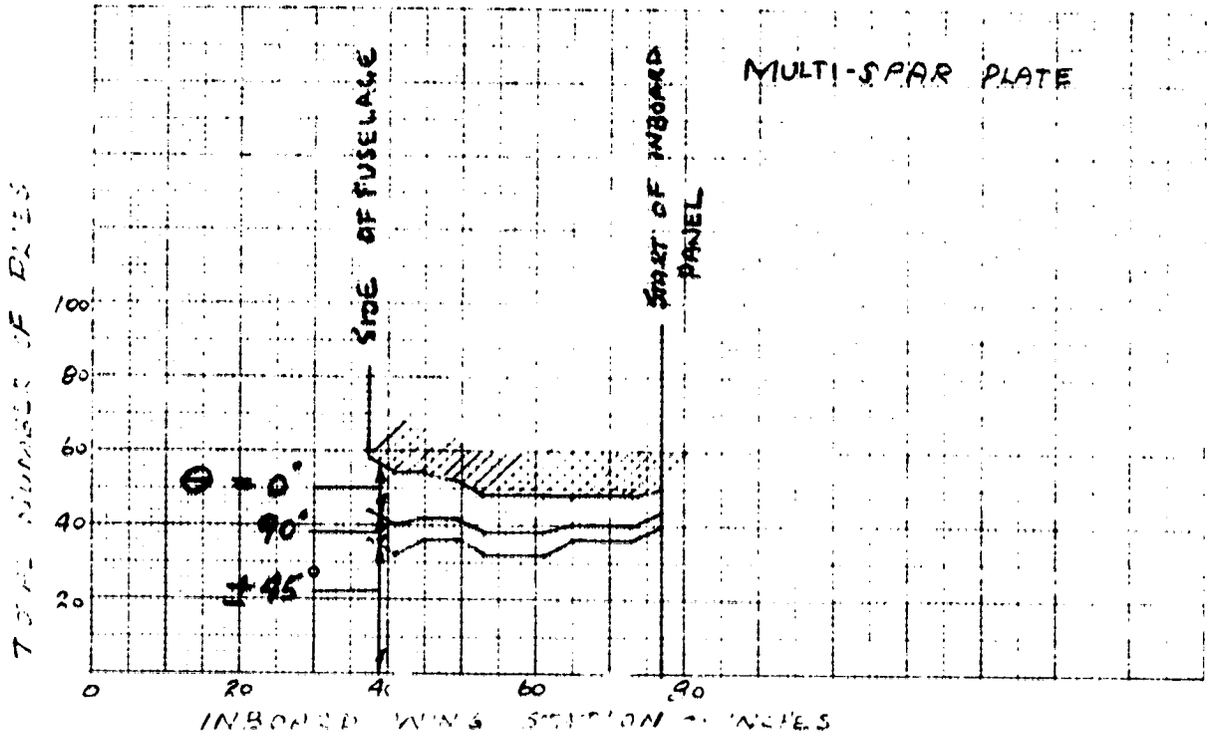

FIGURE 106. INBOARD WING PANEL LOWER COVER PLY BUILD-UP (DSIS-2A)

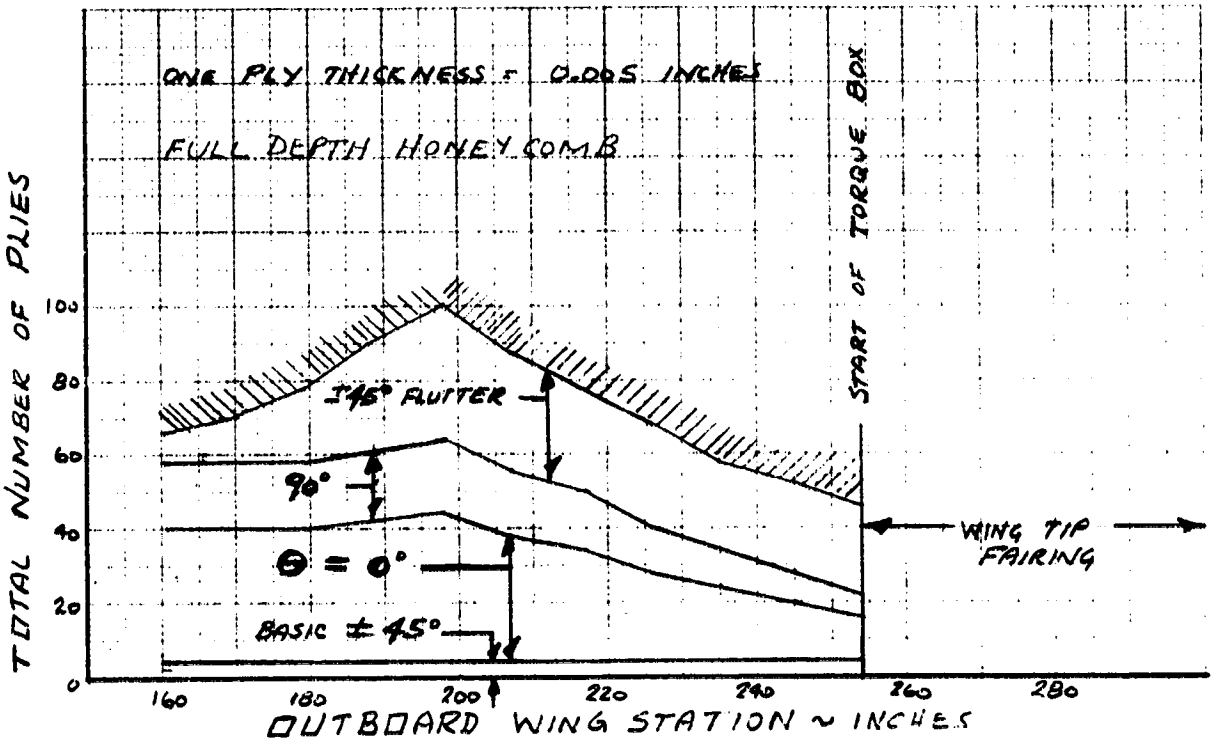

FIGURE 107. OUTBOARD WING PANEL UPPER COVER PLY SCHEDULE (USIS-2A)

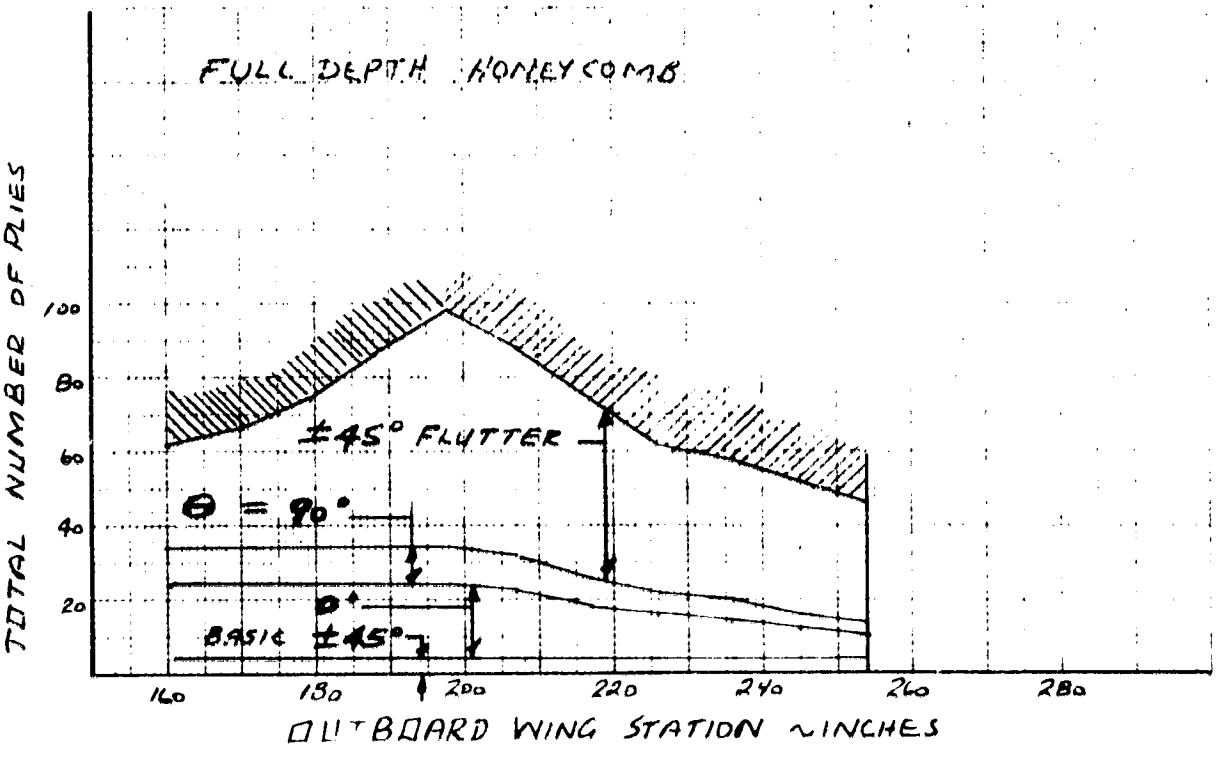

FIGURE 108. OUTBOARD WING PANEL LOWER COVER PLY SCHEDULE (USIS-2A)

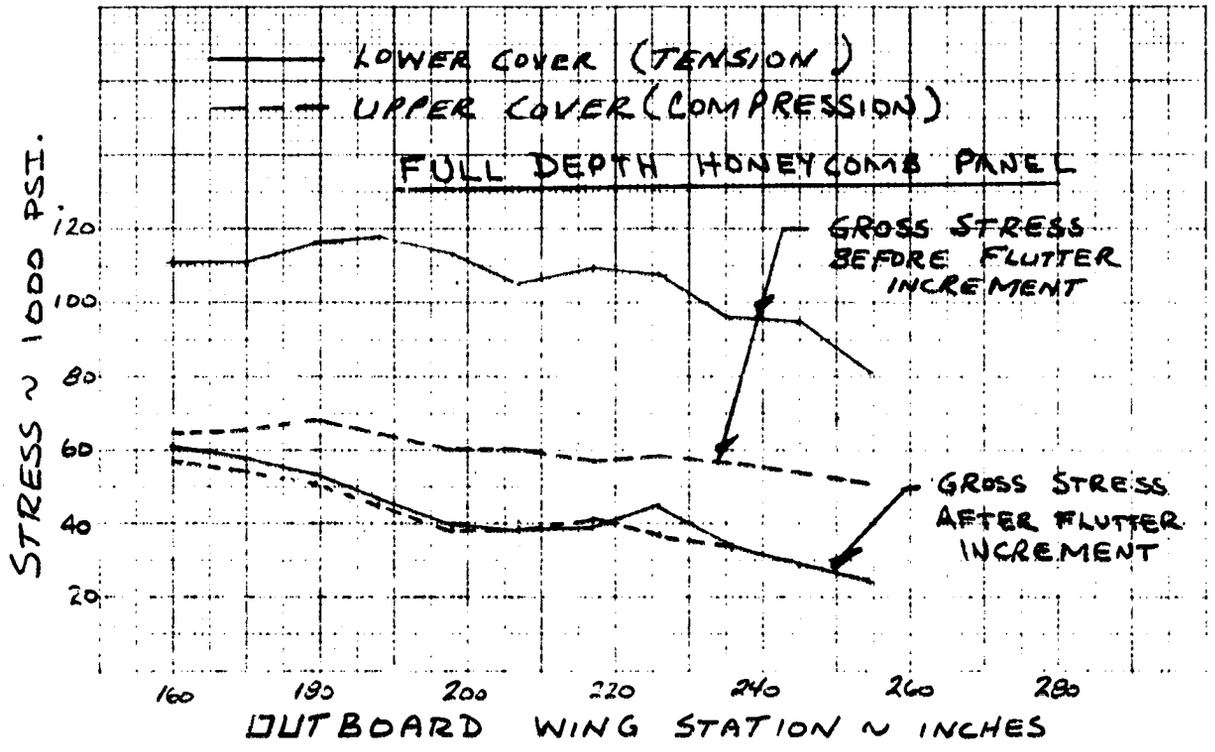

FIGURE 109. OUTBOARD WING PANEL COVER STRESS (DS75-2A)

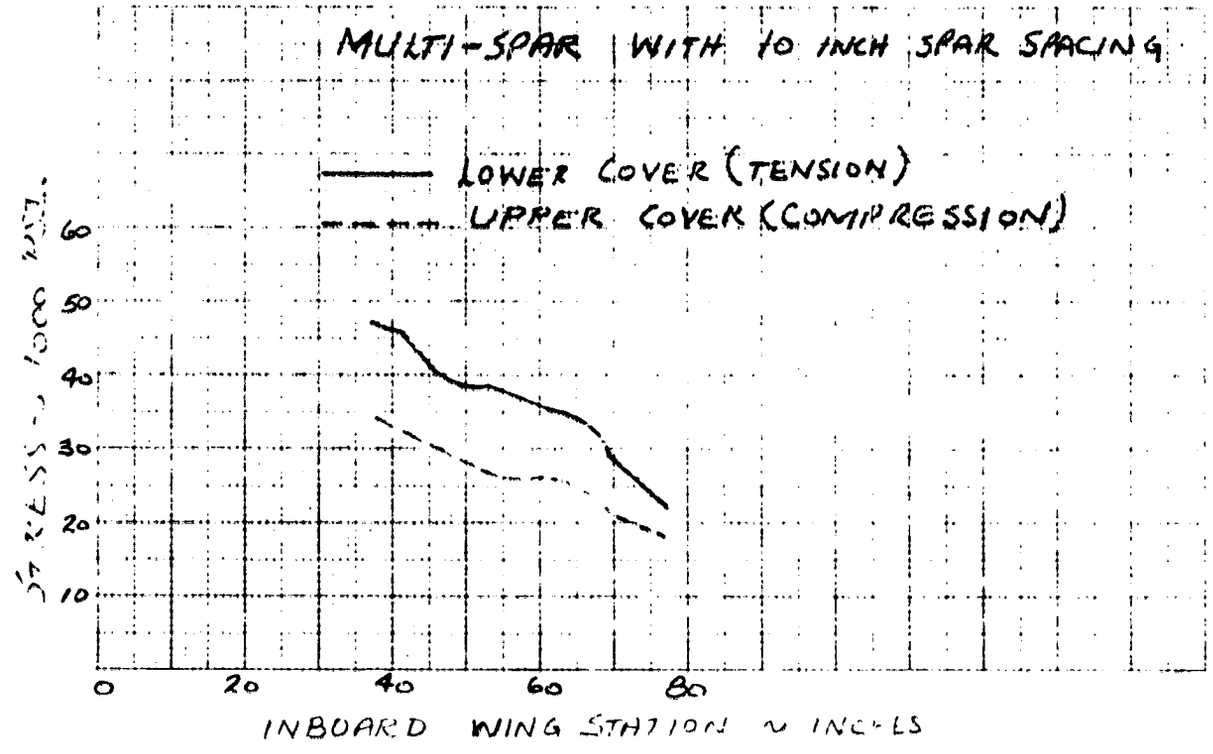

FIGURE 110. INBOARD WING PANEL COVER STRESS (DS15-2A)

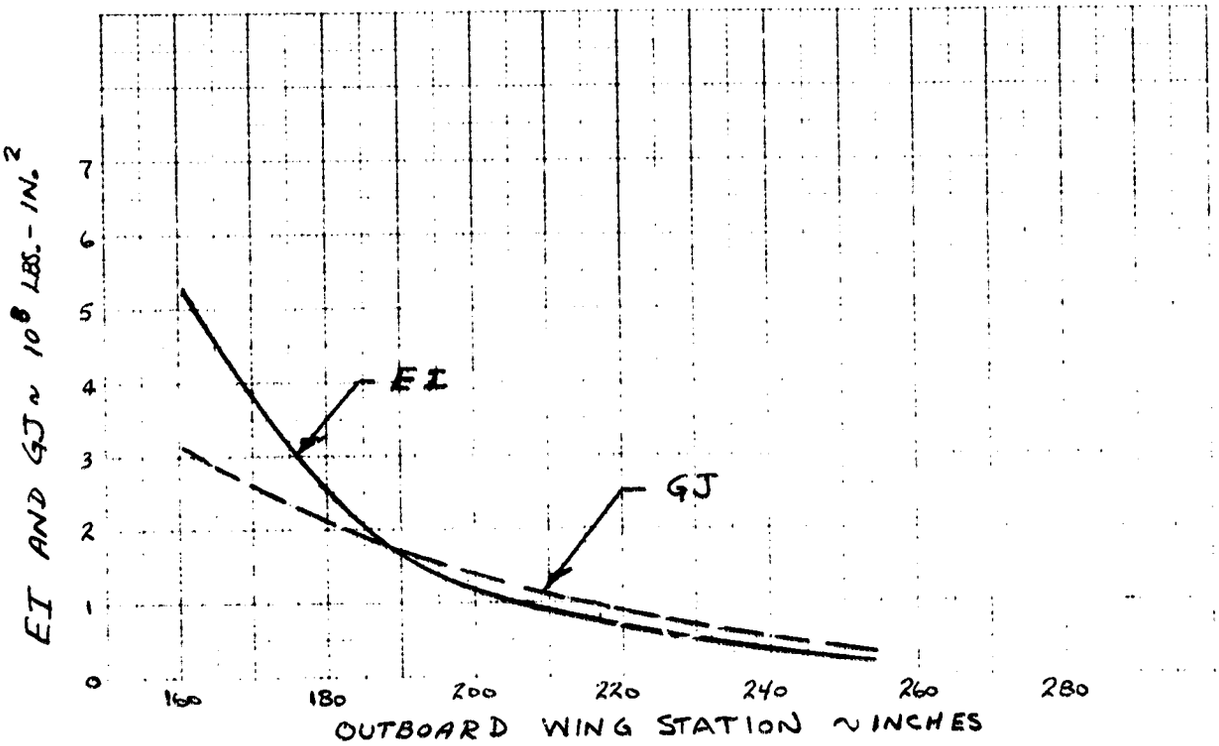

FIGURE 111. BENDING AND TORSIONAL STIFFNESS OUTBOARD WING PANEL (DS1S-2A)

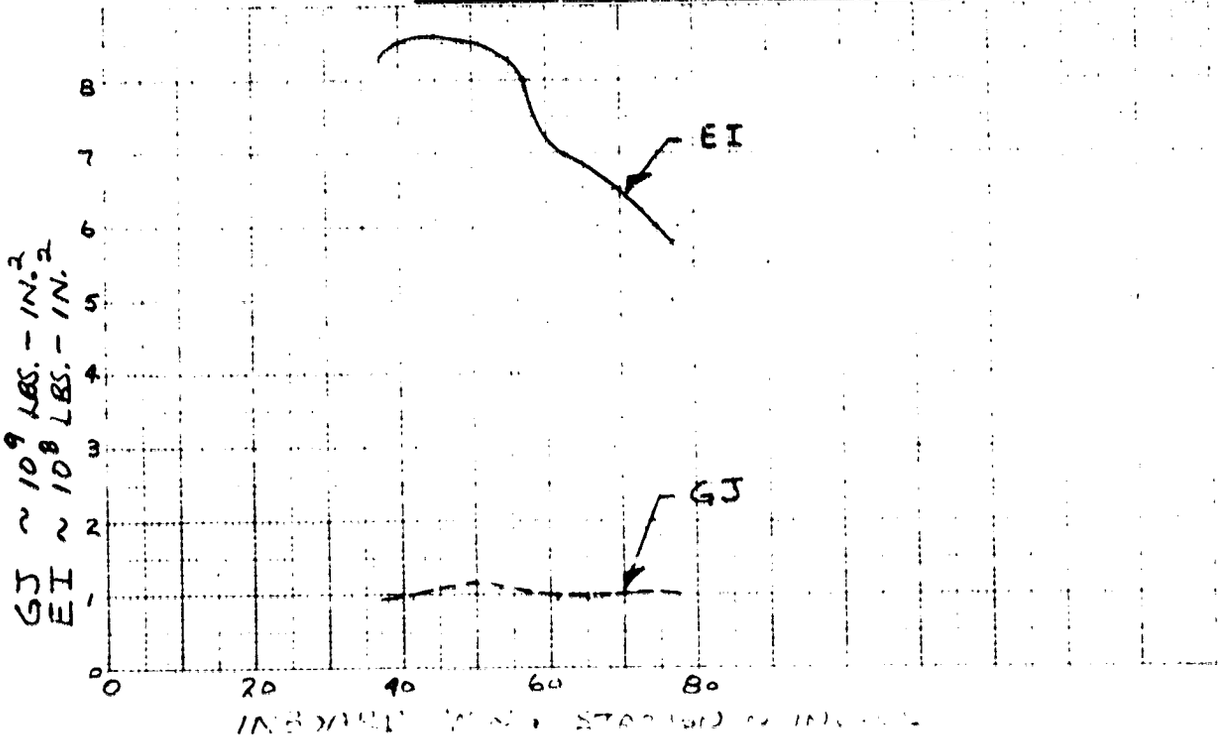

FIG. 112. BENDING AND TORSIONAL STIFFNESS INBOARD WING PANEL (DS1S-2A)

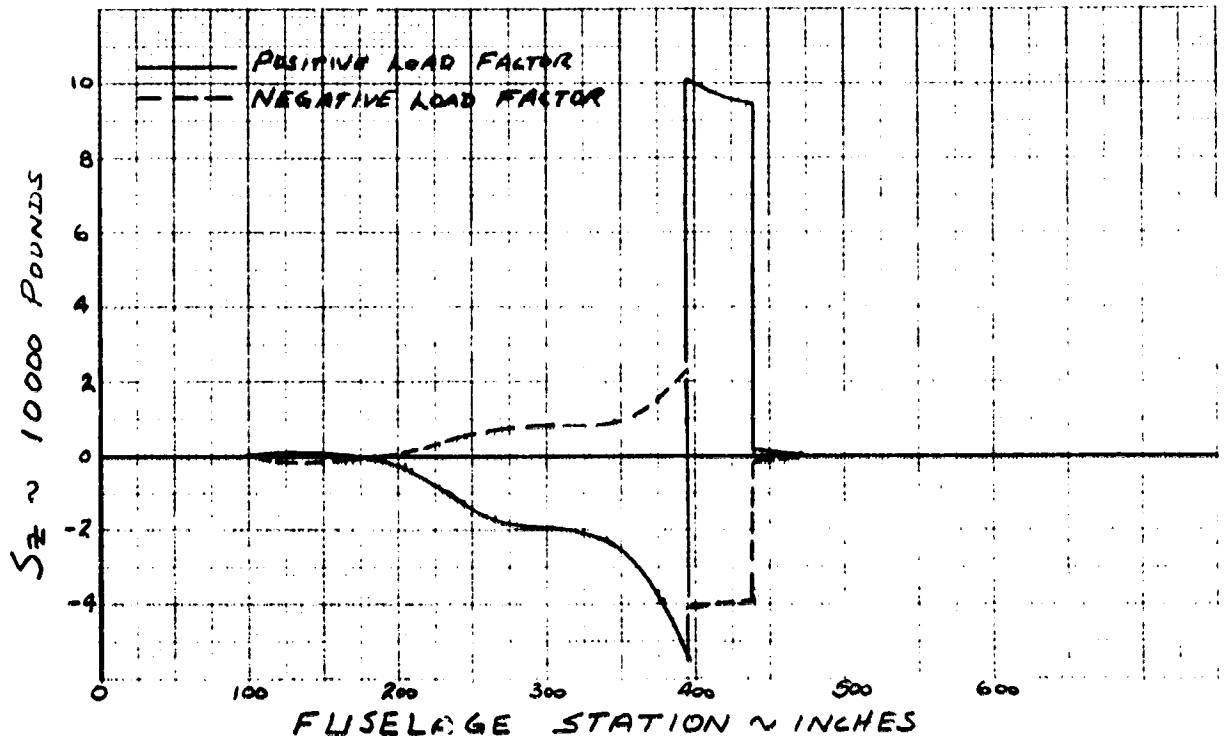

FIGURE 113. ULTIMATE FUSELAGE SHEAR (DS75-2A)

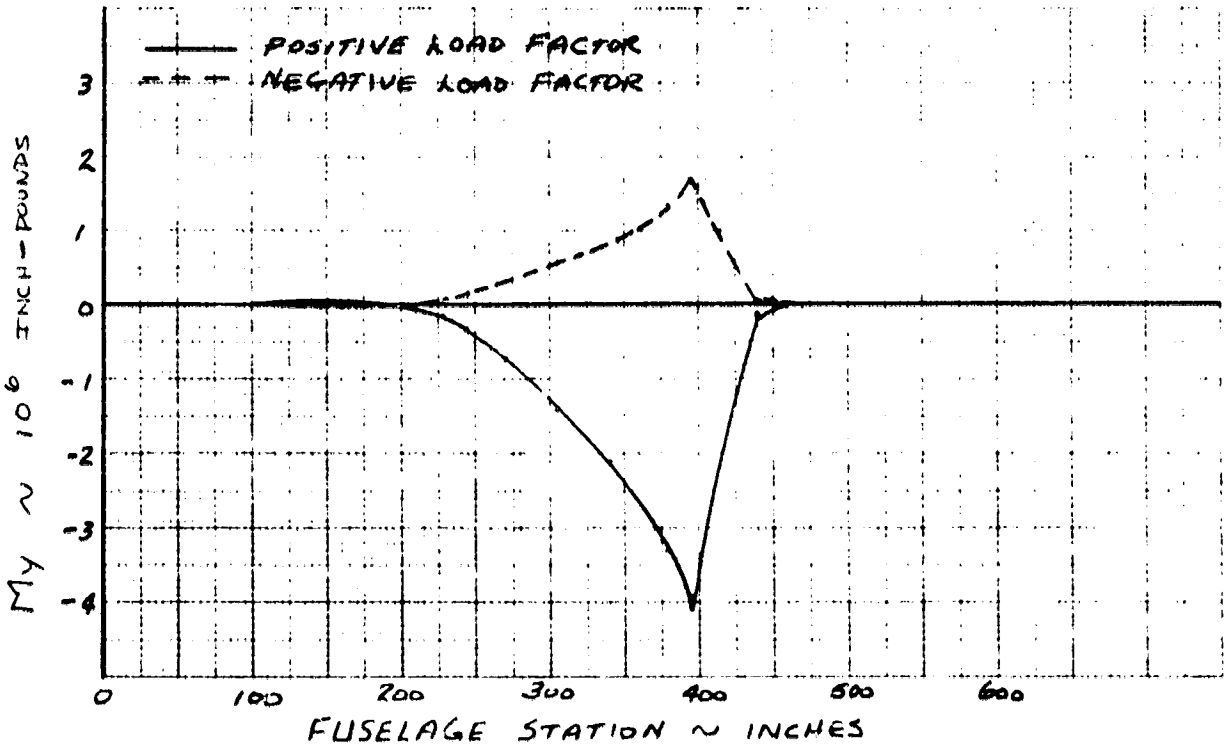

FIGURE 114. ULTIMATE FUSELAGE BENDING LOADS (DS75-2A)

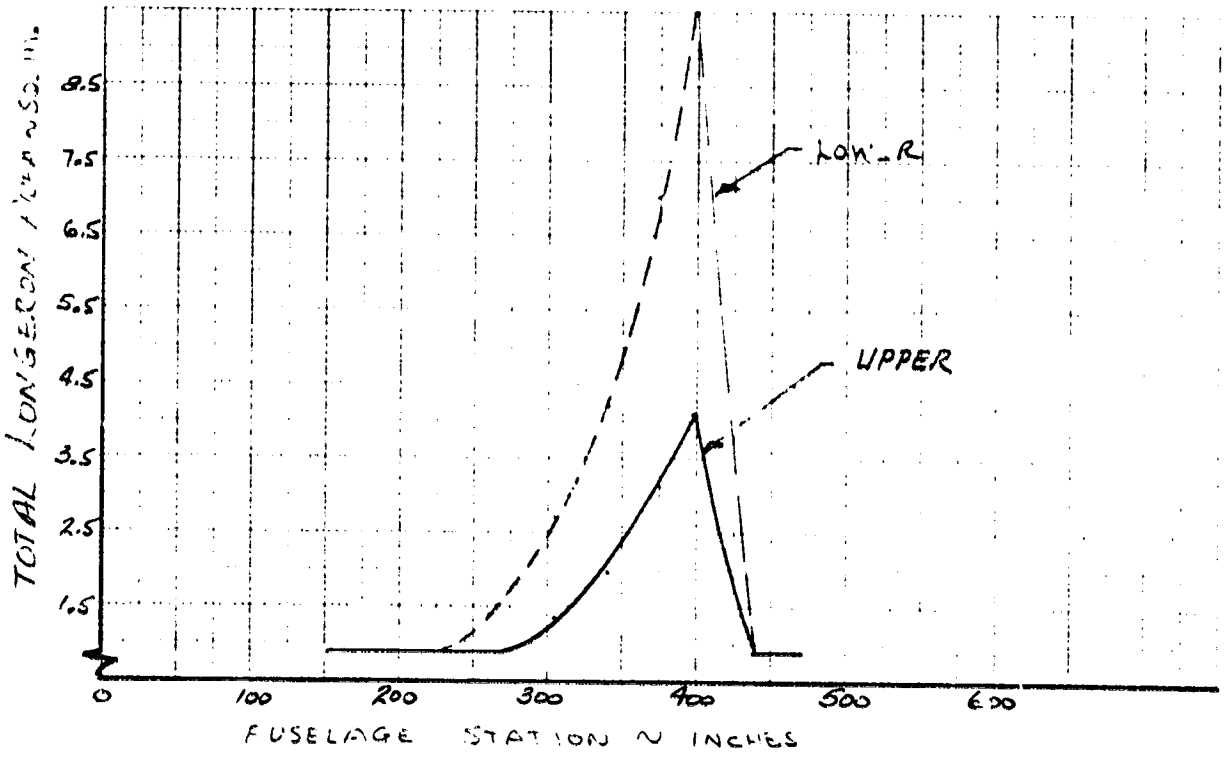

FIGURE 115. ALUMINUM LONGERON AREA VS FUSELAGE STATION (DSV-2A)

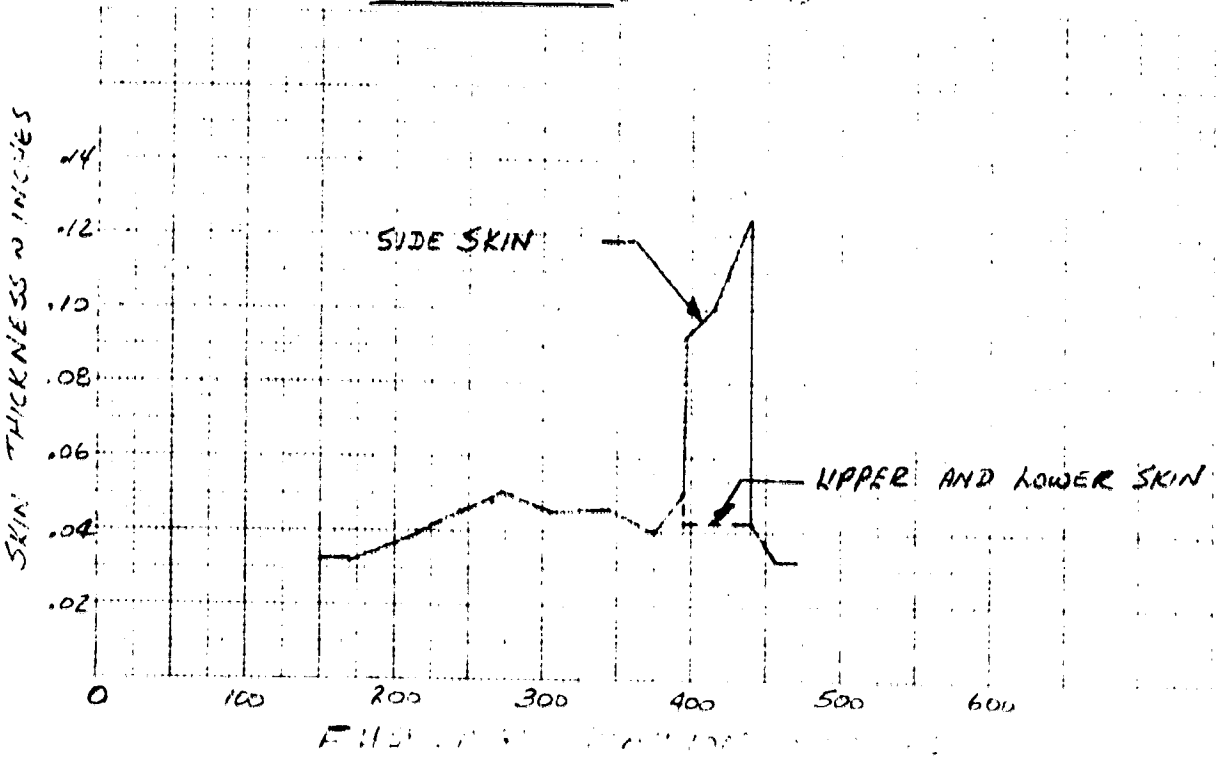

FIGURE 116. ALUMINUM SKIN THICKNESS VS FUSELAGE STATION (DSV-2A)

ORIGINAL PAGE IS
OF POOR QUALITY

	WEIGHT	LOAD FACTOR	LANDING SPEED (FT/SEC)	SINKING SPEED (FT/SEC)
TAKE-OFF	15866.0	1.629	258.8	6.00
LANDING	13549.0	2.748	239.0	10.00

LANDING GEAR LOADS

		MAIN LANDING GEAR		NOSE LANDING GEAR	
		TAKE-OFF	LANDING	TAKE-OFF	LANDING
TWO POINT	AXIAL	7672.	18176.	267.	261.
	NORMAL	947.	2243.	38.	37.
SPIN UP	AXIAL	7024.	14241.	275.	269.
	NORMAL	3935.	7978.	162.	159.
SPRING BACK	AXIAL	7443.	17635.	260.	255.
	NORMAL	5155.	10763.	196.	193.
BRAKED ROLL	AXIAL	12987.	13292.		
	NORMAL	8008.	8197.		
DRIFT LANDING	AXIAL	3807.	9020.		
	NORMAL	3104.	7354.		
UNSYS. BRAKING	AXIAL	11218.	9667.	3920.	3151.
	NORMAL	6917.	5961.	2513.	2019.
TOWING	AXIAL	12273.		1160.	
	NORMAL	3855.		7066.	
TURNING	AXIAL	18737.		413.	
	NORMAL	9715.		212.	

TABLE VIII. LANDING GEAR LOAD SUMMARY (DS75-2A)

TABLE IX. MAIN GEAR WEIGHT AND CRITICAL DESIGN CONDITION INFORMATION (DS75-2A)

MAIN LANDING GEAR WEIGHTS (POUNDS)

OUTER CYLINDER	89.0
PISTON	28.8
AXLE	7.5
OIL	8.8
DRAG STRUT	21.9
SIDE STRUT	19.8
WHEELS	34.0
TIRES	31.0
MISC (CALC.)	186.6
BRAKES	90.0
PODIE	0.0
MISC (INPUT)	0.0
TOTAL	517.4

MAIN LANDING GEAR DESIGN DATA		DESIGN LOAD CONDITION **	AREA (SQ IN)	DIAMETER TO THICKNESS RATIO	BENDING MODULUS OF RUPTURE	TORSIONAL MODULUS OF RUPTURE
OUTER CYLINDER	TOP	22	2.16	24.53	285262.	118847.
	MIDDLE	22	1.48	34.49	262080.	108544.
	BOTTOM	2	0.99	50.00	237500.	98514.
PISTON (20 PCT OF LENGTH FROM AXLE)		22	0.70	45.98	242517.	100408.

PISTON DIAMETER (INCHES)	3.23	CG - BELOW TRUNION POINT	36.3
AFT DEFLECTION (INCHES)	0.0	CG - OUTBOARD (INBOARD) FROM TRUNION POINT	1.3
SIDE DEFLECTION (INCHES)	0.0	CG - AFT (FORWARD) FROM TRUNION POINT	4.9
ANGLE OF TWIST (RADIANS)	0.0		

NOSE LANDING GEAR WEIGHTS (POUNDS) ** LGHT **

OUTER CYLINDER	22.9
PISTON	4.5
AXLE	0.3
OIL	1.6
DRAG STRUT	4.7
SIDE STRUT	0.0
WHEELS	9.5
TIRES	8.5
MISC (CALC.)	52.8
TOTAL	104.7

X. NOSE GEAR WEIGHT AND CRITICAL DESIGN CONDITION INFORMATION (DS75-2A)

NOSE LANDING GEAR DESIGN DATA		DESIGN LOAD CONDITION **	AREA (SQ IN)	DIAMETER TO THICKNESS RATIO	BENDING MODULUS OF RUPTURE	TORSIONAL MODULUS OF RUPTURE
OUTER CYLINDER	TOP	14	1.50	16.67	307668.	129123.
	MIDDLE	14	0.97	24.11	286369.	119349.
	BOTTOM	4	0.44	50.00	237500.	98514.
PISTON (20 PCT OF LENGTH FROM AXLE)		14	0.31	37.08	256994.	106357.

PISTON DIAMETER (INCHES)	1.94	CG - BELOW TRUNION POINT	25.2
AFT DEFLECTION (INCHES)	0.0	CG - OUTBOARD (INBOARD) FROM TRUNION POINT	0.0
SIDE DEFLECTION (INCHES)	0.0	CG - AFT (FORWARD) FROM TRUNION POINT	3.3
ANGLE OF TWIST (RADIANS)	0.0		

** DESIGN LOAD CONDITION INDICATORS

	TAKE-OFF WEIGHT	LANDING WEIGHT
TWO POINT	2	18
SPIN UP	4	20
SPRING BACK	6	22
BRAKED ROLL	8	24
DRIFT LANDING	10	26
UNSYMMETRICAL BRAKING	12	28
TOWING	14	
TURNING	16	

(IF THE DESIGN LOAD CONDITION INDICATORS ARE ALL 0, THE DESIGN LOADS WERE GIVEN IN THE INPUT DATA)

TABLE XI. WEIGHT SUMMARY, D575-2A

	WEIGHT POUNDS	ARM INCHES		MOMENT IN-LBS		
STRUCTURE GROUPS	(3810)	361.7		1379375		
WING GROUP	1140	435				
TAIL GROUP - HORIZONTAL	60	255				
- VERTICAL						
BODY GROUP	1405	295				
ALIGHTING GEAR GROUP - MAIN	520	345				
- AUXILIARY	105	250				
ENGINE SECTION OR NACELLE GROUP	430	435				
AIR INDUCTION SYSTEM	150	400				
PROPULSION GROUP	(2235)	455.8		(1018725)		
ENGINE (AS INSTALLED)	880	460				
ACCESSORY GEAR BOXES & DRIVES	100	465				
EXHAUST SYSTEM	740	510				
COOLING & DRAIN PROVISIONS	10	460				
ENGINE CONTROLS	40	260				
STARTING SYSTEM	40	450				
FUEL SYSTEM	405	365				
FAN (AS INSTALLED)						
HOT GAS DUCT SYSTEM						
LUBRICATING SYSTEM	20	460				
EQUIPMENT GROUPS	(3350)	317.4		(1063125)		
FLIGHT CONTROLS GROUP	625	345				
AUXILIARY POWER PLANT GROUP						
INSTRUMENTS GROUP	190	245				
HYDRAULIC & PNEUMATIC GROUP	340	410				
ELECTRICAL GROUP	445	360				
AVIONICS GROUP	580	215				
ARMAMENT GROUP	670	345				
FURNISHINGS AND EQUIPMENT GROUP	270	240				
AIR CONDITIONING GROUP	220	350				
ANTI-ICING GROUP						
PHOTOGRAPHIC GROUP						
LOAD & HANDLING GROUP	10	370				
TOTAL WEIGHT EMPTY	9395	368.3		3460225		
CREW	215	212				
FUEL - UNUSABLE	60	365				
FUEL - USABLE	3895	345				
OIL - ENGINE	30	460				
PASSENGERS CARGO						
ARMAMENT GUN (M-61)	255	375				
AMMO (300 RDS)	170	380				
2-MADMANS	1000	345				
EQUIPMENT GUN CAMERA	5	185				
N_2	10	365				
O_2	25	230				
TOTAL USEFUL LOAD	(5665)	356.3		2018505		
TAKEOFF GROSS WEIGHT	15060	363.9		5478730		
FLIGHT DESIGN GROSS WEIGHT	13113					
LANDING DESIGN GROSS WEIGHT	12723					

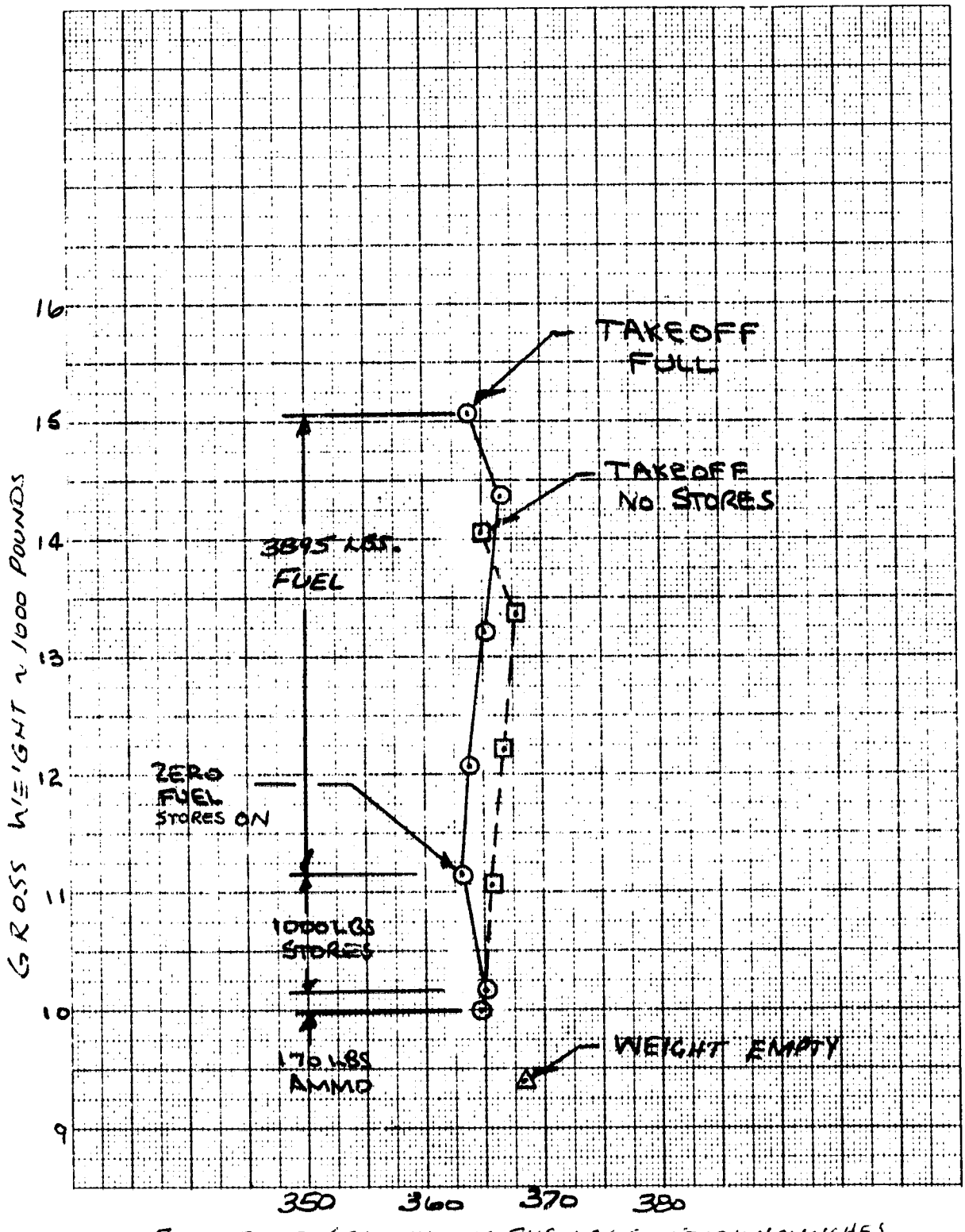

FIGURE 117. GROSS WEIGHT VS CENTER OF GRAVITY (D575-2A)

TABLE XII, WEIGHT SUMMARY, D 575-3

	WEIGHT POUNDS	ARM INCHES		MOMENT IN-LBS		
STRUCTURE GROUPS	(4830)	377.7		1824390		
WING GROUP	1655	465				
TAIL GROUP - HORIZONTAL	60	215				
- VERTICAL						
BODY GROUP	1550	285				
ALIGHTING GEAR GROUP - MAIN	640	345				
- AUXILIARY	130	220				
ENGINE SECTION OR NACELLE GROUP	490	460				
AIR INDUCTION SYSTEM	305	411				
PROPULSION GROUP	(2660)	469.6		1249385		
ENGINE (AS INSTALLED)	1030	480				
ACCESSORY GEAR BOXES & DRIVES	100	485				
EXHAUST SYSTEM	855	535				
COOLING & DRAIN PROVISIONS	10	480				
ENGINE CONTROLS	40	245				
STARTING SYSTEM	40	480				
FUEL SYSTEM	565	364				
FAN (AS INSTALLED)						
HOT GAS DUCT SYSTEM						
LUBRICATING SYSTEM	20	480				
EQUIPMENT GROUPS	(3380)	316.9		1071300		
FLIGHT CONTROLS GROUP	655	350				
AUXILIARY POWER PLANT GROUP						
INSTRUMENTS GROUP	190	230				
HYDRAULIC & PNEUMATIC GROUP	340	420				
ELECTRICAL GROUP	445	370				
AVIONICS GROUP	580	185				
ARMAMENT GROUP	670	370				
FURNISHINGS AND EQUIPMENT GROUP	270	220				
AIR CONDITIONING GROUP	220	330				
ANTI-ICING GROUP						
PHOTOGRAPHIC GROUP						
LOAD & HANDLING GROUP	10	370				
TOTAL WEIGHT EMPTY	(10870)	381.0		4145065		
CREW	215	183				
FUEL - UNUSABLE	80	365				
FUEL - USABLE	5425	365				
OIL - ENGINE	30	480				
PASSENGERS CARGO						
ARMAMENT GUN (M-61)	255	390				
AMMO (300 RDS)	170	400				
2-MADMANS	1000	405				
EQUIPMENT GUN CAMERA	5	160				
N_2	15	365				
O_2	25	200				
TOTAL USEFUL LOAD	(7220)	366.6		2646795		
TAKEOFF GROSS WEIGHT	18090	375.2		6791860		
FLIGHT DESIGN GROSS WEIGHT	15378					
LANDING DESIGN GROSS WEIGHT	14835					

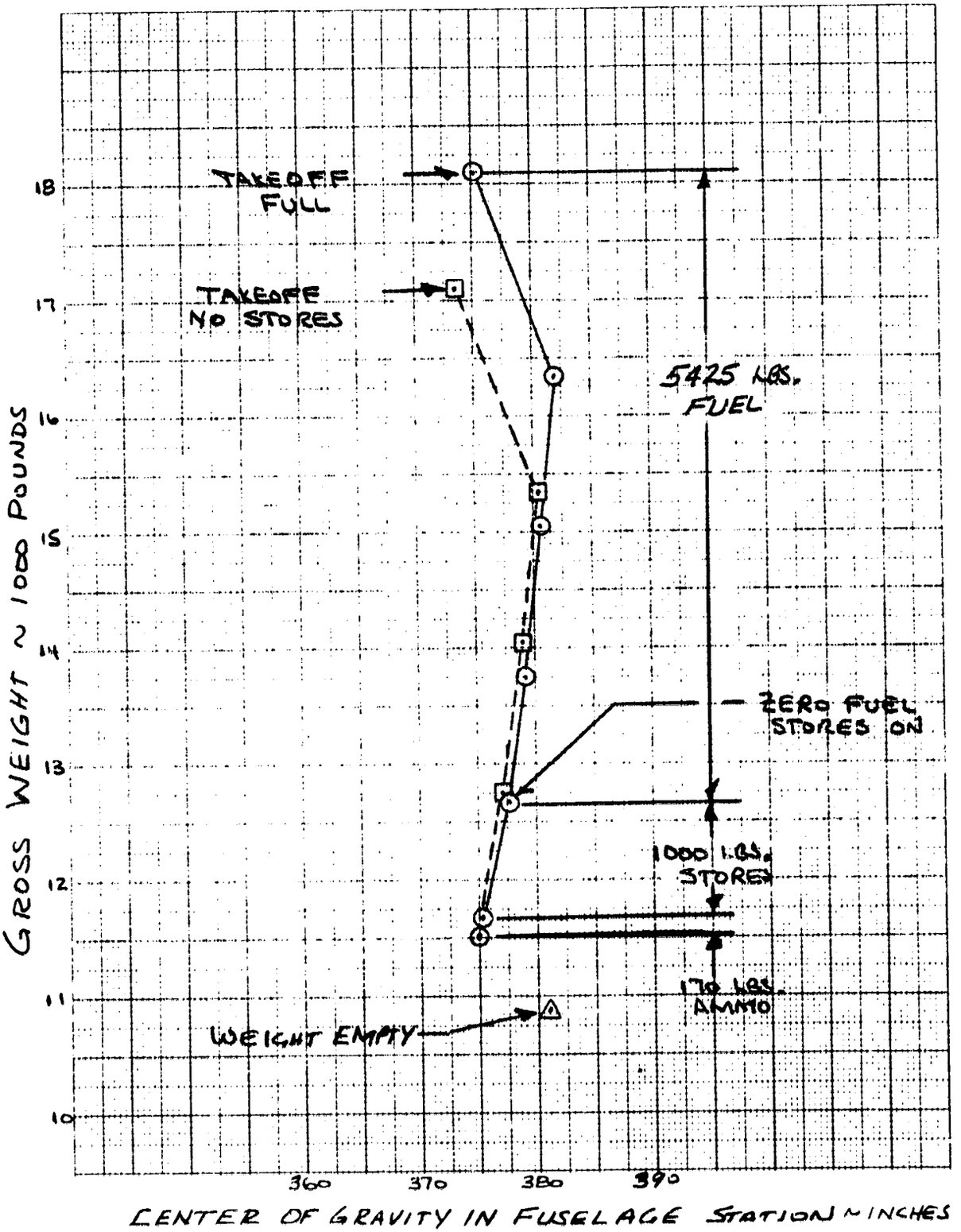

FIGURE 118. GROSS WEIGHT VS. CENTER OF GRAVITY (D575-3)

TABLE XIII. WEIGHT SUMMARY, D575-4

	WEIGHT POUNDS	ARM INCHES		MOMENT IN-LBS		
STRUCTURE GROUPS	(6920)	394.6		2730375		
WING GROUP	2420	490				
TAIL GROUP - HORIZONTAL	60	190				
- VERTICAL						
BODY GROUP	2200	295				
ALIGHTING GEAR GROUP - MAIN	910	350				
- AUXILIARY	185	195				
ENGINE SECTION OR NACELLE GROUP	745	430				
AIR INDUCTION SYSTEM	400	430				
PROPULSION GROUP	(5325)	492.8		1638665		
ENGINE (AS INSTALLED)	1210	510				
ACCESSORY GEAR BOXES & DRIVES	100	515				
EXHAUST SYSTEM	1025	565				
COOLING & DRAIN PROVISIONS	10	510				
ENGINE CONTROLS	40	235				
STARTING SYSTEM	40	510				
FUEL SYSTEM	390	393				
FAN (AS INSTALLED)						
HOT GAS DUCT SYSTEM						
LUBRICATING SYSTEM	20	510				
EQUIPMENT GROUPS	(3430)	319.6		1096125		
FLIGHT CONTROLS GROUP	705	370				
AUXILIARY POWER PLANT GROUP						
INSTRUMENTS GROUP	190	225				
HYDRAULIC & PNEUMATIC GROUP	340	435				
ELECTRICAL GROUP	445	375				
AVIONICS GROUP	580	160				
ARMAMENT GROUP	670	385				
FURNISHINGS AND EQUIPMENT GROUP	270	200				
AIR CONDITIONING GROUP	220	315				
ANTI-ICING GROUP						
PHOTOGRAPHIC GROUP						
LOAD & HANDLING GROUP	10	370				
TOTAL WEIGHT EMPTY	(13675)	399.6		5465165		
CREW	215	153				
FUEL - UNUSABLE	125	393				
FUEL - USABLE	8465	393				
OIL - ENGINE	30	510				
PASSENGERS CARGO						
ARMAMENT GUN (M-61)	255	415				
AMMO (300 RDS)	170	420				
2-MAD MANS	1000	425				
EQUIPMENT GUN CAMERA	5	135				
N_2	20	395				
O_2	25	180				
TOTAL USEFUL LOAD	10310	391.9		4040440		
TAKEOFF GROSS WEIGHT	23985	346.3		9505605		
FLIGHT DESIGN GROSS WEIGHT	19753					
LANDING DESIGN GROSS WEIGHT	18906					

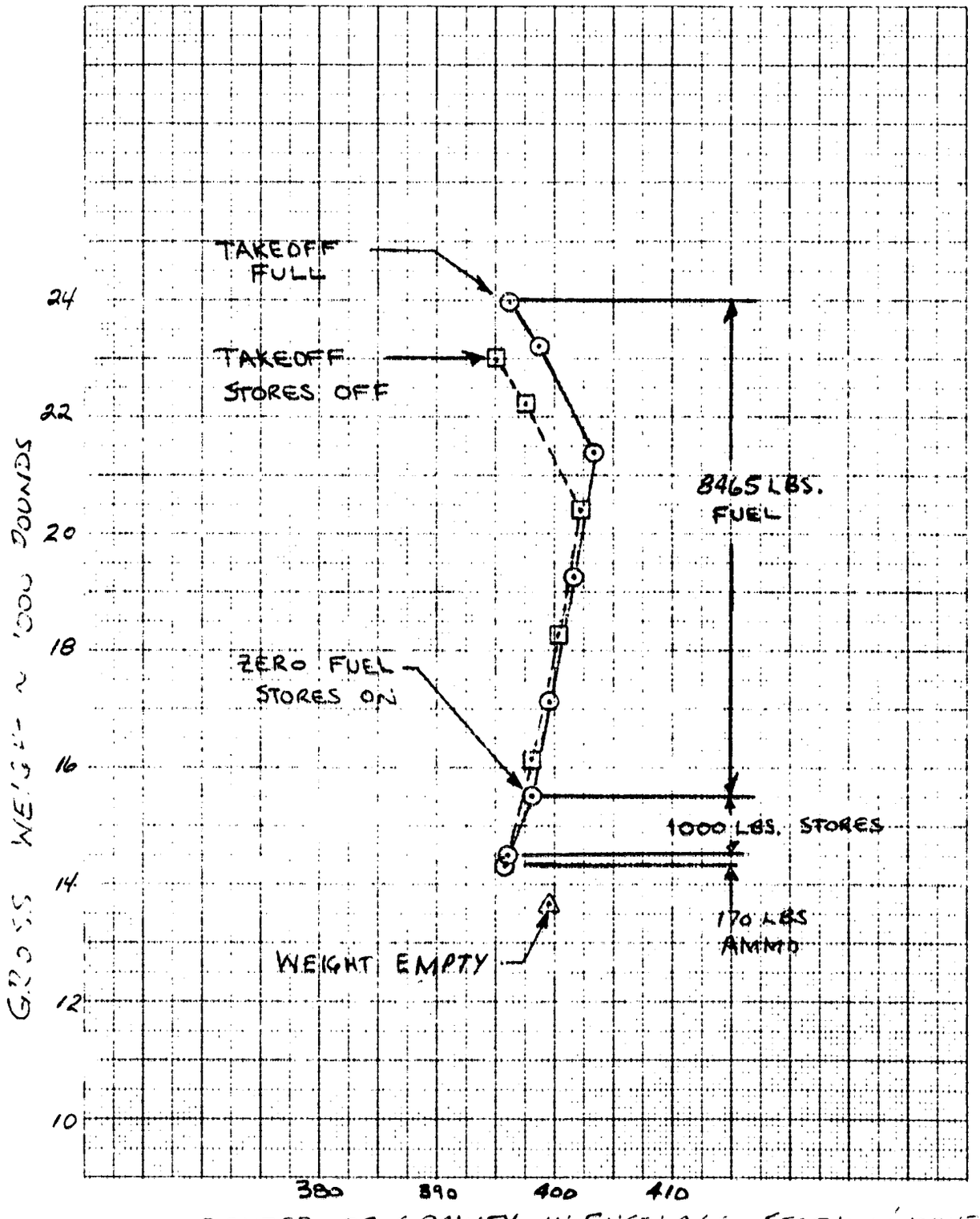

FIGURE 119. GROSS WEIGHT VS. CENTER OF GRAVITY (D515-4)

Section VI

PERFORMANCE

The 1.6, 2.0 and 2.5 Mach cruise airplanes, as resulted from the final iteration of the preliminary sizing process described in Section I, were drawn and aerodynamic and weights estimates made. Performance for each airplane was then calculated using the VSPEP program. The resulting performance and final airplane characteristics are shown in table XIV. A leg-by-leg summary of mission performance is shown in table XV.

Performance trades were run for each airplane. Increments of dead weight and drag at cruise conditions were applied independently and the resulting mission range calculated. All other vehicle parameters, including gross weight, are assumed to remain constant. The results of these trades are shown in figure 120 .

Table XIV

FINAL AIRPLANE CHARACTERISTICS

CRUISE MACH		1.6	2.0	2.5
TOGW	lb	15060	18090	23985
Fuel Wt.	lb	3895	5425	8465
Wing Area	sq ft	185	215	276
Engines	No.-#	2-45.3	2-52.4	2-62.6
Wing Loading	PSF	81.4	84.1	86.9
Thrust-to-Weight		.722	.678	.685
Radius	NM	321	371	467
Takeoff Dist.	Ft	2452	2925	3289
SEP at .9M/30K/5g	FPS	-157	-139	-197

D575-2A

TOGW = 15060 lb FUEL = 3895 lb R = 321 nm

	WEND	M END	H END	DELTA R	DELTA T
WARM UP	14754.7	0.0	0.0	0.0	6.000
TAKEOFF	14501.2	0.8952	0.0	0.0	0.579
CLIMB	14216.6	0.9260	40849.2	22.62	2.552
CRUISE	14072.2	0.9260	41069.7	51.02	5.763
CLIMB	13691.2	1.6000	53774.0	26.38	1.915
CRUISE	13011.5	1.6000	54493.4	221.03	14.451
MANEUVER	12274.3	1.6000	30000.0	0.0	2.129
DROP P/L	11274.3	1.6000	30000.0	0.0	0.0
CRUISE	10771.6	1.6000	60494.1	221.03	14.451
CRUISE	10563.3	0.9280	45554.3	100.00	11.272
LOITER	10162.2	0.3560	0.0	0.0	20.000

D575-3

TOGW = 18090 lb FUEL = 5425 lb R = 371 nm

	WEND	M END	H END	DELTA R	DELTA T
WARM UP	17722.4	0.0	0.0	0.0	6.000
TAKEOFF	17424.1	0.8785	0.0	0.0	0.599
CLIMB	17083.7	0.9120	39997.6	22.37	2.497
CRUISE	16944.6	0.9120	39997.6	41.63	4.775
CLIMB	16286.5	2.0000	54450.1	36.00	2.256
CRUISE	15165.7	2.0000	55889.3	271.84	14.218
MANEUVER	14154.8	2.0000	40000.0	0.0	2.969
DROP P/L	13154.8	2.0000	40000.0	0.0	0.0
CRUISE	12370.0	2.0000	60277.2	271.84	14.218
CRUISE	12132.2	0.9380	46245.3	100.00	11.152
LOITER	11665.3	0.3500	0.0	0.0	20.000

ORIGINAL PAGE IS
OF POOR QUALITY

D575-4

TOGW = 23985 lb FUEL = 8465 lb R = 467 nm

	WEND	M END	H END	DELTA R	DELTA T
WARM UP	23406.2	0.0	0.0	0.0	6.000
TAKEOFF	22989.6	0.9007	0.0	0.0	0.664
CLIMB	22558.1	0.9000	37208.2	18.16	2.029
CRUISE	22477.5	0.9000	37291.3	17.26	2.006
CLIMB	21122.0	2.5000	63640.6	64.48	3.404
CRUISE	19436.4	2.5000	65293.8	367.30	15.369
MANEUVER	17831.0	2.5000	50000.0	0.0	4.466
DROP P/L	16831.0	2.5000	50000.0	0.0	0.0
CRUISE	15597.0	2.5000	67709.8	367.30	15.354
CRUISE	15280.4	0.9000	44075.1	100.00	11.623
LOITER	14523.5	0.3600	0.0	0.0	20.000

TABLE XV. LEG-BY-LEG MISSION SUMMARY

FIGURE 120. WEIGHT AND DRAG TRADES

TOGW CONSTANT

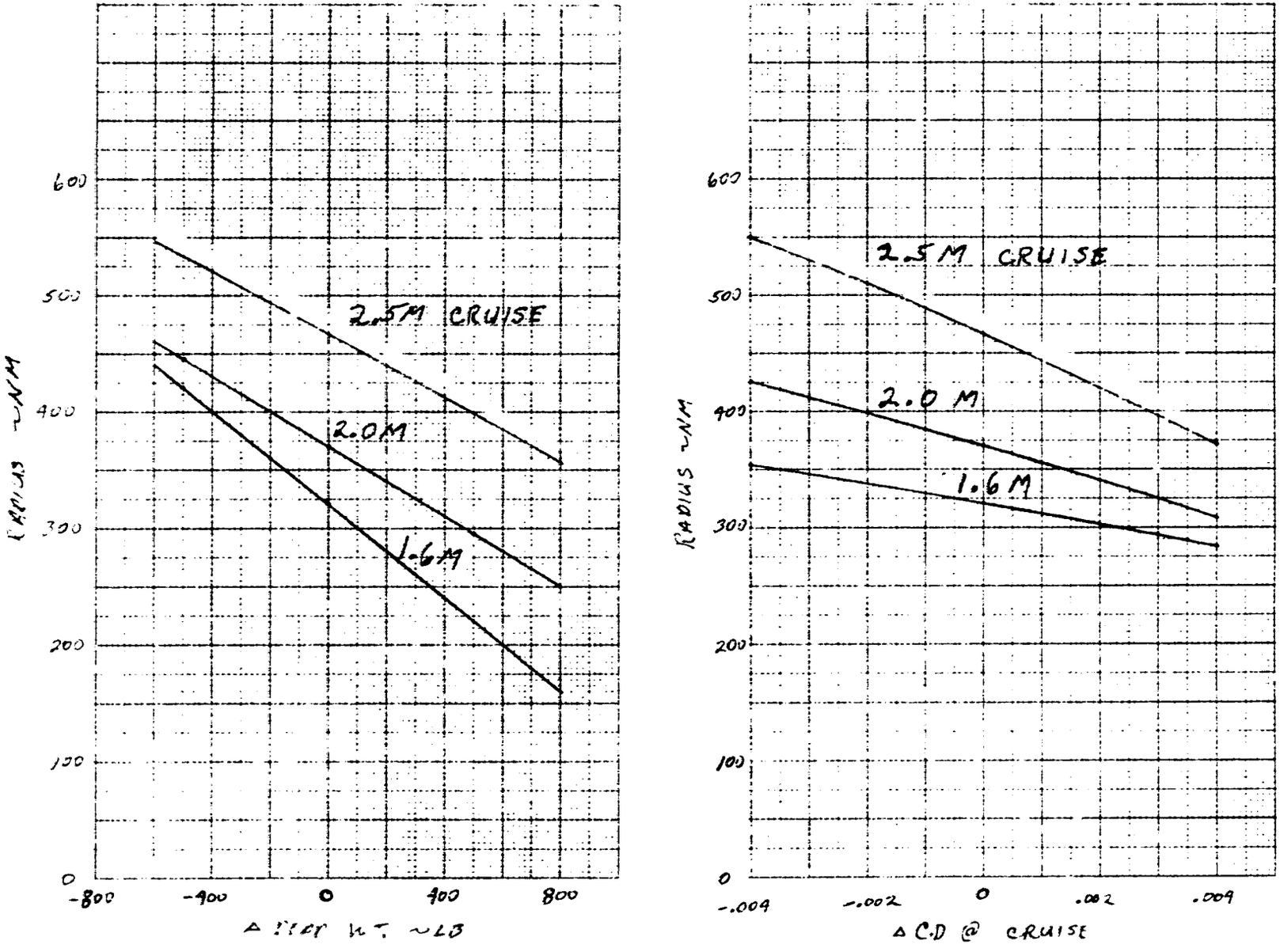

Section VII

CONCLUSIONS

1. The results of this study showed that supersonic dry power cruise fighters in the 15,000 to 23,000 pound class were feasible using the all wing concept, two-dimensional plug nozzles, composite structures, and advanced engines.

2. Due to the high aerodynamic cruise efficiencies required, the supersonic aerodynamic center must be accurately known in the conceptual design phase. This requires verification of the nonplanar lifting surface theory.

3. Off design performance such as transonic maneuverability and subsonic stability and control have major impact on the configuration.

4. Two-dimensional plug nozzles and engine location can result in substantial reductions in wave drag and improvements in stability and control.

RECOMMENDATIONS

1. Design, build, and test wind tunnel model wings to verify the supersonic lifting surface theory for nonplanar wing configurations.

2. Design, build and test wind tunnel models to determine the transonic maneuvering performance of the configuration with a variable camber wing.

3. Conduct a study to determine the optimum combination of wing dihedral, control surface size, two-dimensional nozzle control, and flight control system for optimum maneuvering and flying qualities.

4. Conduct a trade to determine the amount of maneuvering capability in the fighter versus the missile.

Section VIII

REFERENCES

1. Young, L.C., "D575 Supercruiser Inlet Design Synthesis and Performance," TFD-74-911, Rockwell International, 1966.

2. "User's Manual for Parametric Afterburning Turbofan Computer Program CCD-0193-0.2", PWA Inst. 642.

3. Johnson, T.J., "B-1 External Compression Inlet, IP-9, Performance," NA-71-296-4, Rockwell International, 1971.

4. Re, R.J., "An Investigation of Several NACA 1-Series Axisymmetric Inlets at Mach Numbers from 0.4 to 1.28," NASA TM X-2917.

5. Bonner, E., "Theoretical Prediction of Inviscid Three-Dimensional Slender Body Flows," NA-74-787, Rockwell International, 1974.

6. Mac Miller, C.T., "Investigation of Subsonic Duct Distortion," AFFDL TR-69-21.

7. Cawthon, J.A., Truax, P.P., et al, "Supersonic Inlet Design and Airframe-Inlet Integration Programs, Volumes I, II, and III," AFFDL TR-71-124.

8. Martin, R.A., and Hughes, D.L., "Comparisons of Inflight F-111A Inlet Performance for On-and Off-Scheduled Inlet Geometry at Mach Numbers of 0.68 to 2.13," NASA TN D-6490.

9. Nugent, J., and Holzman, J.K., "Flight-Measured Inlet Pressure Transients Accompanying Engine Compressor Surges on the F-111A Airplane," NASA TN D-7696.

10. Young, L.C., and Beaulieu, W.D., "A Review of Hammershock Pressure Distribution in Aircraft Inlets," NA-74-595, Rockwell International, 1974.

11. Chaloff, D., "Inlet Structural Design Pressure and Temperature Determination for Weight Estimation," NA-74-740, Rockwell International, 1974.

12. Hasson, D.F., Fichter, A.B., and Wong, M., "Aerodynamic Characteristics at Mach Numbers from 1.6 to 2.8 of 74° Swept Arrow Wings With and Without Camber and Twist," NASA TM X-8.

13. Donovan, A.F., and Lawrence, H.R., "Aerodynamic Components of Aircraft at High Speeds," Volume VII High Speed Aerodynamics and Jet Propulsion, Princeton University Press, 1957.

14. Bonner, E., "Supersonic Pressure Drag Design by use of Interactive Graphics," NA-72-718, Rockwell International, 1972.

15. Ascani, L., Hayase, G., and Hiyama, R., "A Structural Weight Estimation Program (Sweep) for Aircraft," Volume I thru XI, ASD/XR 74-10, Contract No. F33615-71-C-1929 Rockwell International/Los Angeles Aircraft Division, For Air Force Systems Command, Wright-Patterson Air Force Base, Ohio.

16. Ascani, L., and Hayase, G., "An Integrated Approach to Structural Weight Estimation," Society of Automotive Engineers, October 16,1973.

17. Meledy, T., "Sweep-An Interdisciplinary Approach to Structural Weight Estimation Program," Society of Allied Weight Engineers Paper No. 1016.

18. Cairo, R., and Torczyner, R., "Graphite/Epoxy, Boron-Graphite/Epoxy Hybrid and Boron/Aluminum Design Allowables," AFML-TR-72-230, Contract No. F33615-71-C-1105, Grumman Aerospace Corporation.

19. "Advanced Composites Design Guide"Volume IV Contract No. F33615-71-C-1362, Rockwell International/Los Angeles Aircraft Division, for Air Force Systems Command, Wright-Patterson Air Force Base, Ohio.

20. Wykes, J.H., Sweet, H.R., Joseph, J.A., and Hodson, C.H., "Commercial Supersonic Transport Flutter Studies," ASD TDR-63-817, Contract No. AF33657-8514, North American Aviation/Los Angeles.

21. Goebel, T.P., Sitar, M.D., "Analysis of Low Speed Wind Tunnel Test of A D572-1 Supersonic Cruise Vehicle", NA-74-846, Rockwell International, 1974.

22. Sokolsky, O.M., "Analysis of Low Speed Wind Tunnel Test of A Modified Supersonic Cruise Vehicle", NA-75-129, Rockwell International, 1975.

23. Child, R., "Design and Analysis of A Supersonic Penetration/Maneuvering Fighter", NA-75-118, Appendix , Rockwell International, 1975 (Proprietary Information).